

**Chemical and Enzymatic Footprinting of
Quinoxaline Antibiotics on DNA**

Thesis by
David Mendel

In Partial Fulfillment of the Requirements
for the Degree of
Doctor of Philosophy

California Institute of Technology
Pasadena, California

1989

(Submitted June 1, 1989)

© 1989

David Mendel

All Rights Reserved

To my parents and to Doreen

ACKNOWLEDGEMENTS

I wish to thank my research advisor, Peter Dervan, for his advice and enthusiastic support during the course of my Ph. D. studies and beyond. I am further indebted to him for steering me in the proper direction without navigating too narrow a course. Thanks are also due the alumni of the Dervan group, especially Scott Youngquist, Jim Sluka, Brenda Baker and Dave Horne for their scientific advice, technical assistance and most of all for their friendship.

A number of others deserve special mention for their support of my work. First of all, I thank Dr. Matthew Suffness of the National Cancer Institute, whose generous gift of echinomycin made this study possible; Suzanne Horvath and company of the Caltech microchemical facilities for their assistance with the large-scale oligonucleotide syntheses; Marc Greenberg for his help with the ^{13}C NMR; Delmer, Guy, Toni, Ray and Pavel of the Chemistry machine/mechanic shops, who provided superior service with a genuine concern for my welfare; Richard and Ben of the Caltech photo-lab, whose beautiful work graces the glossy pages of this thesis; to the Midwest Center for Mass Spectrometry for their help in identifying the structures of my reference compounds; Martha Oakley (fellow Carl), Laura Kiessling and Kevin Leubke for their constructive criticism of this manuscript; and special thanks go to the Eastman Kodak Company whose x-ray film and development process provided so much of the data in this work!

Finally, to Doreen and to my parents I am forever grateful for their love, friendship and moral support through all the joys and frustrations of life. Without you, neither this thesis nor I would exist. I am so lucky to have you all around me as I go through life. I can only hope that others may be as fortunate as I.

ABSTRACT

A key element of antitumor drug design is an understanding of how naturally occurring antitumor antibiotics recognize and bind to DNA, the major means by which many of these agents act. Once such an understanding is attained, the salient elements of recognition may be extracted and then extended to create more powerful and more specific antitumor (chemotherapeutic) agents. In an effort to understand G·C recognition, we studied the binding interactions between DNA and the antitumor antibiotics triostin A and echinomycin.

Recent studies by the Rich group at MIT and by the Patel group at Columbia have shown that the naturally occurring antitumor antibiotics triostin A and echinomycin bind four base pairs of DNA and can induce the formation of Hoogsteen base pairs at the first and fourth base pair positions of their binding sites on small oligonucleotides. The central aim of the thesis work described below was to establish whether this novel base-pairing occurs at echinomycin and triostin A binding sites on native DNA and if so, whether this represents a new recognition motif on which to base anticancer drug design.

We find that purines occupying the first and/or fourth base pair positions of echinomycin and triostin A binding sites become hyperreactive to diethyl pyrocarbonate (DEP) in the presence of drug. This finding raised the issue as to whether DEP detects Hoogsteen base-pairing at echinomycin binding sites in solution. We analyzed the products of DEP-purine reaction formed in the presence of echinomycin and ethidium bromide at six different echinomycin binding sites. Two different DEP-purine adducts were identified: 5-carbethoxyamino-4,6-diaminopyrimidine and 5-carbethoxyamino-2,4-diamino-6-hydroxypyrimidine. These products correspond to reaction of DEP at the N7 positions of adenosine and guanosine residues, respectively. The identity of these compounds strongly suggests that DEP responds to local helix unwinding caused by antibiotic intercalation into DNA and not to a Watson-Crick to Hoogsteen base-pairing transition caused by

echinomycin binding to DNA. Nonetheless, DEP is a sensitive and precise probe of echinomycin and triostin A binding to DNA, and we describe this chemical footprinting reagent as the preferred means by which to identify echinomycin and triostin A binding sites on DNA. We also note three new types of echinomycin binding sites (5'-3') GGGG, TCAT, and TCAC not previously identified.

We find that another chemical footprinting reagent, dimethyl sulfate (DMS), demonstrated that isolated C·G Hoogsteen base pairs may exist at echinomycin binding sites within a DNA duplex under acidic conditions. If this is indeed the case, it would be the first example of isolated Hoogsteen base pairs to exist within a DNA fragment in solution. However, at neutral pH, echinomycin and triostin A appear to bind DNA via simple bisintercalation and probably do not form stable Hoogsteen base pairs at their binding sites. Therefore, we conclude that the induction or recognition of Hoogsteen base pairs at drug binding sites does not yet constitute a practical approach to the design of sequence specific DNA binding agents.

In addition, using a series of plasmid DNAs and a battery of enzymatic and chemical probes of DNA structure, we find that echinomycin binding to DNA apparently alters the helix structure of sequences adjacent and distal to its binding sites. Echinomycin can thus be considered an allosteric effector of DNA structure.

TABLE OF CONTENTS

Acknowledgements.....	iv
Abstract.....	v
CHAPTER 1: Characterization of DNA Structure at Occupied Echinomycin Binding Sites.....	1
Introduction.....	2
Chemical Versus Enzymatic Footprinting.....	23
Results	
Gel Studies.....	25
Diethyl Pyrocarbonate Reacts with Purines at Echinomycin Binding Sites.....	25
DEP-Purine Reaction in the Presence of Other Intercalators.....	34
Influence of Methylation upon Echinomycin Binding and DEP-Purine reactivity.....	42
Product Analysis.....	48
DNA Substrates Used for Product Analysis.....	53
DEP/Piperidine Cleavage Patterns on Duplexes 47+48 through 60+61	56
Summary.....	73
HPLC Analysis of DEP-DNA Reaction Products.....	80
Synthesis and Characterization of Reference Compounds.....	99
Identity of DEP-Adenosine and DEP-Guanosine Adducts.....	105
Other Reagents Used to Characterize Echinomycin Binding to DNA.....	117
Discussion and Conclusions.....	123
Nature of the Base-Pairing at Echinomycin Binding Sites in Solution.....	124

CHAPTER 2: Chemical and Enzymatic Probing of DNA Structure	
Adjacent or Distal to Echinomycin Binding Sites.....	128
Introduction.....	129
Results.....	130
Discussion.....	176
Conclusion.....	197
CHAPTER 3: Experimental.....	202
REFERENCES.....	232

LIST OF FIGURES

Figure	Title	Page
Figure 1.	B-DNA structure.....	3
Figure 2.	Helix axis view of Watson-Crick C·G (cytidine·guanosine) and T·A (thymidine·adenosine) base pairs in B-DNA.....	4
Figure 3.	Distamycin A and Netropsin.....	4
Figure 4.	X-ray crystal structure and schematic representation of netropsin complexed to the oligonucleotide d(CGCGAATTCGCG) ₂ as determined by Kopka <i>et al.</i> ³	5
Figure 5.	Structures of echinomycin and triostin A.....	7
Figure 6.	Representation of two triostin A molecules complexed to the d(CGTACG) ₂ hexamer with accompanying helix unwinding angles.....	13
Figure 7.	Minor groove perspective of one-half to the (triostin A) ₂ ·d(CGTACG) ₂ complex structure determined by Wang <i>et al.</i> ¹⁵	14
Figure 8.	Watson-Crick and Hoogsteen T·A base pairs in right-handed DNA.....	15
Figure 9.	Stereodiagram of the (triostin A) ₂ ·d(GCGTACGC) ₂ cocrystal structure determined by Quigley <i>et al.</i> ⁷²	18
Figure 10.	Comparison of H1' to H8 distances for <i>syn</i> versus <i>anti</i> adenosine.....	20
Figure 11.	Comparison of C·G and T·A base pairs in left-handed Z-DNA, right-handed B-DNA and Hoogsteen base-paired, right-handed DNA.....	24
Figure 12.	Structure of diethyl pyrocarbonate (DEP)	26
Figure 13.	MPE·Fe(II) and DEP/piperidine footprinting of echinomycin on a large DNA restriction fragment.....	27
Figure 14.	Densitometric analysis of MPE·Fe(II) and DEP/piperidine footprinting of echinomycin.....	29
Figure 15.	DNase I footprinting of echinomycin.....	32
Figure 16.	Comparison of DNase I and DEP/piperidine footprinting of several intercalators.....	35
Figure 17.	DEP/piperidine cleavage of DNA in the presence of echinomycin and/or ethidium bromide.....	38

Figure	Title	Page
Figure 18.	DEP/piperidine cleavage patterns on about 100 bp of the 629 bp pDMGC11 restriction fragment, as determined by densitometry of the autoradiogram in Figure 17.....	40
Figure 19.	Effects of adenosine methylation on echinomycin binding and DEP/piperidine cleavage	44
Figure 20.	MPE·Fe(II) and DEP/piperidine footprinting of echinomycin bound to about 70 bp of the 628 bp pDMG10 restriction fragment, as determined by densitometry of Figure 19.....	46
Figure 21.	Diagram of T·N ⁶ methyl adenosine base pairs in the Watson-Crick and Hoogsteen geometries	48
Figure 22.	DEP-adenine reaction products determined by N. J. Leonard <i>et al.</i> ⁹⁴	49
Figure 23.	DEP-N ⁹ -substituted adenine reaction products.....	49
Figure 24.	DEP-guanosine reaction product.....	50
Figure 25.	Relative exposure of purine N7 atoms in Z-DNA versus B-DNA for the dinucleotide steps CpG and GpC.....	51
Figure 26.	Design of product analysis experiments.....	52
Figure 27.	Sequences of the oligonucleotides used for product analysis of DNA-DEP reactivity at a number of echinomycin binding sites	54
Figure 28.	Autoradiogram of the high-resolution denaturing polyacrylamide gel used to analyze DEP/piperidine cleavage of the oligonucleotide duplex 47+48 in the presence of echinomycin or ethidium bromide.....	57
Figure 29.	Autoradiogram of the high-resolution denaturing polyacrylamide gel used to analyze DEP/piperidine cleavage of the oligonucleotide duplex 49+50 in the presence of echinomycin or ethidium bromide.....	59
Figure 30.	DEP/piperidine cleavage of oligonucleotide duplexes 47+48 and 49+50 in the presence of echinomycin or ethidium bromide, as determined by densitometry of the autoradiograms in Figures 28 and 29.....	61
Figure 31.	Autoradiogram of the high-resolution denaturing polyacrylamide gel used to analyze DEP/piperidine cleavage of the oligonucleotide duplex 51+52 in the presence of echinomycin or ethidium bromide.....	65
Figure 32.	Autoradiogram of the high-resolution denaturing polyacrylamide gel used to analyze DEP/piperidine cleavage of the oligonucleotide duplex 53 in the presence of echinomycin or ethidium bromide.....	67

Figure	Title	Page
Figure 33.	DEP/piperidine cleavage of oligonucleotide duplexes 51+52 and 53 in the presence of echinomycin or ethidium bromide, as determined by densitometry of the autoradiograms in Figures 31 and 32.....	69
Figure 34.	Autoradiogram of the high-resolution denaturing polyacrylamide gel used to analyze DEP/piperidine cleavage of the oligonucleotide duplex 54+55 in the presence of echinomycin or ethidium bromide.....	74
Figure 35.	Autoradiogram of the high-resolution denaturing polyacrylamide gel used to analyze DEP/piperidine cleavage of the oligonucleotide duplex 60+61 in the presence of echinomycin or ethidium bromide.....	76
Figure 36.	DEP/piperidine cleavage of oligonucleotide duplexes 54+55 and 60+61 in the presence of echinomycin or ethidium bromide, as determined by densitometry of the autoradiograms in Figures 34 and 35.....	78
Figure 37.	Reversed-phase HPLC chromatograms of base-release products obtained by heat/formic acid treatment of 100 nmol scale DEP-oligonucleotide duplex 47+48 reactions	81
Figure 38.	Reversed-phase HPLC chromatograms of base-release products obtained by heat/formic acid treatment of 100 nmol scale DEP-oligonucleotide duplex 49+50 reactions.....	83
Figure 39.	Reversed-phase HPLC chromatograms of base-release products obtained by heat/formic acid treatment of 100 nmol scale DEP-oligonucleotide duplex 51+52 reactions.....	85
Figure 40.	Reversed-phase HPLC chromatograms of base-release products obtained by heat/formic acid treatment of 100 nmol scale DEP-oligonucleotide duplex 53 reactions.....	87
Figure 41.	Reversed-phase HPLC chromatograms of base-release products obtained by heat/formic acid treatment of 100 nmol scale DEP-oligonucleotide duplex 56+57 reactions.....	89
Figure 42.	Reversed-phase HPLC chromatograms of base-release products obtained by heat/formic acid treatment of 100 nmol scale DEP-oligonucleotide duplex 54+55 reactions.....	91
Figure 43.	Reversed-phase HPLC chromatograms of base-release products obtained by heat/formic acid treatment of 100 nmol scale DEP-oligonucleotide duplex 60+61 reactions.....	93
Figure 44.	5-carbethoxyamino-4,6-diaminopyrimidine ("X") and 5-carbethoxyamino-2,4-diamino-6-hydroxypyrimidine ("Y").....	99
Figure 45.	Synthesis of X, 5-carbethoxyamino-4,6-diaminopyrimidine	101
Figure 46.	Synthesis of Y, 5-carbethoxyamino-2,4-diamino-6-hydroxypyrimidine.	101

Figure	Title	Page
Figure 47.	Proton decoupled 22.5 MHz ¹³ C NMR spectrum of 4,5,6-triaminopyrimidine and 5-carbethoxyamino-4,6-diaminopyrimidine hydrochloride.....	102
Figure 48.	400 MHz ¹ H NMR spectrum of 5-carbethoxyamino-4,6-diaminopyrimidine hydrochloride and 5-carbethoxyamino-2,4-diamino-6-hydroxypyrimidine.....	103
Figure 49.	Proton decoupled 22.5 MHz ¹³ C NMR spectrum of 5-carbethoxyamino-2,4-diamino-6-hydroxypyrimidine and [5- ¹⁵ N]-carbethoxyamino-2,4-diamino-6-hydroxypyrimidine.....	104
Figure 50.	Spiking experiments: Reversed-phase HPLC chromatograms of base-release products from 100 nmol scale DEP-oligonucleotide duplex 47+48 reactions.....	109
Figure 51.	Spiking experiments: Reversed-phase HPLC chromatograms of base-release products from 100 nmol scale DEP-oligonucleotide duplex 49+50 reactions.....	111
Figure 52.	Spiking experiments: Reversed-phase HPLC chromatograms of base-release products from 100 nmol scale DEP-oligonucleotide duplex 54+55 reactions.....	113
Figure 53.	Spiking experiments: Reversed-phase HPLC chromatograms of base-release products from 100 nmol scale DEP-oligonucleotide duplex 60+61 reactions.....	115
Figure 54.	Autoradiogram of the high-resolution denaturing polyacrylamide gel used to analyze DMS/piperidine cleavage of the oligonucleotide duplex 60+61 in the presence of echinomycin or ethidium bromide.....	119
Figure 55.	Differential DMS/piperidine cleavage of oligonucleotide duplex 60+61 without drugs or in the presence of echinomycin or ethidium bromide, as determined by densitometry of the autoradiogram shown in Figure 54.....	121
Figure 56.	MPE·Fe(II) and DEP footprinting of echinomycin on a large DNA restriction fragment.....	131
Figure 57.	Densitometric analysis of MPE·Fe(II) and DEP/piperidine footprinting of echinomycin.....	133
Figure 58.	DNase I footprinting of echinomycin.....	135
Figure 59.	MPE·Fe(II) and EDTA·Fe(II) footprinting of echinomycin.....	139

Figure	Title	Page
Figure 60.	MPE·Fe(II) and EDTA·Fe(II) cleavage inhibition patterns on about 100 bp of the 628 bp pDMG10 restriction fragment in the presence of echinomycin, as determined by densitometry of the autoradiogram in Figure 59.....	141
Figure 61.	S1 nuclease probing of echinomycin binding to DNA at various pH values.....	143
Figure 62.	S1 nuclease probing of echinomycin binding to DNA: S1 nuclease unit study.....	145
Figure 63.	KMnO ₄ reactivity in the presence of echinomycin.....	149
Figure 64.	KMnO ₄ /piperidine cleavage patterns in the presence of echinomycin on about 90 bp of the 628 bp restriction fragment from plasmid pDMG10, as determined by densitometry of the autoradiogram in Figure 63.....	151
Figure 65.	Neocarzinostatin (NCS) and Bleomycin A ₂ ·Fe(II) (BLM) footprinting of echinomycin.....	154
Figure 66.	Neocarzinostatin (NCS) footprinting of echinomycin.....	156
Figure 67.	Densitometric analysis of NCS and BLM footprinting of echinomycin...	158
Figure 68.	MPE·Fe(II) and DEP/piperidine footprinting of echinomycin and distamycin A	161
Figure 69.	Densitometric analysis of MPE·Fe(II) and DEP/piperidine footprinting of echinomycin and distamycin A.....	163
Figure 70.	DEP/piperidine footprinting of echinomycin: NaCl concentration dependence.....	167
Figure 71.	NaCl concentration dependence of DEP/piperidine cleavage patterns in the presence of echinomycin on about 100 bp of the 628 bp fragment from pDMG10, as determined by densitometry of the autoradiogram in Figure 70.....	169
Figure 72.	DEP/piperidine footprinting of echinomycin: pH dependence of the reaction.....	172
Figure 73.	pH dependence of DEP/piperidine cleavage patterns in the presence of echinomycin on about 100 bp of the 628 bp fragment from pDMG10, as determined by densitometry of the autoradiogram in Figure 72.....	174
Figure 74.	DEP/piperidine footprinting of echinomycin: pH dependence of the reaction.....	187

Figure	Title	Page
Figure 75.	DNase I, MPE·Fe(II) and DEP/piperidine footprinting of echinomycin on a large DNA restriction fragment.....	189
Figure 76.	pH dependence of DEP/piperidine cleavage patterns in the presence of echinomycin on about 100 bp of the 628 bp restriction fragment from pDMAC10 or pDMAG10, as determined by densitometry of the autoradiograms in Figures 74 and 77, respectively.....	191
Figure 77.	DEP/piperidine footprinting of echinomycin: pH dependence of the reaction.....	194
Figure 78.	DEP/piperidine footprinting of echinomycin: pH dependence of the reaction.....	198
Figure 79.	DEP/piperidine footprinting of echinomycin: NaCl concentration dependence	200
Figure 80.	FPLC [®] solvent gradient used for large-scale oligonucleotide purification.....	207
Figure 81.	Typical FPLC [®] chromatogram illustrating the resolution between DMT-on and DMT-off oligonucleotides.....	208
Figure 82.	Schematic diagram of HPLC solvent gradient RAMP3.....	214
Figure 83.	Schematic diagram of HPLC solvent gradient RAMP9.....	214
Figure 84.	Construction scheme for plasmid pDMG10.....	220

LIST OF TABLES

Table	Title	Page
Table 1.	Association Constants for Echinomycin and Triostin A with DNA Polymers.....	8
Table 2.	Preferred Echinomycin Binding Sites on DNA Restriction Fragments.....	11
Table 3.	Summary of Polyacrylamide Gel Electrophoresis (PAGE) Analysis of DEP-Purine Reaction on Oligonucleotide Duplexes 47+48 through 60+61 in the Presence of Echinomycin and Ethidium Bromide.....	73
Table 4.	Summary of Polyacrylamide Gel Electrophoresis (PAGE) and HPLC Analysis of DEP-Purine Reaction on Oligonucleotide Duplexes 47+48 through 60+61 in the Presence of Echinomycin and Ethidium Bromide..	98
Table 5.	Comparison of Echinomycin-Induced DEP-Purine Hyperreactivity to NMR and X-ray Analyses of Echinomycin·DNA and Triostin A·DNA Complexes.....	125
Table 6.	Oligonucleotides Used for Plasmid Construction.....	219

CHAPTER 1

Characterization of DNA Structure at Occupied Echinomycin Binding Sites

INTRODUCTION

A number of naturally occurring antibiotics bind to DNA and are believed to inhibit the production of disease-causing material by covalently crosslinking DNA, by cleaving DNA or by inhibiting its transcription into RNA.¹ Many of these naturally occurring antibiotics also possess antineoplastic activities but unfortunately, they are also toxic to humans. This is likely because their inherently low sequence binding specificity does not permit the antibiotics to discriminate between the DNA of cancerous cells and the DNA of normal cells. Cancer therapy with such drugs is best viewed as a war of attrition and were it not for the faster proliferation of cancerous cells, it is unlikely that these antibiotics would have significant anticancer activity. The ultimate goal in the treatment of cancer and many other diseases is the construction of molecules that specifically bind a given length and sequence of DNA. Realization of this goal would make it possible, in principle, to specifically inhibit the production of disease-causing material while leaving normal cells and functions untouched, e.g., by selectively binding to oncogenic DNA and preventing its replication or by inhibiting its transcription into RNA. One of the most effective ways to develop new sequence-specific DNA-binding chemotherapeutic agents is to study how nature recognizes DNA, extract the elements of recognition and then build upon these elements to increase and/or change the specificity of DNA recognition. Among the naturally occurring antibiotics to be studied in this manner are netropsin and distamycin A²⁻⁵, CC-1065 and anthramycin⁶, daunomycin⁷, mitomycin C^{8,9}, neocarzinostatin¹⁰, bleomycin¹¹, actinomycin D^{12,13}, echinomycin and triostin A¹⁴⁻¹⁶, Hoechst 33258^{17,18} and chromomycin.^{19,20}

Since the original elucidation of DNA structure by Watson and Crick²¹, the number of alternative DNA structures characterized has grown steadily to include, in addition to the canonical B-form, A-, Z-, D- and H- forms²²⁻²⁷, bent DNA²⁸⁻³⁰, triple-stranded DNA³¹⁻³³ and DNA cruciform loops³⁴⁻³⁶. Surprisingly, some DNA appears to

fold into a complex pseudo-tRNA-like structure which can be aminoacylated by a tRNA synthetase.³⁷ The amazing structural plasticity of DNA raises the issue as to which form of DNA serves as the target for recognition by a given antibiotic. In general, an antibiotic need not even bind to DNA to act. However, all of the aforementioned antibiotics are believed to act primarily via recognition of B-form DNA. Figure 1 shows the structure of B-form DNA. This form of DNA is composed of two antiparallel polynucleotide strands wound into a right-handed double helix possessing a wide major groove, a narrower minor groove and approximately 10.5 base pairs per turn of helix. The helix axis view shown in Figure 2 displays the Watson-Crick base pairs that cement the two antiparallel polynucleotide strands together. In addition, this view shows the atoms of the bases available for hydrogen bond formation with B-DNA-binding antibiotics.

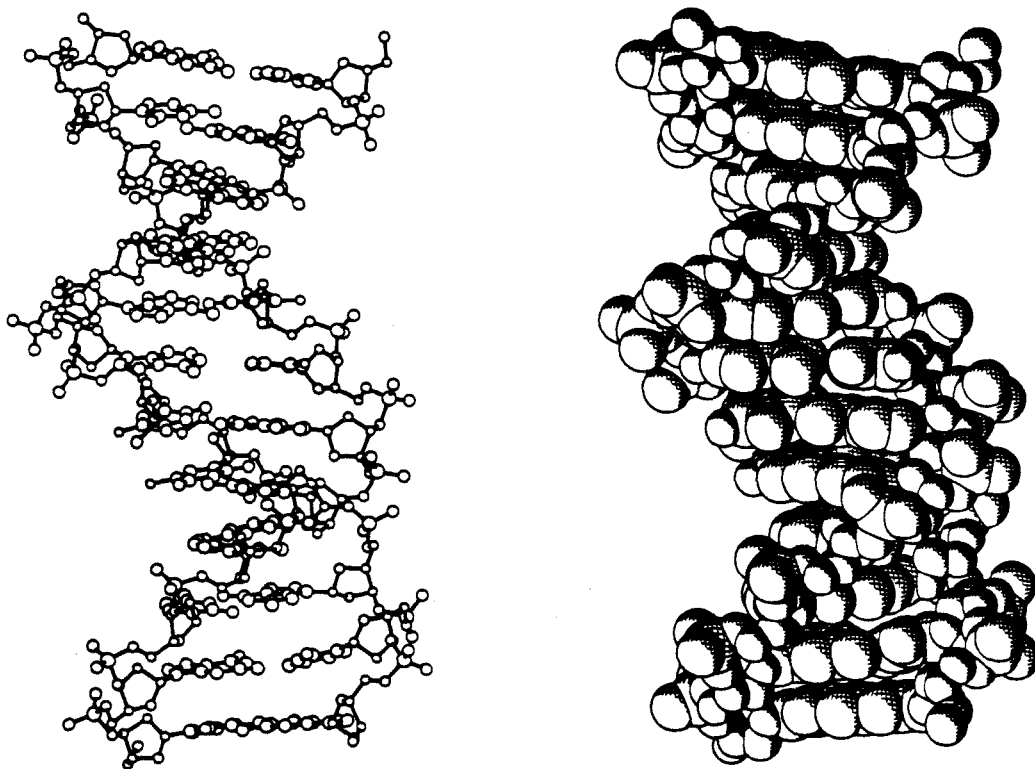


Figure 1. B-DNA structure.

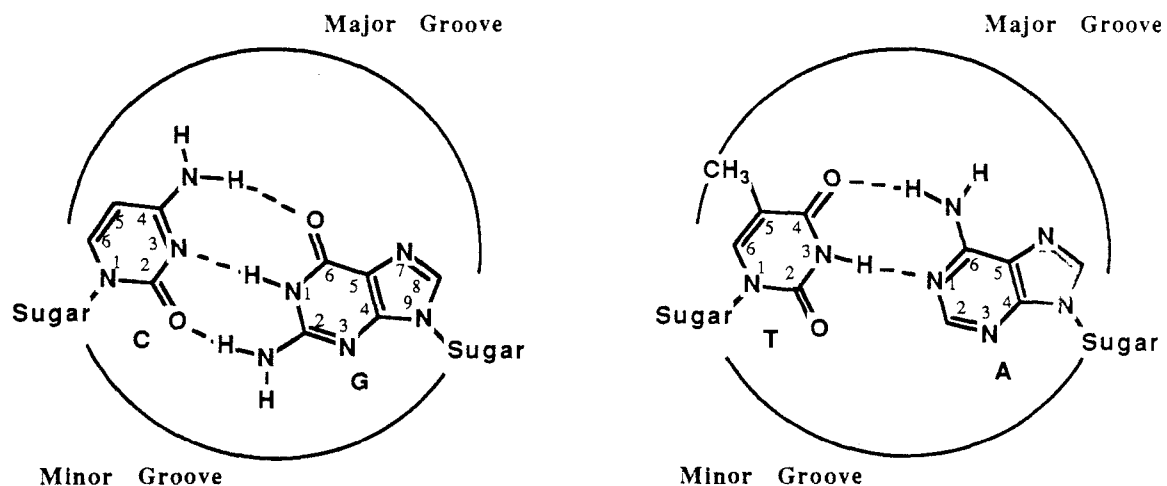


Figure 2. Helix axis view of C·G (cytidine·guanosine) and T·A (thymidine·adenosine) base pairs in B-DNA

A case study of netropsin and distamycin A illustrates how natural products recognize B-DNA and how the salient features of this recognition can be extended to produce more sequence-specific B-DNA binding agents. Figure 3 shows the structures of netropsin and distamycin A, both A-T specific binding small molecules that bind four and five ^{3,5,17} DNA base pairs, respectively.

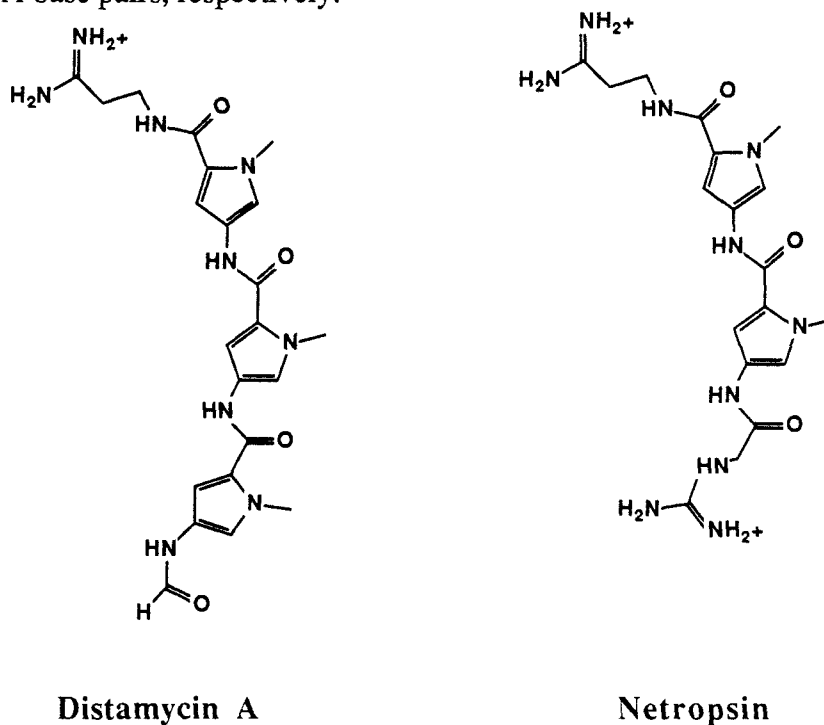


Figure 3. Distamycin A and Netropsin

Footprinting and affinity cleaving studies^{17,38,39} have yielded a binding model for netropsin and distamycin in which the drugs are anchored to the minor groove of B-DNA by a series of bifurcated hydrogen bonds between the oligo-N-methylpyrrole carboxamide NHs and adjacent adenine N3 and thymine O2 atoms on opposite strands. This model has been reinforced by x-ray crystallographic analysis of netropsin·d(CGCGAATTCGCG)₂ and distamycin A·d(CGCAAATTTGCG)₂ complexes.^{3,5} Figure 4 depicts the netropsin·d(CGCGAATTCGCG)₂ complex and a schematic representation of the hydrogen-bonding pattern between antibiotic and nucleic acid.

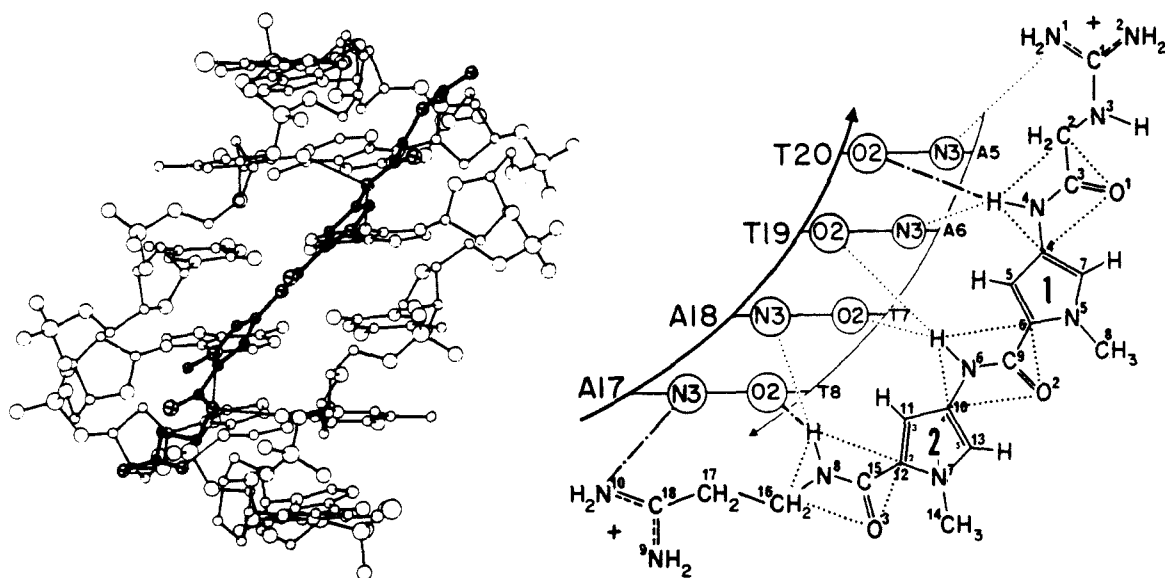


Figure 4. X-ray crystal structure (left) and schematic representation of netropsin complexed to the oligonucleotide d(CGCGAATTCGCG)₂ as determined by Kopka *et al.*³

Schultz and Dervan^{39,40} and Youngquist and Dervan⁴¹ then extended the oligo-N-methylpyrrole carboxamide chain used in netropsin to produce A-T specific, minor groove-binding molecules that recognize up to 11 base pairs of DNA.⁴² Other modifications to the basic N-methylpyrrole carboxamide framework of netropsin and distamycin have produced molecules that recognize up to 16 base pairs of A-T DNA⁴³, molecules that recognize G·C

base pairs in addition to A·T pairs^{44,45} and compounds that bind to DNA in a metal dependent fashion.⁴⁶ Minor groove recognition of A·T base pairs is fairly well understood, based on the successes achieved with these compounds. However, G-C recognition is still poorly understood. It is obviously necessary to understand the elements of G-C recognition so that synthetic antibiotics can be made to recognize any combination of base pairs on DNA. This thesis describes an effort to understand G-C recognition of B-DNA by studying the binding interactions between DNA and the antitumor antibiotics echinomycin and triostin A.

Echinomycin is a member of the quinoxaline antibiotic family. It was originally isolated from cultures of *Streptomyces echinatus* and is also known as quinomycin A.^{47,48} It is a powerful antibiotic, effective against both gram-positive and gram-negative bacteria and displays significant antitumor and cytotoxic activity.^{15,49,50} Echinomycin is currently being used in clinical trials for the treatment of cancer in man.^{50,51} The structures of echinomycin and its close relative triostin A are shown in Figure 5. Both antibiotics are cyclic octapeptides containing D- and L- amino acids, half of which are N-methylated. According to Wang *et al.*¹⁵, these antibiotics are synthesized on special enzymatic systems, which can accept D- and L- as well as N-methylated amino acids. The high degree of N-methylation is a common theme among some of the best characterized naturally occurring antibiotics including actinomycin D, netropsin, and distamycin A. This methylation restricts the number of conformations available to the peptide (see below). Triostin A and echinomycin are each composed essentially of two D-serine, two L-N-methylvaline, two L-alanine and two L-N-methylcysteine residues. Instead of closing the peptide ring with amide bonds, the hydroxyl groups of the two D-serine residues form ester linkages with the carboxyl group of each of the L-N-methylvaline residues. The serine amino functions are used to link two quinoxaline chromophores to the peptide chain. In a formal sense, echinomycin and triostin A can be considered bicyclic peptides because they contain a cross bridge in addition to the lactone linkages. The cross bridge in

echinomycin was originally thought to be a symmetrical dithian ring^{48,52}, but ¹H NMR, ¹³C NMR and mass spectrometry have revealed it to be a thioacetal formed between L-N,S-dimethylcysteine and L-N-methylcysteine residues.^{53,54} Echinomycin is thus pseudo-C₂ symmetric because of the unsymmetrical bridge, whereas triostin A is C₂ symmetric because its cross bridge is a disulfide formed between two L-N-methylcysteine residues.

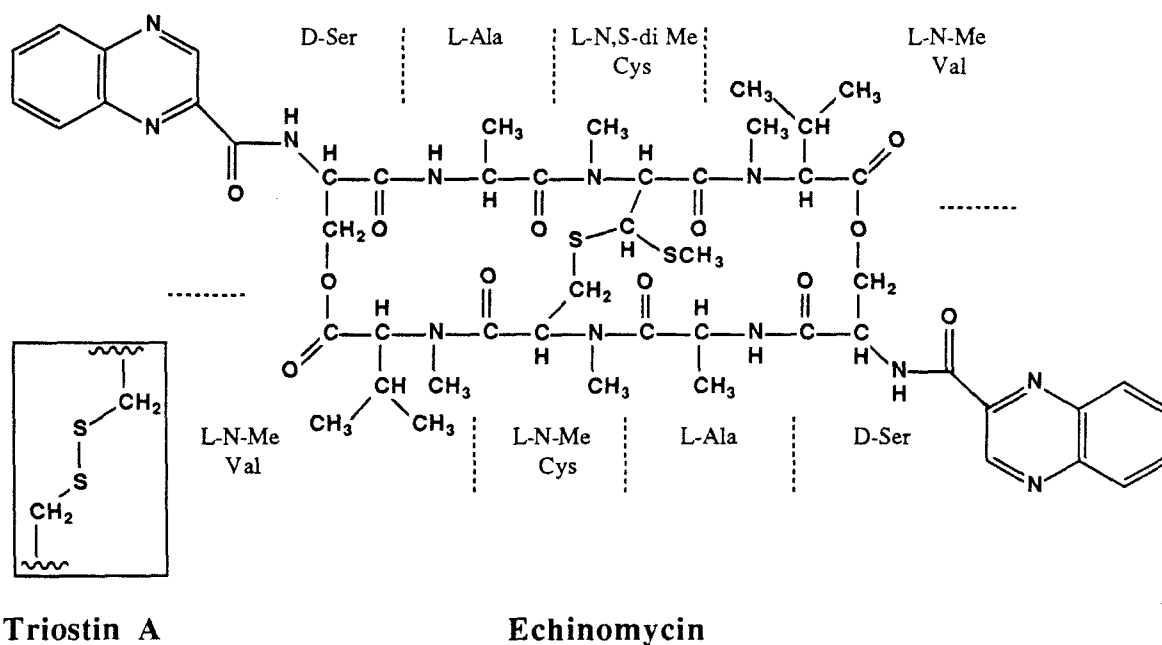


Figure 5. Structures of Echinomycin and Triostin A (insert).

Early studies indicated that echinomycin strongly inhibits the ability of DNA to function as a template for both DNA replication and RNA transcription.^{49,55} Waring and colleagues then investigated the interactions between a number of quinoxaline antibiotics and various nucleic acid polymers via equilibrium binding analysis. Table 1 lists the association constants for echinomycin and triostin A binding to a variety of different DNAs. These values were determined by the solvent partition method of Waring^{56,57} in conjunction with the theoretical analysis of McGhee and von Hippel.⁵⁸ A comparison of the binding affinities to native and heat-denatured calf thymus DNA shows that

echinomycin binds duplex DNA four times stronger than denatured DNA of the same sequence.

Table 1. Association Constants for Echinomycin and Triostin A with DNA Polymers

DNA	G+C (%)	K_a ($10^{-5} \times M^{-1}$)	n	Reference
<u>Echinomycin</u>				
<i>Cl. Perfringens</i>	30	3.44	9.46	59
Calf Thymus	42	5.48	7.17	59
Calf Thymus (heat denatured)	42	1.40	18.49	59
Bacteriophage PM2	42	5.07	7.75	59
<i>M. Lysodeikticus</i>	72	31.0	9.85	59
poly (dG-dC)	100	5.53	5.48	59
poly (dA-dT)	0	3.12	5.65	59
<u>Triostin A</u>				
<i>Cl. Perfringens</i>	30	4.9	8.52	60
Calf Thymus	42	7.0	7.29	60
Bacteriophage PM2	42	4.2	9.42	60
<i>M. Lysodeikticus</i>	72	11.3	7.73	60
poly (dG-dC)	100	4.3	7.41	60
poly (dA-dT)	0	9.7	4.76	60

All assays according to the solvent partition method of Waring^{56,57} at 20°C in 2mM HEPES pH 7.0, 10 uM EDTA, NaCl to I=0.01. K_a and n are the association constant and nucleotides occluded per binding event calculated from Scatchard plots according to McGhee and von Hippel.⁵⁸

When "random sequence" DNAs are considered, echinomycin displays a smooth increase in binding affinity with increasing G+C content of the DNA and binds most avidly to *Micrococcus lysodeikticus* DNA. The same is true for triostin A. However, the situation is different when one considers alternating copolymeric DNA as the binding target. Here, triostin A binds more strongly to alternating dA-dT copolymer than to alternating dG-dC copolymer, while echinomycin maintains its binding preference for high G+C content. Wakelin and Waring⁵⁹ reported an association constant of $15.1 \times 10^5 M^{-1}$ for echinomycin binding to homopolymeric poly dG-poly dC, about three times better than binding to the alternating copolymer, but this result was not found to be reproducible.⁶⁰ This aberrant behavior was ascribed to the lack of structural and stoichiometric homogeneity of the

polymer. In light of the recent discovery that homopolymeric runs of deoxyguanosine DNA can exist as a tetrastranded structure⁶¹, values for the binding affinities between poly dG·poly dC and the quinoxaline antibiotics should be interpreted cautiously. As for other polymers, echinomycin and triostin A bind very poorly to poly dA·poly dT, poly dI·poly dC and to all ribonucleotide polymers.^{59,60} It is clear that triostin A and echinomycin bind most avidly to duplex DNA of irregular base sequence, exemplified by their strong association with *M. lysodeikticus* DNA. This binding suggested to Wakelin and Waring⁵⁹ and to Lee and Waring⁶⁰ that the optimal binding sites for these antibiotics contain all four DNA bases.

Similar equilibrium binding studies also show that the N-methylated amino acids, cyclic peptide backbone and integral cross bridge of triostin A and echinomycin all function together to restrict the conformations of the antibiotic so as to optimize its interaction with DNA. These three structural features appear to be required for antibiotic binding to DNA. For example, if some or all of the peptide N-methyl groups are replaced by hydrogen atoms, the DNA binding affinity of triostin A drops and the sequence binding specificity changes.^{62,63} When either the cross bridge or the lactone linkages of echinomycin are disrupted, the antibiotic no longer binds to DNA.⁶² The fact that these antibiotics contain planar quinoxaline rings suggests that the antibiotics bind via intercalation between DNA base pairs. This is indeed the case because both triostin A and echinomycin remove and eventually reverse the negative supercoils in bacteriophage PM2 DNA.^{56,59,60} The relative helix unwinding angles derived from bouyant density analysis showed that a single echinomycin or triostin A binding event unwinds DNA duplex almost twice as much as does the simple intercalator ethidium bromide. If the corrected unwinding angle of 26° is used for ethidium bromide intercalation⁶⁴, binding of a single quinoxaline antibiotic molecule is estimated to unwind the DNA helix by nearly 50°. Viscometry studies on rod-like DNA fragments also indicate that two intercalation events accompany the binding of a single antibiotic molecule.^{56,59,60} Echinomycin is the first antibiotic observed to bind

DNA by bisintercalation.⁵⁶ The question still remains, however, whether the two intercalation events occur within one or between two DNA duplexes. Macroscopic assays such as bouyant density shifts and viscometry cannot distinguish between these possibilities, but NMR spectroscopy, x-ray crystallography and DNA footprinting methods can be used to differentiate between these two models.

The combined techniques of NMR spectroscopy⁶⁵ and potential energy calculations⁶⁶ suggest very strongly that echinomycin inserts both chromophores within the same DNA duplex upon complexation. Potential energy calculations based on NMR coupling constants of the free antibiotic were used to construct a model where the two quinoxaline rings of echinomycin occupy the same face of the molecule and are parallel to one another. Furthermore, the spacing between the points of ring attachment in this model is approximately 10 Å, very close to the separation required to accommodate a two-base-pair sandwich between the chromophores.⁶⁵ These authors have also suggested that serine and alanine amino groups and alanine carbonyl oxygens might form hydrogen bonds with functional groups in the minor groove of DNA. Minor groove binding appears most likely because echinomycin binds avidly to bacteriophage T2 DNA, whose major groove is encumbered by glycosylated 5-hydroxymethylcytosine residues.⁵⁹ These facts taken together with G+C binding preference of echinomycin implicate the guanine N2 amino group as being vital to the association between antibiotic and DNA. This prediction has been validated by recent footprinting and x-ray crystallographic studies.

Because these methods allow the examination of discrete ligand-binding events on DNA, x-ray crystallography and DNA footprinting techniques have increased the understanding of how echinomycin and triostin A bind to DNA. Footprinting analyses of echinomycin bound to DNA restriction fragments have provided valuable information about both the size and sequence of preferred drug-binding sites. The methidium-propyl-EDTA·Fe(II) (MPE·Fe(II)) footprinting study of Van Dyke and Dervan^{16,19} demonstrated that echinomycin protects four base pairs from MPE·Fe(II) digestion, whereas the DNase I

Table 2. Preferred Echinomycin Binding Sites on DNA Restriction Fragments.

Site (5'-3')	Location	Strength	Reference
ATGT	4317-4314	weak	16
AGGT	4285-4282	weak	16
AGGT	4322-4319	weak	16
CAGT	53-56	weak	16
ACGC	67-70	weak	16
ACGC	4336-4333	weak	16
CCGT	79-82	weak	16
CCGG	410-413	weak	16
TCGG	469-472	medium	16
TCGG	4273-4270	medium	16
TGGT	4301-4298	medium	16
TCGT	4343-4340	strong	16
ACGT	4290-4287	strong	16
GCGG	38-42	strong	16
TCGA	24-27	strong	16
GGCGCG	74-79	weak	14,68
TGCGCC	93-98	weak	14,68
TACGCA	33-38	weak-medium	14,68
CCCGCT	98-103	medium	14,68
AGCGGC	71-76	medium	14,68
CGCGTC	76-81	medium	14,68
TACAGC	68-73	strong	14,68
TCCGTT	14-19	strong	14,68
TACGGA	20-25	strong	14,68
CCCGAT	105-110	strong	14,68
AACGTA	56-61	very strong	14,68

footprinting method ^{14,67} showed echinomycin to protect at least six base pairs of DNA from cleavage by this enzyme. To a first approximation, the regions of protection estimate antibiotic binding site size. The preferred echinomycin binding sites are presented in Table 2. Attempts to footprint triostin A with MPE·Fe(II) were unsuccessful, probably because the reducing agent necessary for MPE·Fe(II)-mediated DNA cleavage, dithiothreitol (DTT), also destroyed the disulfide bridge of triostin A. However, DNase I footprinting of triostin A ⁶⁸ produced footprinting patterns indistinguishable from those obtained with echinomycin.

Assuming that the binding site size derived by MPE·Fe(II) footprinting is correct, sequence analysis of nine strong echinomycin binding sites reveals the consensus sequence for DNA binding:

	5'-	N	N	N	N	-3'
C		2	9			
G		1		8	3	
T		2			4	
A		4		1	2	

In eight of nine cases, the dinucleotide 5'-CG-3' appears in DNA sequences protected by echinomycin from MPE·Fe(II) or DNase I digestion. The exceptional case replaces one purine for another by substituting an adenosine for guanosine. There also exists a preference for A·T base pairs flanking the 5'-CG-3' element. From this analysis, echinomycin prefers to bind the four-base-pair sequence 5'-NCGN-3'. The results obtained by examining a number of individual binding sites agree well with the macroscopic DNA binding properties of echinomycin described earlier, most notably the preference for DNAs with high G+C content and the estimated binding site size derived from equilibrium binding studies (Table 1 and Table 2). Like echinomycin, the 5'-NCGN-3' consensus binding sequence possesses pseudo C-2 symmetry and may in some way

complement the symmetry of the drug. Although footprinting has revealed the consensus sequence for echinomycin binding to DNA, this method cannot describe the specific intermolecular or interatomic contacts which govern this binding. However, x-ray diffraction analysis of quinoxaline antibiotic-DNA cocrystals has provided these details.

In 1984, Wang *et al.*¹⁵ solved the structure of triostin A complexed to the hexamer d(CGTACG)₂. This report provided the first detailed description of the molecular basis for triostin A binding specificity. The structure was refined to 1.67 Å resolution and it was found that two antibiotic molecules bind to the hexamer. A schematic representation of the complex is shown in Figure 6.

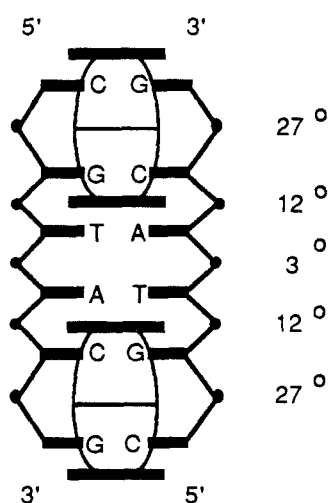


Figure 6. Representation of two triostin A molecules complexed to the d(CGTACG)₂ hexamer¹⁵ with accompanying helix unwinding angles. The peptide backbone of triostin A is schematized as a theta (θ) structure and the planar quinoxaline rings as long bars.

Each triostin A molecule sandwiches the 5'-CG-3' sequence with two quinoxaline rings. In this arrangement, one chromophore of each antibiotic molecule caps the ends of the hexamer, while the second chromophore intercalates between the second and third residues from the 5' end of the oligonucleotide. This does not represent *bona fide* bisintercalation on the part of triostin A because the outer quinoxaline rings extend beyond the helix. Nevertheless, this picture strongly implies that triostin A uses its quinoxaline rings to bracket two base pairs within one DNA duplex as was suggested from calculations

and NMR studies.^{65,66} Figure 7 shows one-half of the (triostin A)₂·d(CG₂TACG)₂ complex viewed from the minor groove of the hexamer duplex.

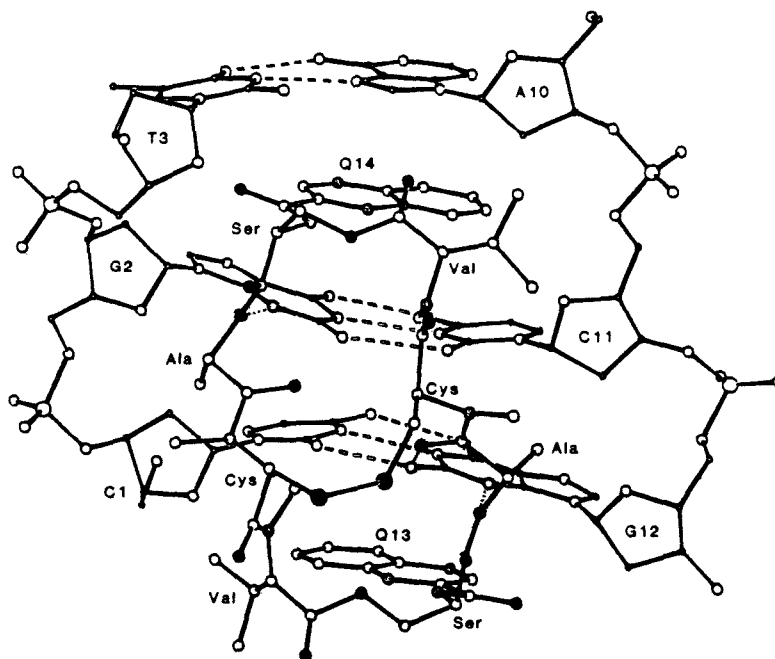


Figure 7. Minor groove perspective of one-half of the (triostin A)₂·d(CG₂TACG)₂ complex structure determined by Wang *et al.*¹⁵

This structure confirms that triostin A binds via the minor groove of B-DNA. The importance of the *D*-configuration for serine residues is clear: This stereochemistry facilitates intercalation by placing the quinoxaline rings parallel to one another, perpendicular to the face of the peptide ring and directed toward the nucleic acid in the complex. In the complex shown in Figure 7, triostin A drives its *L*-alanine methyl groups between the C1-G2 and C11-G12 steps of the hexamer. The *N*-methyl groups of the two *L*-*N*-methylvaline residues are also pushed into the minor groove where they make contact with the O2 atoms of C1 and C11. The wedging of these four methyl groups into the DNA disrupts C1-G2 and C11-G12 base stacking by tilting the guanine bases about 20° from the plane of a normal base pair. Some of the energy lost in this disruption is reclaimed through Van der Waals contacts between the tilted guanine base and the quinoxaline ring.

Another feature of the complex is the nature of the hydrogen bonds formed between antibiotic and nucleic acid. Three hydrogen bonds are observed between each triostin A molecule and the oligonucleotide, occurring between L-alanine amide NH and N3 of G12 (2.91 Å), L-alanine carbonyl oxygen and 2-NH₂ of G12 (3.07 Å) and the second L-alanine amide NH with N-3 of G2 (3.01 Å). These hydrogen bonds are emphasized by shading in Figure 7. The carbonyl oxygen of the second L-alanine residue is too far away (4.1 Å) from the 2-amino group of G2 to form a hydrogen bond. This asymmetric hydrogen-bonding pattern seems unusual when the perfect rotational symmetry of triostin A is considered. Even more surprising than the asymmetric hydrogen-bonding pattern is the nature of the base-pairing within the (triostin A)₂·d(CGTACG)₂ complex. Whereas all four G·C base pairs are held together by the conventional Watson-Crick scheme, the central two A·T base pairs in the complex associate via Hoogsteen base-pairing.⁶⁹ Figure 8 compares Watson-Crick T·A base pairs to Hoogsteen T·A base pairs.

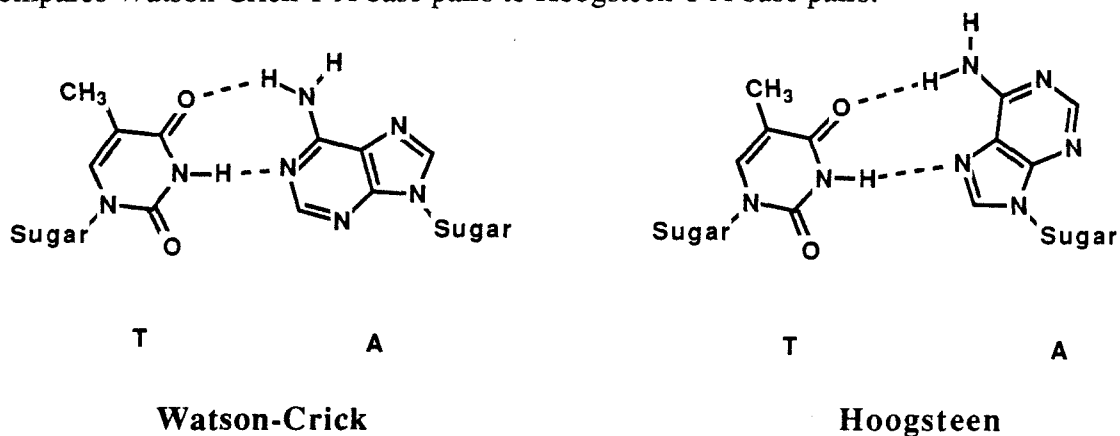


Figure 8. Watson-Crick and Hoogsteen T·A base pairs in right-handed DNA. The minor groove is at bottom.

In the Hoogsteen pairing scheme, the purine base is rotated about its glycosyl bond into the *syn* conformation, and the purine N7 position forms a hydrogen bond with a pyrimidine on the opposite strand. For Watson-Crick pairing, the purine N1 position is used for H-bond formation and the purine is in the *anti* configuration. Hoogsteen base-pairing also reduces the distance between sugar C1' atoms by 2 Å across the minor groove.

In the (trioistin A)₂·d(CGTACG)₂ complex, this contraction draws the sugar-phosphate backbone inward to make Van der Waals contacts with serine α and β carbon atoms and the carbonyl function of L-N-methyl valine residues on the antibiotic. The Hoogsteen arrangement also places the benzenoid portion of quinoxaline Q14 directly below the pyrimidine ring of A10 in the complex (Figure 7 top). Singh *et al.*⁷⁰ have compared the energies of the (trioistin A)₂·d(CGTACG)₂ complex containing either Watson-Crick (WC) or Hoogsteen (HG) A·T base pairs. Their molecular mechanics calculations show that in the absence of bound drug, the WC form is favored by about 8 kcal/mole over the HG form. This large difference was attributed to unfavorable sugar-phosphate and phosphate-base interactions that result from the narrow minor groove in a Hoogsteen base pair. When drug-DNA complexes were considered, the WC model was still favored, but by only 2.5 kcal/mole. The two major factors that reduce the energy gap between WC and HG models for the trioistin A·DNA complex are DNA base-quinoxaline stacking interactions and the Van der Waals contacts formed between the sugar-phosphate backbone of DNA and L-N-methylvaline side chains. These authors note that "...a stereochemically acceptable complex of trioistin A with d(CGTACG)₂ made up only of WC base pairs can be built and is of comparable energy to the structure with T·A HG base pairs."⁷⁰

So far, only the structure of a trioistin A·DNA oligonucleotide complex has been discussed, and this raises the issue of whether the contacts found for trioistin A apply to the related echinomycin. Ughetto *et al.*⁷¹ addressed this problem by comparing the structures of (echinomycin)₂·d(CGTACG)₂ and (trioistin A)₂·d(CGTACG)₂ complexes. The (echinomycin)₂·d(CGTACG)₂ complex was solved at 1.8 Å resolution and the (trioistin A)₂·d(CGTACG)₂ at 1.67 Å resolution. When compared, the structures of these two antibiotic·nucleic acid complexes were remarkably similar. The chief differences between the two complex structures is that the shorter cross bridge of echinomycin leads to tighter packing and thus more Van der Waals contacts between DNA and the amino acid residues of echinomycin. Each echinomycin molecule forms three hydrogen bonds to DNA with the

atoms corresponding to those used by triostin A. Furthermore, the lengths of the hydrogen bonds between antibiotic and nucleic acid are similar in both complexes. The nucleic acid in the echinomycin-hexamer complex also contains the same mixture of Watson-Crick and Hoogsteen base pairs observed for the triostin A-hexamer complex. Therefore, it appears that the different cross bridges of echinomycin and triostin A do not lead to major changes in the precise binding interactions between the antibiotic and the oligonucleotide d(CGTACG)₂. This can probably be extended to other sequences because triostin A and echinomycin produced virtually identical DNase I protection patterns.^{14,68}

More recent work by the Rich group^{72,73} at MIT has characterized the structure of triostin A complexed to the octamer d(GCGTACGC)₂. As for the hexamer above, two triostin A molecules bind to this duplex by sandwiching the 5'-CG-3' dinucleotides between two quinoxaline rings. Figure 9 shows a stereodiagram of the (triostrin A)₂·d(GCGTACGC)₂ complex. This complex is an example of genuine bisintercalation by the antibiotic because all quinoxaline rings are surrounded by DNA base pairs, unlike the (triostrin A)₂·d(CGTACG)₂ structure where one quinoxaline ring from each antibiotic protruded over the ends of the DNA duplex.

Binding contacts between triostin A and the octamer were very similar to the contacts observed for the triostin A-hexamer complex with one major exception (compare Figures 7 and 9). The (triostrin A)₂·d(GCGTACGC)₂ crystal was formed at pH 4.5. Under these conditions, the outermost G·C base pairs of the complex were found to assume the Hoogsteen geometry. Hoogsteen C·G base pair formation requires that the N3 of cytosine be protonated in order to donate a hydrogen bond to the N7 atom of the opposing guanosine residue. The central two A·T base pairs in the (triostrin A)₂·d(GCGTACGC)₂ complex are also Hoogsteen-paired so that the complex contains four Watson-Crick and four Hoogsteen base pairs. This amazing rearrangement of DNA structure appears to be caused solely by triostin A binding. These findings naturally raise

the issue as to whether such novel base-pairing schemes exist in solution at triostin A or echinomycin binding sites within a large DNA duplex.

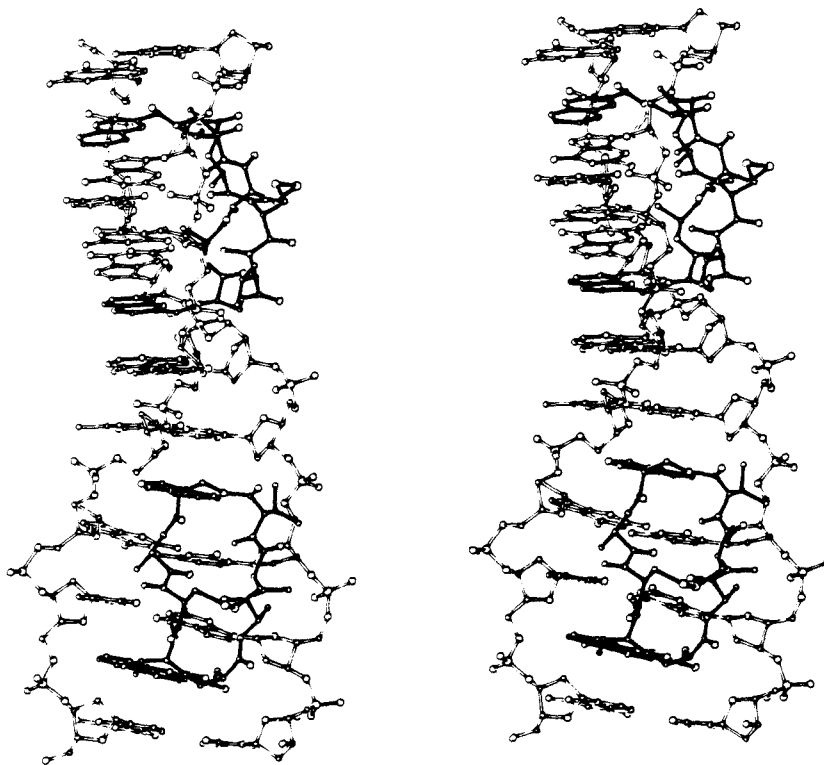


Figure 9. Stereodiagram of the $(\text{triostin A})_2 \cdot \text{d}(\text{GCGTACGC})_2$ cocrystal structure determined by Quigley *et al.*⁷² Triostin A is drawn with solid bonds, the DNA with open bonds.

Recent NMR work on small oligonucleotide·echinomycin complexes demonstrates that Hoogsteen base pairing probably exists in solution. Gao and Patel⁷⁴ have used ^{31}P NMR and ^1H NMR to study the binding of echinomycin to the two tetramers $\text{d}(\text{TCGA})_2$ and $\text{d}(\text{ACGT})_2$. Their findings indicate that the antibiotic-nucleic acid contacts established in the solid-state structure for echinomycin complexed to $\text{d}(\text{CGTACG})_2$ apply to the echinomycin· $\text{d}(\text{TCGA})_2$ and echinomycin· $\text{d}(\text{ACGT})_2$ complexes in solution. These authors completely assigned the nucleic acid and peptide antibiotic protons in both

complexes and then used nuclear Overhauser effects (NOEs) to gauge the distances between nucleic acid and antibiotic protons. Because the H1' and H4' protons of the sugars reside in the minor groove of right-handed B-DNA, the moderate-to-strong NOEs observed between cytidine and guanosine H1' and H4' protons and the L-alanine methyl groups of echinomycin confirmed that the antibiotic binds in the minor groove of d(TCGA)₂ and d(ACGT)₂. Bisintercalation of echinomycin around the C-G dinucleotide unit was suggested by the downfield shift in two of the three phosphate resonances for each complex. Further, the imino proton resonances of the outer base pairs in d(ACGT)₂ and d(TCGA)₂ shifted upfield when echinomycin bound to each tetramer. This upfield shift is characteristic for base pairs adjacent to the site of intercalation and has been observed for actinomycin D-DNA complexes.^{75,76} L-alanine amide protons resonate ~2.7 ppm upfield in free echinomycin compared to their resonance in the echinomycin-d(ACGT)₂ and echinomycin-d(TCGA)₂ complexes. This was interpreted as strong evidence for the formation of intermolecular hydrogen bonds between the L-alanine amide NH and the N3 of guanosine that was observed in the crystal. The third hydrogen bond observed in the crystal between G12 NH₂ and the L-alanine carbonyl oxygen of echinomycin was not described in the NMR study. Numerous NOEs were observed between the nucleic acid and the antibiotic in echinomycin-d(TCGA)₂ and echinomycin-d(ACGT)₂ complexes. Analysis of these NOEs and the aforementioned changes in chemical shift upon complexation lead Gao and Patel⁷⁴ to conclude that antibiotic-DNA contacts within echinomycin-d(TCGA)₂ and echinomycin-d(ACGT)₂ complexes in solution are similar to those in the solid state (echinomycin)₂-d(CGTAACG)₂ complex. Another key issue addressed in this NMR study was the nature of the DNA base pairs surrounding the intercalation site. NOEs were used to establish the existence of either Watson-Crick or Hoogsteen base-pairing in the complex. The strong NOE observed between guanosine imino (N1) and cytidine amino (N4) protons in the echinomycin-d(ACGT)₂ and echinomycin-d(TCGA)₂ complexes implies that the G-C

pairs in both complexes assume the normal Watson-Crick geometry. To determine the A·T pairing scheme, the NOEs between adenosine H8 and H1' protons were examined. Figure 10 shows that the H1' to H8 interproton distance for adenosine in the *syn* conformation is about 1.2 Å shorter than for the *anti* conformation.

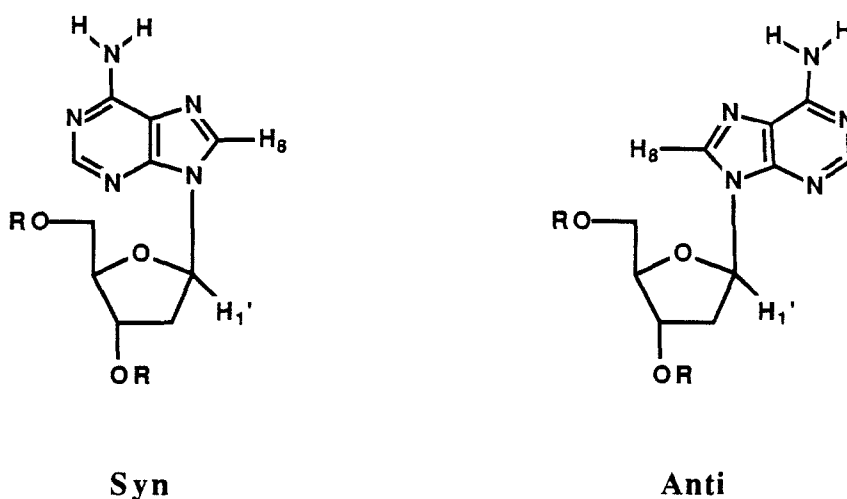


Figure 10. Comparison of the H1' to H8 distances for *syn* (~2.5Å) versus *anti* (~3.7Å) adenosine.

The strong NOE observed between cytidine H5 and H6 protons was used as an internal standard because the approximate 2.5 Å distance between these protons is independent of the base glycosidic torsion angle. At 22° C in D₂O buffer, a strong NOE was observed between the adenosine H8 and H1' protons in the echinomycin-d(ACGT)₂ complex, whereas only a weak NOE was seen between the corresponding protons in the echinomycin-d(TCGA)₂ complex. These results imply that adenosine residues in the former complex assume the *syn* conformation, consistent with Hoogsteen base-pairing, while those in the latter complex assume the *anti* conformation and form Watson-Crick base pairs. If this is the case, it is of interest to understand why one complex forms Hoogsteen base pairs while the other one does not.

A possible explanation for the different structures of the A·T base pairs in the echinomycin·d(ACGT)₂ and echinomycin·d(TCGA)₂ complexes involves the stacking interactions between DNA bases and the antibiotic quinoxaline rings. The solution- and solid-state structures of echinomycin·DNA complexes reveal significant overlap between the pyrimidine ring of purines and the benzenoid portion of the quinoxaline intercalators when the base pairs adjacent the intercalation site are in the Hoogsteen geometry.^{15,71-74} This overlap would be lost if Watson-Crick pairing were to exist at these positions. However, when the purines that stack onto the quinoxaline rings are replaced by pyrimidine residues as in d(ACGT)₂ ----> d(TCGA)₂, quinoxaline-purine overlap may be lost. This would then diminish the amount of π -stacking available to stabilize non-Watson-Crick base pairs. If this is a strong interaction, it appears that the sequence surrounding the C-G dinucleotide of an echinomycin/triostin A binding site determines whether Watson-Crick or Hoogsteen base pairs will be formed when the antibiotic binds to DNA. It is notable that in all triostin A·DNA and echinomycin·DNA complexes containing Hoogsteen base pairs, the DNA within these complexes was made up of a perfectly alternating purine/pyrimidine sequence. Where the purine/pyrimidine alternation was not followed, such as echinomycin complexed to d(TCGA)₂, normal Watson-Crick pairing was found outside the sandwiched C-G dinucleotide. This extends to echinomycin·d(GCGC)₂ and echinomycin·d(CCGG)₂ complexes where the former complex apparently contains two outer Hoogsteen G·C base pairs and the latter is entirely Watson-Crick paired.⁷⁷ Thus, alternating purine/pyrimidine sequences appear to be a prerequisite to Hoogsteen base pair formation at echinomycin and triostin A binding sites on small DNA duplexes. The left-handed Z-form of DNA also prefers alternating purine/pyrimidine sequences and though its base pairs are of the Watson-Crick type, all purines in this structure adopt the *syn* conformation.²⁴ Taken together with the apparent sequence preference for Hoogsteen base pair formation at quinoxaline antibiotic binding sites, this observation implies that an alternating purine/pyrimidine sequence may help purines to assume the *syn* conformation.

The two methods of NMR spectroscopy and x-ray crystallography provide a detailed description of the molecular basis for echinomycin- and triostin A-DNA binding specificity. The precision and thoroughness of these studies provide clear evidence for non-Watson-Crick base pair formation at quinoxaline antibiotic binding sites. In the oligonucleotide-quinoxaline antibiotic complexes characterized to date, Hoogsteen base pairs occur either at the terminal residues of a short DNA duplex or a few base pairs away from the ends of a duplex that has been significantly unwound by intercalated antibiotic molecules. These findings raise the issue as to whether similar novel base-pairing rearrangements will occur when the antibiotic binding sites are buried within a large DNA fragment. Whether these novel structures arise because of DNA end-effects needs to be ascertained. Because end base pairs are constrained by the DNA sugar-phosphate backbone on only one side, they have more degrees of rotational freedom than would a base pair in the middle of a large DNA fragment. Further, the thermal "fraying" of DNA duplex ends at room or body temperature is likely to impart some increased base pair flexibility near the end of a DNA helix compared to the normal "breathing" of base pairs buried within a large DNA duplex. Lesser structural rigidity at or near the ends of a DNA duplex may thus make alternative base-pairing schemes more accessible. It is the purpose of this thesis to determine whether echinomycin binding induces isolated Hoogsteen base pairs to form inside a relatively large DNA duplex and, if so, whether this represents a valid structural motif on which to build synthetic antibiotic/antitumor agents that recognize G·C base pairs.

Examination of the differences between Watson-Crick and Hoogsteen base pairs is necessary to suggest an experimental approach to this problem. Figure 11 compares Watson-Crick C·G and T·A base pairs in Z- and B-DNA to Hoogsteen base pairs in right-handed DNA. In Watson-Crick pairs, guanosine O6, N1(H), 2-NH₂ and adenosine N1, 6-NH₂ positions hydrogen bond with cytosine 4-NH₂, N3, O2 and thymine O4, N3(H), respectively. To switch from Watson-Crick-paired B-DNA to right-handed, Hoogsteen-paired DNA, the purine base rotates from *anti* to *syn* and forms new hydrogen-bonding

arrangements where purine N7 and N1 atoms are transposed. This should be a relatively facile change for T·A pairs because no net hydrogen bonds are lost in the transition. C·G pairs should form the Hoogsteen geometry less readily because such a transition requires protonation of cytosine N3 and results in the loss of one hydrogen bond. A Watson-Crick to Hoogsteen base-pairing transition in right-handed DNA moves guanosine N1, 2-NH₂ and adenosine N1 atoms to the major groove and relieves them of their H-bonding duties. It is well documented that the N1 is the most nucleophilic position of adenosine and is only about three times less nucleophilic than guanosine N7 toward dimethyl sulfate.⁷⁸ In the B-DNA duplex, adenosine N1 is unavailable for reaction because it resides in the center of the helix and is masked by a hydrogen bond to thymine N4(H). The availability of adenine N1 changes dramatically upon the formation of a Hoogsteen base pair in right-handed DNA and it is possible, in principle, that chemical probes will react with this center when it is exposed. If this is the case, then one should be able to map Hoogsteen base pairs within a DNA restriction fragment by cleaving the DNA at the positions of base modification via Maxam-Gilbert chemical sequencing methods.⁷⁹

Chemical versus enzymatic footprinting.

We used a combination of footprinting methods to characterize echinomycin-DNA binding interactions. Two major types of footprinting exist: enzymatic and chemical. Enzymatic footprinting techniques employ a relatively sequence-neutral DNA cleaving agent such as DNase I⁶⁷ or MPE·Fe(II)^{16,19} to digest DNA. In the absence of DNA-binding ligands, these reagents cleave DNA in a random fashion and produce an even "ladder" when the cleavage products are visualized on a high-resolution Maxam-Gilbert sequencing gel.⁷⁹ If DNA digestion by these reagents is performed in the presence of DNA-binding ligands, however, strong DNA-binding molecules directly block DNase I or MPE·Fe(II) from binding and cleaving DNA. A gap or "footprint" in the ladder of DNA cleavage products is then observed when compared to the cleavage product ladder

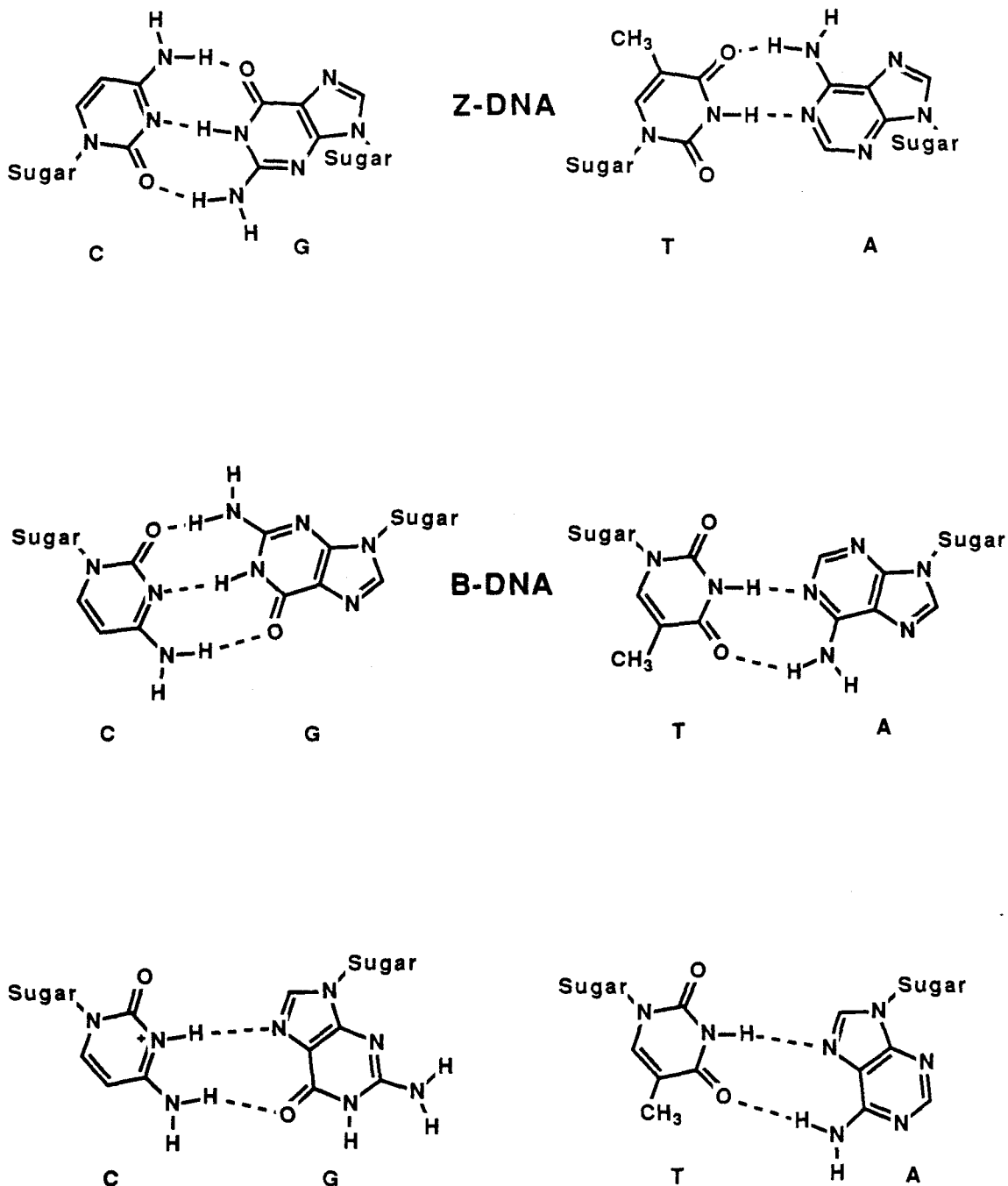


Figure 11. Comparison of the C·G and T·A base pairs in left-handed Z-DNA (top), right-handed B-DNA (middle) and Hoogsteen base-paired, right-handed DNA (bottom). Z-DNA and B-DNA are made up of Watson-Crick base pairs with purines *syn* for Z-DNA and *anti* for B-DNA. Hoogsteen base-paired, right-handed DNA has purines in the *syn* conformation. For B-DNA and Hoogsteen-paired DNA, the minor groove is shown at the top of each base pair.

obtained with unbound DNA. The sequence binding preference and binding site size of a given ligand on DNA can then be assigned by reading the sequences where gaps appear in the cleavage pattern. Chemical footprinting is similar to but distinct from enzymatic footprinting. Unlike DNase I or MPE·Fe(II), chemical probes are sequence-selective because they preferentially modify certain nucleobase atoms. An exception to this generalization is ethyl methane sulfonate (EMS), a reagent that modifies phosphate residues with little sequence preference. Though it can be used to map preferred DNA ligand-binding sites in a manner similar to enzymatic footprinting, chemical footprinting is more frequently used as a probe of nucleic acid structure. When the atom centers modified by a particular reagent are known, the relative efficiencies of modification describe the accessibility of a nucleobase atom under different conditions. Such knowledge can then be used to infer gross DNA structure at any given sequence. Chemical footprinting is much more sensitive than enzymatic footprinting because chemical footprinting agents act by simple bimolecular reactions with DNA bases. Consequently, no binding occurs between DNA and chemical probe. Therefore, a chemical probe is unlikely to displace a weakly bound ligand, whereas DNase I or MPE·Fe(II) might do so because these reagents must bind to DNA before cleaving.

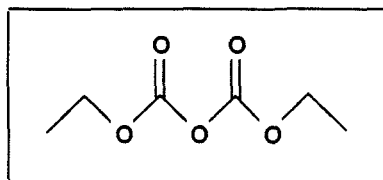
Below we compare enzymatic and chemical footprinting of small molecule binding to DNA.

RESULTS

Diethyl pyrocarbonate reacts with purines at echinomycin binding sites.

Diethyl pyrocarbonate (DEP) is a useful probe of nucleic acid structure. DEP reacts preferentially with adenosine and guanosine residues and has been used to characterize RNA secondary structure⁸⁰⁻⁸², Z-DNA⁸³⁻⁸⁵, H-DNA²⁷ and DNA cruciform loops.^{86,87} Because B-DNA is relatively unreactive to DEP, we tested the ability of DEP to detect Hoogsteen base-pairing on DNA in the presence of echinomycin and triostin A. Indeed,

purines at echinomycin and triostin A binding sites become hyperreactive to DEP upon drug binding.⁸⁸



DEP

Figure 12. Structure of diethyl pyrocarbonate (DEP).

The patterns of MPE·Fe(II)- and DEP/piperidine-mediated cleavage of a ³²P end-labeled 628 base pair (bp) *Eco* RI-*Bgl* I restriction fragment from plasmid pDMG10 are presented in Figure 13. pDMG10 was constructed by inserting a synthetic 33 base pair oligonucleotide duplex into the 4.0 kilobase (kb) *Hind* III-*Bam* HI fragment of pBR322 (see experimental section). In the absence of echinomycin, MPE·Fe(II) produced an even cleavage pattern (lanes 2 and 17) and DEP reacted only slightly with the DNA (lanes 7 and 22). Both cleavage patterns changed markedly upon addition of echinomycin to the system. Echinomycin at 12.5 to 50 micromolar concentrations protected several regions on the fragment from MPE·Fe(II) cleavage (lanes 3-6 and 18-21) and caused DEP to react very strongly with several purines (lanes 8-11 and 23-26). Figure 14 presents a densitometric analysis of the MPE·Fe(II) protection and DEP reaction patterns from the gel of Figure 13. Based on diminution of MPE·Fe(II) cleavage intensity, echinomycin protects the sequences (5'-3') TCGA, GGGGGGGGGG, TCGA, TCCT, ACGCCGGACGC, TCGT, CCGG, TCACCGG, GCCA, AGGT and GCGG on 100 of the 628 base pairs (bp) of this fragment. Close inspection of the DEP cleavage patterns in the presence of echinomycin revealed that DEP reacted more strongly with adenosine residues than with guanosine residues and that the reactivity, in decreasing order, occurred at purines straddling the dinucleotides (5'-3') CG > CC~GG > CA. Comparison of Figure 14 entries A-D with entries E-H shows a nearly one-to-one correspondence between purines reactive to DEP in

Figure 13. MPE·Fe(II) and DEP/piperidine footprinting of echinomycin on a large DNA restriction fragment. Autoradiogram of 5' (lanes 1-13) and 3' (lanes 14-26) ³²P end-labeled 628 bp *Eco* RI-*Bgl* I restriction fragment from plasmid pDMG10. Lanes: 1 and 16, intact DNA; 2 and 17, MPE·Fe(II) cleavage of DNA in the absence (-) of echinomycin; 3-6 and 18-21, MPE·Fe(II) cleavage of DNA in the presence (+) of echinomycin at 12.5, 25, 50 and 100 μM, respectively; 7 and 22, DEP/piperidine cleavage of DNA in the absence (-) of echinomycin; 8-11 and 23-26, DEP/piperidine cleavage of DNA in the presence (+) of echinomycin at 12.5, 25, 50 and 100 μM, respectively; 12 and 14, Maxam-Gilbert ⁷⁹ chemical sequencing G-specific reaction; 13 and 15, Maxam-Gilbert chemical sequencing purine-specific reaction. The gel was scanned from the bottom to the arrow (at left). Brackets denote the 5' (T-A)₆ segment hyperreactive to DEP. Reaction conditions were 10 mM Tris·HCl pH 7.4, 50 mM NaCl, 400 μM DNA base pairs (bp) and 10%(v/v) methanol.

MPE/E DEP/E G G+A MPE/E DEP/E
- + + + + + + + + G G+A - + + + + - + + + +
1 2 3 4 5 6 7 8 9 10 11 12 13 14 15 16 17 18 19 20 21 22 23 24 25 26

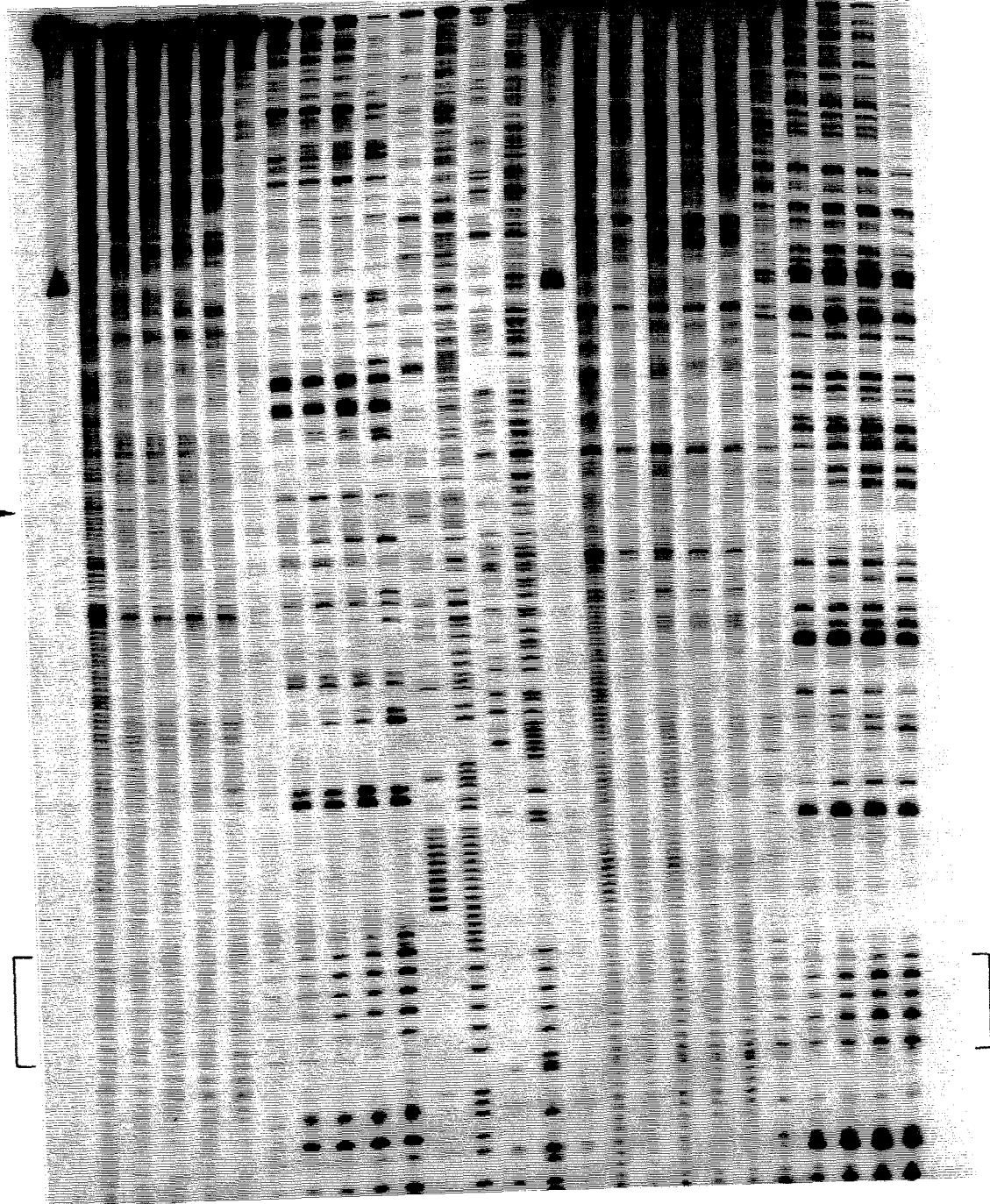


Figure 14. Densitometric analysis of MPE·Fe(II) and DEP/piperidine footprinting of echinomycin. (A-D) MPE·Fe(II) cleavage inhibition patterns of DNA in the presence of echinomycin at 12.5, 25, 50 and 100 μ M, respectively, bound to 100 bp of the 628 bp restriction fragment, as determined by densitometry from the autoradiogram in Figure 13. (E-H) DEP/piperidine cleavage patterns on DNA in the presence of 12.5, 25, 50 and 100 μ M echinomycin, respectively, bound to the same 100 bp of DNA, as determined by densitometry of the autoradiogram in Figure 13. MPE·Fe(II) cleavage inhibition patterns (A-D) are shown as histograms or bars with the height proportional to the reduction of cleavage at each nucleotide compared with MPE·Fe(II) cleavage of unprotected DNA. DEP/piperidine cleavage patterns (E-H) are shown as arrows, with the height proportional to the enhancement of cleavage at each nucleotide compared to DEP/piperidine cleavage of unbound DNA. The scale at the bottom corresponds to the first 5' thymidine in the *Eco* RI site of plasmid pDMG10 defined as position 1. Boxes are the assigned echinomycin binding sites based on the model in References 4 and 16.

A 5'-ATCGATAAGCTTATATATATATAAAAAAGGGGGGGGGTTCGATAGGATCCTCTACGCCGGACCGCATCGTGC CCGGCATCACCGGC GCCACAGGTGCGGTTG
3'-TAGCTATTGGAATATATATATATATTTTTTCCCCCCCCCAGCTATCCTAGGAGATGCGGCCTGCGTAGCACCGGCC TAGTGGCCGCGGTGTCCACGCCAAC

B 5'-ATCGATAAGCTTATATATATATAAAAAAGGGGGGGGGTTCGATAGGATCCTCTACGCCGGACCGCATCGTGC CCGGCATCACCGGC GCCACAGGTGCGGTTG
3'-TAGCTATTGGAATATATATATATATTTTTTCCCCCCCCCAGCTATCCTAGGAGATGCGGCCTGCGTAGCACCGGCC TAGTGGCCGCGGTGTCCACGCCAAC

C 5'-ATCGATAAGCTTATATATATATAAAAAAGGGGGGGGGTTCGATAGGATCCTCTACGCCGGACCGCATCGTGC CCGGCATCACCGGC GCCACAGGTGCGGTTG
3'-TAGCTATTGGAATATATATATATATTTTTTCCCCCCCCCAGCTATCCTAGGAGATGCGGCCTGCGTAGCACCGGCC TAGTGGCCGCGGTGTCCACGCCAAC

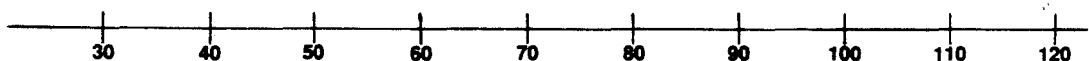
D 5'-ATCGATAAGCTTATATATATATAAAAAAGGGGGGGGGTTCGATAGGATCCTCTACGCCGGACCGCATCGTGC CCGGCATCACCGGC GCCACAGGTGCGGTTG
3'-TAGCTATTGGAATATATATATATATTTTTTCCCCCCCCCAGCTATCCTAGGAGATGCGGCCTGCGTAGCACCGGCC TAGTGGCCGCGGTGTCCACGCCAAC

E 5'-ATCGATAAGCTTATATATATATAAAAAAGGGGGGGGGTTCGATAGGATCCTCTACGCCGGACCGCATCGTGC CCGGCATCACCGGC GCCACAGGTGCGGTTG
3'-TAGCTATTGGAATATATATATATATTTTTTCCCCCCCCCAGCTATCCTAGGAGATGCGGCCTGCGTAGCACCGGCC TAGTGGCCGCGGTGTCCACGCCAAC

F 5'-ATCGATAAGCTTATATATATATAAAAAAGGGGGGGGGTTCGATAGGATCCTCTACGCCGGACCGCATCGTGC CCGGCATCACCGGC GCCACAGGTGCGGTTG
3'-TAGCTATTGGAATATATATATATATTTTTTCCCCCCCCCAGCTATCCTAGGAGATGCGGCCTGCGTAGCACCGGCC TAGTGGCCGCGGTGTCCACGCCAAC

G 5'-ATCGATAAGCTTATATATATATAAAAAAGGGGGGGGGTTCGATAGGATCCTCTACGCCGGACCGCATCGTGC CCGGCATCACCGGC GCCACAGGTGCGGTTG
3'-TAGCTATTGGAATATATATATATATTTTTTCCCCCCCCCAGCTATCCTAGGAGATGCGGCCTGCGTAGCACCGGCC TAGTGGCCGCGGTGTCCACGCCAAC

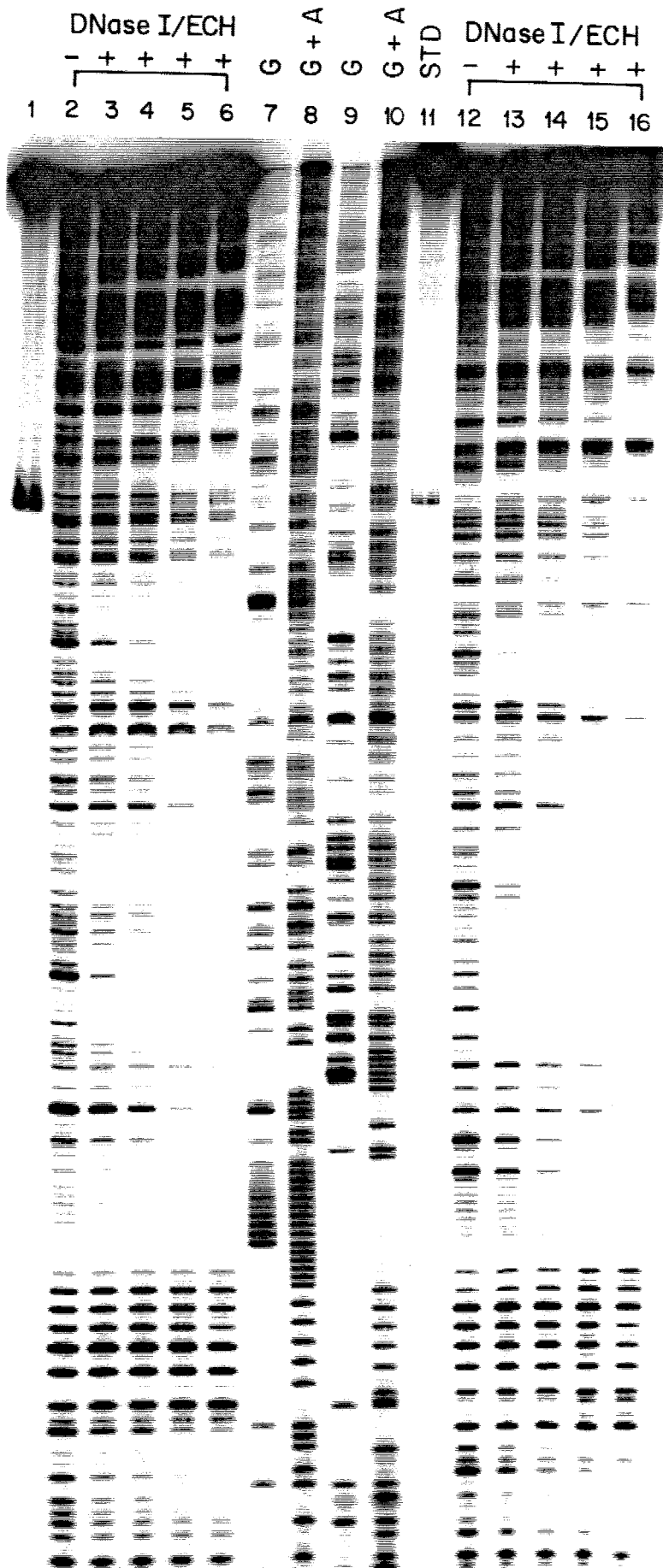
H 5'-ATCGATAAGCTTATATATATATAAAAAAGGGGGGGGGTTCGATAGGATCCTCTACGCCGGACCGCATCGTGC CCGGCATCACCGGC GCCACAGGTGCGGTTG
3'-TAGCTATTGGAATATATATATATATTTTTTCCCCCCCCCAGCTATCCTAGGAGATGCGGCCTGCGTAGCACCGGCC TAGTGGCCGCGGTGTCCACGCCAAC



the presence of echinomycin and the regions of DNA protected by echinomycin from MPE·Fe(II) cleavage. Specifically, MPE·Fe(II) footprinting yielded a minimum binding site size of four base pairs for echinomycin. Importantly, purines (A>G) that correspond to the first and/or fourth positions of these sites reacted with DEP only in the presence of drug. Because these sites were not reactive to DEP in the absence of echinomycin, it appeared that DEP responded to some type of local DNA structural modification. It is noteworthy that the DEP reactive purines occupied the first and/or fourth base-pair positions of echinomycin binding sites, those found to be Hoogsteen base-paired in the triostin A·DNA and echinomycin·DNA cocrystal structures.

A major exception to the correlation between MPE·Fe(II) cleavage inhibition and DEP hyperreactivity is the d(T-A)₆ segment beginning at position 34. Adenosine residues within this segment became increasingly reactive to DEP as the concentration of echinomycin was raised (Figure 13). The adenosine-DEP reactivity pattern in this region is pseudo-C₂ symmetric and is shifted to the 3' side (Figure 14 E-H), but there was no apparent protection of this region from MPE·Fe(II) cleavage, even at the highest concentration of echinomycin tested (Figure 14 D). Echinomycin also failed to protect the d(T-A)₆ segment from digestion by the enzyme deoxyribonuclease I (DNase I). Figure 15 shows the autoradiogram of the 628 bp pDMG10 fragment subjected to DNase I cleavage in the presence of various amounts of echinomycin. DNase I cleaved unprotected DNA in a less sequence neutral fashion than MPE·Fe(II) (lanes 2 and 12). At high echinomycin concentrations (lanes 6 and 16) the drug protected large spans of the DNA from cleavage by DNase I, but the d(T-A)₆ segment at the bottom quarter of the gel was still cleaved efficiently by DNase I. Therefore, the d(T-A)₆ segment that became reactive to DEP at high echinomycin concentrations did not appear to constitute an echinomycin binding site and yet it was at least 6 bp away from a strong (5'-TCGA-3') echinomycin binding site. The nature of the DEP hyperreactivity of this *distal* segment will be addressed in Chapter 2.

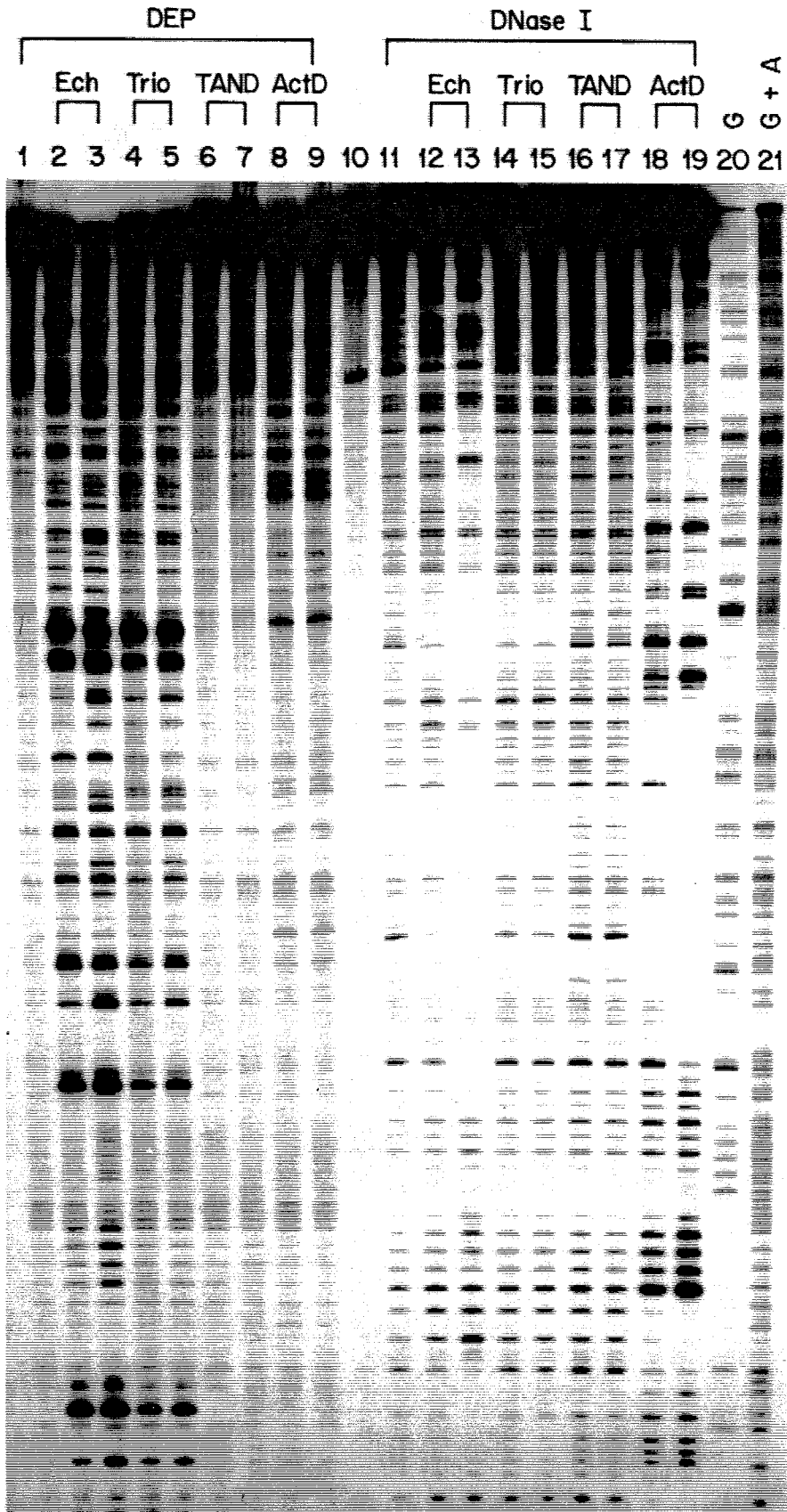
Figure 15. DNase I footprinting of echinomycin. Autoradiogram of 5' (lanes 1-8) and 3' (lanes 9-16) ^{32}P end-labeled 628 bp *Eco* RI-*Bgl* I restriction fragment from pDMG10. Lanes: 1 and 11, intact DNA; 2 and 12, DNase I cleavage of unprotected DNA; 3-6 and 13-16, DNase I cleavage of DNA in the presence of 6.25, 12.5, 25 or 50 μM echinomycin, respectively, bound to the DNA restriction fragment; 7 and 9, Maxam-Gilbert chemical sequencing G-specific reactions; 8 and 10, Maxam-Gilbert chemical sequencing purine-specific reactions. Reaction conditions were 10 mM Tris·HCl pH 7.9, 10 mM KCl, 10 mM MgCl_2 , 5 mM CaCl_2 , 10% (v/v) methanol and 200 μM DNA base pairs. DNA was digested for 2 minutes at room temperature with 1.32 ng of DNase I.



DEP-purine reaction in the presence of other intercalators.

As described above, the majority of purines that react with DEP in the presence of echinomycin occur within the echinomycin binding sites determined by MPE·Fe(II) footprinting. Other known intercalating agents were tested for the ability to promote DNA-DEP hyperreactivity. Figure 16 compares the DNA-DEP reactivity and DNase I cleavage inhibition patterns of echinomycin, triostin A, TANDEM (des-N-methyl triostin A) and actinomycin D on a 628 bp restriction fragment from plasmid pDMAG10. As seen before, DEP reacted weakly with DNA in the absence of bound drugs (Figure 16, lane 1) but moderate amounts of echinomycin dramatically enhanced DNA-DEP reaction (Figure 16, lanes 2 and 3). At slightly higher concentrations, triostin A produced a DNA-DEP reactivity pattern virtually identical to that observed for echinomycin but with less intensity (lanes 4 and 5). High concentrations of TANDEM failed to produce any DEP reaction over background (lanes 6-7), and high actinomycin D concentrations produced DNA-DEP reactivity marginally above background levels (lanes 8-9). Echinomycin (lanes 12-13) and actinomycin D (lanes 18-19) each protected large regions of the DNA from DNase I cleavage, whereas triostin A (lanes 14-15) and TANDEM (lanes 16-17) did not significantly protect the DNA (compare to DNase I control cleavage, lane 11). TANDEM is known to bind DNA more weakly than either triostin A or echinomycin, and it is possible that the concentrations used in Figure 16 were too low to permit DNase I detection of bound TANDEM. Another possibility is that our TANDEM sample decomposed over the ca. six-year storage period because Portugal *et al.*⁸⁹ found specific and significant enhancement of DEP reactivity on another DNA restriction fragment at high TANDEM binding densities. The inability of DNase I to detect triostin A binding to our restriction fragment was somewhat puzzling in that it was not due to the presence of DTT in the buffer (see Figure 16 legend), but it is clear that the DNA-DEP hyperreactivity patterns were almost identical for both echinomycin and triostin A. Although strong actinomycin D binding can be detected on this fragment, the drug did not appear to enhance DNA-DEP

Figure 16. Comparison of DNase I and DEP/piperidine footprinting of several intercalators. Autoradiogram of 5' ³²P end-labeled 628 bp *Eco* RI-*Bgl* I restriction fragment from plasmid pDMAG10. Lanes 1-9 are DEP/piperidine cleavage of DNA in the presence of : lane 1, no drug; lanes 2-3, 12.5-50 μ M echinomycin; lanes 4-5, 16-64 μ M triostin A; lanes 6-7, 400-800 μ M TANDEM and lanes 8-9, 50-200 μ M actinomycin D. Lane 10 is intact DNA. Lanes 11-19 are DNase I digestion patterns of the restriction fragment in the presence of: lane 11, no drug; lanes 12-13, 12.5-50 μ M echinomycin; lanes 14-15, 16-64 μ M triostin A; lanes 16-17, 400-800 μ M TANDEM and lanes 18-19, 50-200 μ M actinomycin D. Lanes 20 and 21 are the Maxam-Gilbert chemical sequencing G- and purine-specific reactions, respectively. Reaction conditions for both DEP and DNase I cleavage reactions were 10 mM Tris·HCl pH 7.9, 10 mM KCl, 10 mM MgCl₂, 5 mM CaCl₂, 10% (v/v) methanol and 200 μ M DNA base pairs. DNase I reactions also contained 100 μ M DTT, but identical results were obtained when the DTT was omitted.



reaction to a significant extent. Thus, it appears that DNA-DEP reactivity may not be due to helix unwinding caused by drug intercalation. To further investigate this hypothesis, the simple intercalator ethidium bromide was tested for its ability to promote DNA-DEP hyperreactivity.

Ethidium bromide is a small mono-intercalating agent that binds DNA with low sequence preference and unwinds the helix by about 26° at each point of intercalation.⁶⁴ Figure 17 presents the results of DNA-DEP reaction in the presence of various amounts of ethidium bromide (EB) and/or echinomycin (ECH). Lanes 1 and 16 indicate that 1000 μM EB did not nick the DNA during handling and lanes 6 and 21 show that DEP did not react with DNA in the absence of intercalating agents. There was a proportional increase in the level of DNA-DEP reactivity as the ethidium bromide concentration was increased from 10 μM to 1000 μM (lanes 2-5 and 17-20). Reaction occurred at purines (A>G) and there was little variation in band intensity throughout the DEP reaction containing 1000 μM EB (lanes 5 and 20). The DEP reaction executed in the presence of 50 μM echinomycin (lanes 7 and 22) yielded a reaction pattern similar to those presented in Figures 13 and 16. Purines (A>G) reacted with DEP in the presence of echinomycin and a wide range of different band intensities could be seen (Figure 17, compare lane 5 with lane 7 and 20 with 22). The addition of 10-1000 μM ethidium bromide to the reactions containing 50 μM echinomycin changed the DEP-DNA reactivity pattern slightly. These results are displayed as histograms in Figure 18. Most of the nucleotides that reacted with DEP in the presence of 50 μM echinomycin grew even more reactive to DEP when 10-1000 μM ethidium bromide was included with the echinomycin (Figure 17, lanes 8-11 and 23-26 and Figure 18 D). However, some nucleotides actually became *less* reactive to DEP under the same circumstances. These occurred near the 3' ends of the d(T-A)₆ segment and at the assigned echinomycin binding sites (5'-3') ACGC, CCGG, TCGT, TCAC and GCCA (Figure 18 D). It is important to note that except for TCGT, these sequences constitute weak-to-medium-strength echinomycin binding sites. This result suggests that ethidium bromide can

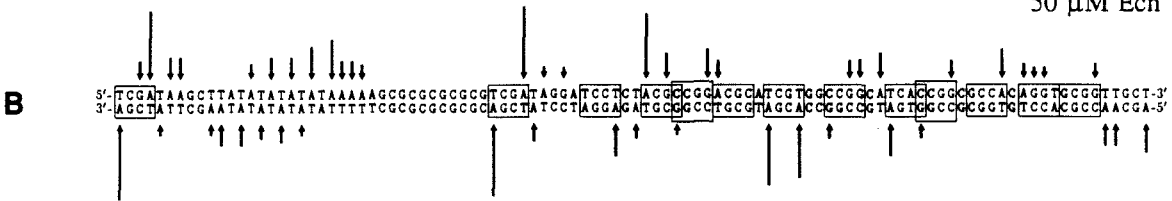
Figure 17. DEP/piperidine cleavage of DNA in the presence of echinomycin and/or ethidium bromide. Autoradiogram of 5' (lanes 1-13) and 3' (lanes 14-26) ^{32}P end-labeled 629 bp *Eco* RI-*Bgl* I restriction fragment from plasmid pDMGC11. DEP/piperidine cleavage patterns of the DNA in the presence of: Lanes 1 and 16, 1000 μM ethidium bromide (EB) UV nicking controls heated with piperidine but without DEP; 2-5 and 17-20, 1, 10, 100 or 1000 μM EB, respectively; lanes 6 and 21, no intercalator present; lanes 7 and 22, 50 μM echinomycin (ECH); lanes 8-11 and 23-26, 50 μM ECH plus 1, 10, 100 or 1000 μM EB, respectively. Lanes 12 and 14 are the Maxam-Gilbert chemical sequencing G-specific reactions; lanes 13 and 15 are the Maxam-Gilbert chemical sequencing purine-specific reactions. Buffer conditions were 100 mM Tris·HCl / 100 mM NaOAc pH 7.0, 10% (v/v) methanol and 200 μM DNA base pairs. The gel used for analysis contained 8% (w/v) polyacrylamide, crosslinked 1:20, 50% (w/v) urea and 1X TBE as the running buffer. Dimensions were 0.2 mm thick at the top, 0.6 mm thick at the base, 40 cm long and 34 cm wide. Electrophoresis at 1900 V was carried out until the BPB marker dye migrated about 42 cm.

Figure 18. DEP/piperidine cleavage patterns on about 100 bp of the 629 bp pDMGC11 restriction fragment, as determined by densitometry of the autoradiogram in Figure 17. Entries represent DEP/piperidine cleavage of DNA in the presence of 1000 μM ethidium bromide (A), 50 μM echinomycin (B) or 50 μM echinomycin plus 1000 μM ethidium bromide (C) and are shown as arrows with the height proportional to the cleavage enhancement at that nucleotide relative to DEP/piperidine cleavage of DNA in the absence of intercalator. Entry D displays the differential cleavage pattern between reactions containing 50 μM echinomycin only and those containing both 50 μM echinomycin and 1000 μM ethidium bromide, obtained by subtracting B from C. Those nucleotides cleaved more efficiently in the presence of both drugs relative to echinomycin only are shown as arrows and those cleaved less efficiently are shown as bars. For entry D only, arrow and bar height is proportional to the difference in cleavage intensity between entries C and B.

1000 μ M EB



50 μ M Ech



50 μ M Ech + 1000 μ M EB



(C-B)



compete with echinomycin for the binding of some sequences on DNA. The results of Figure 17 clearly demonstrate that high concentrations of ethidium bromide can significantly enhance DNA-DEP reactivity. Recent studies have shown that bleomycin, phleomycin⁹⁰ and 9-aminoacridine⁹¹ also induce DEP-purine hyperreactivity. These investigations question the nature of the DEP-DNA reactivity at triostin A and echinomycin binding sites: Is the observed reactivity due to a novel structural rearrangement of DNA such as Hoogsteen base-pairing, to simple unwinding of the DNA helix by quinoxaline intercalation, or is the reactivity a combination of these two possibilities? Figure 17 shows that many adenosine residues became intensely reactive to DEP in the presence of 50 μM echinomycin and that even 1000 μM ethidium bromide did not induce such intense reactivity (compare lanes 5 and 7). It can be argued that the DEP reactivity of adenosine residues in the presence of echinomycin results from helix unwinding and that the greater reactivity of these residues can be ascribed to the inherently greater binding specificity and/or longer residence times of echinomycin on DNA relative to ethidium bromide. However, the prospect that echinomycin binding to DNA induces a Watson-Crick to Hoogsteen base pair transition and exposes a highly reactive adenosine atom is equally tenable. In an attempt to elucidate the cause of DNA-DEP reactivity in the presence of triostin A and echinomycin, another study was undertaken.

Influence of methylation upon echinomycin binding and DEP-purine reactivity.

The sequence 5'-TCGA-3' is both a strong echinomycin binding site and the recognition site for the enzyme *Taq* I methylase (*M.Taq* I). When the site was bound by echinomycin, the adenosine residues at position four on both strands reacted intensely with DEP (see Figures 13 and 14). These adenosine residues are also modified by the action of *M.Taq* I in the presence of S-adenosylmethionine (SAM): *Taq* I methylase catalyzes the sequence specific and atom specific transfer of a methyl group from SAM to the exocyclic

N6 atom of the adenosine residue of the sequence 5'-TCGA-3'. This enabled us to study the effects of adenosine N6 methylation upon echinomycin binding affinity and echinomycin-induced DEP-DNA reactivity at these sites.

Were echinomycin binding to 5'-TCGA-3' to induce the T·A pairs to adopt the Hoogsteen geometry and if DEP reacts with the N1 atom of adenosine residues in this configuration, then we expected that N6 methylation of adenosine residues would sterically block the N1 position and would attenuate the DEP reactivity of those residues. The results of this experiment are presented in Figure 19. Because *Taq* I endonuclease cannot cleave 5'-TCGA-3' sites containing N6 methyl adenosine residues⁹², lanes 1-2 and 17-18 confirm the action of *M. Taq* I and SAM: Untreated DNA was digested by *Taq* I endonuclease (lanes 1 and 17), but DNA treated with *M. Taq* I and SAM prior to *Taq* I endonuclease digestion remained intact (lanes 2 and 18). MPE·Fe(II) footprinting analysis shows that N6 methylation of adenosines in the 5'-TCGA-3' sequences did not alter the apparent affinity of echinomycin for those sites, nor did it affect the binding of echinomycin at adjacent sites (compare Figure 19 lanes 5-6 with 7-8 and 21-22 with 23-24). These results have been analyzed by densitometry and are presented in Figure 20. Outside of the 5'-TCGA-3' sites, DEP/piperidine cleavage patterns in the presence of echinomycin were identical for both unmodified and methylated DNA (Figure 19 lanes 11-12 and 27-28 and Figure 20 C-D). However, N6 methylation selectively and totally abolished adenosine-DEP reactivity at 5'-TCGA-3' sites in the presence of 50 μ M echinomycin (Figure 19, compare lane 11 with lane 12 and 27 with 28 and Figure 20 C with D). That N6 methylation totally inhibited adenosine-DEP reactivity is entirely consistent with the formation of Hoogsteen base pairs at occupied echinomycin binding sites 5'-TCGA-3' in solution within a large piece of DNA. However, model building showed that N6 methylation of adenosine within a Watson-Crick pair can also sterically block the N7 position of adenosine from reacting with DEP (Figure 21).

Figure 19. Effects of adenosine methylation on echinomycin binding and DEP/piperidine cleavage. Autoradiogram of 5' (lanes 1-14) and 3' (lanes 15-28) ^{32}P end-labeled 628 bp restriction fragment from pDMG10. Odd-numbered lanes are unmodified DNA and the DNA in all even-numbered lanes except 14 and 16 was treated with *M.Taq* I and S-adenosyl methionine. Lanes are: 1-2 and 17-18, *Taq* I restriction endonuclease digestion of the labeled restriction fragment (*Taq* I); 3-4 and 19-20, intact DNA (STD); 5-6 and 21-22, MPE·Fe(II) cleavage of unprotected DNA; 7-8 and 23-24, MPE·Fe(II) cleavage of DNA in the presence of 50 μM echinomycin; 9-10 and 25-26, DEP/piperidine control cleavage in the absence of echinomycin; 11-12 and 27-28, DEP/piperidine cleavage of DNA in the presence of 50 μM echinomycin; 13 and 15, Maxam-Gilbert chemical sequencing G-specific reactions; 14 and 16, Maxam-Gilbert chemical sequencing purine-specific reactions. Buffer conditions, except lanes 1-2 and 13-18, were 100 mM Tris / 100 mM NaOAc pH 7.0, 10% (v/v) methanol and 200 μM DNA base pairs. For lanes 1-2 and 17-18, approximately 1.3 μg of DNA was digested with 7 units of *Taq* I endonuclease at 65°C for 1h according to standard procedures. The large, dark bands at the bottom of the gel correspond to the *Taq* I site nearest the label, position 24 on this fragment.

Taq I STD MPE/E DEP/E G A G A Taq I STD MPE/E DEP/E
┌ ┌ ┌ ┌ G A G A ┌ ┌ ┌ ┌
1 2 3 4 5 6 7 8 9 10 11 12 13 14 15 16 17 18 19 20 21 22 23 24 25 26 27 28

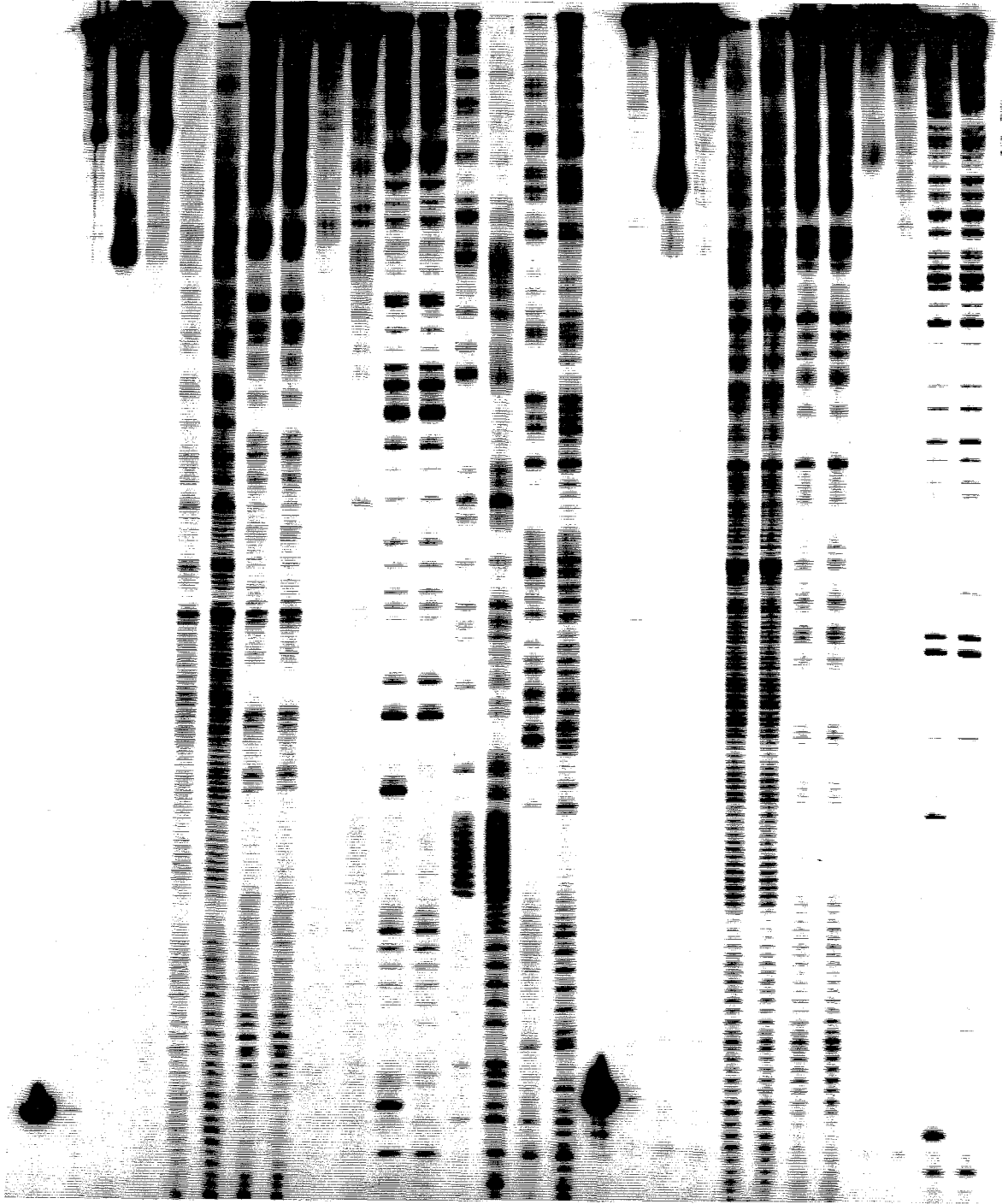
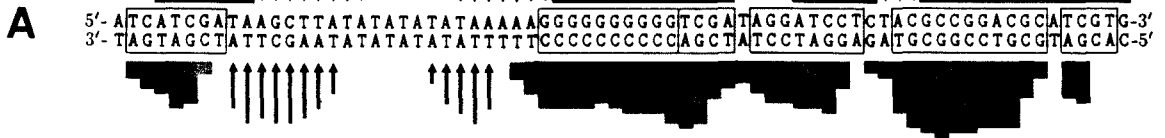
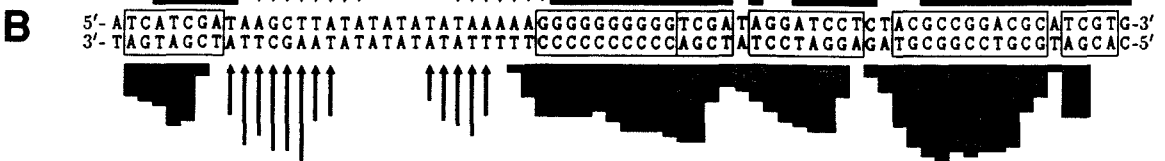


Figure 20. MPE·Fe(II) and DEP/piperidine footprinting of 50 μ M echinomycin bound to about 70 bp of the 628 bp pDMG10 restriction fragment, as determined from densitometry of the autoradiogram in Figure 19. DNA was either unmodified (A and C) or was specifically methylated by *M.Taq* I and SAM (B and D). Two of the three *Taq* I sites on this fragment can be seen beginning at positions 24 and 60 (see scale at bottom). MPE·Fe(II) footprinting patterns (A-B) are shown as bars with height proportional to the reduction of cleavage at each nucleotide and as arrows with height proportional to the enhancement of MPE·Fe(II) cleavage compared to MPE·Fe(II) cleavage of unbound DNA. DEP/piperidine cleavage patterns (C-D) are shown as arrows with height proportional to the enhancement of cleavage at each nucleotide compared to DEP/piperidine cleavage of unbound DNA. Boxes are the assigned echinomycin binding sites based on the model in References 4 and 16.

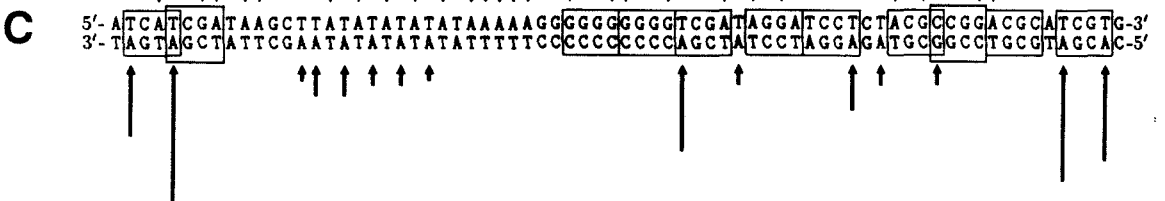
M. Taq I-



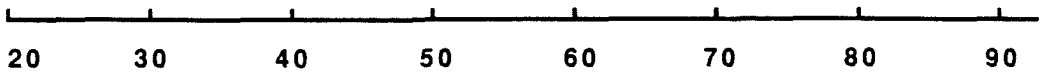
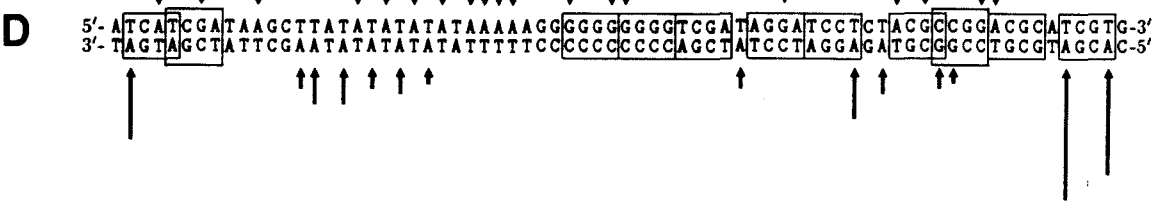
M. Taq I+



M. Taq I-



M. Taq I+



The result of the *Taq* I methylation experiment, though consistent with Hoogsteen base pair formation in solution, did not unequivocally demonstrate the existence of this novel structure because the adenosine atom responsible for the observed DEP hyperreactivity remained unknown. We determined the purine atoms responsible for the observed DEP hyperreactivity in order to describe the echinomycin·DNA complex structure in solution.

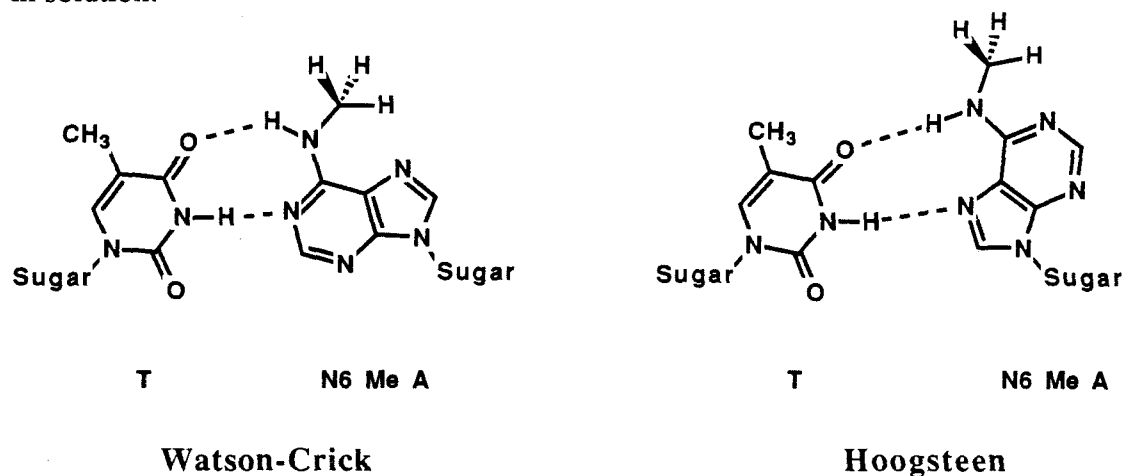


Figure 21. Diagram of T·N⁶-methyl adenosine (N6 Me A) base pairs in the Watson-Crick and Hoogsteen geometries. N⁶ methylation occludes adenosine N1 in a Hoogsteen base pair and adenosine N7 in a Watson-Crick base pair in right-handed DNA.

PRODUCT ANALYSIS

In the early 1970's, Nelson Leonard and coworkers elucidated the structures of DEP-nucleoside and DEP-nucleobase products formed in aqueous solution. Elemental analysis, NMR, UV-Visible and mass spectrometry were used to show that N1 and N3 atoms of adenine and 6-alkyladenines react with DEP to give a substituted imidazole.^{93,94} Carbon C2 is believed to be lost as formate during the course of the reaction (Figure 22). When adenine is substituted at its N9 position, such as 9-propyl adenine and adenosine, primary reaction occurs instead at the exocyclic N6 and/or the N7 to yield substituted pyrimidines (Figure 23).⁹⁴

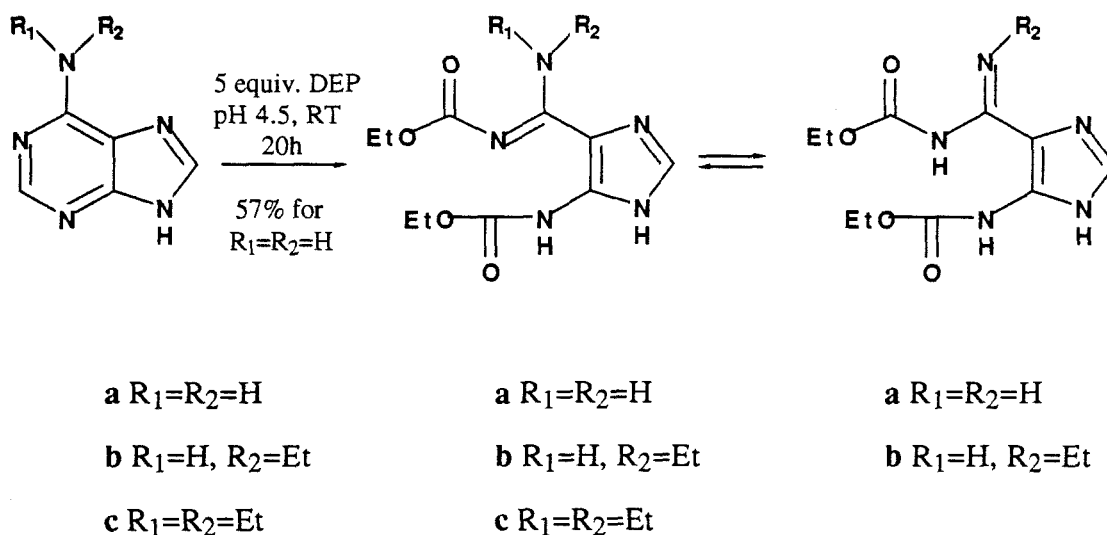


Figure 22. DEP-adenine reaction products determined by N. J. Leonard *et al.*⁹⁴

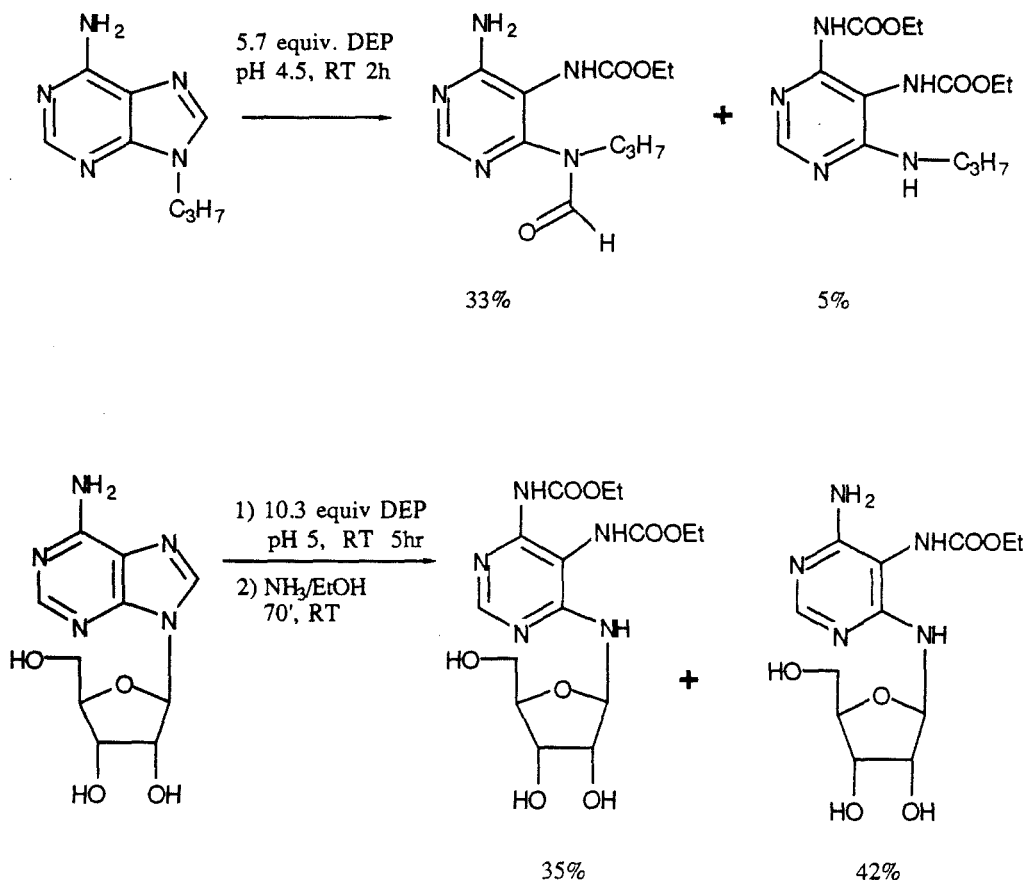


Figure 23. DEP-N9-substitued adenine reaction products.

Free base guanine did not react under similar conditions, probably because of its extremely poor water solubility. Guanosine is less reactive to DEP than adenosine and DEP reacts exclusively with guanosine N7, not with the exocyclic N2 amino function as seen for adenosine N6 above (Figure 24).⁹⁵

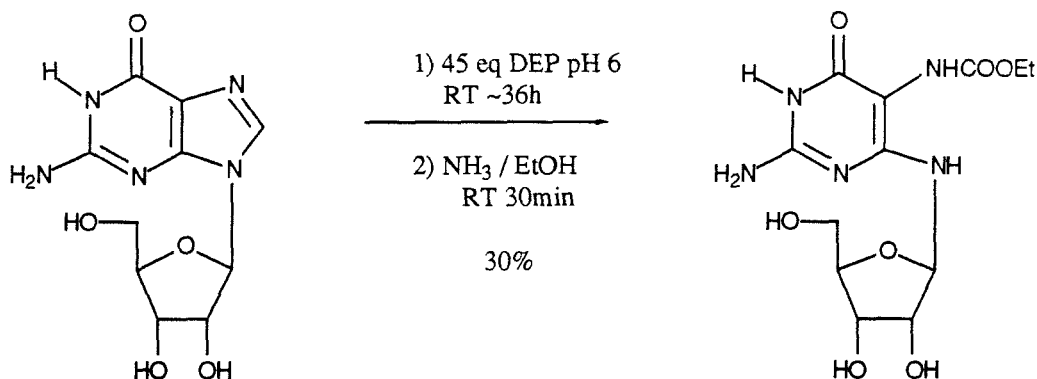


Figure 24. DEP-guanosine reaction product.

In general, it appears that the N7, not the N1 atom of N9-substituted purines reacts with DEP in aqueous solution. Because the purine bases in DNA and RNA are N9-substituted, it is assumed that DNA/RNA reactivity toward DEP occurs at purine N7 atoms. However, it remained to be seen whether the DEP-nucleobase reaction products formed on a large nucleic acid with extensive secondary structure were the same as those formed with nucleic acid constituents lacking such structure.⁹⁶ Numerous studies have shown that B-DNA is relatively unreactive to DEP. This lack of reactivity is somewhat surprising because the N7 position of guanosine residues within B-DNA is available for reaction with dimethyl sulfate (DMS).⁷⁹ DEP readily modifies adenosine and guanosine residues within Z-DNA⁸³⁻⁸⁵, single-stranded nucleic acids⁹⁴ and unpaired cruciform loops.^{86,87} For the case of Z-DNA, the assertion that purine N7 atoms within large DNA react with DEP appears valid because the N1 center is masked by a hydrogen bond, and the

B \rightarrow Z transition moves purine N7 atoms to the convex surface of the Z-DNA helix, making the N7 more accessible to electrophiles in solution (Figure 25). For unpaired cruciform loops and single-stranded nucleic acids, the situation is less clear because both N1 and N7 atoms are probably available for reaction with DEP. Even more intriguing is the possibility that Hoogsteen base-pairing leads to DEP hyperreactivity. Hoogsteen base-pairing exposes purine N1 centers to and protects N7 centers from electrophiles in solution (see Figure 11). A detailed analysis of the products formed between DEP and large DNA was required to determine precisely the purine centers responsible for the observed DEP-purine hyperreactivity in the presence of echinomycin and ethidium bromide.

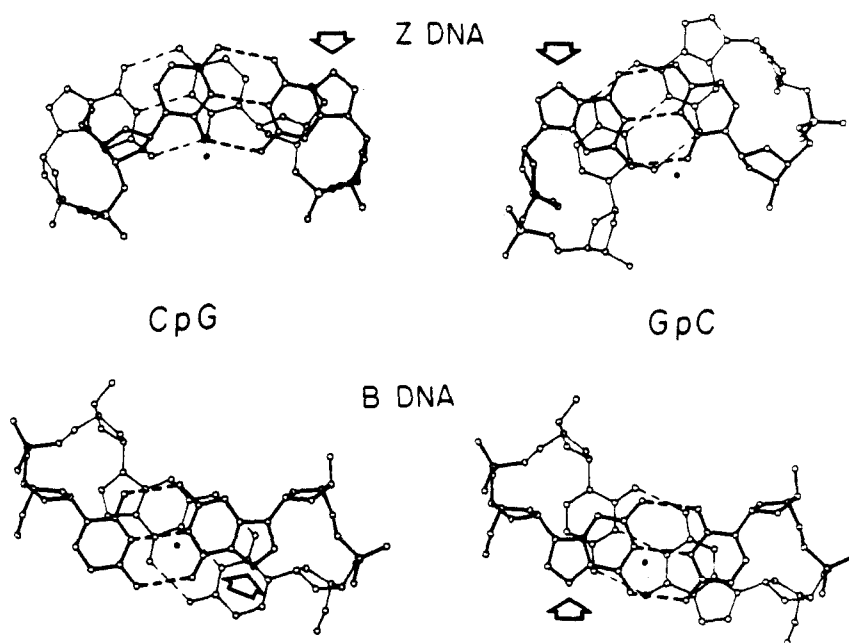


Figure 25. Relative exposure of purine N7 atoms (arrows) in Z-DNA versus B-DNA for the dinucleotide steps CpG and GpC. ²⁴

Figure 26 summarizes the method we used to identify the products of DEP-DNA reactivity at echinomycin and ethidium bromide binding sites on DNA. Precise characterization of the DNA-DEP adducts formed in the presence of echinomycin, or ethidium bromide was then used to describe the nature of base-pairing at filled echinomycin binding sites on DNA.

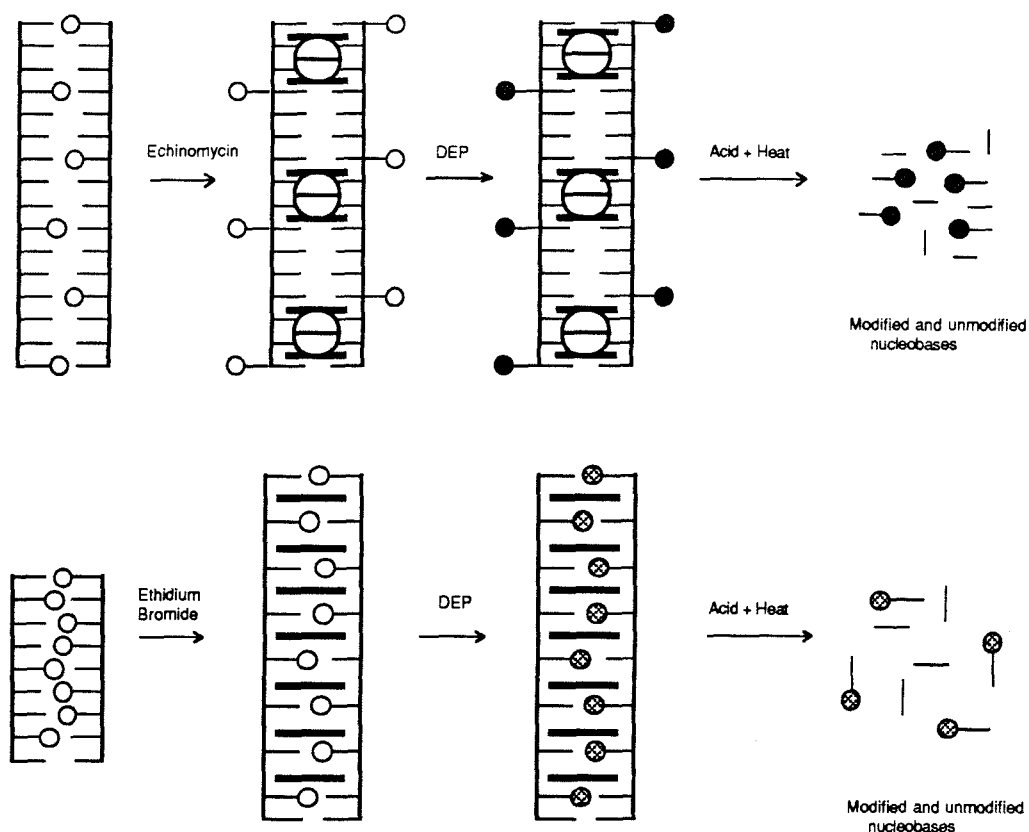


Figure 26. Design of product analysis experiments. (Top) Echinomycin (theta structure) bisintercalates into DNA and exposes reactive purine centers (white circles) either by inducing Hoogsteen base-pairing at its binding sites (shown) or by unwinding the DNA duplex. Exposed purine centers then react with DEP to give modified purines (shaded circles) which can be liberated from the DNA strand by heat and acid. (Bottom) Ethidium bromide, represented as a dark bar, intercalates into DNA and increases the accessibility of purine N7 atoms (white circles) to solution by helix unwinding. These centers then react with DEP to give a modified base (stippled circles) that is released from the DNA by depurination. Base release products were then analyzed by HPLC after which their structures were determined by a combination of IR, NMR, UV-Visible and mass spectrometric methods. The DNA structure at drug binding sites was then inferred from a knowledge of the purine atoms responsible for the observed DEP hyperreactivity. Details of this analysis are presented in the experimental section.

DNA substrates used for product analysis.

The NMR work of Patel and coworkers cited above showed that the base sequence probably determines whether Hoogsteen or Watson-Crick base pairs will be found at the first and fourth positions of echinomycin binding sites in solution. If random sequence DNA such as calf thymus DNA were used as the substrate for product analysis, we would not have been able to assign a given DEP-base adduct to a specific echinomycin binding site. The use of calf thymus or other large DNA as substrate would be further complicated by the fact that after sonication, the DNA would likely contain significant amounts of single-stranded regions that would react with DEP and could mask the DEP-base adducts formed at the echinomycin or ethidium bromide binding sites. For these reasons, a series of oligonucleotides was designed and synthesized to investigate the nucleic acid structure at a series of *specific* echinomycin binding sites. The oligonucleotides range in length from 32 to 36 nucleotides and contain the preferred echinomycin binding sequences (5'-3') TCGA, ACGT, ACGC, GCGT, CCGG and GCGC. The sequences of these oligonucleotides are presented in Figure 27. Each oligonucleotide pair forms a flush-ended duplex containing four to six copies of a specific echinomycin binding site. Although these oligonucleotides do not qualify as "large DNA" such as a restriction fragment, they are certain to reflect more realistically the environment of a large DNA fragment than do oligonucleotides shorter than 10 base pairs. Each oligonucleotide was synthesized on a 10 μ mol scale and was purified by FPLC before annealing to its complementary strand (see Experimental section). Native polyacrylamide gel electrophoresis showed nearly quantitative annealing of oligonucleotide pairs, thus discounting the possibility that DEP-DNA products resulted from DEP reaction with single-stranded DNA. The results of DEP-oligonucleotide reaction in the presence of ethidium bromide or echinomycin are presented below. For each oligonucleotide pair (except **56+57**), the DEP-DNA reaction was analyzed from two different but complementary perspectives: From the perspective of the DNA strands (shown as high-resolution denaturing polyacrylamide gel autoradiograms) and from the

Figure 27. Sequences of the oligonucleotides used for product analysis of DNA-DEP reactivity at a number of echinomycin binding sites. In all cases, the preferred four base pair echinomycin binding sites are boxed. Oligonucleotides **47** and **48** form a 34 base pair duplex containing five (5'-3') TCGA sites. Oligonucleotides **49** and **50** form a 34 base pair duplex containing five (5'-3') ACGT sites. The flanking sequences between echinomycin binding sites are identical for both **47+48** and **49+50**. Oligonucleotides **51** and **52** form a 36 base pair duplex containing six (5'-3') ACGT sites within the context of a perfectly alternating purine/pyrimidine helix. Oligonucleotide **53** is a self-complementary 32 base pair duplex composed of four repeats of the octamer sequence used by Quigley *et al.*⁷² in the (trioestin A)₂·d(GCGTACGC)₂ structure. This alternating purine/pyrimidine duplex contains four copies each of the echinomycin binding sites (5'-3') GCGT and ACGC. Oligonucleotides **56** and **57** also contain these sequences, but not all directly adjacent to one another. Oligonucleotides **54** and **55** contain five copies of the site (5'-3') CCGG, while oligonucleotides **60** and **61** contain five copies of the site (5'-3') GCGC. The sequences flanking the echinomycin binding sites are the same for duplexes **54+55** and **60+61**.

47 5'- C T C G A T T G T C G A T T G T C G A T C T T C G A G T G T C G A G -3'
 48 3'- G A G C T A A C A G C T A A C A G C T A G A A G C T C A C A G C T C -5'

49 5'- C A C G T T T G A C G T T T G A C G T T C T A C G T G T G A C G T G -3'
 50 3'- G T G C A A A C T G C A A A C T G C A A G A T G C A C A C T G C A C -5'

51 5'- C A C G T G T A C G T G T A C G T G T A C G T G T A C G T G T A C G T G -3'
 52 3'- G T G C A C A T G C A C A T G C A C A T G C A C A T G C A C A T G C A C -5'

53 5'- G C G T A C G C G C G T A C G C G C G T A C G C G C G T A C G C -3'
 3'- C G C A T G C G C G C A T G C G C G C A T G C G C G C A T G C G -5'

56 5'- G C G T A C G C A C A C G C G T A C G C A C A C G C G T A C G C -3'
 57 3'- C G C A T G C G T G T G C G C A T G C G T G T G C G C A T G C G -5'

54 5'- T C C G G T G T C C G G T G T C C G G T G T C C G G T G T C C G G T -3'
 55 3'- A G G C C A C A G G C C A C A G G C C A C A G G C C A C A G G C C A -5'

60 5'- T G C G C T G T G C G C T G T G C G C T G T G C G C T G T G C G C T -3'
 61 3'- A C G C G A C A C G C G A C A C G C G A C A C G C G A C A C G C G A -5'

perspective of the DNA bases (shown as HPLC traces). In all cases, the reaction conditions for gel electrophoretic analysis were identical to those for the HPLC analysis except that a heat/piperidine workup was used to mark the positions of DEP-modified bases for gel analysis, whereas a heat/formic acid workup was used to release DEP-modified bases from the DNA strand for HPLC analysis and structural characterization. Different treatment was required because heat/piperidine treatment degraded the bases modified by DEP.

DEP/piperidine cleavage patterns on duplexes 47+48 through 60+61.

Figure 28 displays the DEP/piperidine cleavage patterns produced on duplex 47+48 without intercalators and in the presence of 120 μ M echinomycin or 3 mM ethidium bromide. As observed for large DNA restriction fragments, DEP did not significantly modify unbound DNA (lanes 2-4 and 16-18), but reacted readily with DNA when echinomycin (lanes 5-7 and 19-21) or ethidium bromide (lanes 8-10 and 22-24) was present. At 120 μ M echinomycin, DEP reacted very strongly with adenosine residues of the 5'-TCGA-3' echinomycin binding sites and less so with adenosines outside of these sequences. Guanosine residues were not significantly modified by DEP on this duplex in the presence of echinomycin. When 3 mM ethidium bromide was allowed to bind the 47+48 duplex, DEP modified virtually all of the purines, reacting preferentially with adenosine residues. Densitometric analysis of the autoradiogram of Figure 28 is presented in Figure 30 A and B. On this duplex, ethidium bromide produced a more even but less intense overall DEP/piperidine cleavage pattern than did echinomycin (compare Figure 30 A and B). Further, the degree of DEP-duplex reaction was significantly lower for ethidium bromide than for echinomycin, even though the concentration of ethidium bromide was twenty-five times greater than that of echinomycin. Similar results were obtained in the modified base-release assay (see below). The products of DEP/piperidine cleavage comigrated with the products of chemical sequencing lanes on this and all following 15% polyacrylamide gels, indicating that the cleavage products possessed 3' phosphate termini.

Figure 28. Autoradiogram of the high-resolution denaturing polyacrylamide gel used to analyze DEP/piperidine cleavage of the oligonucleotide duplex **47+48** in the presence of echinomycin or ethidium bromide. Both 5' ³²P end-labeled **47** (lanes 1-12) and **48** (lanes 13-24) were used for opposite strand analysis on this duplex. Lanes are: 1 and 15, intact DNA standards (STD) incubated as for all other reactions on the gel but not treated with DEP or piperidine; 2-4 and 16-18, DEP/piperidine control cleavage of DNA in the absence of drugs (DEP); 5-7 and 19-21, DEP/piperidine cleavage of the duplex in the presence of 120 μ M echinomycin (DEP/ECH); 8-10 and 22-24, DEP/piperidine cleavage of DNA in the presence of 3 mM ethidium bromide (DEP/EB). After reaction with DEP, the reaction mixture was precipitated, divided into three portions and heated with 100 mM piperidine at 90°C for different lengths of time to insure that complete strand cleavage occurred at bases modified by DEP. The piperidine/heat reaction times are 15, 30 or 60 minutes reading from left to right in a given series. For example, lanes 5, 6, and 7 were heated with piperidine for 15, 30, and 60 minutes, respectively. Lanes 11 and 13 are the Maxam-Gilbert chemical sequencing G-specific reactions, lanes 12 and 14 are the Maxam-Gilbert chemical sequencing purine-specific reactions. The DEP reaction conditions were 100 mM Tris / 100 mM sodium acetate (NaOAc), pH 7.0, 0.3 mM MgCl₂, 10% (v/v) methanol, 600 μ M oligonucleotide base pairs, 200 mM DEP (~330 equivalents to bp), and either 120 μ M echinomycin (ECH:DNA bp = 1:5) or 3 mM ethidium bromide (EB:DNA bp = 5:1). The gel contained 15% (w/v) polyacrylamide, crosslinked 1:20, 50% (w/v) urea, 1X TBE buffer (see Experimental) and 2% (v/v) glycerol to prevent cracking of the gel when drying. Gel dimensions were 0.4 mm thick at the top, 1.2 mm thick at the base, 40 cm long and 34 cm wide. Electrophoresis at 1500 V was continued until the bromophenol blue (BPB) marker dye had migrated 25 cm from the origin.

STD 1 2 3 4 5 6 7 8 9 10 11 12 13 14 15 16 17 18 19 20 21 22 23 24

DEP DEP/ECH DEP/EB

STD G+Δ G STD G+Δ G DEP DEP/ECH DEP/EB

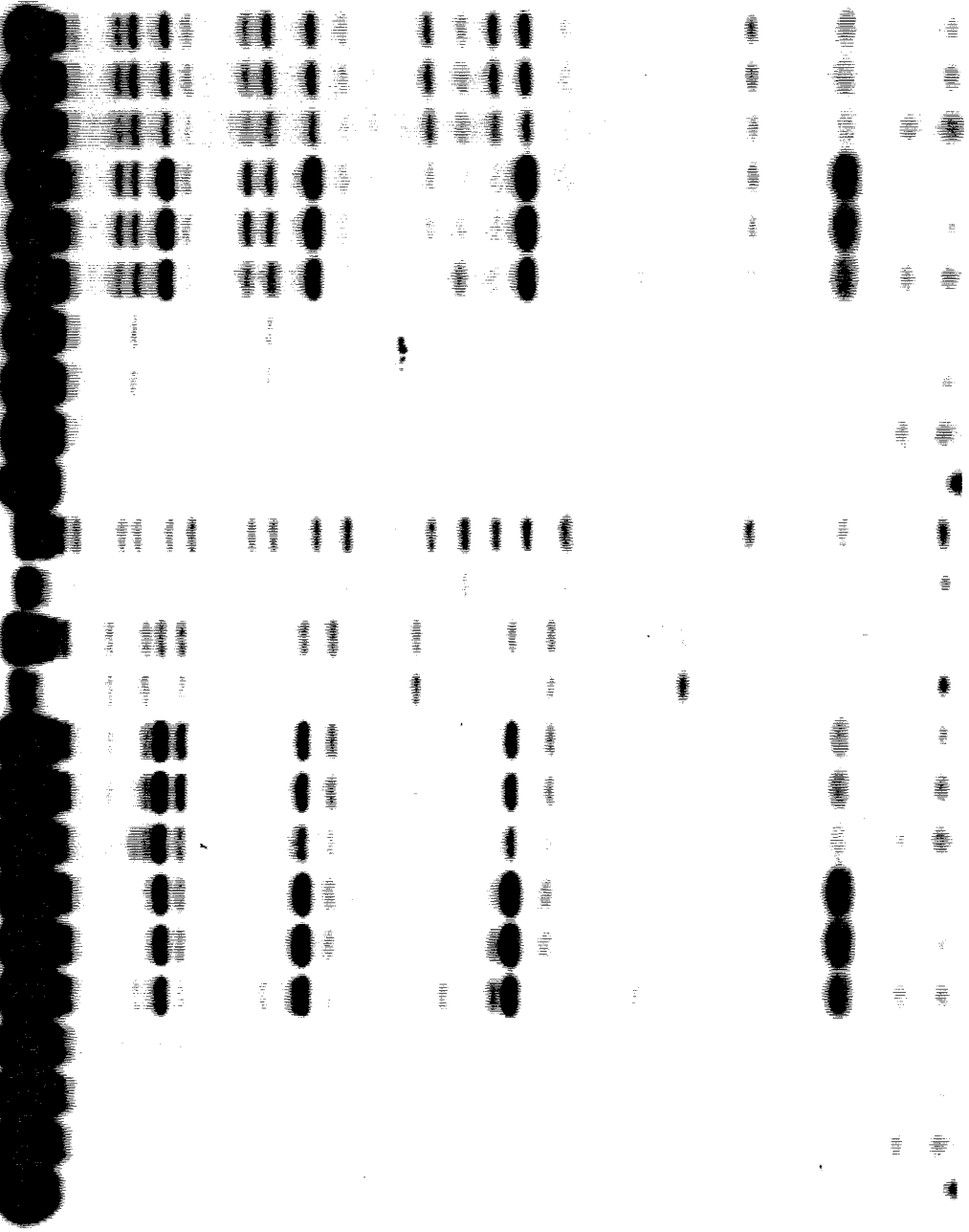


Figure 29. Autoradiogram of the high-resolution denaturing polyacrylamide gel used to analyze DEP/piperidine cleavage of the oligonucleotide duplex **49+50** in the presence of echinomycin or ethidium bromide. Both 5' ³²P end-labeled **49** (lanes 1-12) and **50** (lanes 13-24) were used for opposite strand analysis on this duplex. Lanes are: 1 and 15, intact DNA standards (STD) incubated as for all other reactions on the gel but not treated with DEP or piperidine; 2-4 and 16-18, DEP/piperidine control cleavage of DNA in the absence of drugs (DEP); 5-7 and 19-21, DEP/piperidine cleavage of the duplex in the presence of 120 μ M echinomycin (DEP/ECH); 8-10 and 22-24, DEP/piperidine cleavage of DNA in the presence of 3 mM ethidium bromide (DEP/EB). After reaction with DEP, the reaction mixture was precipitated, divided into three portions and heated with 100 mM piperidine at 90°C for different lengths of time to insure that complete strand cleavage occurred at bases modified by DEP. The piperidine/heat reaction times are 15, 30 or 60 minutes reading from left to right in a given series. For example, lanes 5, 6, and 7 were heated with piperidine for 15, 30, and 60 minutes, respectively. Lanes 11 and 13 are the Maxam-Gilbert chemical sequencing G-specific reactions, lanes 12 and 14 are the Maxam-Gilbert chemical sequencing purine-specific reactions. The DEP reaction conditions were 100 mM Tris / 100 mM NaOAc, pH 7.0, 0.3 mM MgCl₂, 10% (v/v) methanol, 600 μ M oligonucleotide base pairs, 200 mM DEP (~330 equivalents to bp), and either 120 μ M echinomycin (ECH:DNA bp = 1:5) or 3 mM ethidium bromide (EB:DNA bp = 5:1). The gel contained 15% (w/v) polyacrylamide, crosslinked 1:20, 50% (w/v) urea, 1X TBE buffer (see Experimental) and 2% (v/v) glycerol to prevent cracking of the gel when drying. Gel dimensions were 0.4 mm thick at the top, 1.2 mm thick at the base, 40 cm long and 34 cm wide. Electrophoresis at 1500 V was continued until the bromophenol blue (BPB) marker dye had migrated 25 cm from the origin.

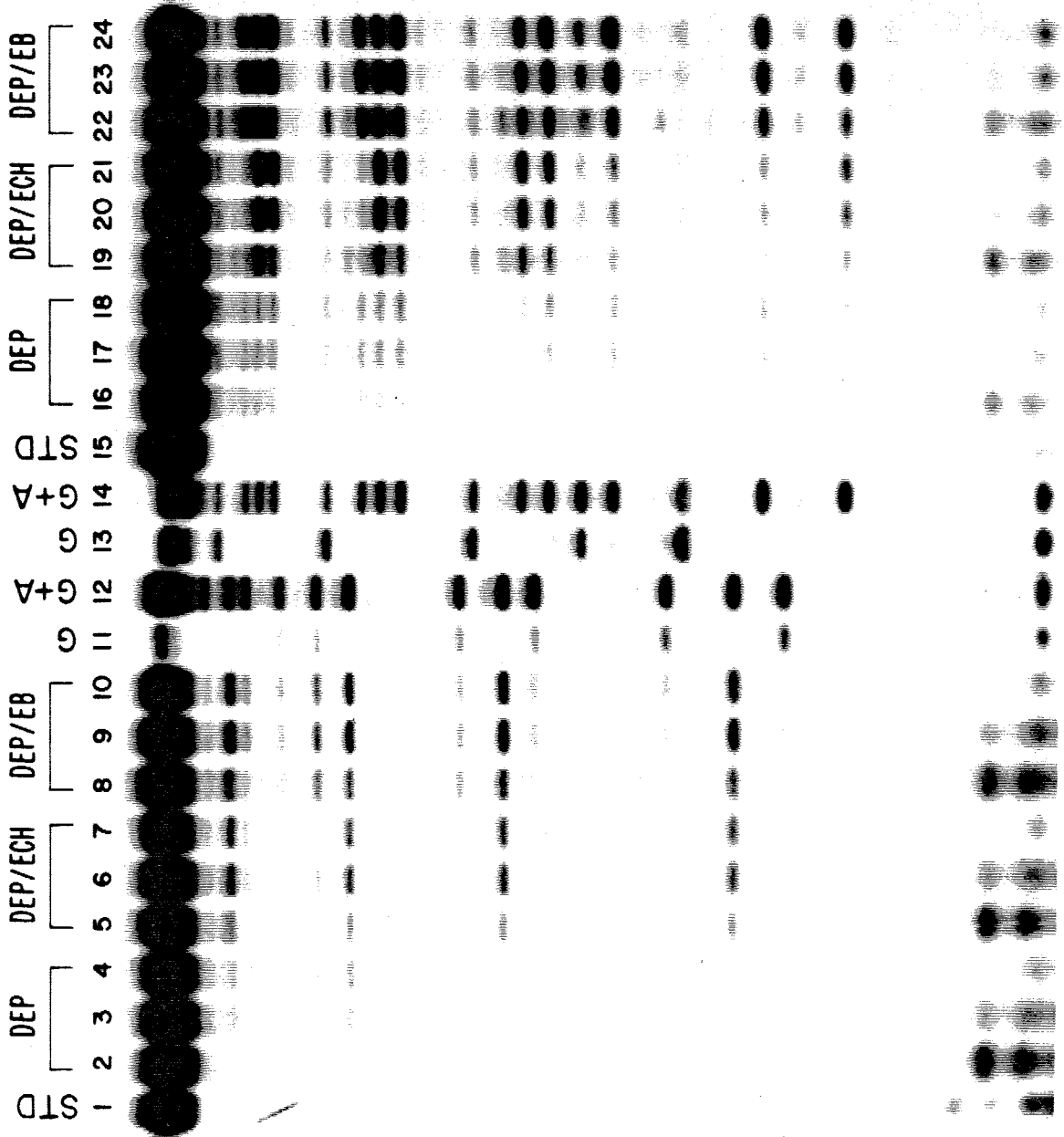
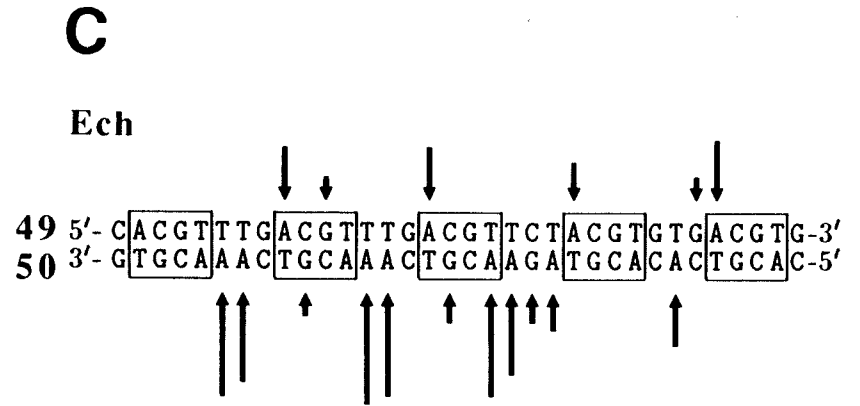
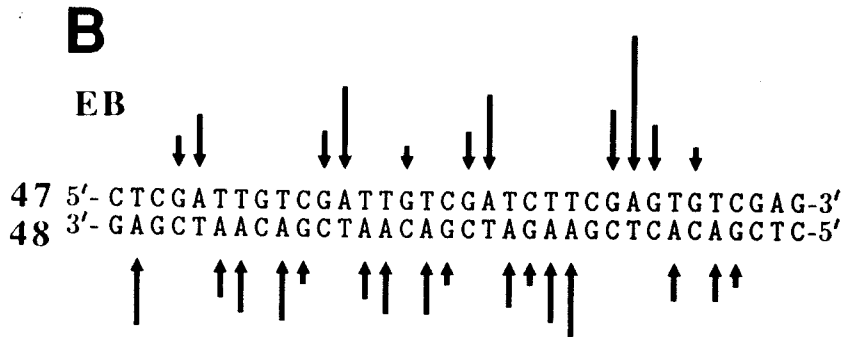
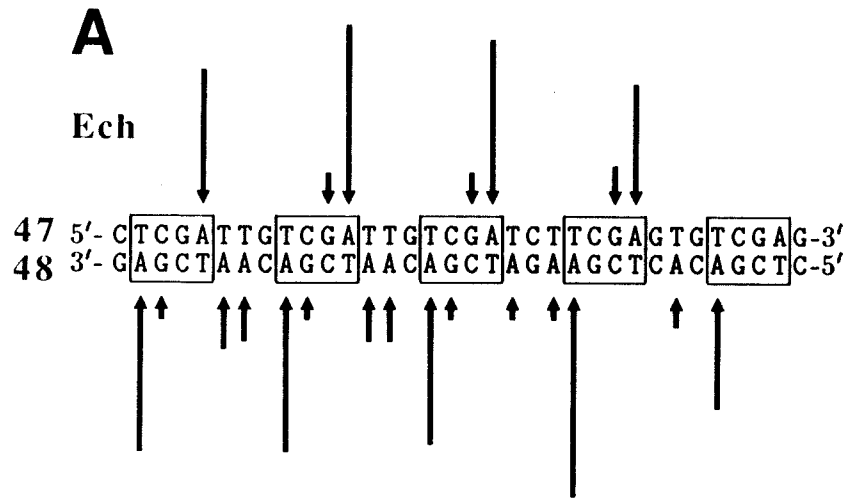


Figure 30. (A-D) DEP/piperidine cleavage of oligonucleotide duplexes **47+48** (A-B) and **49+50** (C-D) in the presence of 120 μ M echinomycin, A and C, or 3 mM ethidium bromide, B and D, as determined by densitometry of the autoradiograms of Figures 28 and 29. Lanes 4 and 18 were scanned to analyze DEP/piperidine cleavage of unbound DNA, 7 and 21 for DEP/piperidine cleavage of DNA bound by echinomycin, and 10 and 24 for DEP/piperidine cleavage of DNA bound by ethidium bromide. DEP/piperidine cleavage patterns are shown as arrows with height proportional to the enhancement of cleavage at each nucleotide compared to DEP/piperidine cleavage of unbound DNA. No data are available for the 5' and 3' terminal three to four base pairs of each oligonucleotide because of the limits of 15% polyacrylamide gel resolution. Designed four base pair echinomycin binding sites are boxed in A and C.



The end products of DEP/piperidine cleavage in the presence of echinomycin or ethidium bromide probably resulted from nucleobase modification followed by base-catalyzed phosphate elimination and sugar degradation.

Under the same conditions used for duplex **47+48**, duplex **49+50** gave markedly different DEP/piperidine cleavage patterns. Figure 29 presents these results. Again, DEP did not react with DNA in the absence of intercalators (lanes 2-4 and 16-18). It is obvious that on the **49+50** duplex, echinomycin (lanes 5-7 and 19-21) induced *less* DEP-DNA reaction than did ethidium bromide (lanes 8-10 and 22-24). Figure 30 shows the densitometric analysis of DEP-DNA reactivity in the presence of 120 μ M echinomycin (C) or 3 mM ethidium bromide (D) on duplex **49+50**. Adenosine residues within 5'-ACGT-3' echinomycin binding sites reacted to varying degrees with DEP when echinomycin was present. All adenosines within the 5'-ACGT-3' sequences on the upper strand in Figure 29 reacted moderately with DEP, but the situation was different on the lower strand (Figure 30 C). The adenosine residue within the central 5'-ACGT-3' sequence on the lower strand reacted with DEP, but adenosine residues of the other 5'-ACGT-3' sites on this strand did not react with DEP above background when echinomycin was included in the reaction mixture. Most interesting of the unreactive sequences are two copies of the sequence 5'-AAACGT-3' near the 3' end of the lower strand. At 120 μ M echinomycin, the first two 5' adenosines of this sequence reacted with DEP, but the third adenosine corresponding to the first residue of the echinomycin binding site failed to react with DEP above background levels (Figure 30 C). However, all three adenosine residues of this sequence reacted strongly with DEP in the presence of 3 mM ethidium bromide (Figure 30 D). The possibility that echinomycin did not bind to these sites seemed unlikely because all adenosines corresponding to the first position of echinomycin binding sites did react with DEP on the top strand. It is interesting that some adenosine residues occupying the first or fourth positions of strong echinomycin binding sites did not react with DEP, contrary to the general trend seen in Figures 13, 14, 16 and 28. This failure to react may tell us as much

about the base-pairing at echinomycin binding sites as does the extreme hyperreactivity to DEP seen at other echinomycin binding sites. If DEP-adenosine reaction at 5'-ACGT-3' echinomycin binding sites occurs at N1, the failure of these residues to react with DEP suggests Watson-Crick pairing at these positions. If the adenosine-DEP reaction is at N7, then the failure of these residues to react with DEP indicates protection of N7, consistent with Hoogsteen base-pairing at these sites in solution.

We constructed a duplex containing 5'-ACGT-3' sites within the context of an alternating purine/pyrimidine sequence to see if this had any effect upon purine-DEP reaction in the presence of echinomycin. Figure 31 presents the DEP/piperidine cleavage patterns of duplex **51+52** without intercalators (lanes 2-4 and 16-18) or in the presence of 144 μ M echinomycin (lanes 5-7 and 19-21) or 3.6 mM ethidium bromide (lanes 8-10 and 22-24). Bands were not sharp for the **51** label (lanes 1-12), and DEP/piperidine control cleavage was not as clean as observed for either **47+48** or **49+50** duplexes. This result was repeated with three different syntheses of the oligomer and could not be improved. Purity of **51** and its hybridization characteristics appeared to be as good as or better than all the other oligonucleotides used. Strong and relatively even DEP-DNA reactivity above background was observed in the presence of 3.6 mM ethidium bromide. Nearly all purines were modified by DEP at this concentration of ethidium bromide. DEP/piperidine cleavage in the presence of echinomycin was less clear. When **51** was labeled, there appeared slight protection from, rather than enhanced, reactivity to DEP at 144 μ M echinomycin (Figure 31, lanes 5-7). However, there was moderate DEP-DNA reactivity above background with labeled **52** under the same conditions (lanes 19-21). Figure 33 (A and B) presents the densitometric analysis of these results. As with duplex **49+50**, the overall level of DEP-DNA reactivity was less for echinomycin than for ethidium bromide on duplex **51+52**. Adenosine residues within 5'-ACGT-3' sequences reacted only weakly with DEP on the lower strand, whereas the adenosine residues immediately 3' adjacent to these sites reacted more strongly with DEP in the presence of 144 μ M echinomycin. This pattern of adenosine

Figure 31. Autoradiogram of the high-resolution denaturing polyacrylamide gel used to analyze DEP/piperidine cleavage of the oligonucleotide duplex **51+52** in the presence of echinomycin or ethidium bromide. Both 5' ³²P end-labeled **51** (lanes 1-12) and **52** (lanes 13-24) were used for opposite strand analysis on this duplex. Lanes are: 1 and 15, intact DNA standards (STD) incubated as for all other reactions on the gel but not treated with DEP or piperidine; 2-4 and 16-18, DEP/piperidine control cleavage of DNA in the absence of drugs (DEP); 5-7 and 19-21, DEP/piperidine cleavage of the duplex in the presence of 140 μ M echinomycin (DEP/ECH); 8-10 and 22-24, DEP/piperidine cleavage of DNA in the presence of 3.6 mM ethidium bromide (DEP/EB). After reaction with DEP, the reaction mixture was precipitated, divided into three portions and heated with 100 mM piperidine at 90°C for different lengths of time to insure that complete strand cleavage occurred at bases modified by DEP. The piperidine/heat reaction times are 15, 30 or 60 minutes reading from left to right in a given series. For example, lanes 5, 6, and 7 were heated with piperidine for 15, 30, and 60 minutes, respectively. Lanes 11 and 13 are the Maxam-Gilbert chemical sequencing G-specific reactions, lanes 12 and 14 are the Maxam-Gilbert chemical sequencing purine-specific reactions. The DEP reaction conditions were 100 mM Tris / 100 mM NaOAc, pH 7.0, 0.3 mM MgCl₂, 10% (v/v) methanol, 700 μ M oligonucleotide base pairs, 240 mM DEP (~330 equivalents to bp), and either 140 μ M echinomycin (ECH:DNA bp ~ 1:5) or 3.6 mM ethidium bromide (EB:DNA bp ~ 5:1). The gel contained 15% (w/v) polyacrylamide, crosslinked 1:20, 50% (w/v) urea, 1X TBE buffer (see Experimental) and 2% (v/v) glycerol to prevent cracking of the gel when drying. Gel dimensions were 0.4 mm thick at the top, 1.2 mm thick at the base, 40 cm long and 34 cm wide. Electrophoresis at 1500 V was continued until the bromophenol blue (BPB) marker dye had migrated 25 cm from the origin.

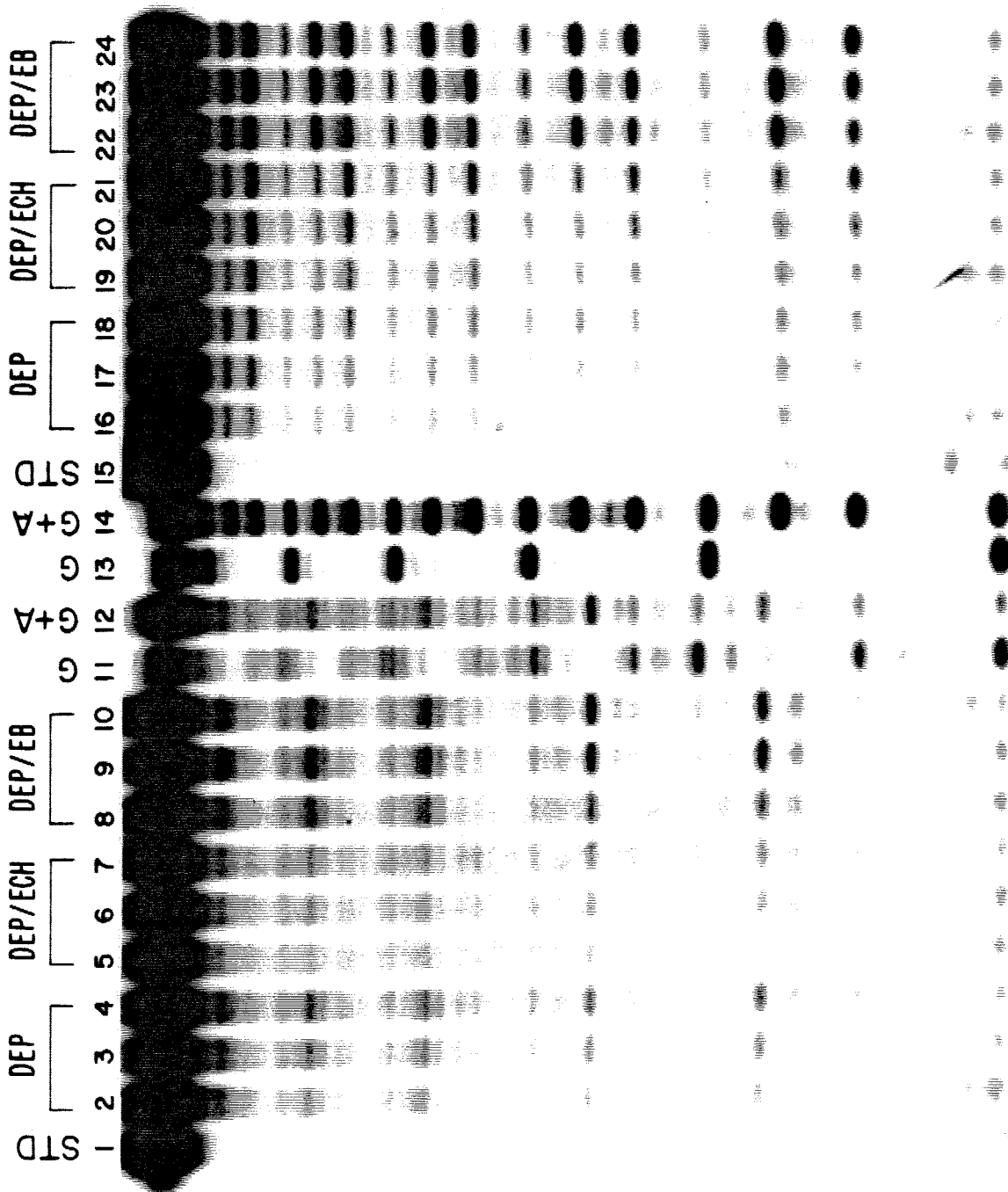


Figure 32. Autoradiogram of the high-resolution denaturing polyacrylamide gel used to analyze DEP/piperidine cleavage of the self-complementary oligonucleotide duplex **53** in the presence of echinomycin or ethidium bromide at pH 7.0 (lanes 1-10) or pH 4.7 (lanes 13-22). Exposure time was twice as long as the other autoradiograms presented in this series. 5' ^{32}P end-labeled **53** was sufficient for opposite strand analysis on this duplex. Lanes are: 1 and 13, intact DNA standards (STD) incubated as for all other reactions on the gel but not treated with DEP or piperidine; 2-4 and 14-16, DEP/piperidine control cleavage of DNA in the absence of drugs (DEP); 5-7 and 17-19, DEP/piperidine cleavage of the duplex in the presence of 120 μM echinomycin (DEP/ECH); 8-10 and 20-22, DEP/piperidine cleavage of DNA in the presence of 3 mM ethidium bromide (DEP/EB). After reaction with DEP, the reaction mixture was precipitated, divided into three portions and heated with 100 mM piperidine at 90°C for different lengths of time to insure that complete strand cleavage occurred at bases modified by DEP. The piperidine/heat reaction times are 15, 30 or 60 minutes reading from left to right in a given series. For example, lanes 5, 6, and 7 were heated with piperidine for 15, 30, and 60 minutes, respectively. Lane 11 is the Maxam-Gilbert chemical sequencing G-specific reaction, lane 12 is the Maxam-Gilbert chemical sequencing purine-specific reaction. The DEP reaction conditions were 100 mM Tris / 100 mM NaOAc, pH 7.0 or 4.7, 0.3 mM MgCl_2 , 10% (v/v) methanol, 600 μM oligonucleotide base pairs, 200 mM DEP (~330 equivalents to bp), and either 120 μM echinomycin (ECH:DNA bp = 1:5) or 3 mM ethidium bromide (EB:DNA bp = 5:1). The denaturing 15%, 1:20 crosslinked polyacrylamide gel contained 1X TBE buffer (see Experimental), 50% (w/v) urea and 2% (v/v) glycerol to prevent cracking of the gel when drying. The wedge-shaped gel was 0.4 mm thick at the top, 1.2 mm thick at the base, 40 cm long and 34 cm wide. Electrophoresis at 1500 V was continued until the bromophenol blue (BPB) marker dye had migrated 25 cm from the origin.

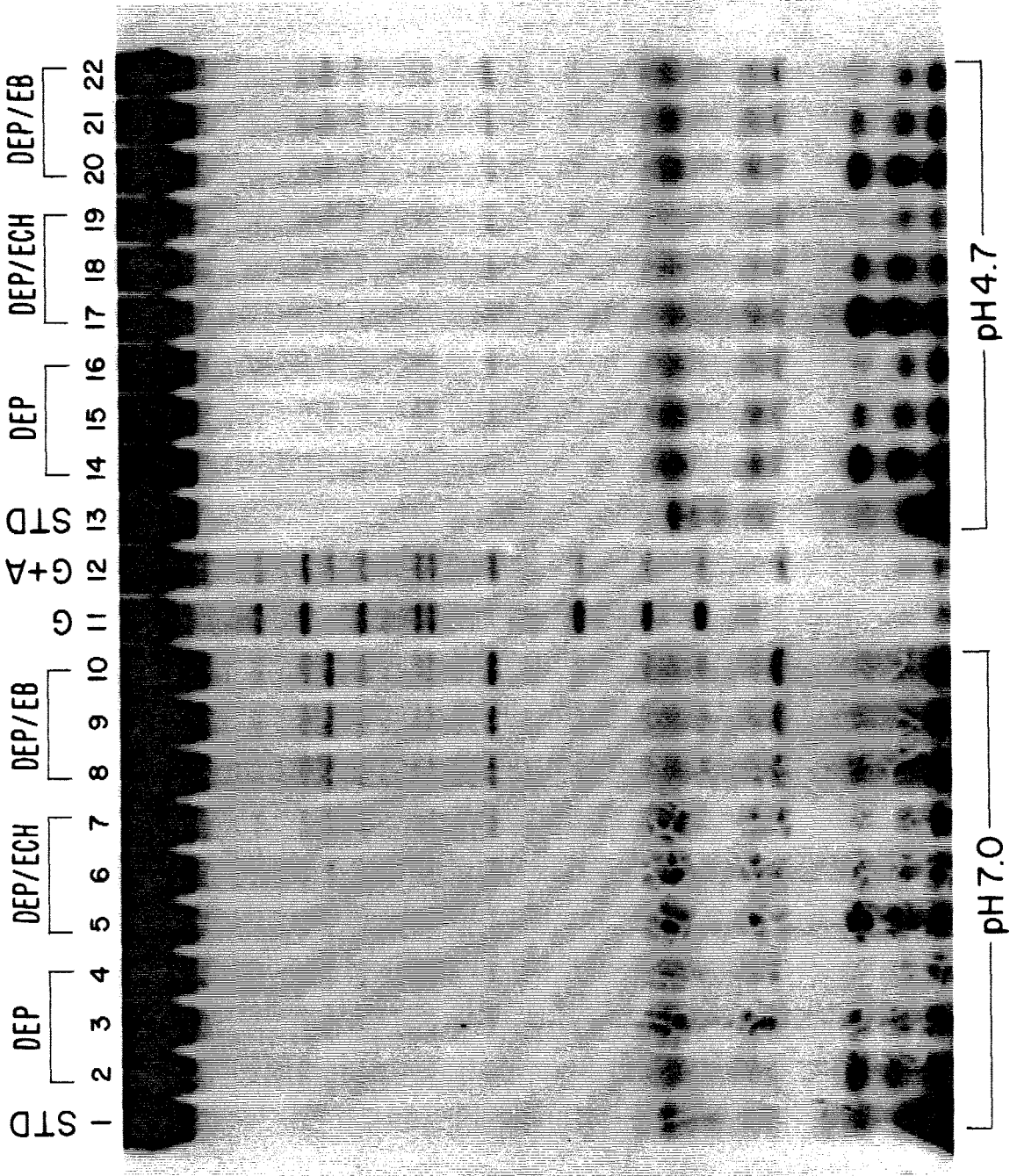
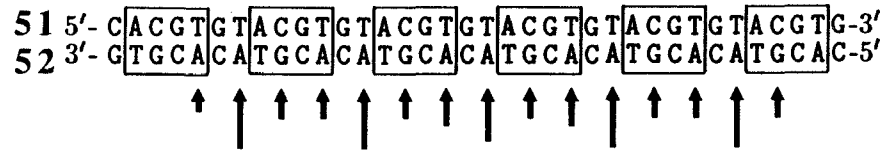


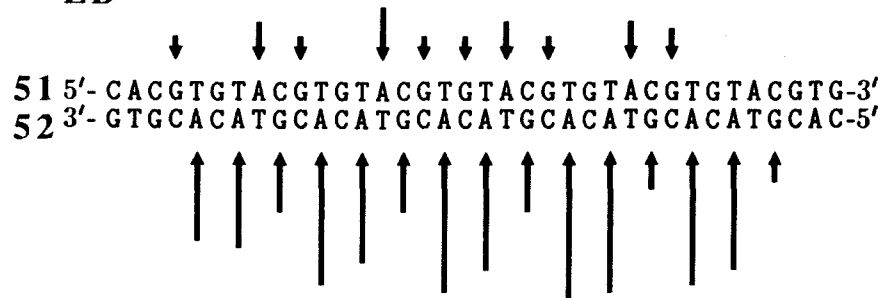
Figure 33. (A-D) DEP/piperidine cleavage of oligonucleotide duplexes **51+52** (A-B) and **53** (C-D) in the presence of 140-120 μ M echinomycin, A and C, or 3.6-3 mM ethidium bromide, B and D, as determined by densitometry of the autoradiograms of Figures 31 and 32. Referring to Figure 31, lanes 4 and 18 were scanned to analyze DEP/piperidine cleavage of unbound **51+52**, 7 and 21 for DEP/piperidine cleavage of **51+52** bound by echinomycin, and 10 and 24 for DEP/piperidine cleavage of **51+52** bound by ethidium bromide. For duplex **53**, Figure 32 lanes 4, 7, and 10 were scanned to determine the amounts of DEP/piperidine cleavage of duplex **53** either unbound or in the presence of echinomycin or ethidium bromide, respectively. DEP/piperidine cleavage patterns are shown as arrows with height proportional to the enhancement of cleavage at each nucleotide compared to DEP/piperidine cleavage of unbound DNA. No data are available for the 5' and 3' terminal three to four base pairs of each oligonucleotide because of the limits of 15% polyacrylamide gel resolution. Designed four base pair echinomycin binding sites are boxed in A and C.

A

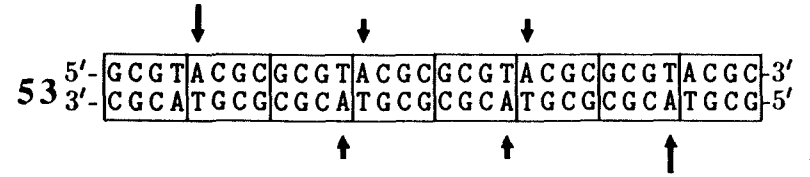
Ech

**B**

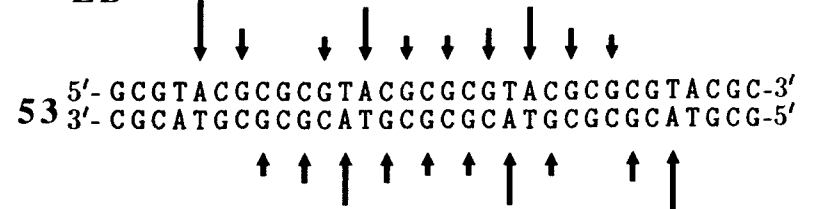
EB

**C**

Ech

**D**

EB



reactivity paralleled that observed for echinomycin bound to duplex **49+50**, where adenosine residues adjacent to 5'-ACGT-3' sequences reacted more strongly with DEP than did those occupying the first/fourth positions of the echinomycin binding site. When bound by echinomycin, this DEP-purine reactivity pattern appeared to be general for 5'-ACGT-3' sites, fundamentally different from that observed at 5'-TCGA-3' sequences. The DEP/piperidine cleavage pattern for echinomycin bound to (5'-3') GCGT and ACGC sites was also unique.

Self-complementary duplex **53** contains four copies of the 5'-GCGTACGC-3' sequence used by Quigley *et al.*⁷² to elucidate the triostin A·octamer complex structure. The complex forms both T·A and C·G Hoogsteen base pairs at pH 4.5. Figure 32 displays the effect of pH on DEP-duplex **53** reactivity in the presence of echinomycin and ethidium bromide. At pH 7.0 and 120 μ M echinomycin, DEP reactivity with duplex **53** was barely above background (Figure 32, lanes 5-7). 3 mM ethidium bromide produced slightly better DEP-**53** reactivity, but still much weaker than that observed with duplexes **47+48**, **49+50** and **51+52** under similar reaction conditions. Densitometric analysis of these results is shown in Figure 33 C and 33 D. All the adenosine residues resolved on the gel reacted feebly with DEP, and no DEP-guanosine reaction could be seen in the presence of echinomycin (Figure 33 C). Figure 33 D shows that most purines reacted weakly (A>G) with DEP when 3 mM ethidium bromide bound to duplex **53**. At pH 4.7 (Figure 32, lanes 14-22), overall purine-DEP reactivity was severely attenuated relative to the reaction at pH 7.0, regardless of the intercalator present. If Hoogsteen C·G base pairs formed at this pH within bound 5'-GCGT-3' or 5'-ACGC-3' echinomycin sites, DEP did not appear to detect the transition. In hopes of identifying the DEP-guanosine adduct and thus the base-pairing scheme at other echinomycin binding sites, we chose to examine the DEP/piperidine cleavage patterns of echinomycin and ethidium bromide bound to the sites 5'-CCGG-3' and 5'-GCGC-3'. The autoradiogram showing DEP/piperidine cleavage of duplex **54+55** without intercalators or in the presence of 140 μ M echinomycin or 3.4 mM ethidium

bromide appears in Figure 34. Very little DEP modification of the duplex was observed in the absence of intercalators (lanes 2-4 and 16-18). When 140 μ M echinomycin bound the duplex, guanosine residues occupying the first and fourth base-pair positions of 5'-CCGG-3' sites reacted strongly with DEP (lanes 5-7 and 19-21). Densitometric analysis revealed this reaction pattern to be specific, with minimal secondary reaction of other purines under these conditions (Figure 36 A). 3.4 mM ethidium bromide produced a different DEP/piperidine cleavage pattern (Figure 34, lanes 8-10 and 22-24). DEP reaction on the top strand was minimal and occurred at both guanosine residues of 5'-CCGG-3' sequences. On the lower strand at 3.4 mM ethidium bromide (Figure 34, lanes 22-24 and Figure 36 B), DEP reacted indiscriminately with all purines, A slightly greater than G. Ethidium bromide induced less overall DEP-guanosine and more overall DEP-adenosine reaction than did echinomycin on this duplex.

Figure 35 presents DEP/piperidine cleavage promoted by 140 μ M echinomycin and 3.4 mM ethidium bromide on duplex **60+61** that contains five 5'-GCGC-3' sequences. The top strand, labeled **60**, displayed only weak DEP reaction above background in the presence of either intercalator (Figure 35, lanes 2-10). When the lower strand was labeled, echinomycin yielded significant DEP-purine reactivity above background levels (lanes 19-21). Densitometric analysis of these lanes (Figure 36 C) shows that guanosines at the first or fourth base-pair positions of 5'-GCGC-3' sites reacted moderately with DEP, but not as efficiently as did adenosine residues immediately 5' adjacent to the 5'-GCGC-3' sites. Ethidium bromide gave rise to a less specific DEP/piperidine cleavage pattern on duplex **60+61** than did echinomycin: Most purines reacted with DEP and showed the usual A>G extent of reactivity (Figure 35 lanes 22-24 and Figure 36 D). It is interesting to note that in the presence of 140 μ M echinomycin, DEP-guanosine reactivity at 5'-GCGC-3' sites was less intense and less specific than that observed at 5'-CCGG-3' sites (compare Figure 36 A with Figure 36 C). This is very similar to what was observed at 5'-TCGA-3' and 5'-ACGT-3' sites where the 5'-TCGA-3' sites gave more intense and specific DEP-adenosine

reactivity in the presence of echinomycin (Figure 30 A and 30 C). This trend may be general for echinomycin binding sites of the class 5'-YCGU-3'.

Summary.

In preparation for the base release analysis of DEP-purine reaction products, it is helpful to recap the results of DEP/piperidine cleavage obtained by sequencing gel electrophoresis. Table 3 summarizes the results of DEP-purine reaction on all of the oligonucleotide duplexes studied so far.

Table 3. Summary of Polyacrylamide Gel Electrophoresis (PAGE) Analysis of DEP-Purine Reaction on Oligonucleotide Duplexes **47+48** through **60+61** in the Presence of Echinomycin and Ethidium Bromide.

Duplex	Sites (5'-3')	DEP reaction @ 1:5 Ech:bp	Overall DEP-A cleavage	Overall DEP-G cleavage
47+48	TCGA	Strong at sites, weak adjacent to sites	Ech>EB	--
49+50	ACGT	Moderate at sites, stronger adjacent to sites	EB>Ech	--
51+52	ACGT	Weak at sites, moderate adjacent to sites	EB>Ech	--
53	GCGT, ACGC	Very weak overall	EB>Ech	--
54+55	CCGG	Moderate to strong at site, very specific modification	EB>Ech (weak)	Ech>EB
60+61	GCGC	Moderate at sites, stronger adjacent to sites	EB>Ech	Ech~EB

Figure 34. Autoradiogram of the high-resolution denaturing polyacrylamide gel used to analyze DEP/piperidine cleavage of the oligonucleotide duplex **54+55** in the presence of echinomycin or ethidium bromide. Both 5' ³²P end-labeled **54** (lanes 1-12) and **55** (lanes 13-24) were used for opposite strand analysis on this duplex. Lanes are: 1 and 15, intact DNA standards (STD) incubated as for all other reactions on the gel but not treated with DEP or piperidine; 2-4 and 16-18, DEP/piperidine control cleavage of DNA in the absence of drugs (DEP); 5-7 and 19-21, DEP/piperidine cleavage of the duplex in the presence of 140 μ M echinomycin (DEP/ECH); 8-10 and 22-24, DEP/piperidine cleavage of DNA in the presence of 3.4 mM ethidium bromide (DEP/EB). After reaction with DEP, the reaction mixture was precipitated, divided into three portions and heated with 100 mM piperidine at 90°C for different lengths of time to insure that complete strand cleavage occurred at bases modified by DEP. The piperidine/heat reaction times are 15, 30 or 60 minutes reading from left to right in a given series. For example, lanes 5, 6, and 7 were heated with piperidine for 15, 30, and 60 minutes, respectively. Lanes 11 and 13 are the Maxam-Gilbert chemical sequencing G-specific reactions, lanes 12 and 14 are the Maxam-Gilbert chemical sequencing purine-specific reactions. The DEP reaction conditions were 100 mM Tris / 100 mM NaOAc, pH 7.0, 0.3 mM MgCl₂, 10% (v/v) methanol, 680 μ M oligonucleotide base pairs, 230 mM DEP (~330 equivalents to bp), and either 140 μ M echinomycin (ECH:DNA bp ~ 1:5) or 3.4 mM ethidium bromide (EB:DNA bp ~ 5:1). The gel contained 15% (w/v) polyacrylamide, crosslinked 1:20, 50% (w/v) urea, 1X TBE buffer (see Experimental) and 2% (v/v) glycerol to prevent cracking of the gel when drying. Gel dimensions were 0.4 mm thick at the top, 1.2 mm thick at the base, 40 cm long and 34 cm wide. Electrophoresis at 1500 V was continued until the bromophenol blue (BPB) marker dye had migrated 25 cm from the origin.

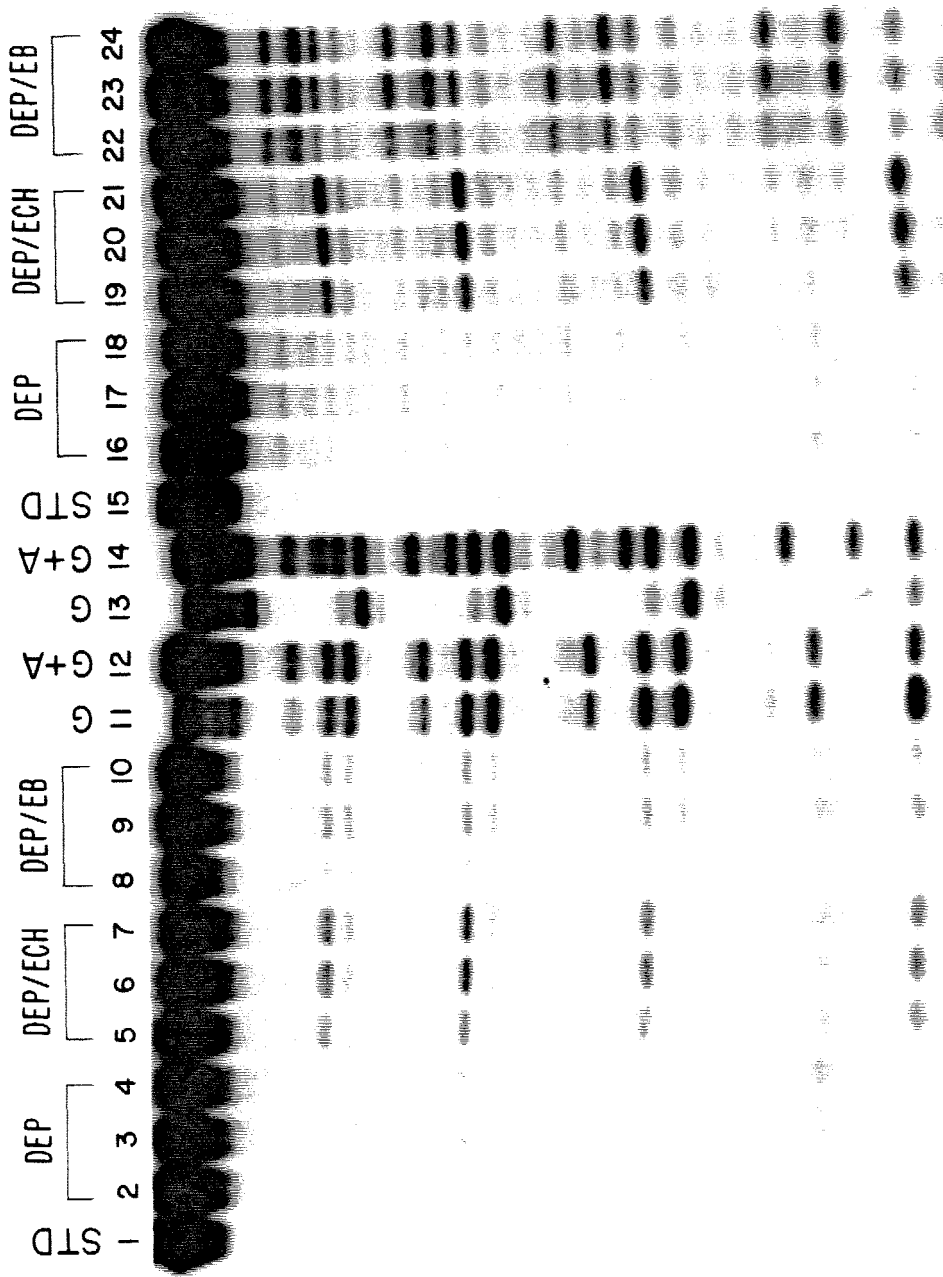


Figure 35. Autoradiogram of the high-resolution denaturing polyacrylamide gel used to analyze DEP/piperidine cleavage of the oligonucleotide duplex **60+61** in the presence of echinomycin or ethidium bromide. Both 5' ³²P end-labeled **60** (lanes 1-12) and **61** (lanes 13-24) were used for opposite strand analysis on this duplex. Lanes are: 1 and 15, intact DNA standards (STD) incubated as for all other reactions on the gel but not treated with DEP or piperidine; 2-4 and 16-18, DEP/piperidine control cleavage of DNA in the absence of drugs (DEP); 5-7 and 19-21, DEP/piperidine cleavage of the duplex in the presence of 140 μ M echinomycin (DEP/ECH); 8-10 and 22-24, DEP/piperidine cleavage of DNA in the presence of 3.4 mM ethidium bromide (DEP/EB). After reaction with DEP, the reaction mixture was precipitated, divided into three portions and heated with 100 mM piperidine at 90°C for different lengths of time to insure that complete strand cleavage occurred at bases modified by DEP. The piperidine/heat reaction times are 15, 30 or 60 minutes reading from left to right in a given series. For example, lanes 5, 6, and 7 were heated with piperidine for 15, 30, and 60 minutes, respectively. Lanes 11 and 13 are the Maxam-Gilbert chemical sequencing G-specific reactions, lanes 12 and 14 are the Maxam-Gilbert chemical sequencing purine-specific reactions. The DEP reaction conditions were 100 mM Tris / 100 mM NaOAc, pH 7.0, 0.3 mM MgCl₂, 10% (v/v) methanol, 680 μ M oligonucleotide base pairs, 230 mM DEP (~330 equivalents to bp), and either 140 μ M echinomycin (ECH:DNA bp ~ 1:5) or 3.4 mM ethidium bromide (EB:DNA bp ~ 5:1). The gel contained 15% (w/v) polyacrylamide, crosslinked 1:20, 50% (w/v) urea, 1X TBE buffer (see Experimental) and 2% (v/v) glycerol to prevent cracking of the gel when drying. Gel dimensions were 0.4 mm thick at the top, 1.2 mm thick at the base, 40 cm long and 34 cm wide. Electrophoresis at 1500 V was continued until the bromophenol blue (BPB) marker dye had migrated 25 cm from the origin.

STD 1
2 3 4 DEP
5 6 7 DEP/ECH
8 9 10 DEP/EB
11 G
12 G+A
13 G
14 G+A
15 STD
16 17 18 DEP
19 20 21 DEP/ECH
22 23 24 DEP/EB

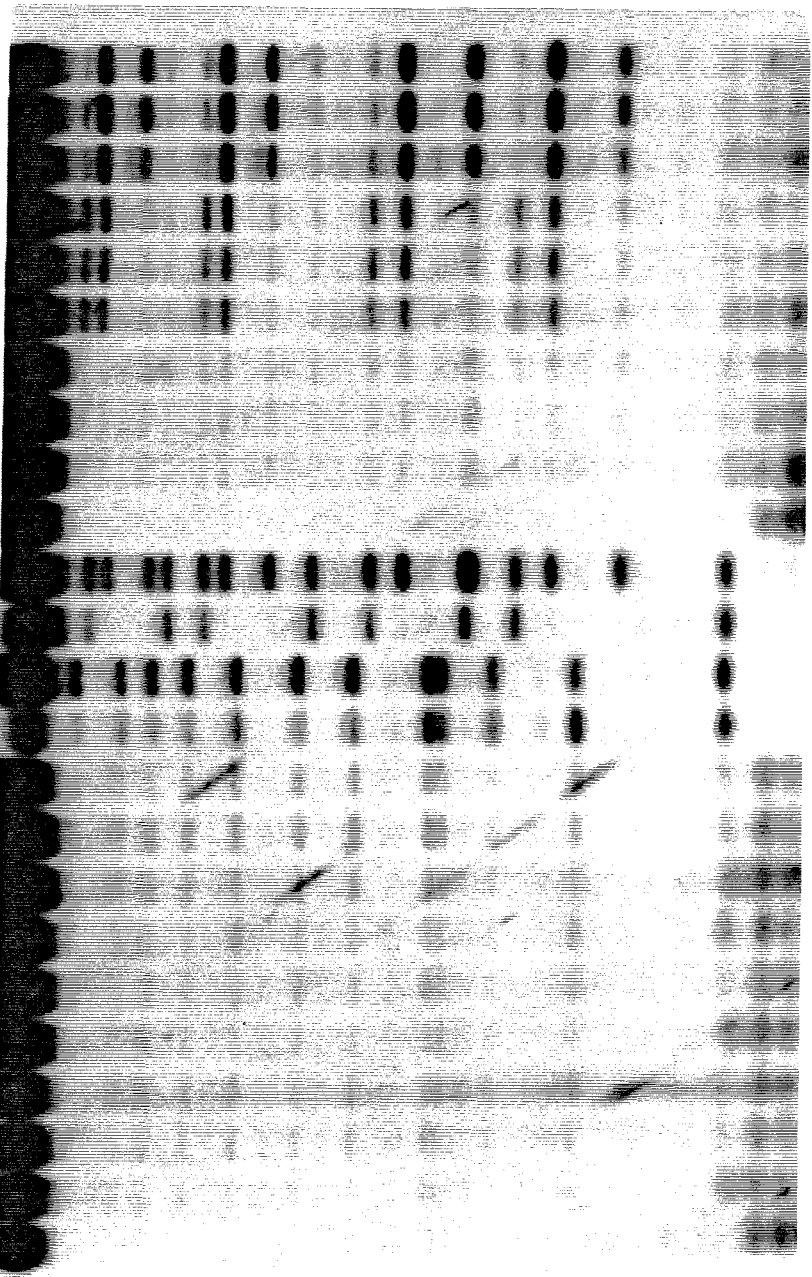
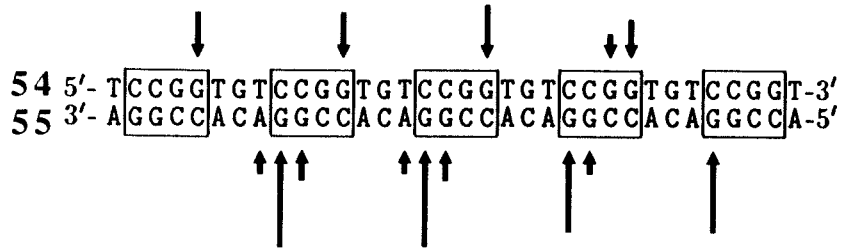


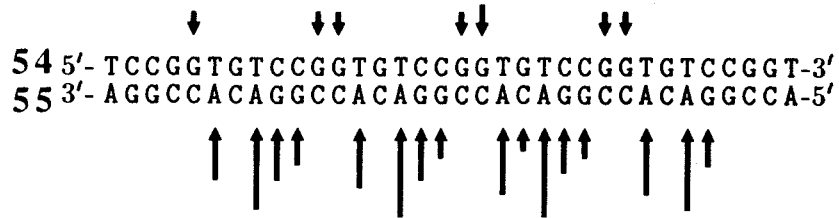
Figure 36. (A-D) DEP/piperidine cleavage of oligonucleotide duplexes **54+55** (A-B) and **60+61** (C-D) in the presence of 120 μ M echinomycin, A and C, or 3 mM ethidium bromide, B and D, as determined by densitometry of the autoradiograms of Figures 34 and 35. Lanes 4 and 18 were scanned to analyze DEP/piperidine cleavage of unbound DNA, 7 and 21 for DEP/piperidine cleavage of DNA bound by echinomycin, and 10 and 24 for DEP/piperidine cleavage of DNA bound by ethidium bromide. DEP/piperidine cleavage patterns are shown as arrows with height proportional to the enhancement of cleavage at each nucleotide compared to DEP/piperidine cleavage of unbound DNA. No data are available for the 5' and 3' terminal three to four base pairs of each oligonucleotide because of the limits of 15% polyacrylamide gel resolution. Designed four base pair echinomycin binding sites are boxed in A and C.

A

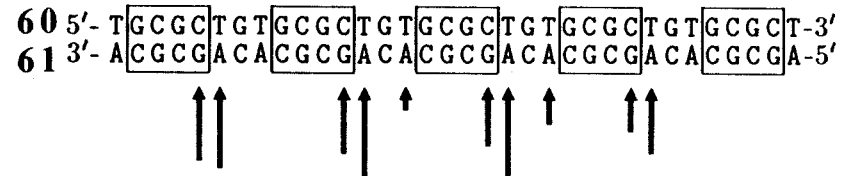
Ech

**B**

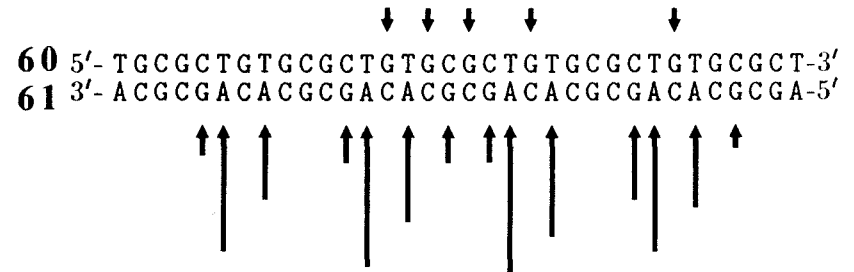
EB

**C**

Ech

**D**

EB



HPLC analysis of DEP-DNA reaction products.

Although the DEP/piperidine cleavage patterns shown in Figures 28 to 36 describe the intensity and specificity of DEP-purine reaction produced by echinomycin and ethidium bromide binding to various DNA sequences, the purine centers responsible for the observed reactivity were still unknown at this point. By scaling up the DEP-oligonucleotide reactions and then depurinating the DNA, we identified the purine-DEP adducts that correspond to the cleavage bands shown in the autoradiograms above. This analysis allowed us to describe the nucleic acid structure of echinomycin·DNA complexes at *specific* binding sites in solution. Figures 37 to 43 display the HPLC chromatograms of depurinated large-scale oligonucleotide-DEP reactions performed without intercalators or in the presence of ethidium bromide or echinomycin. Reaction conditions for the large-scale DEP-oligonucleotide reactions were virtually identical to those employed for gel electrophoretic analysis except for the depurination step.

There was good correspondence between the HPLC chromatograms and the autoradiograms presented above. For example, Figures 37 to 39 present the HPLC traces of bases released from reaction of DEP with duplexes **47+48**, **49+50** and **51+52**, respectively. When reactions were conducted in the absence of intercalating agents (Figures 37 A to 39 A), unmodified bases cytosine (peak 1), guanine (peak 2), and adenine (peak 4) as well as relatively small amounts of another material (peak 3) were released from the DNA. In the presence of 140 μ M echinomycin, DEP-duplex reactions produced more peak 3 relative to unbound DNA in the order **47+48** > **49+50** ~ **51+52** (Figures 37 B to 39 B). Furthermore, DEP-duplex reactions in the presence of 3.4 mM ethidium bromide also produced more peak 3 material relative to controls in the order **51+52** ~ **49+50** > **47+48** (Figures 37 C to 39 C). Both of these findings correlated well with the extent of DEP/piperidine cleavage at adenosine residues observed on these duplexes in the autoradiograms of Figures 28, 29 and 31. It thus appeared that peak 3 was a DEP-adenosine adduct. Peak 3 had the same HPLC retention time and UV spectrum for both

Figure 37. (A-C) Reversed-phase HPLC chromatograms of base-release products obtained by heat/formic acid treatment of 100 nmol scale DEP-oligonucleotide duplex **47+48** reactions either in the absence of intercalators (A) or in the presence of 136 μ M echinomycin (B) or 3.4 mM ethidium bromide (C). Peaks: 1, cytosine; 2, guanine; 3, DEP-adenosine adduct; 4, adenine; 5, internal standard *p*-anisaldehyde; 6, DEP-ethidium bromide adduct. Peak assignment was based on identical ultraviolet spectra and HPLC retention times (coelution) of reference compounds. The ultraviolet spectrum of DEP-adenosine adduct peak 3 is displayed in panel D. HPLC method RAMP3 (see Experimental) was used to separate the reaction products.

DEP-Duplex 47+48 Reaction Products

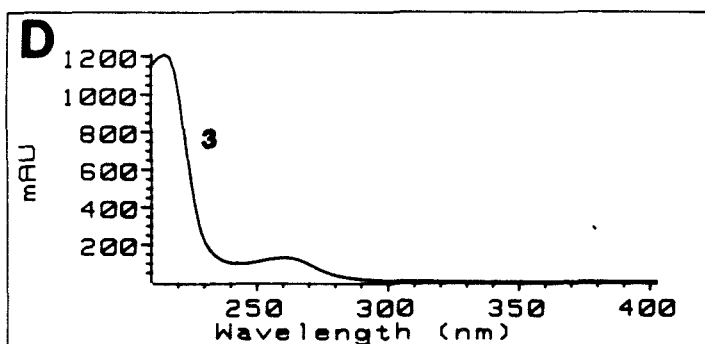
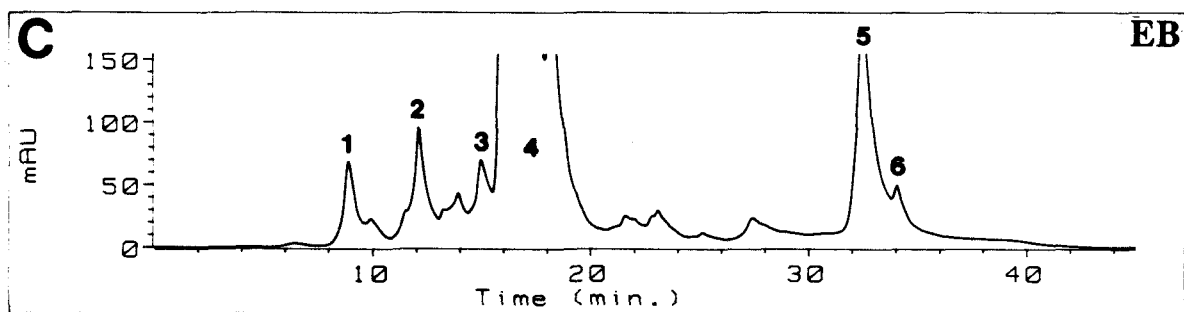
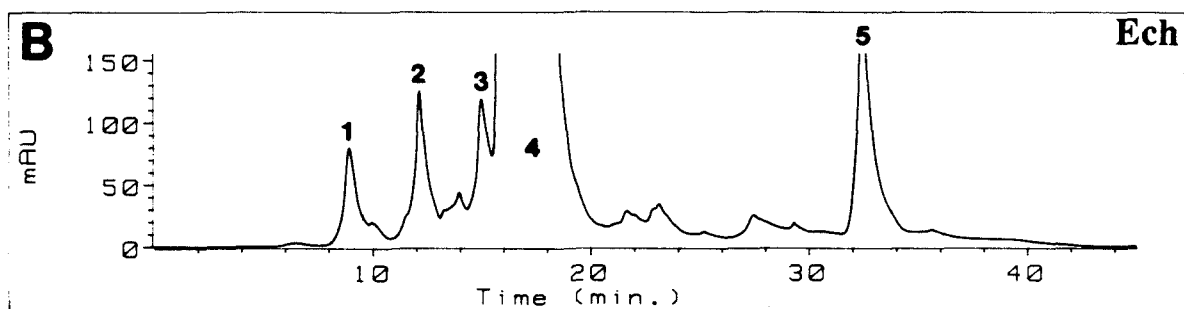
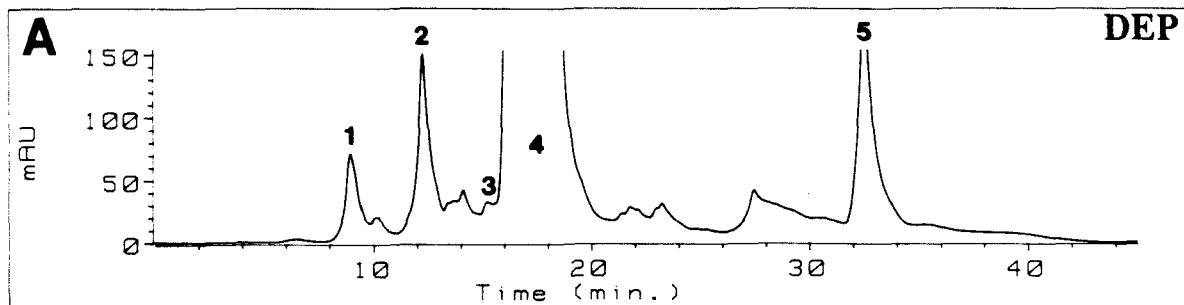


Figure 38. (A-C) Reversed-phase HPLC chromatograms of base-release products obtained by heat/formic acid treatment of 100 nmol scale DEP-oligonucleotide duplex **49+50** reactions either in the absence of intercalators (A) or in the presence of 136 μ M echinomycin (B) or 3.4 mM ethidium bromide (C). Peaks: 1, cytosine; 2, guanine; 3, DEP-adenosine adduct; 4, adenine; 5, internal standard *p*-anisaldehyde; 6, DEP-ethidium bromide adduct. Peak assignment was based on identical ultraviolet spectra and HPLC retention times (coelution) of reference compounds. The ultraviolet spectrum of DEP-adenosine adduct peak 3 is displayed in panel D. HPLC method RAMP3 (see Experimental) was used to separate the reaction products.

DEP-Duplex 49+50 Reaction Products

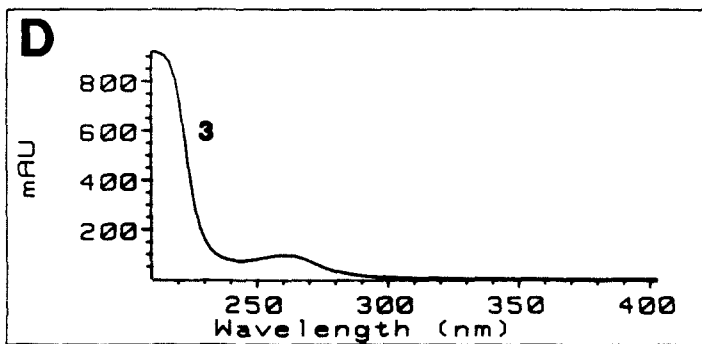
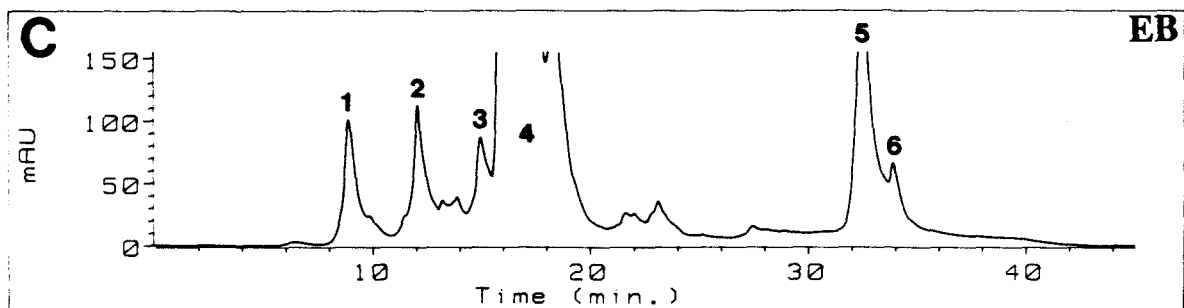
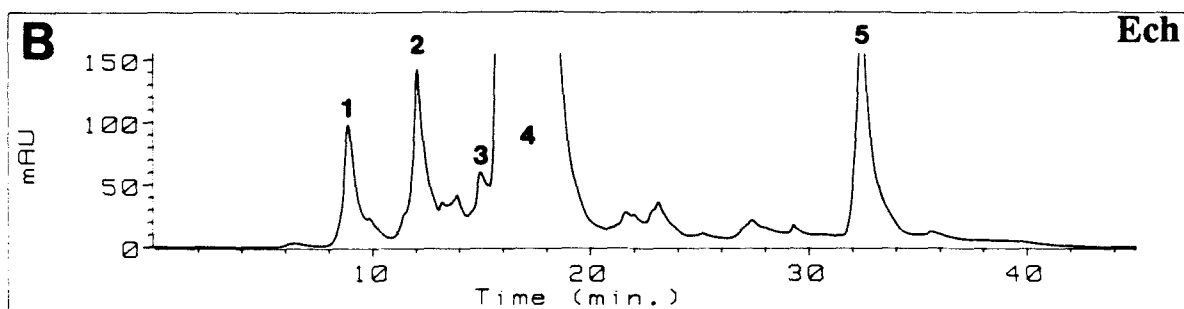
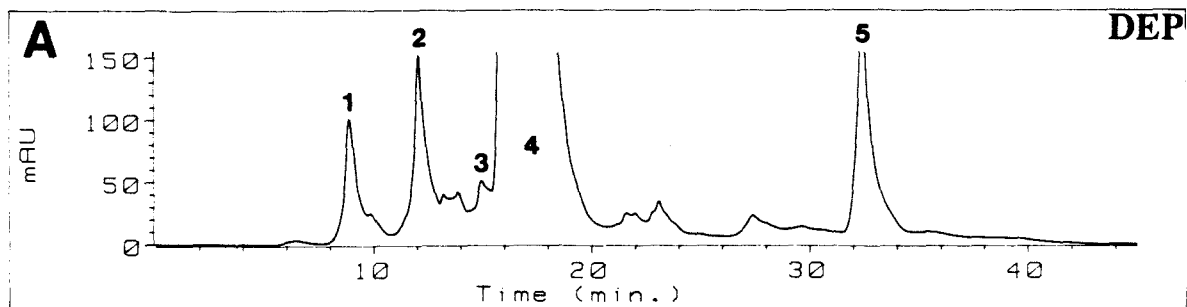


Figure 39. (A-C) Reversed-phase HPLC chromatograms of base-release products obtained by heat/formic acid treatment of 100 nmol scale DEP-oligonucleotide duplex **51+52** reactions either in the absence of intercalators (A) or in the presence of 144 μ M echinomycin (B) or 3.6 mM ethidium bromide (C). Peaks: 1, cytosine; 2, guanine; 3, DEP-adenosine adduct; 4, adenine; 5, internal standard *p*-anisaldehyde; 6, DEP-ethidium bromide adduct. Peak assignment was based on identical ultraviolet spectra and HPLC retention times (coelution) of reference compounds. The ultraviolet spectrum of DEP-adenosine adduct peak 3 is displayed in panel D. HPLC method RAMP3 (see Experimental) was used to separate the reaction products.

DEP-Duplex 51+52 Reaction Products

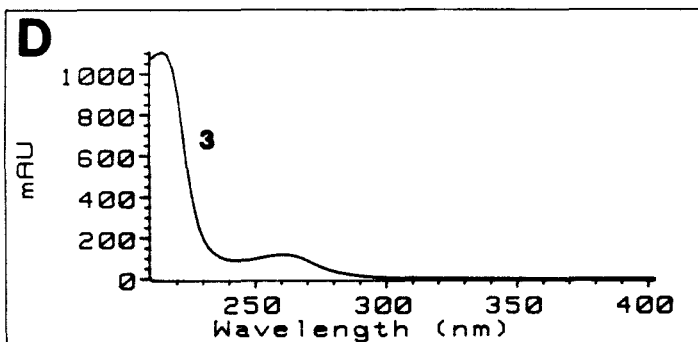
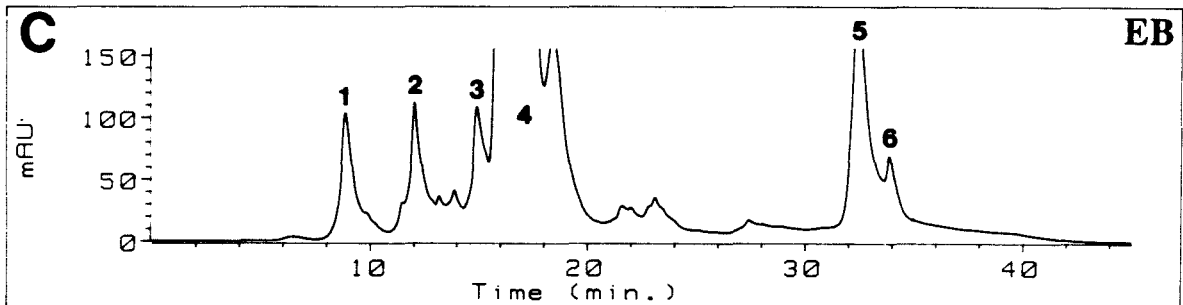
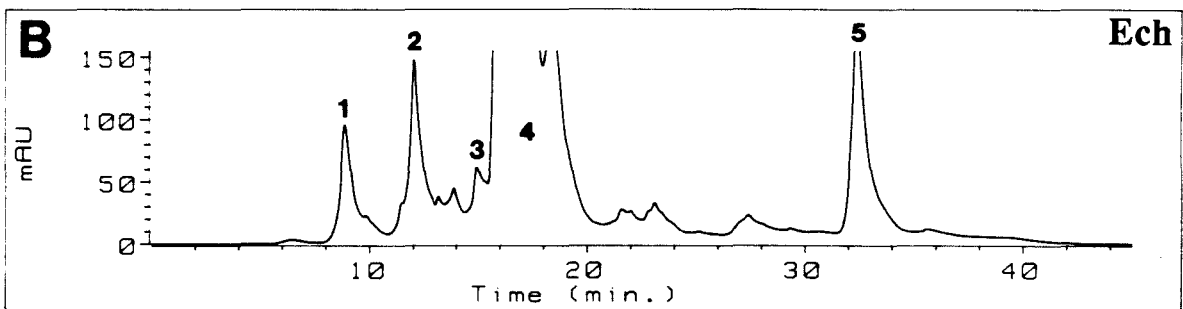
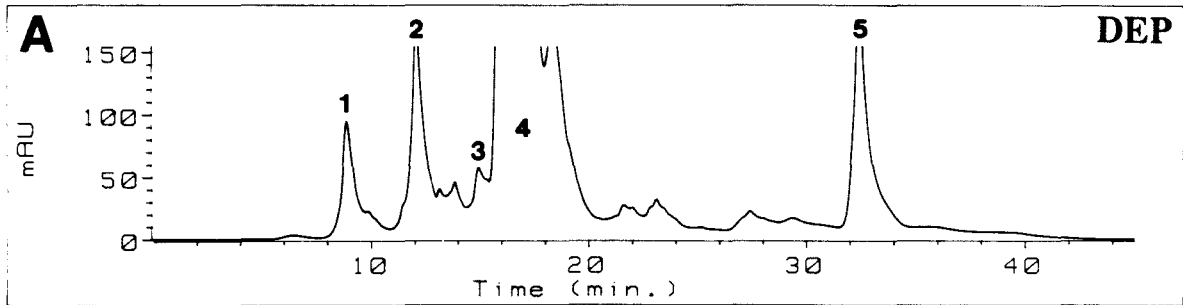


Figure 40. (A-C) Reversed-phase HPLC chromatograms of base-release products obtained by heat/formic acid treatment of 100 nmol scale DEP-oligonucleotide duplex **53** reactions either in the absence of intercalators (A) or in the presence of 128 μ M echinomycin (B) or 3.2 mM ethidium bromide (C). Peaks: 1, cytosine; 2 (shoulder), DEP-guanine adduct; 3, guanine; 4, DEP-adenine adduct; 5, adenine; 6, unknown; 7, internal standard *p*-anisaldehyde; 8, DEP-ethidium bromide adduct. Peak assignment was based on identical ultraviolet spectra and HPLC retention times (coelution) of reference compounds. The ultraviolet spectra of DEP-guanosine and DEP-adenosine adducts peaks 2 and 4 are displayed in panels D and E, respectively. HPLC method RAMP3 (see Experimental) was used to separate the reaction products.

DEP-Duplex 53 Reaction Products

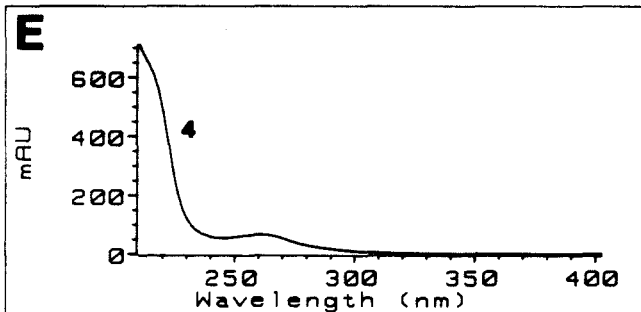
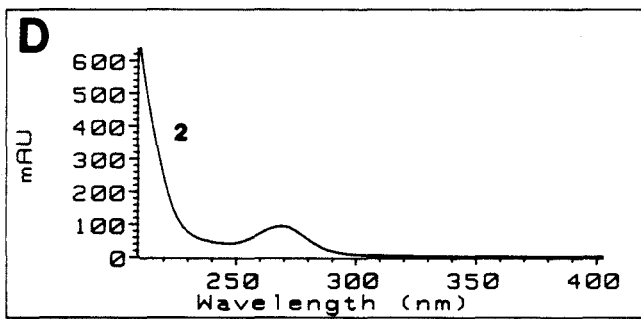
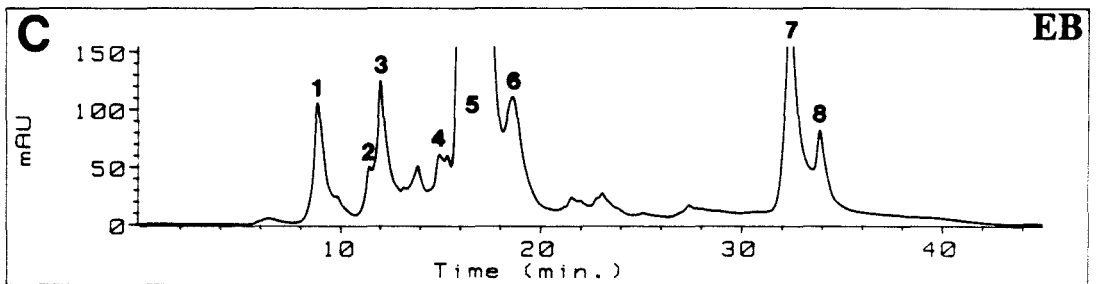
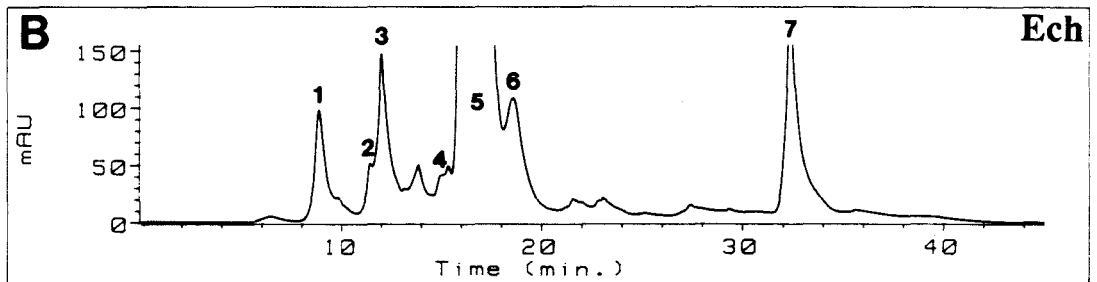
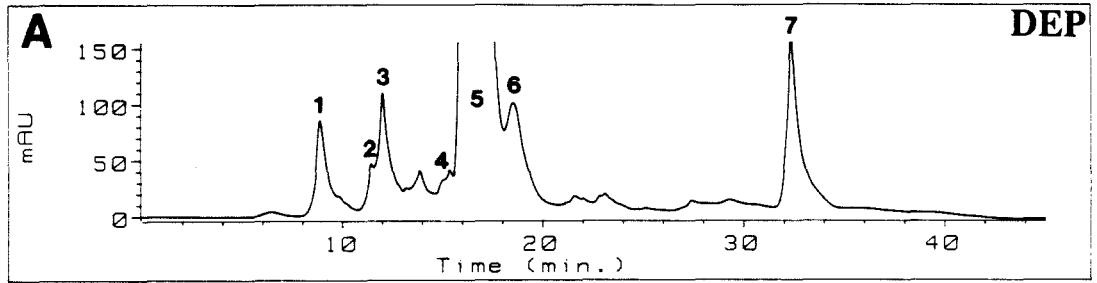


Figure 41. (A-C) Reversed-phase HPLC chromatograms of base-release products obtained by heat/formic acid treatment of 100 nmol scale DEP-oligonucleotide duplex **56+57** reactions either in the absence of intercalators (A) or in the presence of 128 μ M echinomycin (B) or 3.2 mM ethidium bromide (C). Peaks: 1, cytosine; 2, DEP-guanosine adduct; 3, guanine; 4, DEP-adenosine adduct; 5, adenine; 6, internal standard *p*-anisaldehyde; 7, DEP-ethidium bromide adduct; 8, echinomycin from previous injection. Peak assignment was based on identical ultraviolet spectra and HPLC retention times (coelution) of reference compounds. The ultraviolet spectra of DEP-guanosine and DEP-adenosine adducts peaks 2 and 4 are displayed in panels D and E, respectively. HPLC method RAMP9 (see Experimental) was used to separate the reaction products.

DEP-Duplex 56+57 Reaction Products

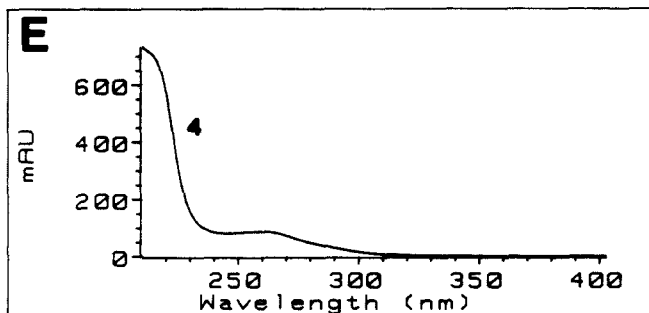
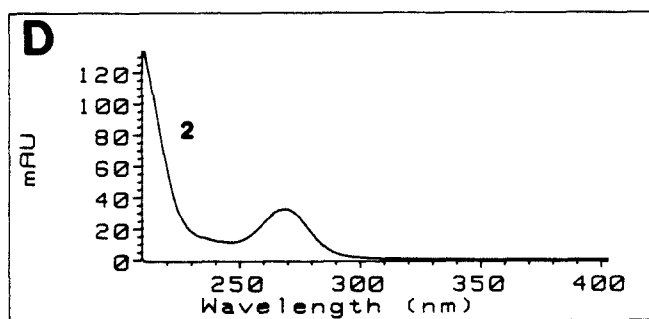
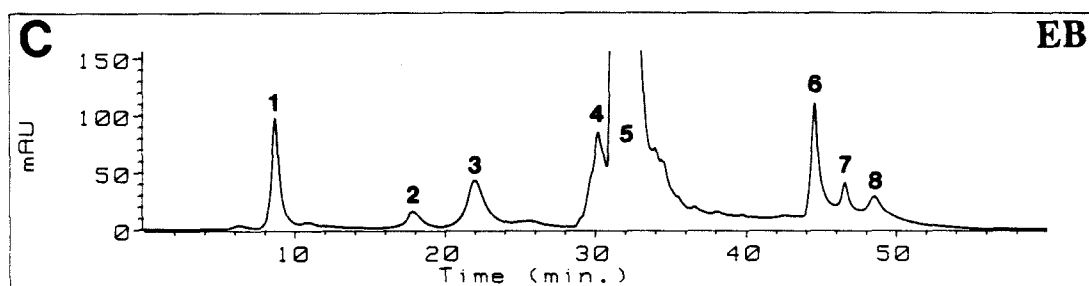
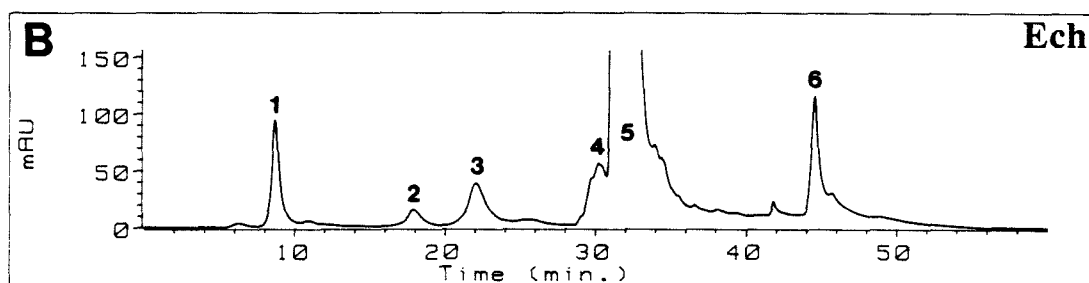
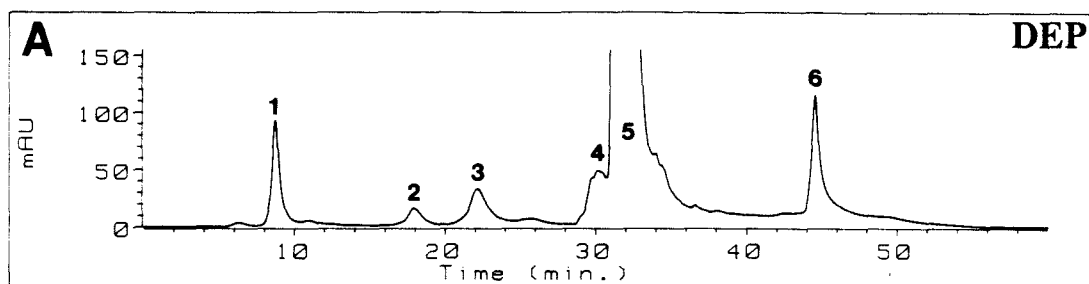


Figure 42. (A-C) Reversed-phase HPLC chromatograms of base-release products obtained by heat/formic acid treatment of 100 nmol scale DEP-oligonucleotide duplex **54+55** reactions either in the absence of intercalators (A) or in the presence of 136 μ M echinomycin (B) or 3.4 mM ethidium bromide (C). Peaks: 1, cytosine; 2, DEP-guanosine adduct; 3, guanine; 4, DEP-adenosine adduct; 5, adenine; 6, internal standard *p*-anisaldehyde; 7, DEP-ethidium bromide adduct; 8, echinomycin from previous injection. Peak assignment was based on identical ultraviolet spectra and HPLC retention times (coelution) of reference compounds. The ultraviolet spectra of DEP-guanosine and DEP-adenosine adducts peaks 2 and 4 are displayed in panels D and E, respectively. HPLC method RAMP9 (see Experimental) was used to separate the reaction products.

DEP-Duplex 54+55 Reaction Products

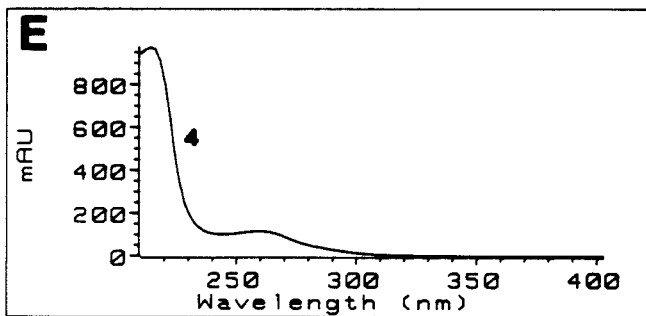
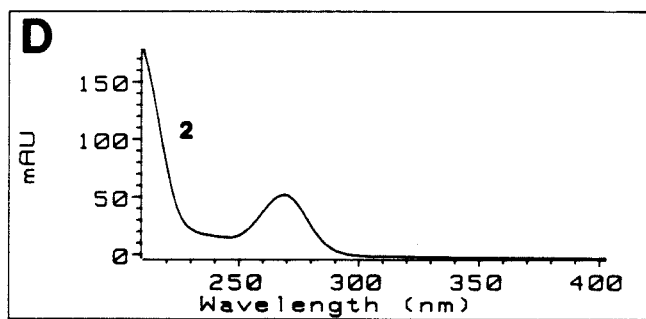
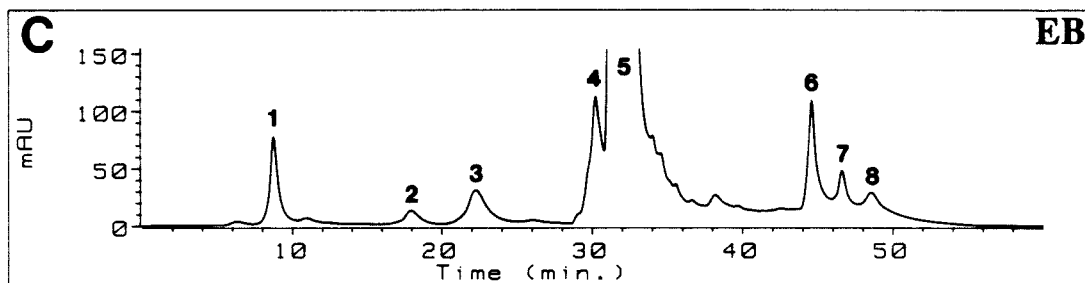
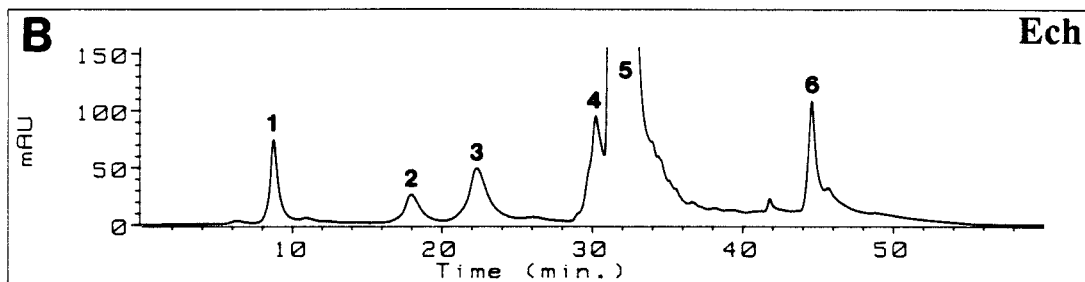
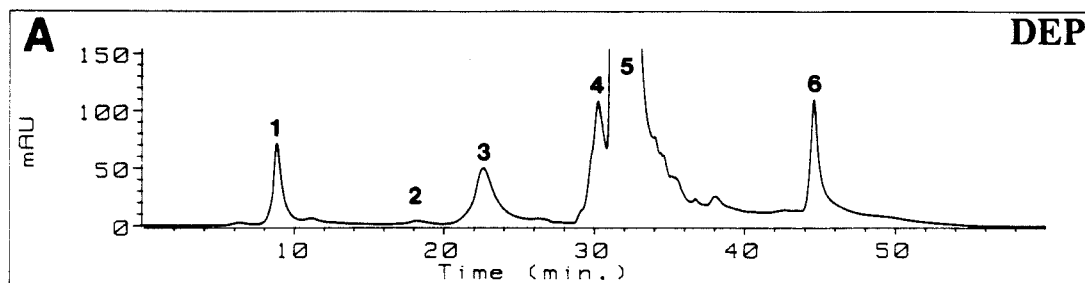
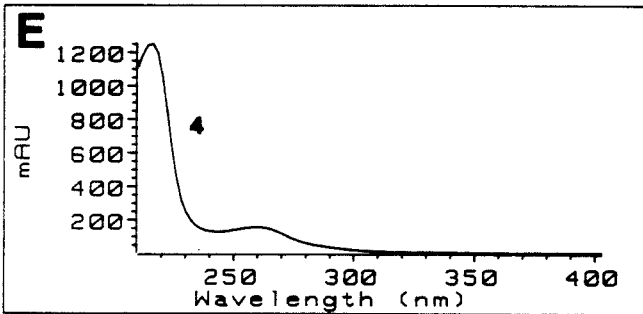
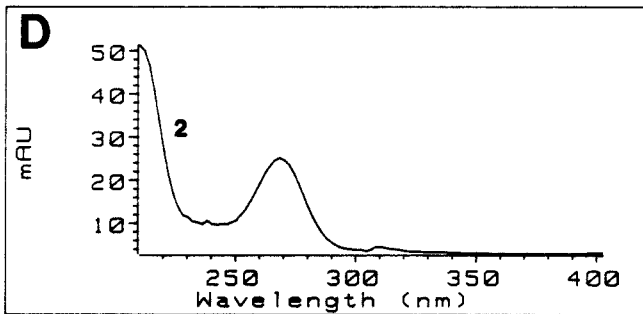
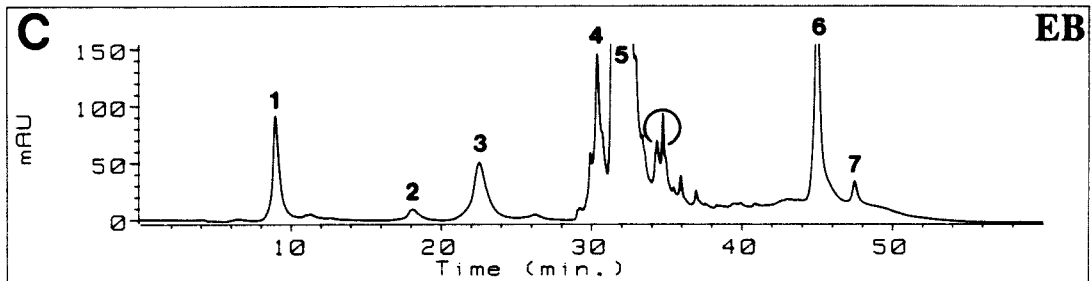
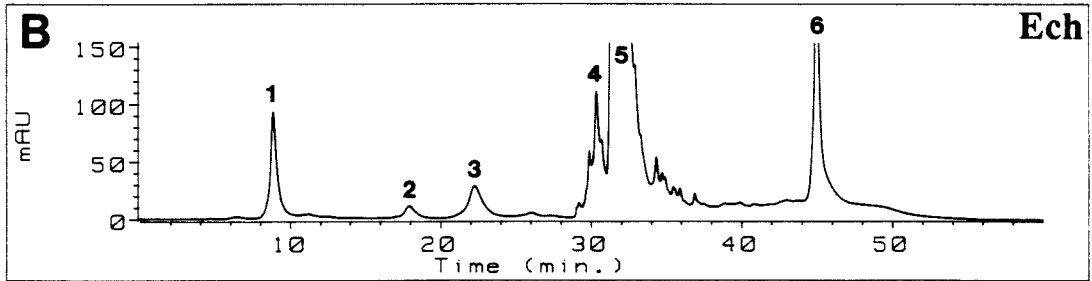
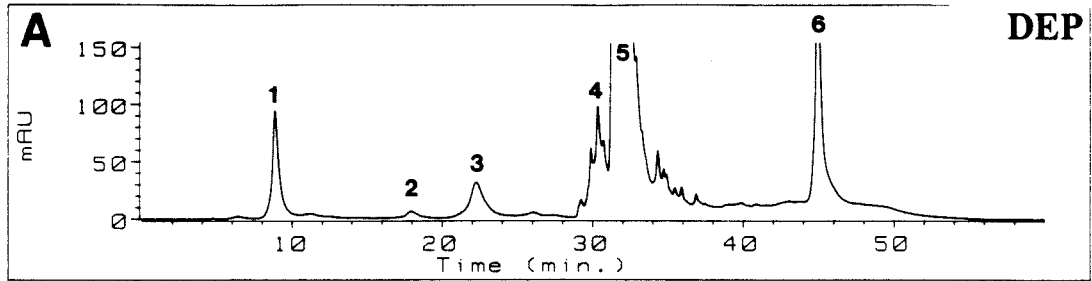


Figure 43. (A-C) Reversed-phase HPLC chromatograms of base-release products obtained by heat/formic acid treatment of 100 nmol scale DEP-oligonucleotide duplex **60+61** reactions either in the absence of intercalators (A) or in the presence of 136 μ M echinomycin (B) or 3.4 mM ethidium bromide (C). Peaks: 1, cytosine; 2, DEP-guanosine adduct; 3, guanine; 4, DEP-adenosine adduct; 5, adenine; 6, internal standard *p*-anisaldehyde; 7, DEP-ethidium bromide adduct. The circled peaks in panel C have not been assigned but appear to be small DNA fragments. Peak assignment was based on identical ultraviolet spectra and HPLC retention times (coelution) of reference compounds. The ultraviolet spectra of DEP-guanosine and DEP-adenosine adducts peaks 2 and 4 are displayed in panels D and E, respectively. HPLC method RAMP9 (see Experimental) was used to separate the reaction products.

DEP-Duplex 60+61 Reaction Products



echinomycin and ethidium bromide containing DEP-DNA reactions (Figures 37 D to 39 D). Therefore, bound echinomycin and ethidium bromide both gave rise to the same DEP-adenosine adduct, but in different amounts depending on nucleic acid sequence. The identity of the DEP-adenosine adduct will be discussed shortly.

HPLC chromatograms of base-release products from DEP-oligonucleotide **53** and **56+57** duplex reactions are presented in Figures 40 and 41, respectively. Panels A-C of Figure 40 show little difference in the array of DEP-modified bases whether the reaction was performed without intercalators or in the presence of 120 μ M echinomycin or 3.2 mM ethidium bromide. This is not surprising since DEP/piperidine cleavage of duplex **53** was very weak in the autoradiogram of Figure 32. **56+57**-DEP reaction products were resolved using a different HPLC solvent gradient to better resolve peaks 2 and 3 (Figure 41). Duplex **56+57** contained the same 5'-ACGC-3' and 5'-GCGT-3' echinomycin binding sites as did duplex **53**, but in a slightly different arrangement. In this instance, no comparison between base-release and DEP/piperidine cleavage could be made because the high resolution PAGE analysis of DEP/piperidine cleavage on duplex **56+57** was not performed. Like **53**, the products released from **56+57**-DEP reactions did not differ a great deal whether intercalators were absent or present (Figure 41 A-C). When 3.2 mM ethidium bromide was present, a small increase was observed in the amount of peak 4 produced relative to **56+57**-DEP reactions in the absence of intercalator (Figure 41 C and A). Peak 4 in Figures 40 and 41 appeared to be a DEP-adenosine adduct. In fact, when chromatographed under identical conditions, this peak coeluted with peak 3 shown in Figures 37-39, suggesting that they were the same adduct.

Figures 42 and 43 display the HPLC chromatograms of depurinated DEP-duplex **54+55** and DEP-duplex **60+61** reactions, respectively. In the absence of intercalators, panels A, formic acid/heat treatment released cytosine (peak 1), guanine (peak 3), and adenine (peak 5) as well as a small amount of another compound (peak 2) from the strands. DEP-duplex **54+55** reactions in the presence of 140 μ M echinomycin give a more intense

peak 2 signal (Figure 42 A and 42 B). For DEP-**54+55** reactions containing 3.4 mM ethidium bromide, more peak 2 was produced relative to DEP control reactions, but less than that produced in the presence of 140 μ M echinomycin (Figure 42 C). For duplex **60+61**-DEP reactions the extent of peak 2 formation was significantly less than that observed for duplex **54+55**-DEP reactions (Figure 43) . Here, the amount of peak 2 formed in reactions containing either echinomycin (Figure 43 B) or ethidium bromide (Figure 43 C) was only slightly above background levels (Figure 43 A). On duplexes **54+55** and **60+61**, there was good correlation between the amount of peak 2 formed in the base release analysis and the degree of DEP/piperidine cleavage observed at guanosine residues on the high-resolution gel assay (see Table 4 below). This suggested very strongly that peak 2 in Figures 42 and 43 was a DEP-guanosine adduct. It is important to note that peak 2 had the same UV spectrum and HPLC retention time whether produced in reactions containing ethidium bromide or echinomycin. By these criteria, echinomycin and ethidium bromide gave rise to identical DEP-guanosine adducts just as they gave rise to identical DEP-adenosine adducts on other duplexes.

A steady increase in the amount of peak 4 formed in DEP-duplex **60+61** reactions was observed on going from reactions performed without intercalator to those containing 140 μ M echinomycin and then 3.4 mM ethidium bromide (Figure 43 A, B and C, respectively). A similar trend was observed on the high-resolution gel analysis of identical reactions where the amount of DEP/piperidine cleavage at *adenosine* residues on duplex **60+61** followed the order EB > Ech > control (Figures 35-36). Peak 4 in Figures 43 A-C thus appeared to be a DEP-adenosine adduct. It was judged to be the same DEP-adenosine adduct assigned as peak 3 in the DEP-**47+48**, **49+50** and **51+52** reactions because their HPLC retention times and UV spectra were identical when chromatographed under the same conditions.

Table 4 compares the level of DEP/piperidine cleavage at purines on oligonucleotide duplexes **47+48** through **60+61** in the presence of echinomycin or ethidium bromide on denaturing polyacrylamide gels to the amount of DEP-purine adducts formed in the base-release assay under identical DEP reaction conditions. There was good agreement between the overall purine-DEP cleavage observed on gels and the amount of specific DEP-purine adducts formed in the base-release assay. This agreement strongly implied that the formic acid/heat treatment released all the nucleobases modified by DEP. Therefore, it appeared that the DEP-purine adducts formed on these duplexes in the presence of intercalators possess labile glycosidic bonds such that DEP-base modification can be developed into a DNA strand scission event by heating with piperidine. Figures 37-43 demonstrate that although different amounts of DEP-purine adducts were formed on DNA in the presence of echinomycin and ethidium bromide, both intercalators led to the formation of the same DEP-adenosine and DEP-guanosine adducts based on identical HPLC retention times and UV spectra. Furthermore, only one DEP-adenosine and one DEP-guanosine adduct appeared to be formed regardless of the intercalator or DNA base sequence used in the reaction. This finding immediately argued that DEP did not detect Hoogsteen base-pairing in solution but rather simple helix unwinding caused by antibiotic intercalation.

Table 4. Summary of Polyacrylamide Gel Electrophoresis (PAGE) and HPLC Analysis of DEP-Purine Reaction on Oligonucleotide Duplexes 47+48 through 60+61 in the Presence of Echinomycin and Ethidium Bromide.

Duplex	Sites (5'-3')	DEP reaction @ 1:5 Ech:bp	PAGE Overall DEP-A cleavage	PAGE Overall DEP-G cleavage	HPLC Overall DEP-A adduct	HPLC Overall DEP-G adduct
47+48	TCGA	Strong at sites, weak adjacent to sites	Ech>EB	--	Ech>EB	--
49+50	ACGT	Moderate at sites, stronger adjacent to sites	EB>Ech	--	EB>Ech	--
51+52	ACGT	Weak at sites, moderate adjacent to sites	EB>Ech	--	EB>Ech	--
53	GCGT ACGC	Very weak overall	EB>Ech	--	EB>Ech	--
56+57	GCGT ACGC	Very weak on HPLC	--	--	EB>Ech (weak)	--
54+55	CCGG	Moderate to strong at site, very specific modification	EB>Ech (weak)	Ech>EB	EB>Ech (weak)	Ech>EB
60+61	GCGC	Moderate at sites, stronger adjacent to sites	EB>Ech	Ech~EB	EB>Ech	Ech~EB

Synthesis and characterization of reference compounds.

That both echinomycin and ethidium bromide led to DEP-purine adducts with labile glycosidic bonds suggested that DEP-purine reaction on "large DNA" occurs at purine N7 centers as demonstrated by the studies of N. J. Leonard and co-workers.⁹³⁻⁹⁶ If this were the case, depurination of DEP-modified DNA should give 5-carbethoxyamino-4,6-diaminopyrimidine and 5-carbethoxyamino-2,4-diamino-6-hydroxypyrimidine as the DEP-adenosine and DEP-guanosine adducts, respectively. Figure 44 depicts the structures of these compounds.

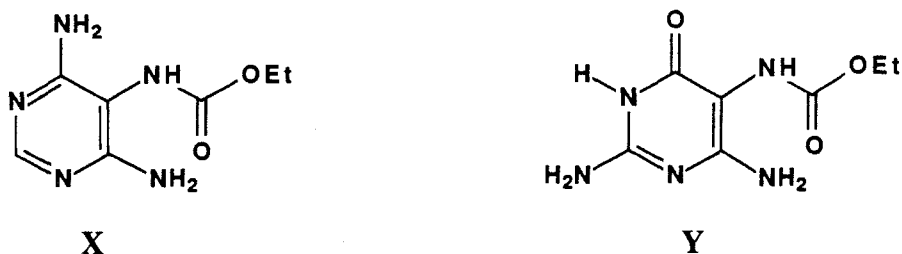


Figure 44. 5-carbethoxyamino-4,6-diaminopyrimidine ("X") and 5-carbethoxyamino-2,4-diamino-6-hydroxypyrimidine ("Y").

Each HPLC injection in Figures 37 to 43 consumed about 30% of the total 100 nmol scale oligonucleotide-DEP reaction. Reactions of this scale could not provide enough material for characterization by NMR spectroscopy, and this necessitated the synthesis and characterization of reference compounds. We then assigned the structures of DEP-purine adducts formed on duplexes **47+48** through **60+61** based on reference compounds whose HPLC retention characteristics and ultraviolet spectra matched those DEP-purine adduct peaks found in the HPLC chromatograms of Figures 37 to 43. This in turn revealed the purine atom centers responsible for DNA-DEP hyperreactivity in the presence of echinomycin or ethidium bromide and also described the DNA base-pairing at echinomycin binding sites in solution.

From the data presented above, the two pyrimidines shown in Figure 44 were likely to represent the DEP-purine adducts and were thus chosen as the first synthetic targets. Pyrimidine **X** is a known compound, synthesized by reacting a low concentration of ethyl chloroformate with 4,5,6-triaminopyrimidine in pyridine at 0°C (see Figure 45).⁹⁴ The reported proton NMR and mass spectra of this compound were consistent with the assigned structure, but assignment of the positional isomer was still equivocal. This was an easy problem to solve: If substitution occurs on the 5-amino group as assigned, the product is symmetrical about a mirror plane passing through the C2 and C5 atom centers. Therefore, carbons 4 and 6 are equivalent and the ¹³C NMR spectrum should show only six different carbon signals. Seven different carbon signals would be observed if substitution occurred at the 4 or 6 positions. We synthesized **X** according to the published procedure and found its mass and ¹H NMR spectra to be as reported (see Experimental section and Figure 48 A). The completely proton decoupled ¹³C NMR spectrum of **X** and its precursor base 4,5,6-triaminopyrimidine are shown in Figure 47. Peak assignments were made based on the chemical shift values given by Silverstein, Bassler and Morrill.⁹⁷ As expected, the precursor base 4,5,6-triaminopyrimidine showed only three different resonances (at 151.5, 147.6 and 106.6 ppm relative to internal standard DMSO-d₆ at 39.5 ppm, Figure 47 A). Product **X** clearly showed only six different carbon resonances at 156.4, 154.4, 147.2, 93.1, 60.7 and 14.4 ppm (Figure 47 B). Based on this finding, product **X** was unequivocally 5-carbethoxyamino-4,6-diaminopyrimidine.

Product **Y** was made according to the scheme presented in Figure 46 (see Experimental section for more details). The conversion of **A** to **C** via nitrosation and reduction has been known for nearly 90 years.⁹⁸ Reaction of ethyl chloroformate with **C** under slightly basic conditions formed a white precipitate. When recrystallized from hot water, this material gave about 30% **Y** as pale yellow needles. The assigned ¹H NMR spectrum of **Y** is shown in Figure 48 B. Synthetic material had a mass of 213 g/mole (C₇H₁₁N₅O₃) and showed carbonyl absorptions in the infrared. Thus, structure **Y** was

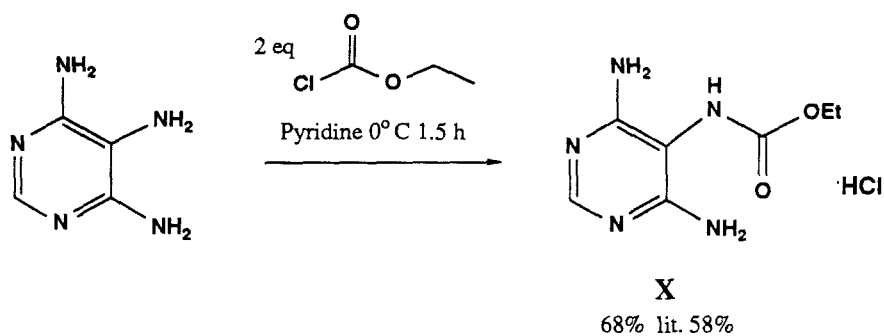


Figure 45. Synthesis of X, 5-carbethoxyamino-4,6-diaminopyrimidine.

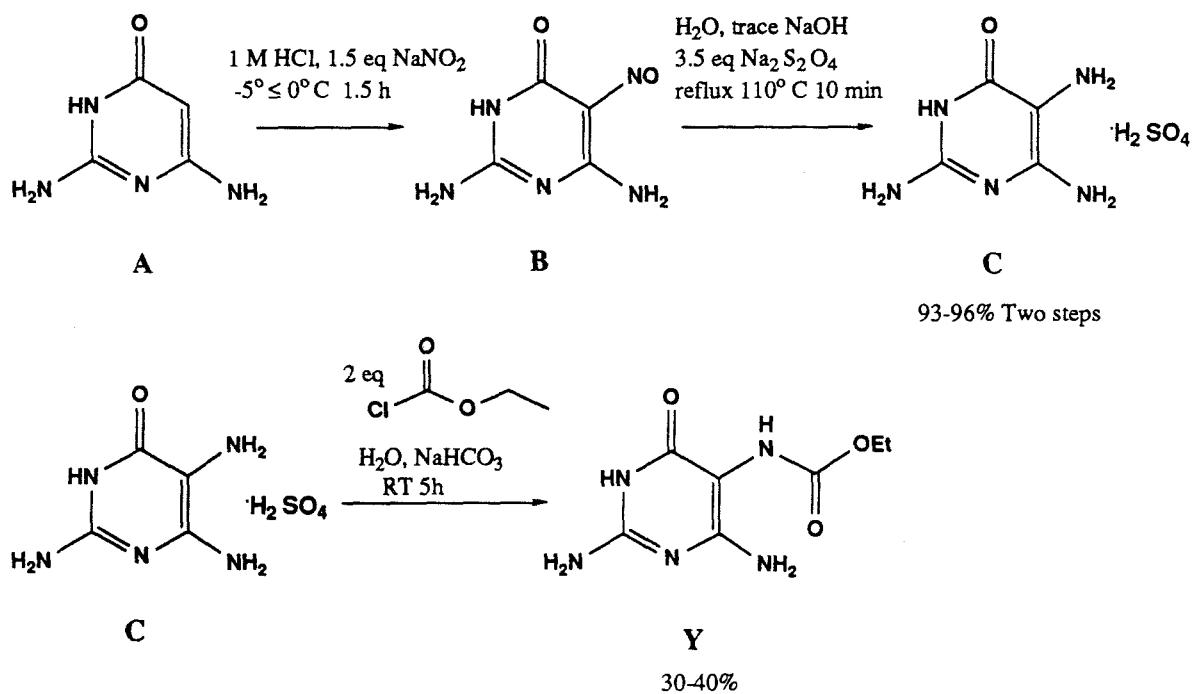
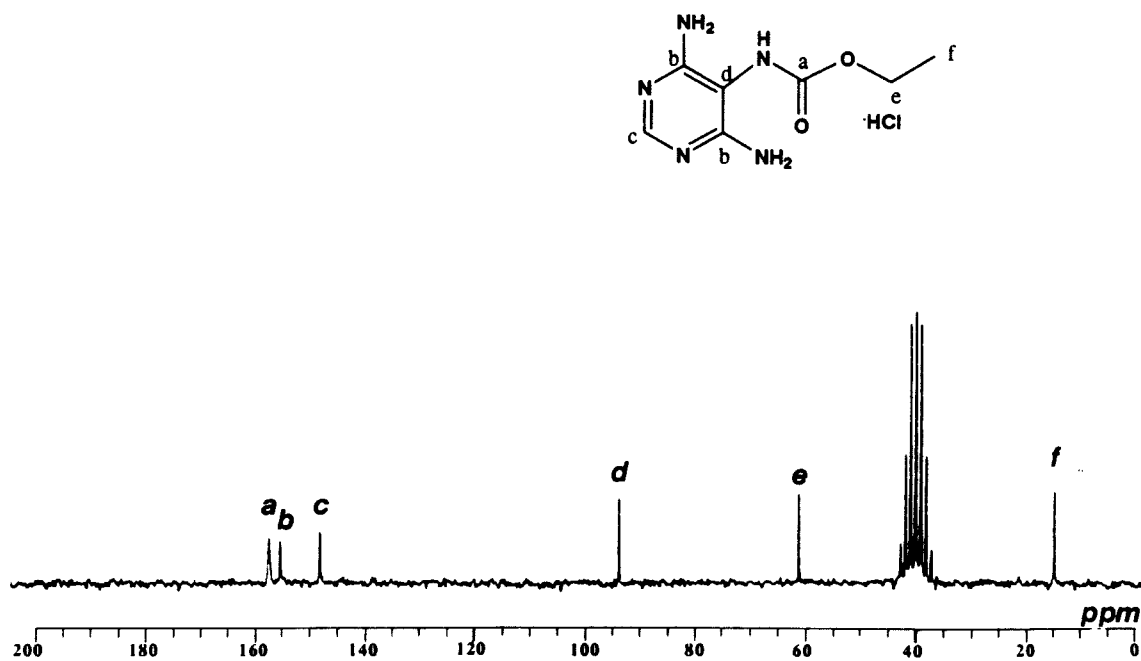
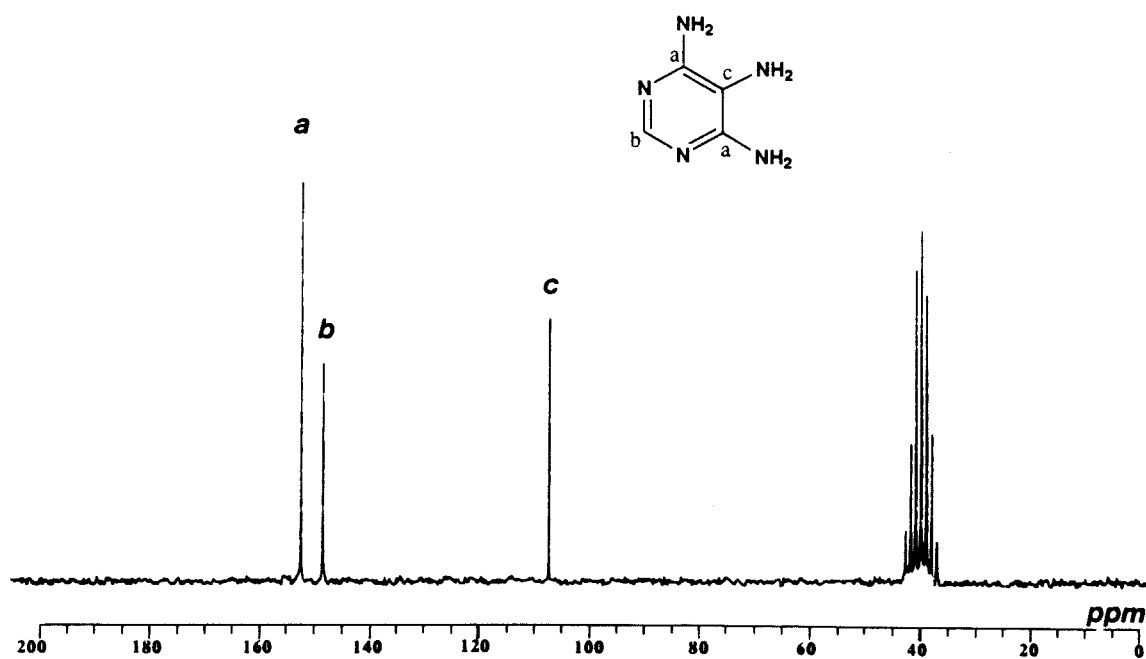


Figure 46. Synthesis of Y, 5-carbethoxyamino-2,4-diamino-6-hydroxypyrimidine.



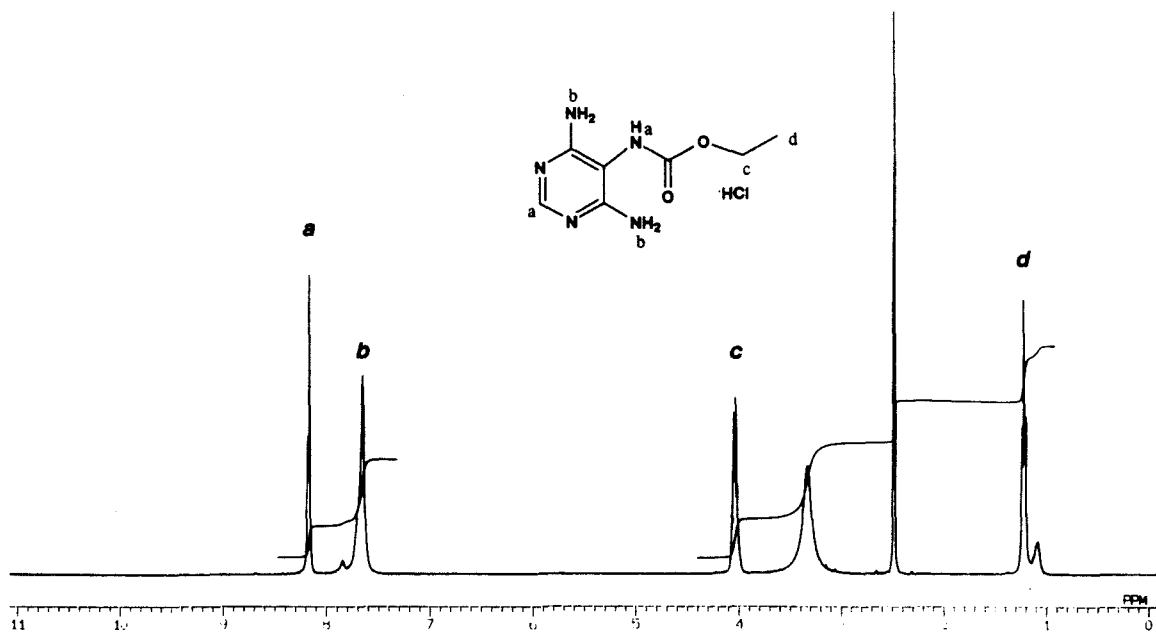


Figure 48 A. 400 MHz ¹H NMR spectrum of 5-carbethoxyamino-4,6-diaminopyrimidine hydrochloride.

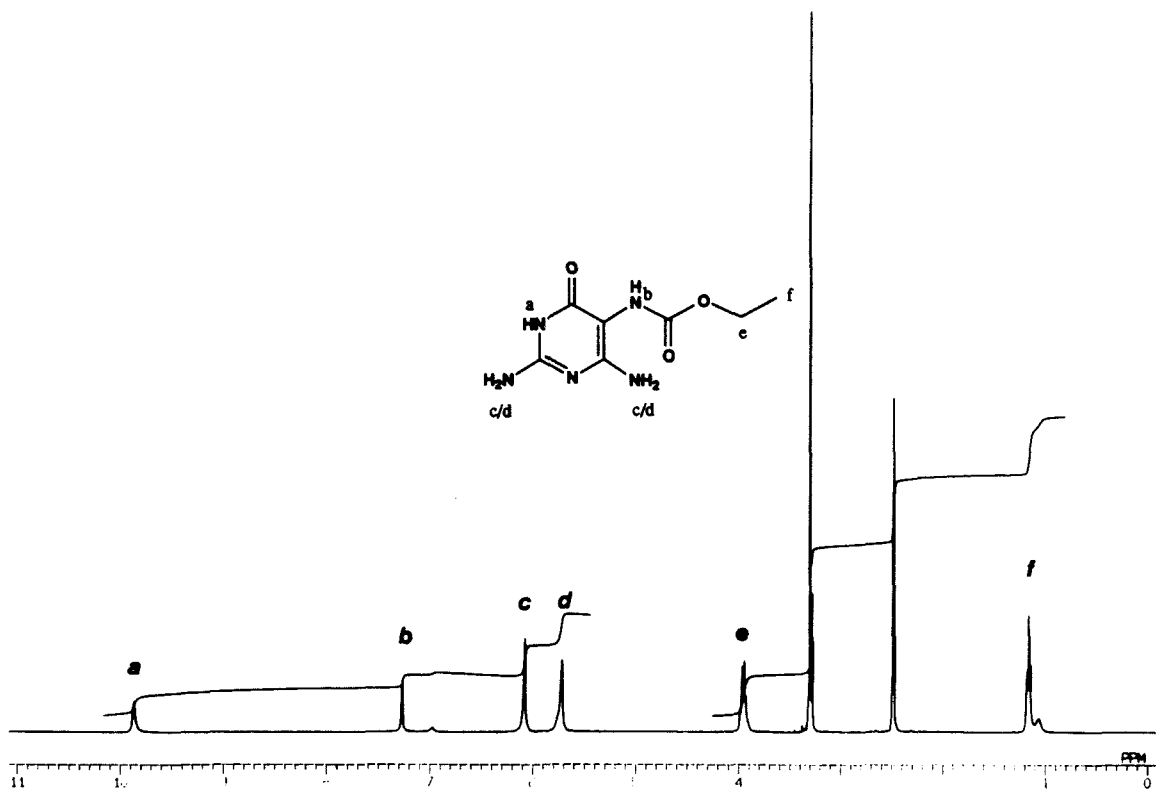


Figure 48 B. 400 MHz ¹H NMR spectrum of 5-carbethoxyamino-2,4-diamino-6-hydroxypyrimidine.

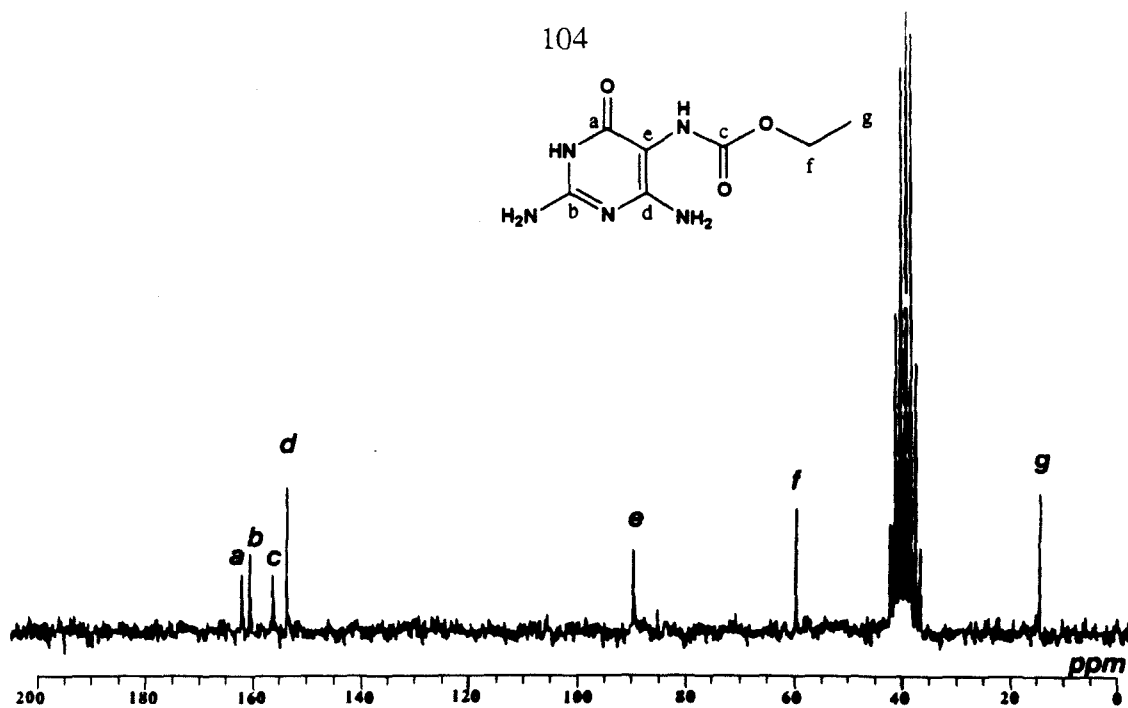


Figure 49 A. Proton decoupled 22.5 MHz ^{13}C NMR spectrum of 5-carbethoxyamino-2,4-diamino-6-hydroxypyrimidine.

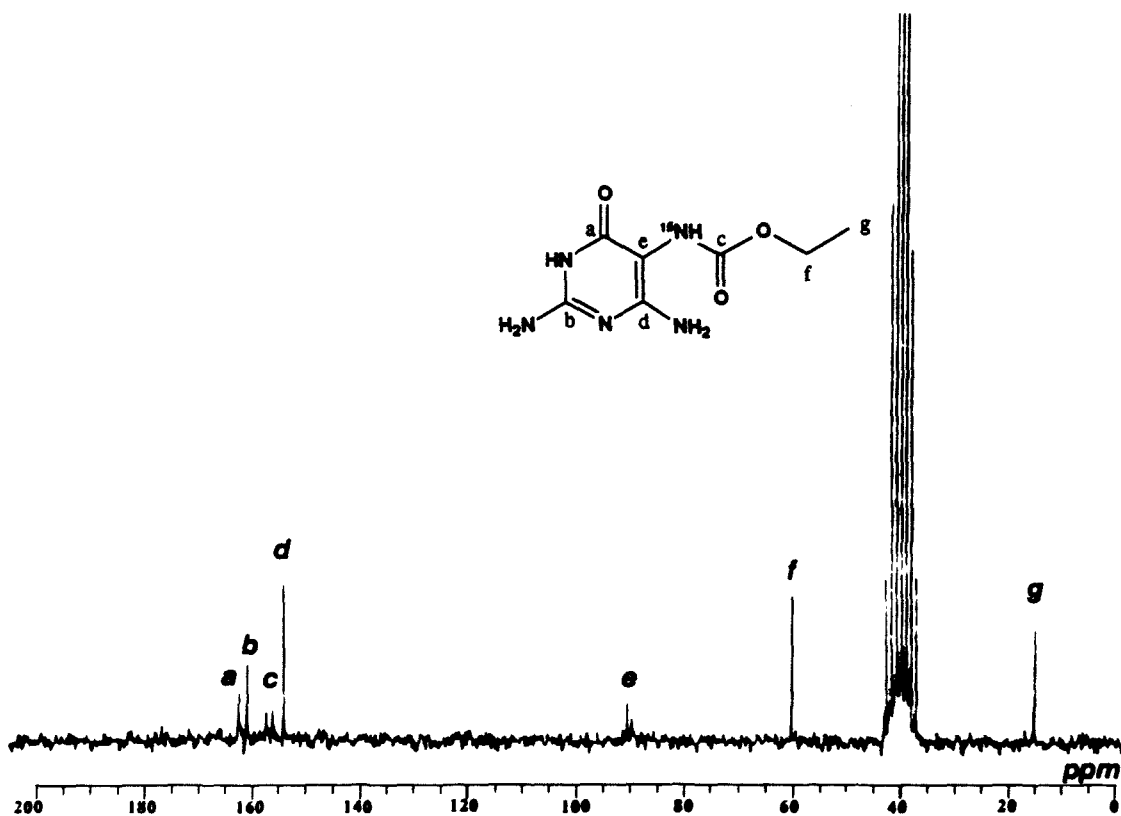


Figure 49 B. Proton decoupled 22.5 MHz ^{13}C NMR spectrum of [5- ^{15}N]-carbethoxyamino-2,4-diamino-6-hydroxypyrimidine.

consistent with the NMR, IR and mass spectral data, but ethyl chloroformate reaction at the 2 or 4 amino groups would have yielded the same data. The structure assigned to **Y** was substantiated by making **C** with either $\text{Na}^{14}\text{NO}_2$ or >99% enriched $\text{Na}^{15}\text{NO}_2$. Conversion of **C** to **Y** (Figure 46) then gave either 5-carbethoxyamino-2,4-diamino-6-hydroxypyrimidine or $[5\text{-}^{15}\text{N}]$ carbethoxyamino-2,4-diamino-6-hydroxypyrimidine, depending on which nitrogen source was used to make the precursor base **C**. Because ^{15}N has a nuclear spin of 1/2, carbon atoms directly attached to the ^{15}N atom should give a doublet in the ^{13}C NMR spectrum. Therefore, if the ethyl chloroformate modifies the 5 position of **C** made with $\text{Na}^{15}\text{NO}_2$, two doublets should appear in the ^{13}C NMR spectrum of **Y** relative to **Y** made with $\text{Na}^{14}\text{NO}_2$. If reaction is at the 2 or 4 positions, only the carbon 5 resonance will be split in the ^{13}C NMR of **Y**. Figure 49 shows the completely proton decoupled ^{13}C NMR spectra of synthetic **Y**. Two carbon signals at 155.9 and 89.5 ppm were split into doublets ($J = 26$ and 19 Hz, respectively) on going from **Y** made with $\text{Na}^{14}\text{NO}_2$ to that made with >99% enriched $\text{Na}^{15}\text{NO}_2$. The signal at 89.5 ppm represents ring carbon 5 and that at 155.9 ppm, the ethyl carbamate carbonyl carbon. Furthermore, $[5\text{-}^{15}\text{N}]$ -**Y** had a mass of 214 g/mole ($\text{C}_7\text{H}_{11}\text{N}_4\text{O}_3$ ^{15}N) and showed an electron impact mass spectrum fragmentation pattern nearly identical to $[^{14}\text{-N}]$ **Y**, except that major fragmentation peaks differed by one mass unit (see Experimental section). These results unequivocally demonstrated **Y** to be 5-carbethoxyamino-2,4-diamino-6-hydroxypyrimidine. The chromatographic properties and ultraviolet spectra of **X** and **Y** were then compared with the products of DEP-oligonucleotide duplex reactions.

Identity of DEP-adenosine and DEP-guanosine adducts.

When injected alone, reference compound **X** eluted at about 15 minutes under the HPLC method RAMP3 (Figure 50 E). This retention time was very close to that of the suspected DEP-adenosine adduct (peak 3) resulting from depurination of DEP-duplex **47+48** reactions conducted in the presence of echinomycin or ethidium bromide (Figure 50

A and C, respectively). When the product mixture from DEP-duplex **47+48** reactions performed with echinomycin was spiked with synthetic compound **X**, no new peaks were seen in the HPLC chromatogram, but the intensity of peak 3 increased (compare Figure 50 A and B). The same was true for DEP-**47+48** reactions performed with ethidium bromide and spiked with synthetic **X** (Figure 50 C and D). Note that for product mixtures spiked with **X**, only enough material was added to approximately double the intensity of peak 3. If the retention times of peak 3 and **X** were not identical, this amount of added **X** would have clearly shown two peaks or a shoulder at peak 3 in Figure 50 B and 50 D. Also, the amount of added **X** was small enough not to drown out the signal of peak 3 and thus could not give the illusion of a single peak if, in fact, two different peaks were to exist. These spiking experiments clearly demonstrated that compound **X** coeluted with peak 3 produced in DEP-**47+48** reactions containing either echinomycin or ethidium bromide. Furthermore, the ultraviolet spectrum of compound **X** was identical to that of peak 3 (Figure 50 F and 50 G). Therefore, peak 3 was identified as 5-carbethoxyamino-4,6-diaminopyrimidine because its UV spectrum and HPLC retention characteristics were identical to those of authentic material.

Figure 51 shows the results of spiking experiments conducted on DEP-**49+50** reaction product mixtures. As with **47+48** above, compound **X** had a retention time similar to peak 3 produced in DEP-**49+50** reactions containing echinomycin or ethidium bromide (compare Figure 51 A, 51 C and 51 E). Small amounts of added synthetic **X** to the mixtures of 51 A and 51 C led only to an increase in peak 3 intensity. No new peaks or shoulders about peak 3 could be seen (Figure 51 B and 51 D). Figure 51 F and 51 G shows that the UV spectrum of peak 3 in DEP-**49+50** reactions was identical to that obtained for compound **X**. Therefore, as with duplex **47+48**, the DEP-**49+50** reaction product formed in the presence of echinomycin or ethidium bromide was identified as 5-carbethoxyamino-4,6-diaminopyrimidine based on identical electronic spectra and HPLC retention characteristics of authentic material.

Similar spiking experiments were conducted on product mixtures resulting from oligonucleotides containing echinomycin binding sites composed entirely of G·C base pairs. Synthetic compound **Y** eluted at about 18 minutes on HPLC method RAMP9 (Figure 52 E). This retention time was very similar to peak 2 seen in DEP-**54+55** reactions performed with echinomycin or ethidium bromide present (Figure 52 A and 52 C). As with the spiking controls carried out on duplex **47+48** and **49+50** reaction product mixtures, only a small amount of reference compound was added to duplex **54+55** reaction product mixtures to demonstrate coelution. Comparison of Figure 52 A and 52 B shows that upon addition of reference compound **Y**, the intensity of peak 2 increased and no new peaks could be seen in the spiked sample (Figure 52 B). Figure 52 C and 52 D shows similar results. Compound **Y** therefore coeluted with peak 2 produced in DEP-**54+55** reactions containing echinomycin or ethidium bromide. Panels F and G of Figure 52 demonstrate that peak 2 and compound **Y** have identical UV spectra. Therefore, peak 2 produced in DEP-**54+55** reactions was identified as 5-carbethoxyamino-2,4-diamino-6-hydroxypyrimidine based on shared HPLC retention properties and UV spectra with authentic reference material.

The results of spiking experiments on DEP-**60+61** reaction products were very similar to those observed for DEP-**54+55** reactions. Compound **Y** (Figure 53 E) eluted very close to peak 2 produced in DEP-**60+61** reactions containing echinomycin (Figure 53 A) or ethidium bromide (Figure 53 C). Addition of synthetic **Y** to the reaction mixtures of Figures 53 A and 53 C yielded identical chromatograms, except for an increase in peak 2 intensity (Figure 53 B and 53 D). No new peaks appeared and no shoulders were seen about peak 2 in the spiked samples. This result indicated that compound **Y** coeluted with peak 2 produced in DEP-**60+61** reactions containing echinomycin or ethidium bromide. Compound **Y** and peak 2 also shared ultraviolet spectra (Figure 53 F and 53 G). Therefore, DEP-**60+61** reaction in the presence of echinomycin or ethidium bromide leads to the formation of 5-carbethoxyamino-2,4-diamino-6-hydroxypyrimidine. This represents the

DEP-guanosine reaction product. However, significant DEP reaction also occurred at adenosine residues on this duplex (Figures 35 and 43). Thus, some 5-carbethoxyamino-4,6-diaminopyrimidine was also produced in these reactions and appears as peak 4 in Figure 53.

Summary.

High-resolution PAGE analysis of DEP/piperidine cleavage at adenosine and guanosine residues on DNA and HPLC analysis of bases released from DEP-DNA reactions containing echinomycin or ethidium bromide showed that one DEP-adenosine and/or one DEP-guanosine adduct appeared to be formed regardless of the intercalator present during the course of DEP-DNA reaction. Different DNA sequences yielded different quantities of each product, but the constitution of DEP-guanosine and DEP-adenosine adducts formed was independent of DNA base sequence. The DEP-adenosine adduct was identified as 5-carbethoxyamino-4,6-diaminopyrimidine and the DEP-guanosine adduct as 5-carbethoxyamino-2,4-diamino-6-hydroxypyrimidine. These two products demonstrate that DEP-purine reaction in the presence of echinomycin or ethidium bromide occurs at the N7 atom center, forcing us to conclude that DEP hyperreactivity of purine residues at echinomycin binding sites is caused by increased solvent accessibility of purine N7 atoms.

Figure 50. (A-E) Spiking experiments: Reversed-phase HPLC chromatograms of base-release products from 100 nmol scale DEP-oligonucleotide duplex **47+48** reactions. Panels are: A, **47+48**-DEP reaction containing 140 μ M echinomycin; B, A spiked with synthetic **X**; C, **47+48**-DEP reactions containing 3.4 mM ethidium bromide; D, C spiked with synthetic **X**; E, synthetic **X** alone; F, UV spectrum of peak 3; G, UV spectrum of synthetic **X**. Peaks: 1, cytosine; 2, guanine; 3, **X**; 4, adenine; 5, internal standard *p*-anisaldehyde; 6, DEP-ethidium bromide adduct. Peak assignment was based on identical ultraviolet spectra and HPLC retention times (coelution) of reference compounds.

Duplex 47+48 Spike

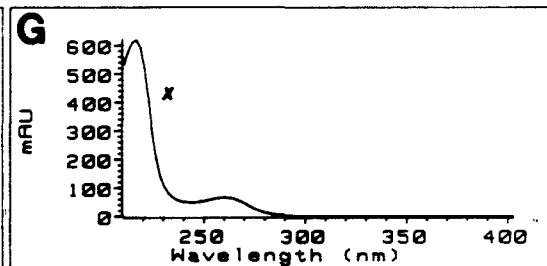
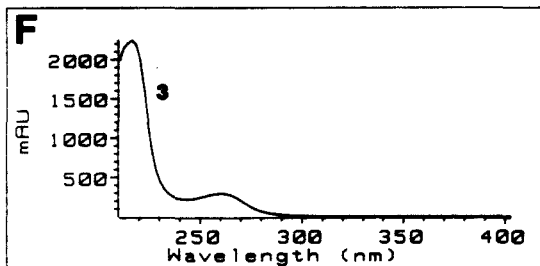
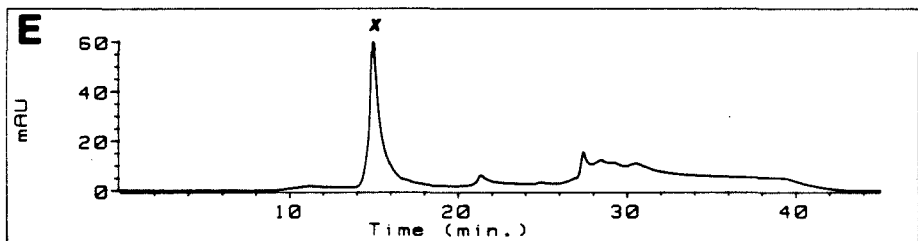
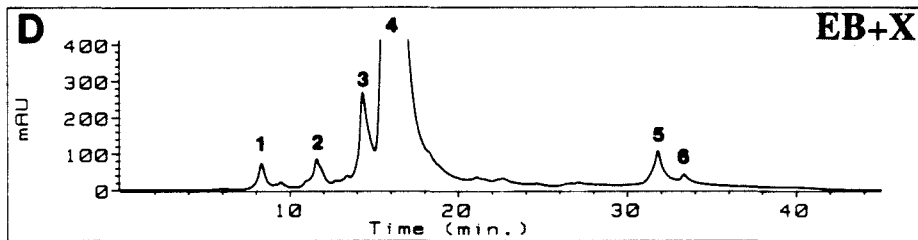
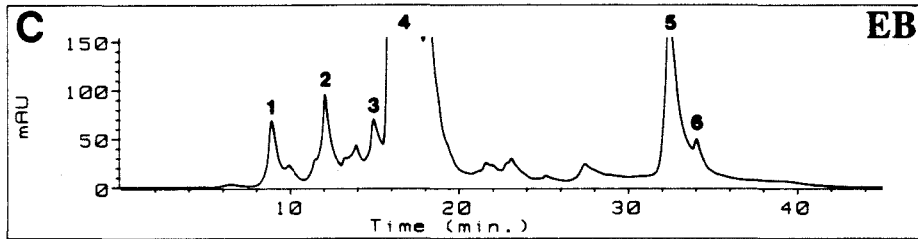
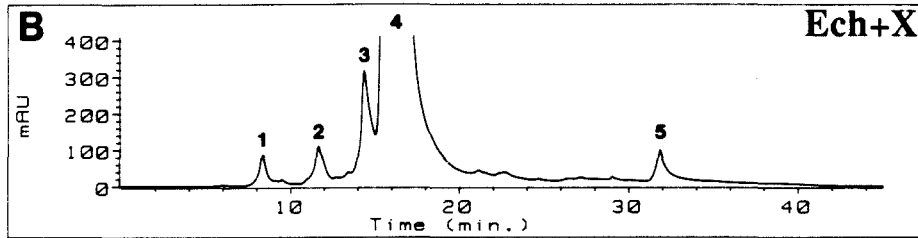
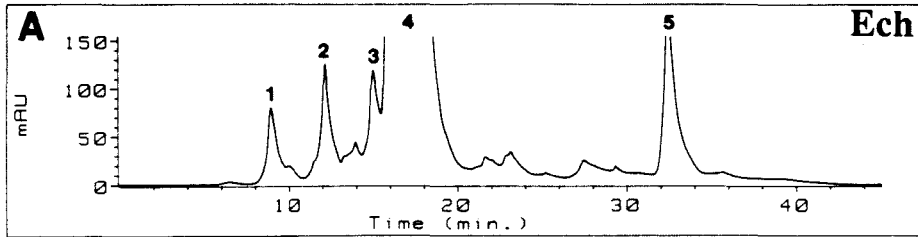


Figure 51. (A-E) Spiking experiments: Reversed-phase HPLC chromatograms of base-release products from 100 nmol scale DEP-oligonucleotide duplex **49+50** reactions. Panels are: A, **49+50**-DEP reaction containing 140 μ M echinomycin; B, A spiked with synthetic **X**; C, **49+50**-DEP reactions containing 3.4 mM ethidium bromide; D, C spiked with synthetic **X**; E, synthetic **X** alone; F, UV spectrum of peak 3; G, UV spectrum of synthetic **X**. Peaks: 1, cytosine; 2, guanine; 3, **X**; 4, adenine; 5, internal standard *p*-anisaldehyde; 6, DEP-ethidium bromide adduct. Peak assignment was based on identical ultraviolet spectra and HPLC retention times (coelution) of reference compounds.

Duplex 49+50 Spike

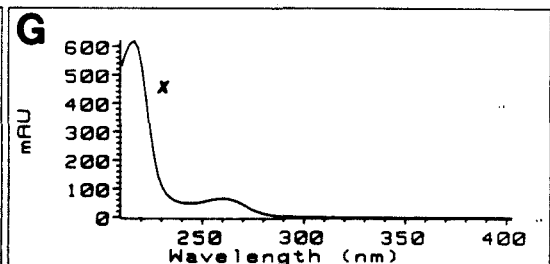
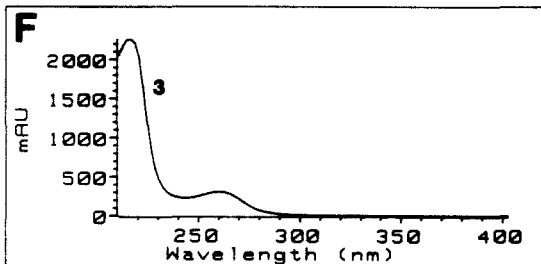
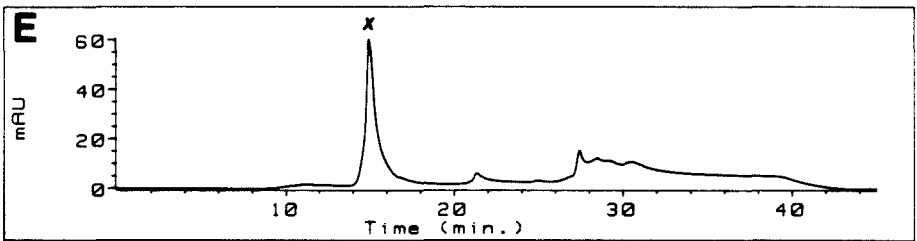
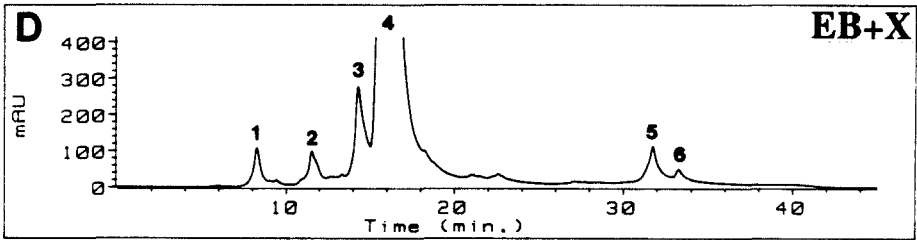
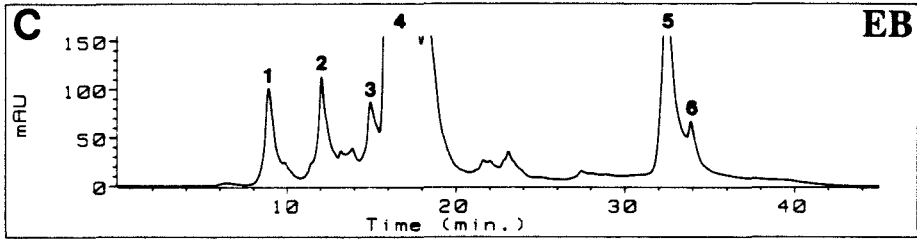
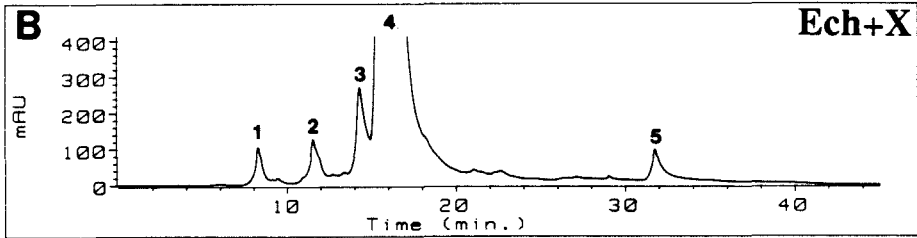
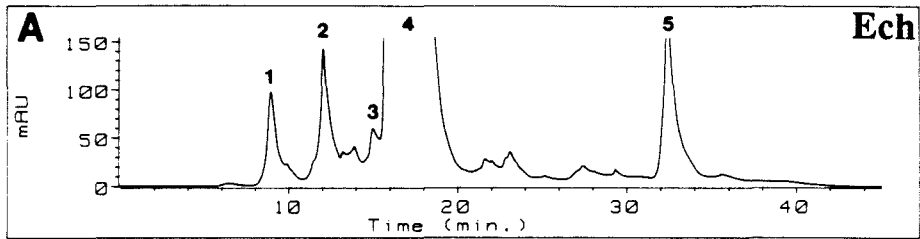


Figure 52. (A-E) Spiking experiments: Reversed-phase HPLC chromatograms of base-release products from 100 nmol scale DEP-oligonucleotide duplex **54+55** reactions. Panels are: A, **54+55**-DEP reaction containing 140 μ M echinomycin; B, A spiked with synthetic **Y**; C, **54+55**-DEP reactions containing 3.4 mM ethidium bromide; D, C spiked with synthetic **Y**; E, synthetic **Y** alone; F, UV spectrum of peak 3; G, UV spectrum of synthetic **Y**. Peaks: 1, cytosine; 2, **Y**; 3, guanine; 4, **X**; 5, adenine, 6; internal standard *p*-anisaldehyde; 7, DEP-ethidium bromide adduct. Peak assignment was based on identical ultraviolet spectra and HPLC retention times (coelution) of reference compounds.

Duplex 54+55 Spike

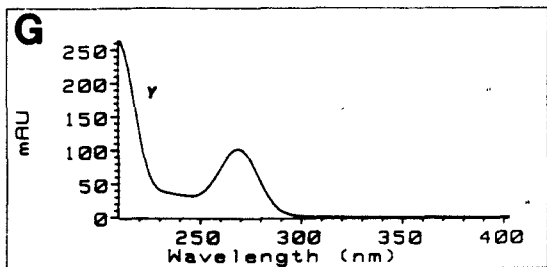
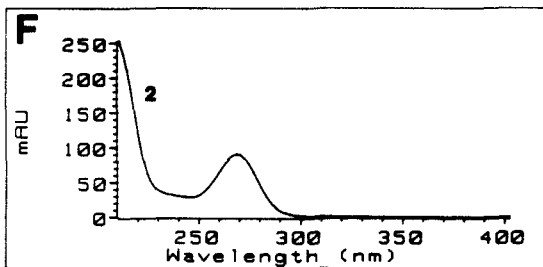
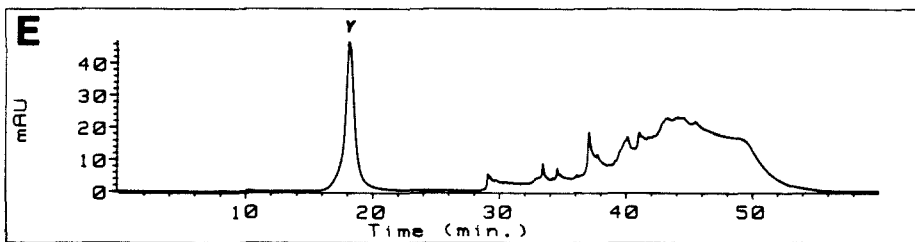
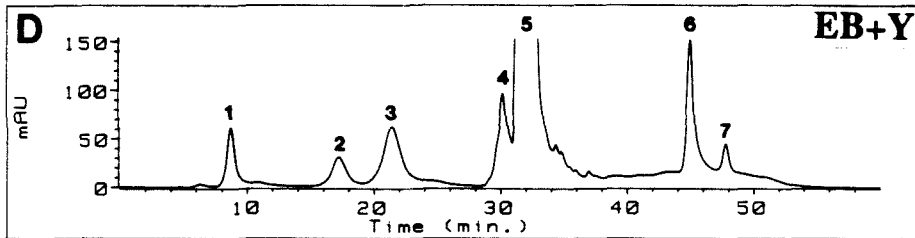
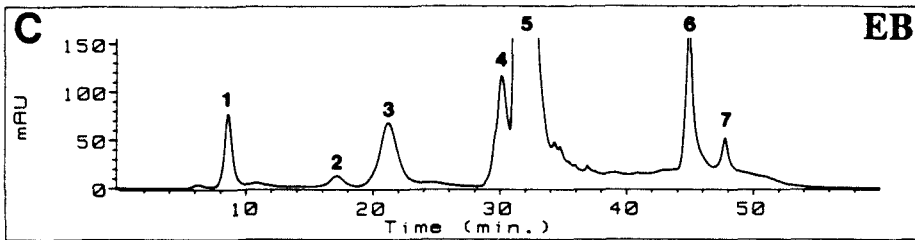
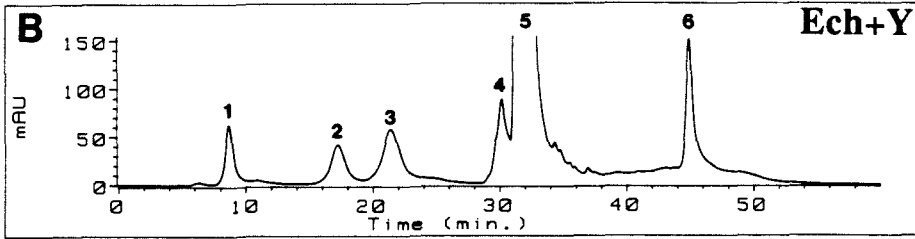
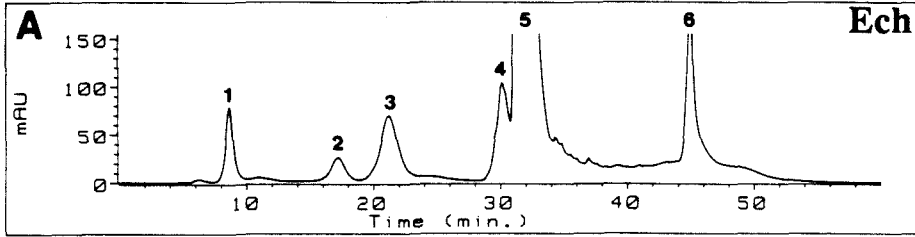
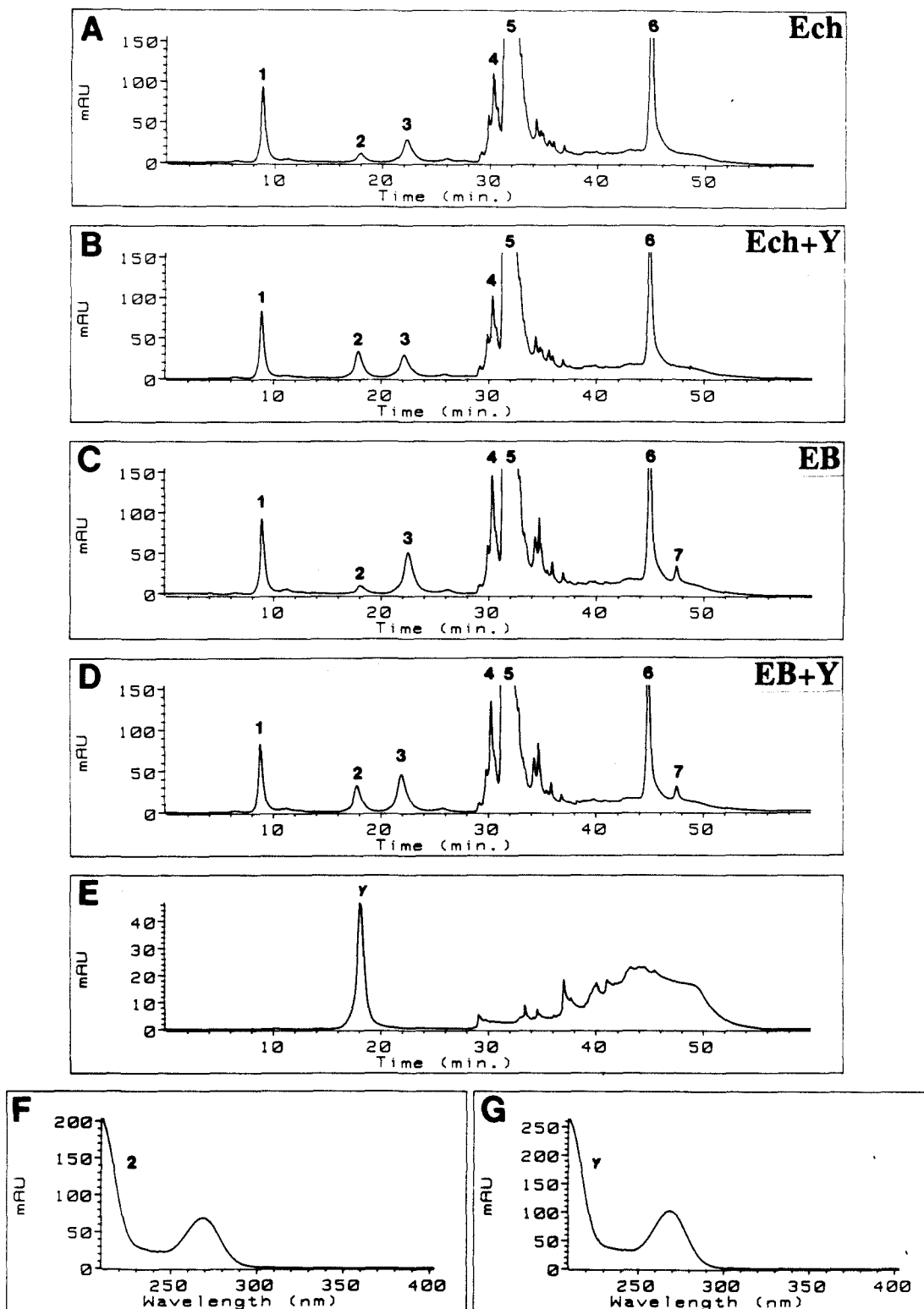


Figure 53. (A-E) Spiking experiments: Reversed-phase HPLC chromatograms of base-release products from 100 nmol scale DEP-oligonucleotide duplex **60+61** reactions. Panels are: A, **60+61**-DEP reaction containing 140 μ M echinomycin; B, A spiked with synthetic **Y**; C, **60+61**-DEP reactions containing 3.4 mM ethidium bromide; D, C spiked with synthetic **Y**; E, synthetic **Y** alone; F, UV spectrum of peak 3; G, UV spectrum of synthetic **Y**. Peaks: 1, cytosine; 2, **Y**; 3, guanine; 4, **X**; 5, adenine; 6, internal standard *p*-anisaldehyde; 7, DEP-ethidium bromide adduct. Peak assignment was based on identical ultraviolet spectra and HPLC retention times (coelution) of reference compounds.

Duplex 60+61 Spike



Other reagents used to characterize echinomycin-DNA complexes in solution.

The results presented above suggest that DEP does not detect Hoogsteen base-pairing at echinomycin binding sites, but rather helix unwinding caused by antibiotic intercalation into DNA. Other chemical probes of nucleic acid structure were used to characterize echinomycin-DNA complexes in solution. Bromoacetaldehyde, specific for adenosine N1 and N6 positions, did not react measurably with any DNA sequence tested, whether echinomycin was present or not. Dimethyl sulfate (DMS), however, was useful for probing nucleic acid structure at echinomycin-d(GCGC)₂ binding sites because this reagent preferentially methylates the N7 of guanosine. This event can be converted into a DNA strand scission via Maxam-Gilbert⁷⁹ workup and allows visualization of guanosine N7 methylation. Recall that in a Hoogsteen base pair, the N7 atom is masked by a hydrogen bond (Figure 11). Further, Hoogsteen C-G base pairs should be favored at low pH because the cytosine base must be protonated to form a hydrogen bond with guanosine N7 in this arrangement. Because DMS reacts primarily with guanosine N7, we tested the ability of DMS to detect Hoogsteen C-G base pairs at echinomycin binding sites under acidic conditions.

DMS probing of echinomycin and ethidium bromide bound to duplex 60+61 is shown in Figure 54. In the absence of DNA-binding small molecules, DMS modified all guanosine residues evenly (lanes 2-3 and 13-14). DMS-guanosine reactivity was more efficient at pH 3.7 (lanes 2 and 13) than at pH 8.0 (lanes 3 and 14). In the presence of ethidium bromide (lanes 6-7 and 17-18), DMS modification was still fairly even, but was much more efficient than in the absence of intercalator (Figure 54, compare lanes 2-3 with 6-7 and 13-14 with 17-18). However, in the presence of echinomycin, some guanosine residues were methylated *less* efficiently by DMS at pH 3.7 than at pH 8.0 (lanes 4-5 and 15-16). The diminution of methylation at these bases was moderate but detectable and is presented in histogram form as Figure 55 B. Figure 55 represents the difference in DMS

methylation efficiency at pH 3.7 versus pH 8.0. For each set of DMS reactions, the amount of cleavage and thus the extent of DMS modification at each guanosine residue obtained at pH 8.0 was subtracted from that obtained at pH 3.7. Arrows symbolize more efficient DMS modification and bars less efficient DMS modification at pH 3.7 relative to pH 8.0. Figure 55 A and 55 C showed uniformly more efficient DMS methylation at pH 3.7 for both DMS control reactions and those conducted in the presence of ethidium bromide. Echinomycin yielded a very different pH-dependent DMS methylation pattern (Figure 55 B). Here, moderate *inhibition* of DMS action was seen at the guanosine residues occupying the first and fourth base pair positions of the echinomycin binding sites 5'-GCGC-3'. Weak inhibition was also visible at two of the guanosine residues between the 5'-GCGC-3' sequences. In addition to the inhibition of DMS methylation at the first and fourth positions of 5'-GCGC-3' sites, there was weak-to-moderate enhancement of DMS action at the internal guanosine residues of this sequence at pH 8.0 relative to pH 3.7.

It should be noted that we attempted to use DMS to probe echinomycin binding sites where A·T pairs occupy the first and fourth base pair positions because DMS readily alkylates adenosine N1 positions. In a Hoogsteen A·T base pair, adenosine N1 is exposed to solvent and we would expect it to be modified by DMS. We substituted DMS for DEP in the large-scale oligonucleotide duplex reactions and looked for the appearance of 1-methyl adenosine. Unfortunately, the signal-to-noise ratio of the data from these experiments did not allow us to detect significant amounts of 1-methyl adenosine in the absence or presence of echinomycin or ethidium bromide. Furthermore, 1-methyl adenosine residues cannot be mapped via Maxam-Gilbert sequencing workup like 7-methyl guanosine residues and thus it was not possible to compare the amount of 1-methyl adenosine formation to a cleavage band on an autoradiogram. Therefore, although DMS can in principle detect non-Watson-Crick A·T base pairs, the reagent did not produce clear data in our assay and was best suited for characterization of G·C base pair structure.

Figure 54. Autoradiogram of the high-resolution denaturing polyacrylamide gel used to analyze DMS/piperidine cleavage of the oligonucleotide duplex **60+61** in the presence of echinomycin or ethidium bromide. Both 5' ³²P end-labeled **60** (lanes 1-9) and **61** (lanes 10-18) were employed for opposite strand analysis on this duplex. DMS modification reactions were performed in Tris-acetate buffer at pH 3.7 (lanes 2,4,6, 13,15,17) or pH 8.0 (lanes 3,5,7, 14,16,18). Lanes are: 1 and 12, intact DNA standards (STD) incubated as for all other reactions on the gel but not treated with DMS or piperidine; 2-3 and 13-14, DMS/piperidine control cleavage of DNA in the absence of drugs (DMS); 4-5 and 15-16, DMS/piperidine cleavage of the duplex in the presence of 140 μM echinomycin (ECH); 6-7 and 17-18, DMS/piperidine cleavage of DNA in the presence of 3.4 mM ethidium bromide (EB); 8 and 10, Maxam-Gilbert chemical sequencing G-specific reaction; 9 and 11, Maxam-Gilbert chemical sequencing purine-specific reaction. DMS reaction conditions were 100 mM Tris / 100 mM NaOAc, pH 3.7 or 8.0, 0.3 mM MgCl₂, 10% (v/v) methanol, 680 μM oligonucleotide base pairs, 10 X dilution of DMS saturated in H₂O and either 140 μM echinomycin (ECH:DNA bp ~ 1:5) or 3.4 mM ethidium bromide (EB:DNA bp ~ 5:1). The gel contained 15% (w/v) polyacrylamide, crosslinked 1:20, 50% (w/v) urea, 1X TBE buffer (see Experimental) and 2% (v/v) glycerol to prevent cracking of the gel when drying. Gel dimensions were 0.4 mm thick at the top, 1.2 mm thick at the base, 40 cm long and 34 cm wide. Electrophoresis at 1500 V was continued until the bromophenol blue (BPB) marker dye had migrated 25 cm from the origin.

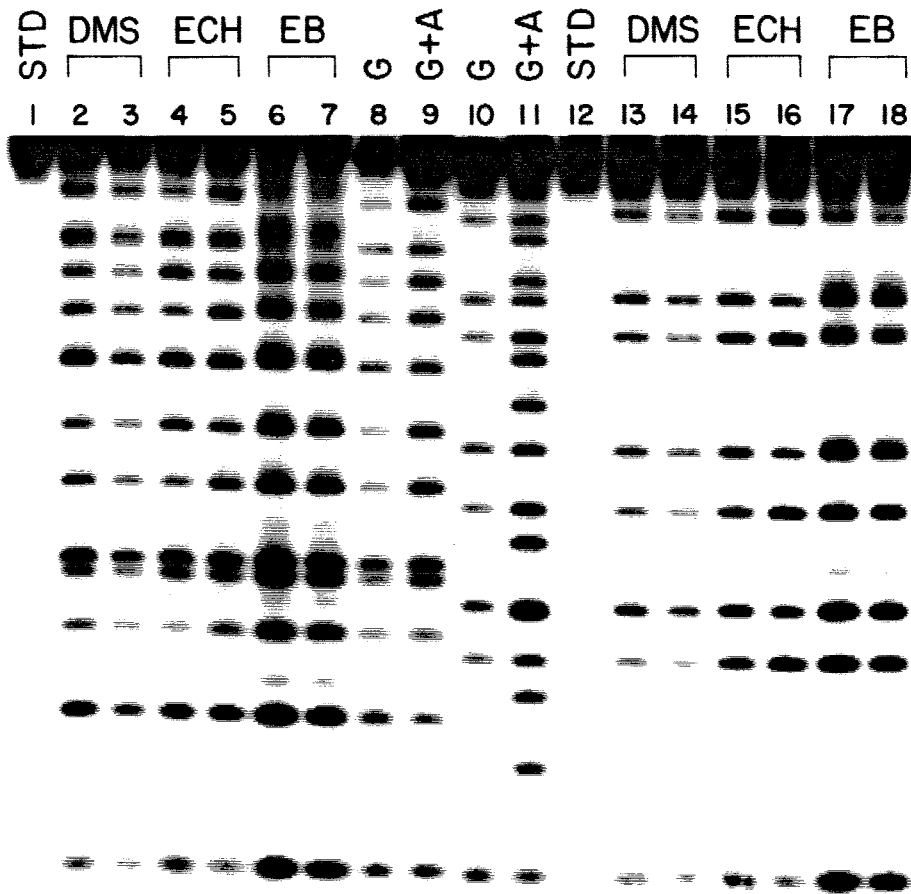
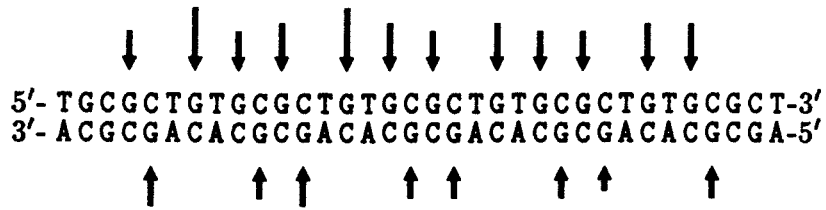
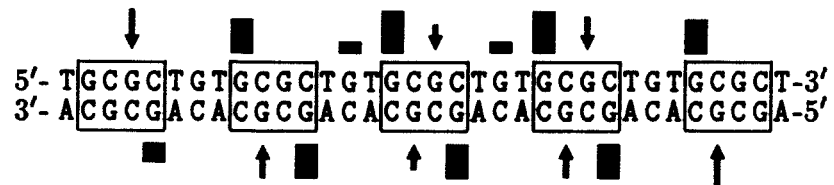
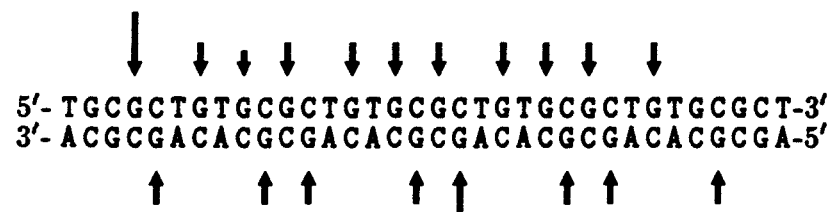


Figure 55. (A-C) Differential DMS/piperidine cleavage of oligonucleotide duplex **60+61** at pH 3.7 or pH 8.0 either without drugs, A, or in the presence of 140 μ M echinomycin, B, or 3.4 mM ethidium bromide, C, as determined by densitometry of the autoradiogram shown in Figure 54. Differential DMS/piperidine cleavage patterns were obtained by subtracting cleavage bands at pH 8 from those at pH 3.7. For example, panel A was obtained by subtracting the bands of lane 3 from lane 2 and lane 14 from lane 13 in Figure 54. Difference DMS/piperidine cleavage patterns are shown as arrows with height proportional to cleavage enhancement or bars with height proportional to cleavage inhibition at pH 3.7 relative to pH 8.0.

A**B****C**

DISCUSSION AND CONCLUSIONS

Our results clearly show that echinomycin, triostin A, and ethidium bromide binding to DNA enhances reaction between purines and diethyl pyrocarbonate. In general, adenosine residues were modified more readily than were guanosine residues, probably because of the inherently greater reactivity of adenosine residues toward DEP. The inherent sequence-binding specificity of triostin A and echinomycin leads to specific DEP modification of purines at or near their binding sites when the drugs bind to DNA. Further, we found that because DEP detects bound quinoxaline antibiotics at nucleotide resolution, DEP can be considered the preferred reagent for footprinting DNA-bound quinoxaline antibiotics, especially in cases where several binding sites are clustered or where they overlap. In most cases, the finer precision of DEP over MPE·Fe(II) is accompanied by greater sensitivity of the former reagent. This is probably because MPE·Fe(II) competes with echinomycin for DNA binding sites, whereas DEP does not. In the presence of echinomycin, purines occupying the first and/or fourth base pair positions of echinomycin binding sites (5'-3') reacted with DEP in decreasing order TCGA > CCGG ~ ACGT > GCGC >> ACGC ~ GCGT. Strongest DEP modification occurred at echinomycin binding sites of the class 5'-YCGU-3' and weakest modification at binding sites of the class 5'-UCGY-3'. For duplexes **49+50** and **60+61** containing (5'-3') ACGT and GCGC sites, respectively, greater DEP modification actually occurred immediately *adjacent* to rather than within drug binding sites.

Detailed product analysis on a number of different oligodeoxynucleotide duplexes showed that regardless of DNA sequence or intercalator used to enhance DEP-DNA reaction, only one DEP-adenosine adduct and one DEP-guanosine adduct were formed. Based on identical HPLC retention characteristics and electronic spectra with authentic reference compounds, the DEP-adenosine adduct was identified as 5-carbethoxyamino-4,6-diaminopyrimidine and the DEP-guanosine adduct as 5-carbethoxyamino-2,4-diamino-6-hydroxypyrimidine. These products correspond to N7 modification of adenosine and

guanosine residues on the DNA strand in the presence of echinomycin and ethidium bromide. Therefore, DEP cannot respond to Hoogsteen base-pairing at occupied echinomycin binding sites because Hoogsteen base-pairing would *protect* the N7 atom from DEP modification. Instead, DEP-purine hyperreactivity in the presence of echinomycin, triostin A or ethidium bromide appears to result from helix unwinding at the points of antibiotic intercalation into DNA. We postulate that DEP is apparently too large to reach purine N7 atoms in B-DNA, but that unwinding of the helix by intercalated small molecules changes the dimensions of DNA and allows DEP access to these centers.

Nature of the base-pairing at echinomycin binding sites in solution.

It is helpful to compare our results with the NMR and x-ray crystallographic analyses of echinomycin·DNA and triostin A·DNA complexes. Table 5 shows that those sequences observed to form Hoogsteen (HG) base pairs in the presence of echinomycin or triostin A; i.e., d(CGCTACGC)₂ or d(ACGT)₂, showed only weak to moderate DEP hyperreactivity. Those sequences observed to be entirely Watson-Crick (WC) paired in the presence of echinomycin; i.e., d(CCGG)₂ and d(TCGA)₂, showed moderate to strong DEP hyperreactivity in our assay.

Apparently, either WC or HG base pairs can exist at strong echinomycin and triostin A binding sites in solution. This suggests that an equilibrium between WC and HG base pairs may exist at these binding sites and that the sequence determines the distribution between WC and HG pairing in the presence of echinomycin or triostin A. Gao and Patel observed strong purine H8-H1' nuclear Overhauser effects in echinomycin·d(GCGC)₂ and echinomycin·d(ACGT)₂ complexes and took this as evidence for *syn* purine conformation and thus Hoogsteen pairing in solution. However, one does not necessarily know from the NOE signal where the HG = WC equilibrium lies. Although DEP does not appear to detect Hoogsteen base-pairing by reacting with exposed purine N1 centers, the relative intensity of DEP modification at a given echinomycin binding site may describe the equilibrium

between Watson-Crick and Hoogsteen base pairs at that site. If we assume that the strong purine H8-H1' NOE observed at echinomycin·d(ACGT)₂ and echinomycin·d(GCGC)₂ complexes indicates that the equilibrium favors the HG form, then we would expect limited exposure of purine N7 atoms and thus relatively weak DEP reactivity. The absence of purine H8-H1' NOE in echinomycin·d(TCGA)₂ and echinomycin·d(CCGG)₂ complexes probably indicates equilibrium on the WC side, and here we would expect greater exposure of purine N7 centers and thus stronger DEP reaction. We observed this pattern. We conclude that strong DEP reactivity of purines at echinomycin binding sites indicates that Watson-Crick base-pairing predominates. Weak DEP reactivity at these sites may indicate that Hoogsteen pairing predominates at these sites, but we have no positive evidence for their existence.

Table 5. Comparison of Echinomycin-Induced DEP-Purine Hyperreactivity to NMR and X-ray Analyses of Echinomycin·DNA and Triostin A·DNA Complexes.

Sequence	Antibiotic	Method (Ref.)	HG or WC @ 1,4 positions	DEP reaction 1,4 positions*
d(CGTACG) ₂	triestin A	X-ray (15)	HG	weak
d(CGTACG) ₂	echinomycin	X-ray (71)	HG	weak
d(GCGTACGC) ₂	triestin A	X-ray (72)	HG	weak
d(ACGTACGT) ₂	echinomycin	NMR (100)	HG, more stable at helix ends	weak-moderate
d(ACGT) ₂	echinomycin	NMR (74)	HG	weak-moderate
d(GCGC) ₂	echinomycin	NMR (77)	WC, pH > 5.2 HG, pH < 5.2	moderate @ pH 7.0
d(TCGA) ₂	echinomycin	NMR (74)	WC	strong
d(CCGG) ₂	echinomycin	NMR (77)	WC	moderate-strong

*DEP reaction (echinomycin present) at site buried within a ~34 bp oligonucleotide.

Dimethyl sulfate (DMS) reactivity patterns suggested that isolated C·G Hoogsteen base pairs can occur at echinomycin binding sites within a DNA fragment at low pH. Figures 54 and 55 B show that at pH 3.7, echinomycin inhibits DMS methylation of guanosine residues occupying the first and fourth base pair positions of 5'-GCGC-3' sequences. Because DMS specifically methylates guanosine N7 positions, the observed inhibition indicates pH-dependent protection of guanosine N7 by echinomycin at these sites. Similar experiments by McLean and Waring⁹⁹ shows a similar result, but this was apparently not detected by these authors. Gao and Patel⁷⁷ observed a pH-dependent transition from WC to HG base-pairing at the terminal residues on an echinomycin·d(GCGC)₂ complex with an apparent transition pK_a of about 5.2. We believe that the observed protection of guanosine residues from DMS methylation at 5'-GCGC-3' echinomycin binding sites indicates a least a partial WC to HG transition at the points of methylation inhibition. If this is indeed the case, this would be the first example of an isolated Hoogsteen base pair to occur within an otherwise normal DNA duplex in solution. It is somewhat surprising that C·G base pairs appear to form isolated Hoogsteen base pairs at echinomycin binding sites within a DNA duplex while T·A pairs do not. T·A pairs were expected to adopt the Hoogsteen form more readily than C·G base pairs because there is a net loss of hydrogen bonds in C·G pairs, whereas the number of H-bonds remains constant for T·A pairs in a WC to HG transition. However, our failure to obtain direct evidence for Hoogsteen T·A base pairs may reflect the bias of DEP toward the N7 atom center of purines.

Even though Hoogsteen base pairs exist at quinoxaline·DNA complexes in the solid and solution states, it appears more difficult for them to form when isolated within a DNA duplex. Recent NMR work bears this out. Gao and Patel⁷⁷ showed that while Hoogsteen base-pairing occurred at the outermost base pairs of an echinomycin·d(ACGT)₂ complex, the echinomycin·d(AAACGTTT)₂ complex was entirely Watson-Crick paired. Comparable results were found by Feigon and co-workers, who described the structure of an

echinomycin₂·d(ACGTACGT)₂ complex.¹⁰⁰ They state: "In the echinomycin-DNA complex reported here, we observe that stable Hoogsteen AT base pairs are formed at the ends of the DNA helix. In contrast, Hoogsteen AT base pairs in the center of the duplex which are constrained by the helix are much less stable."¹⁰⁰ Both of these NMR studies support the assertion that echinomycin does not induce Hoogsteen base-pairing at its 5'-ACGT-3' binding sites *within* DNA. Other than our findings with DMS, no data are available for echinomycin-d(GCGC) complexes residing within a larger helix, but we would expect that isolated Hoogsteen C·G base pairs can exist at low pH within the context of a large DNA duplex. However, at neutral pH, it appears that echinomycin and triostin A bind DNA by simple bisintercalation and do not induce Hoogsteen base pair formation at their binding sites. Therefore, we do not yet feel that the design of DNA binding molecules that recognize or stabilize Hoogsteen base pairs is a practical approach toward the design of G·C-specific DNA binding ligands.

CHAPTER 2

**Chemical and Enzymatic Probing of DNA Structure
Adjacent or Distal to Echinomycin Binding Sites**

INTRODUCTION

Chapter one of this thesis shows that DEP is a valuable tool for sensitive and precise footprinting of quinoxaline antibiotics bound to DNA. We have also established that DEP reacts specifically with the N7 atom of purines within DNA when the helix is unwound by an intercalator. From this knowledge and studies by other groups, we feel that either Watson-Crick or Hoogsteen base pairs can exist at triostin A·DNA and echinomycin·DNA complexes in solution. Along with the results that led to these conclusions, we found that an alternating d(A-T)₆ segment became hyperreactive to DEP in the presence of echinomycin, although this tract did not appear to constitute a strong echinomycin binding site. The nearest strong echinomycin binding site was six base pairs distant from the d(A-T)₆ segment, and it appeared that distal echinomycin binding events in some way caused the d(A-T)₆ tract to react with DEP. The d(A-T)₆ segment does not appear to be B-form DNA because the B-form is refractory to DEP modification. Using DNase I and DNase II to footprint echinomycin, Low *et al.* observed dramatic cleavage enhancement by both enzymes at A-T-rich sequences near strong echinomycin binding sites. They state that: "This increased susceptibility to nuclease attack can be attributed to an altered helix conformation in the vicinity of the bis-intercalated echinomycin molecule."¹⁴ We believe that the DEP reactivity at the A-T segment in the presence of echinomycin is another measure of altered helix structure caused by echinomycin binding to DNA. Apparently, a distal echinomycin binding event can transmit helix unstructuring into the A-T segment, causing it to react with DEP. In this chapter, we characterize the d(A-T)₆ segment structure in the presence of echinomycin, using a variety of enzymatic and chemical probes. Further, we find that other repeating sequences adjacent to strong echinomycin binding sites exhibit increased reactivity to DEP in the presence of echinomycin, and we discuss these results in terms of allosteric effects of echinomycin

binding to DNA. In general, echinomycin binding to DNA appeared to unwind or otherwise alter the structure of DNA adjacent and/or distal to its binding sites.

RESULTS

Purines distal to strong echinomycin binding sites react with DEP in the presence of echinomycin.

Figure 56 presents the autoradiogram of MPE·Fe(II) and DEP/piperidine footprinting of echinomycin on the 628 bp restriction fragment from plasmid pDMG10. In the absence of echinomycin, DEP does not react with the DNA to a significant extent (lanes 7 and 22), but in the presence of 12.5 to 100 μ M echinomycin (lanes 8-11 and 23-26), numerous purines reacted with DEP and these showed up as dark bands in the autoradiogram. Densitometric analysis of these results is presented as Figure 57. Most of the purines reactive to DEP in the presence of echinomycin mapped to echinomycin binding sites independently determined by MPE·Fe(II) footprinting (compare Figure 57 A and 57 E). An exception to this correspondence is the A-T-rich tract of DNA centered at about position 40 (see scale at bottom of Figure 57). Even 100 μ M echinomycin failed to protect the A-T tract from MPE·Fe(II) digestion (Figure 57 D), but as little as 12.5 μ M added echinomycin increased the DEP-reactivity of purines within this segment (Figure 57 E). Increasing from 12.5 to 100 μ M echinomycin concentration, the DEP-adenosine reaction intensity increased and the reaction pattern spread outward until all but the last 5' adenosine residues of the A-T segment reacted with DEP (Figure 57 H). Interestingly, the reaction pattern within this segment was shifted toward the 3' side, even though DEP reacts with purine N7 atoms in the major groove of DNA. Because MPE·Fe(II) intercalates into DNA, it may be that weak echinomycin binding to the A-T segment increased the DEP reactivity of adenosine residues there, but that MPE·Fe(II) readily displaced weakly bound echinomycin and thus showed no cleavage inhibition. We checked the ability of DNase I to

Figure 56. MPE·Fe(II) and DEP/piperidine footprinting of echinomycin on a large DNA restriction fragment. Autoradiogram of 5' (lanes 1-13) and 3' (lanes 14-26) ³²P end-labeled 628 bp *Eco* RI-*Bgl* I restriction fragment from plasmid pDMG10. Lanes: 1 and 16, intact DNA; 2 and 17, MPE·Fe(II) cleavage of DNA in the absence (-) of echinomycin; 3-6 and 18-21, MPE·Fe(II) cleavage of DNA in the presence (+) of echinomycin at 12.5, 25, 50 and 100 μM, respectively; 7 and 22, DEP/piperidine cleavage of DNA in the absence (-) of echinomycin; 8-11 and 23-26, DEP/piperidine cleavage of DNA in the presence (+) of echinomycin at 12.5, 25, 50 and 100 μM, respectively; 12 and 14, Maxam-Gilbert ⁷⁹ chemical sequencing G-specific reaction; 13 and 15, Maxam-Gilbert chemical sequencing purine-specific reaction. The gel was scanned from the bottom to the arrow (at left). Brackets denote the 5' (T-A)₆ segment hyperreactive to DEP. Reaction conditions were 10 mM Tris pH 7.4, 50 mM NaCl, 400 μM DNA calf thymus base pairs, 10%(v/v) methanol and 0, 12.5, 25, 50 or 100 μM echinomycin.

MPE/E					DEP/E					G	G+A	G	G+A	MPE/E					DEP/E							
-	+	+	+	+	+	+	+	+	+	+	G	G+A	G	G+A	-	+	+	+	+	+	-	+	+	+	+	+
1	2	3	4	5	6	7	8	9	10	11	12	13	14	15	16	17	18	19	20	21	22	23	24	25	26	

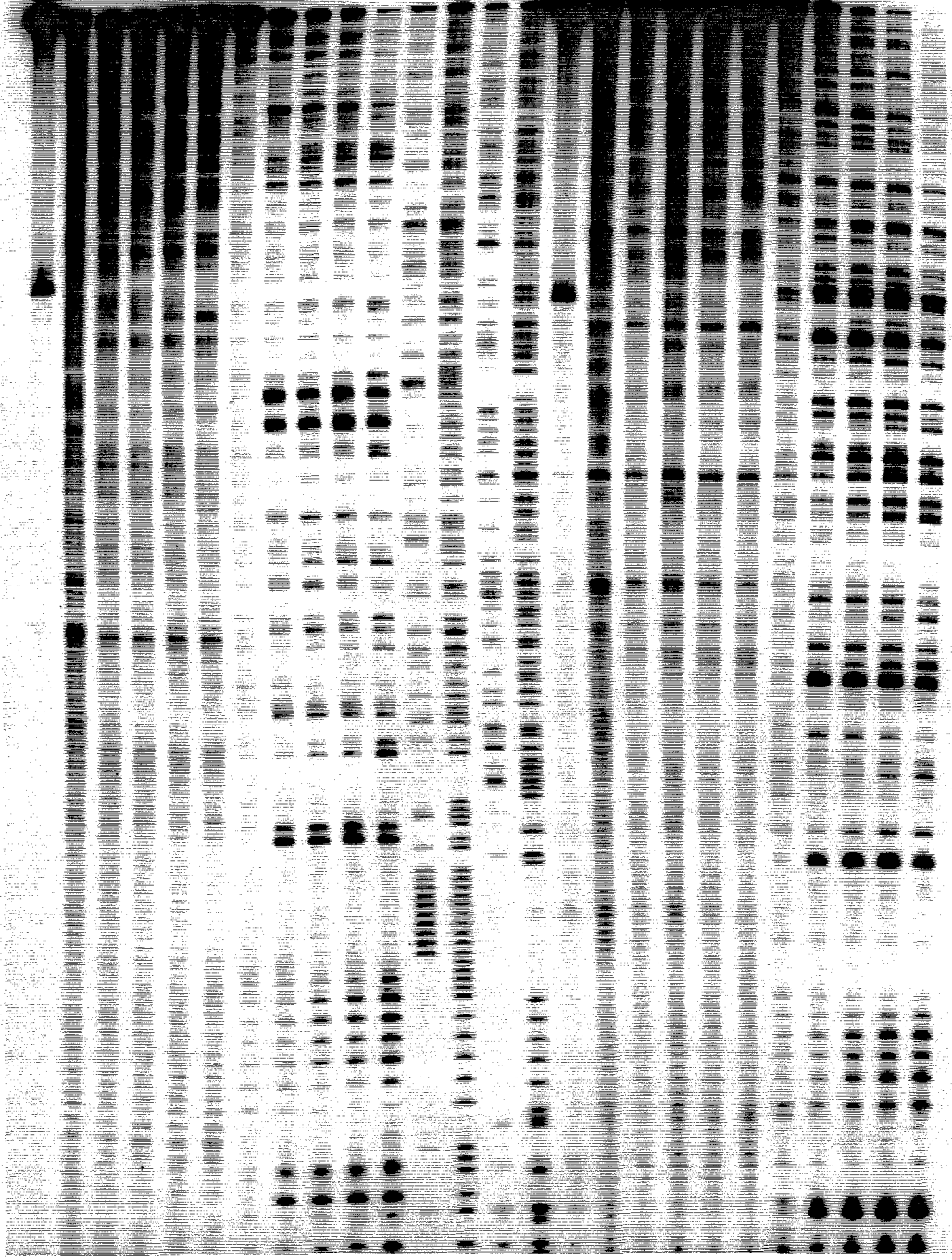


Figure 57. Densitometric analysis of MPE·Fe(II) and DEP/piperidine footprinting of echinomycin. (A-D) MPE·Fe(II) cleavage inhibition patterns of DNA in the presence of echinomycin at 12.5, 25, 50 and 100 μ M, respectively, bound to 100 bp of the 628 bp restriction fragment, as determined by densitometry from the autoradiogram in Figure 56. (E-H) DEP/piperidine cleavage patterns on DNA in the presence of 12.5, 25, 50 and 100 μ M echinomycin, respectively, bound to the same 100 bp of DNA, as determined by densitometry of the autoradiogram in Figure 56. MPE·Fe(II) cleavage inhibition patterns (A-D) are shown as histograms or bars with the height proportional to the reduction of cleavage at each nucleotide compared with MPE·Fe(II) cleavage of unprotected DNA. DEP/piperidine cleavage patterns (E-H) are shown as arrows, with the height proportional to the enhancement of cleavage at each nucleotide compared to DEP/piperidine cleavage of unbound DNA. The scale at the bottom corresponds to the first 5' thymidine in the *Eco* RI site of plasmid pDMG10 defined as position 1. Boxes are the assigned echinomycin binding sites based on the model in References 4 and 16.

A 5'-ATCGATAAGCTTATATATATATAAAAAAGGGGGGGGGTTCGATAGGATCCTCTACGCCGGACCGCATCGCTGC CCGGCATCACCGGCCGCCACAGGTGCGGTTG
 3'-TAGCTATTTCGAATATATATATATATTTTTCCCCCCCCCAGCTATCCTAGGAGATGCGGCCCTGCGTAGCACCGGCCATAGTGGCCGCGGTGTCCACGCCAAC

B 5'-ATCGATAAGCTTATATATATATAAAAAAGGGGGGGGGTTCGATAGGATCCTCTACGCCGGACCGCATCGCTGC CCGGCATCACCGGCCGCCACAGGTGCGGTTG
 3'-TAGCTATTTCGAATATATATATATATTTTTCCCCCCCCCAGCTATCCTAGGAGATGCGGCCCTGCGTAGCACCGGCCATAGTGGCCGCGGTGTCCACGCCAAC

C 5'-ATCGATAAGCTTATATATATATAAAAAAGGGGGGGGGTTCGATAGGATCCTCTACGCCGGACCGCATCGCTGC CCGGCATCACCGGCCGCCACAGGTGCGGTTG
 3'-TAGCTATTTCGAATATATATATATATTTTTCCCCCCCCCAGCTATCCTAGGAGATGCGGCCCTGCGTAGCACCGGCCATAGTGGCCGCGGTGTCCACGCCAAC

D 5'-ATCGATAAGCTTATATATATATAAAAAAGGGGGGGGGTTCGATAGGATCCTCTACGCCGGACCGCATCGCTGC CCGGCATCACCGGCCGCCACAGGTGCGGTTG
 3'-TAGCTATTTCGAATATATATATATATTTTTCCCCCCCCCAGCTATCCTAGGAGATGCGGCCCTGCGTAGCACCGGCCATAGTGGCCGCGGTGTCCACGCCAAC

E 5'-ATCGATAAGCTTATATATATATAAAAAAGGGGGGGGGTTCGATAGGATCCTCTACGCCGGACCGCATCGCTGC CCGGCATCACCGGCCGCCACAGGTGCGGTTG
 3'-TAGCTATTTCGAATATATATATATATTTTTCCCCCCCCCAGCTATCCTAGGAGATGCGGCCCTGCGTAGCACCGGCCATAGTGGCCGCGGTGTCCACGCCAAC

F 5'-ATCGATAAGCTTATATATATATAAAAAAGGGGGGGGGTTCGATAGGATCCTCTACGCCGGACCGCATCGCTGC CCGGCATCACCGGCCGCCACAGGTGCGGTTG
 3'-TAGCTATTTCGAATATATATATATATTTTTCCCCCCCCCAGCTATCCTAGGAGATGCGGCCCTGCGTAGCACCGGCCATAGTGGCCGCGGTGTCCACGCCAAC

G 5'-ATCGATAAGCTTATATATATATAAAAAAGGGGGGGGGTTCGATAGGATCCTCTACGCCGGACCGCATCGCTGC CCGGCATCACCGGCCGCCACAGGTGCGGTTG
 3'-TAGCTATTTCGAATATATATATATATTTTTCCCCCCCCCAGCTATCCTAGGAGATGCGGCCCTGCGTAGCACCGGCCATAGTGGCCGCGGTGTCCACGCCAAC

H 5'-ATCGATAAGCTTATATATATATAAAAAAGGGGGGGGGTTCGATAGGATCCTCTACGCCGGACCGCATCGCTGC CCGGCATCACCGGCCGCCACAGGTGCGGTTG
 3'-TAGCTATTTCGAATATATATATATATTTTTCCCCCCCCCAGCTATCCTAGGAGATGCGGCCCTGCGTAGCACCGGCCATAGTGGCCGCGGTGTCCACGCCAAC

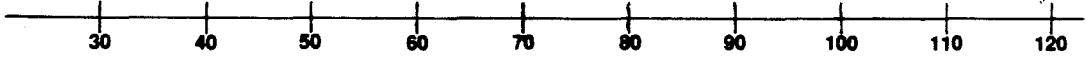


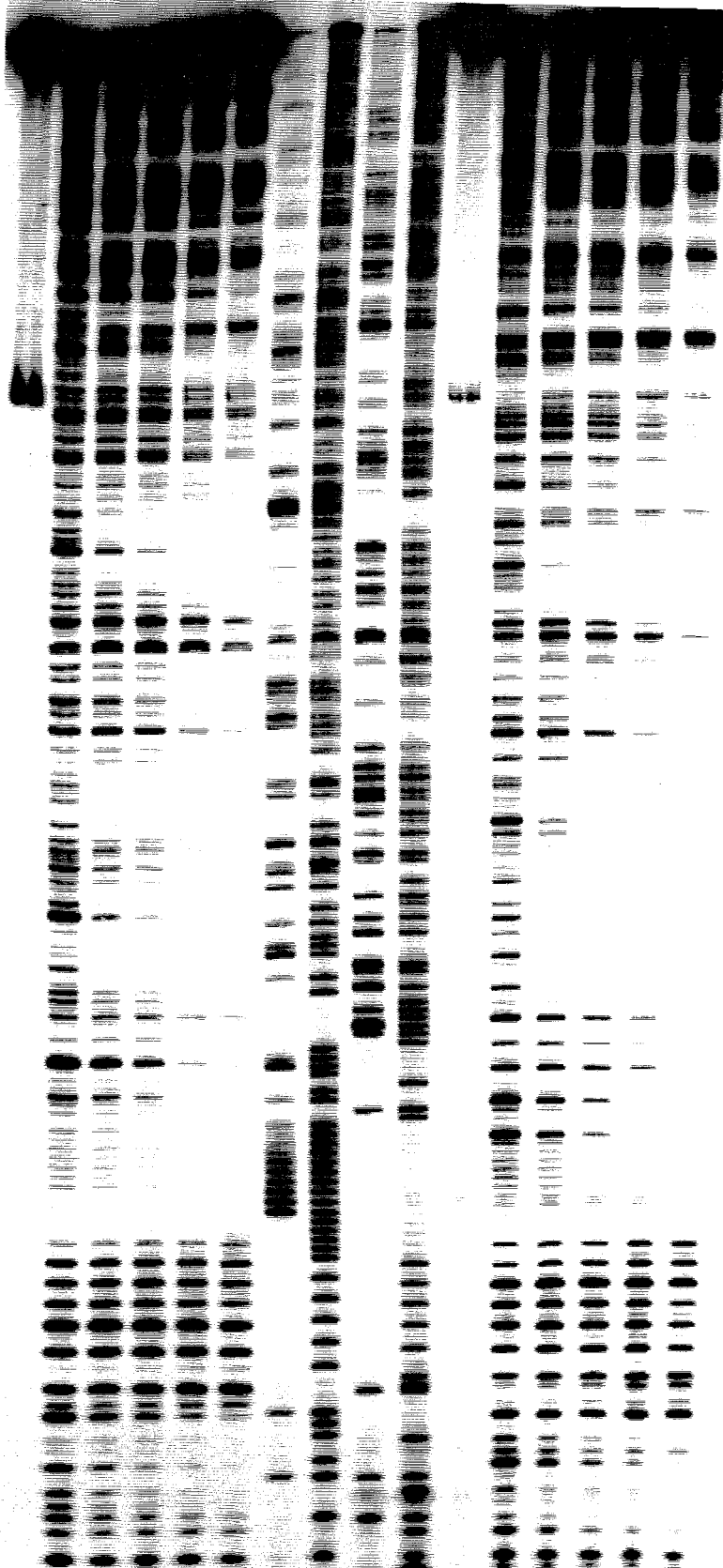
Figure 58. DNase I footprinting of echinomycin. Autoradiogram of 5' (lanes 1-8) and 3' (lanes 9-16) ³²P end-labeled 628 bp *Eco* RI-*Bgl* I restriction fragment from pDMG10. Lanes: 1 and 11, intact DNA; 2 and 12, DNase I cleavage of unprotected DNA; 3-6 and 13-16, DNase I cleavage of DNA in the presence of 6.25, 12.5, 25 or 50 μM echinomycin, respectively; 7 and 9, Maxam-Gilbert chemical sequencing G specific reactions; 8 and 10, Maxam-Gilbert chemical sequencing purine specific reactions. Reaction conditions were 10 mM Tris·HCl pH 7.9, 10 mM KCl, 10 mM MgCl₂, 5 mM CaCl₂, 10% (v/v) methanol and 200 μM DNA base pairs. DNA was digested for 2 minutes at room temperature with 1.32 ng of DNase I.

DNase I/ECH
- + + + +
1 2 3 4 5 6

G G + A
7 8 9 10

STD 11

DNase I/ECH
- + + + +
12 13 14 15 16



detect echinomycin binding at the A-T segment. Although DNase I also binds to DNA, its ability to displace bound ligands is believed to be much less than that of MPE·Fe(II) because DNase I is a much more sensitive footprinting reagent than is MPE·Fe(II).¹⁰¹

Figure 58 shows DNase I footprinting of echinomycin on the same restriction fragment used for MPE·Fe(II) and DEP footprinting. In the absence of echinomycin, DNase I cleaved the DNA efficiently, but with a moderate degree of sequence preference (lanes 2 and 12). As 6.25 to 50 μ M echinomycin was added (lanes 3-6 and 13-16), large spans of DNA were protected from DNase I cleavage. However, at the highest echinomycin concentration tested, the A-T rich segment of DNA at the bottom quarter of Figure 58 was still cleaved efficiently by DNase I. Thus, any echinomycin binding to this segment must be very weak.

Echinomycin does not protect the A-T segment from cleavage by MPE·Fe(II) or EDTA·Fe(II).

The ultimate test for weak binding to DNA is to use a footprinting reagent that does not bind to DNA and thus cannot displace weakly bound ligands. To this end, we tested EDTA·Fe(II) for its ability to detect echinomycin binding at the A-T segment. EDTA·Fe(II) is a very small and thus precise footprinting tool. In the presence of an appropriate reducing agent and hydrogen peroxide, the EDTA·Fe(II) complex is thought to generate hydroxyl radicals via Fenton chemistry.¹⁰² The hydroxyl radicals then oxidatively damage nucleic acid sugars in a fashion similar to MPE·Fe(II)-mediated DNA cleavage.^{103,104} The advantage of EDTA·Fe(II) is that it possesses a net negative charge and is thus unlikely to interact with DNA because of electrostatic repulsion. A comparison of MPE·Fe(II) and EDTA·Fe(II) footprinting of echinomycin bound to the 628 bp pDMG10 restriction fragment is presented in Figure 59. In the absence of echinomycin, EDTA·Fe(II) produced a sequence neutral cleavage ladder (lanes 5 and 16). At 12.5 or 50 μ M echinomycin (lanes 6-7 and 17-18), several discrete points of inhibition appeared in the EDTA·Fe(II) cleavage

pattern, each covering only one to three residues. These are displayed as histograms in Figure 60 along with the MPE·Fe(II) cleavage inhibition patterns produced under identical reaction conditions. There was good correspondence between the MPE·Fe(II) and EDTA·Fe(II) cleavage inhibition patterns, the major differences being size and intensity of the cleavage inhibition pattern for each reagent. Where echinomycin yielded intense and relatively long regions of MPE·Fe(II) cleavage inhibition (Figure 60 A and B), protection from EDTA·Fe(II) cleavage was much less intense and extended over only one to three residues (Figure 60 C and D). Echinomycin appeared to protect only the one to two 3' extreme residues of its binding sites from EDTA·Fe(II) cleavage on both strands. The cleavage inhibition patterns for both MPE·Fe(II) and EDTA·Fe(II) were shifted to the 3' side, consistent with echinomycin binding via the minor groove of DNA. However, neither pattern revealed any protection of the A-T segment by echinomycin. Because EDTA·Fe(II) does not bind to DNA, its apparent failure to detect echinomycin binding to the A-T segment cannot be due to displacement of weakly bound antibiotic at this region. Thus, three different reagents, MPE·Fe(II), DNase I and EDTA·Fe(II) all showed that echinomycin does not bind the A-T-rich segment of this DNA restriction fragment with high affinity.

The cause of adenosine-DEP hyperreactivity in this segment in the presence of echinomycin was still unknown, but we feel that an alternate DNA structure may underlie the observed hyperreactivity. We next employed a variety of reagents and buffer conditions in order to describe the structure of the A-T segment in the presence of echinomycin.

Echinomycin does not induce S1 nuclease hypersensitivity at the A-T segment.

S1 nuclease is a valuable enzymatic probe of nucleic acid structure. It specifically cleaves single-stranded DNA under acidic conditions with optimal activity occurring at about pH 4.3.¹⁰⁵ Figure 61 shows S1 nuclease cleavage of the 628 bp restriction fragment

Figure 59. MPE·Fe(II) and EDTA·Fe(II) footprinting of echinomycin. Autoradiogram of the high-resolution denaturing 8% polyacrylamide gel containing 5' (lanes 1-9) or 3' (lanes 10-18) ³²P end-labeled 628 bp *Eco* RI-*Bgl* I restriction fragment from plasmid pDMG10. Lanes: 1 and 12, buffered, intact DNA (STD) incubated with sodium L-ascorbate but without MPE·Fe(II) or EDTA·Fe(II); 2 and 13, MPE·Fe(II) control cleavage of unbound DNA; 3-4 and 14-15, MPE·Fe(II) cleavage of DNA bound by 12.5-50 μM echinomycin; 5 and 16, EDTA·Fe(II) control cleavage of unbound DNA; 6-7 and 17-18, EDTA·Fe(II) cleavage of DNA bound by 12.5-50 μM echinomycin; 8 and 10, Maxam-Gilbert chemical sequencing G-specific reactions; 9 and 11, Maxam-Gilbert chemical sequencing purine-specific reactions. MPE·Fe(II) reaction conditions were 10 mM Tris·HCl pH 7.4, 50 mM NaCl, 200 μM calf thymus DNA bp, 4 μM MPE, 8 μM Fe(NH₄)₂(SO₄)₂ (FAS), 1 mM sodium L-ascorbate and 0, 12.5 or 50 μM echinomycin. EDTA·Fe(II) reaction conditions were identical except that MPE and iron were replaced by 200 μM EDTA and 400 μM FAS. MPE·Fe(II) digestion of DNA was carried out for 2 minutes at 37°C, EDTA·Fe(II) digestion of DNA for 10 minutes at 37°C.

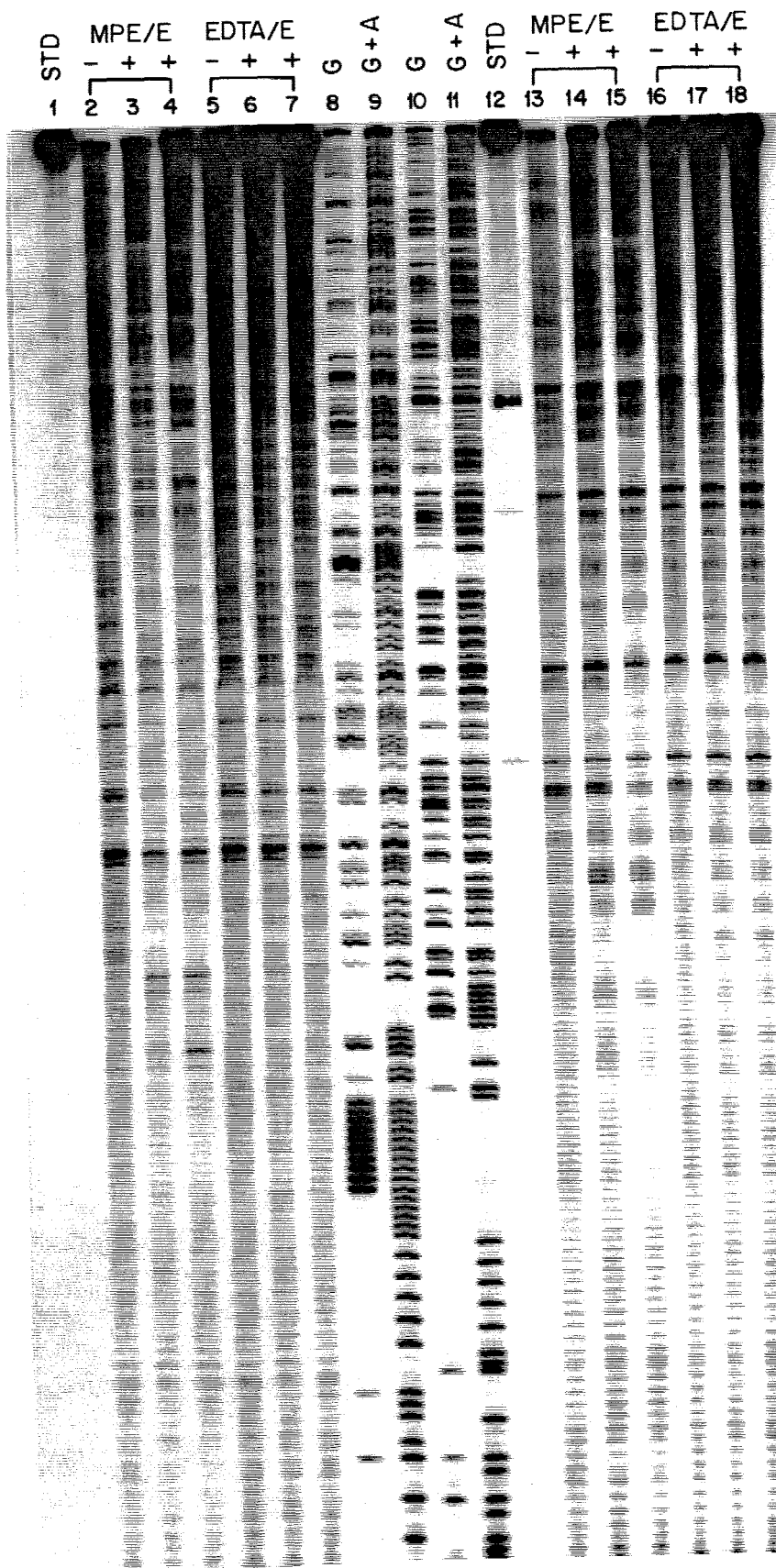
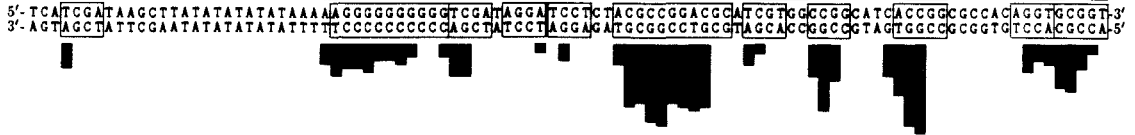


Figure 60. MPE·Fe(II) (A-B) and EDTA·Fe(II) (C-D) cleavage inhibition patterns on about 100 bp of the 628 bp pDMG10 DNA restriction fragment in the presence of 12.5 μ M echinomycin (A and C) or 50 μ M echinomycin (B and D), as determined by densitometry from the autoradiogram in Figure 59. MPE·Fe(II) and EDTA·Fe(II) cleavage inhibition patterns are shown as histograms or bars with the height proportional to the reduction of cleavage at each nucleotide compared with MPE·Fe(II) or EDTA·Fe(II) cleavage of unprotected DNA. Boxes are the assigned echinomycin binding sites based on the model in References 4 and 16.

MPE·Fe(II) / 12.5 μM Ech

A



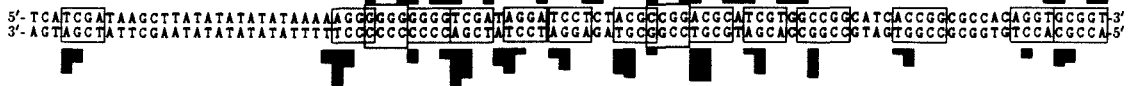
MPE·Fe(II) / 50 μM Ech

B



EDTA·Fe(II) / 12.5 μM Ech

C



EDTA·Fe(II) / 50 μM Ech

D

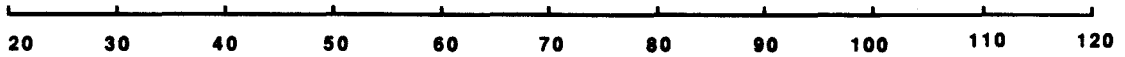
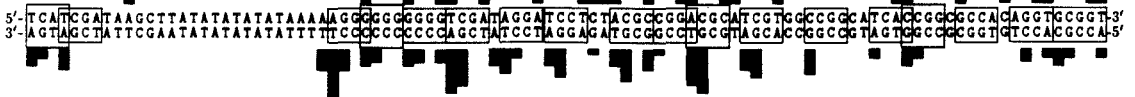


Figure 61. S1 nuclease probing of echinomycin binding to DNA at various pH values. Autoradiogram of high-resolution denaturing 8% polyacrylamide gel containing 5' (lanes 1-6, 19-20 and 23) or 3' (lanes 7-18, 21-22 and 24) ³²P end-labeled 628 bp *Eco* RI-*Bgl* I restriction fragment from plasmid pDMG10. 4 units of S1 nuclease were used to digest either unbound DNA (lanes 1-12) or DNA in the presence of 50 μM echinomycin (lanes 13-18). Digestion was carried out at pH 2.7 (lanes 1, 7, 13), pH 3.7 (lanes 2, 8, 14), pH 4.7 (lanes 3, 9, 15), pH 5.7 (lanes 4, 10, 16), pH 7.0 (lanes 5, 11, 17) or pH 8.0 (lanes 6, 12, 18). Lanes 23 and 24 are intact DNA (STD). Lanes 19 and 21 are the Maxam-Gilbert chemical sequencing G-specific reactions, lanes 20 and 22 the Maxam-Gilbert chemical sequencing purine-specific reactions on this fragment. S1 nuclease digestion conditions were 100 mM Tris / 100 mM sodium acetate (NaOAc) pH 2.7, 3.7, 4.7, 5.7, 7.0 or 8.0 with HCl, 0.5 mM ZnSO₄, 10% (v/v) methanol, 200 μM calf thymus DNA bp and 0 or 50 μM echinomycin. Digestion was for 10 minutes at 37°C.

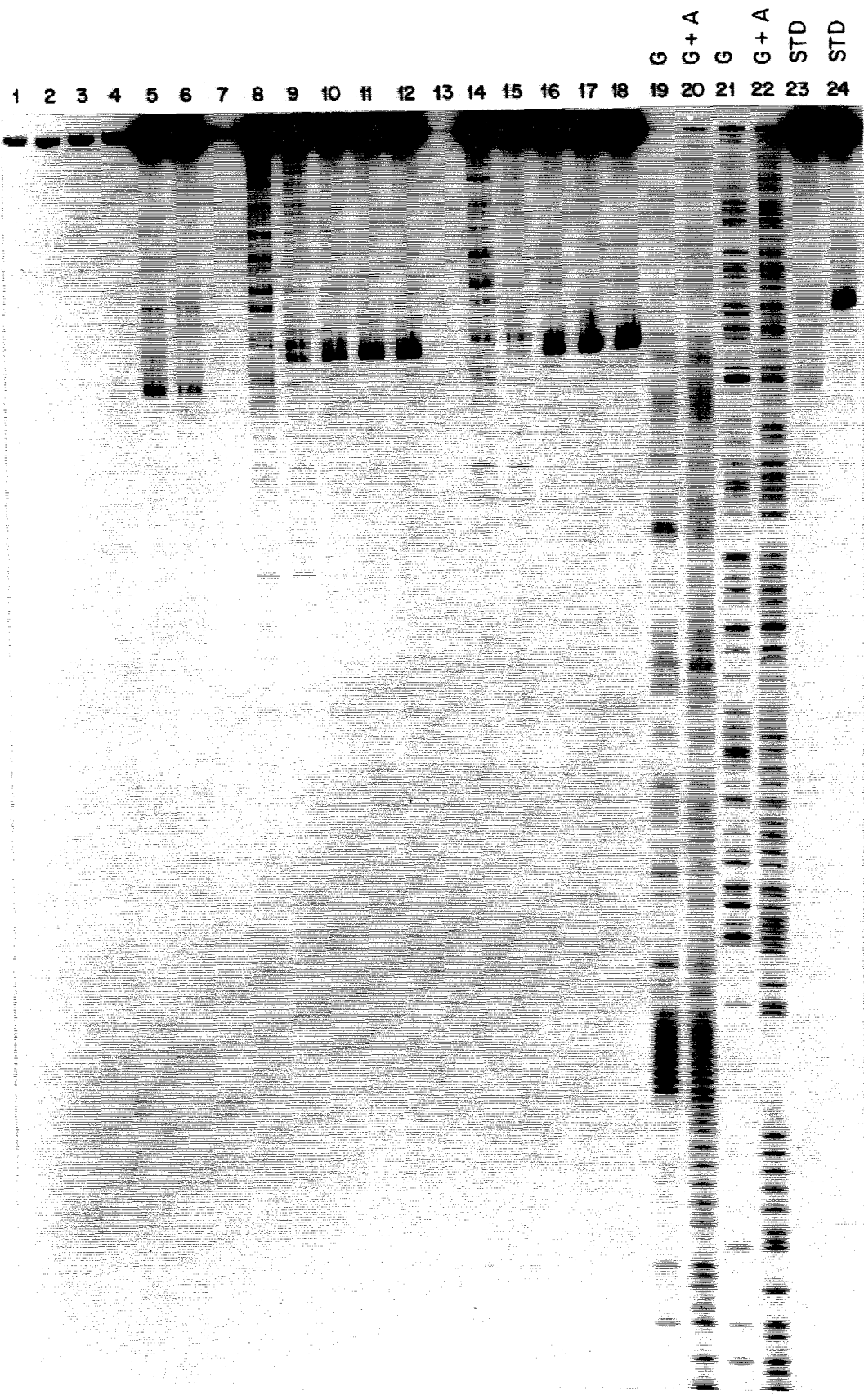
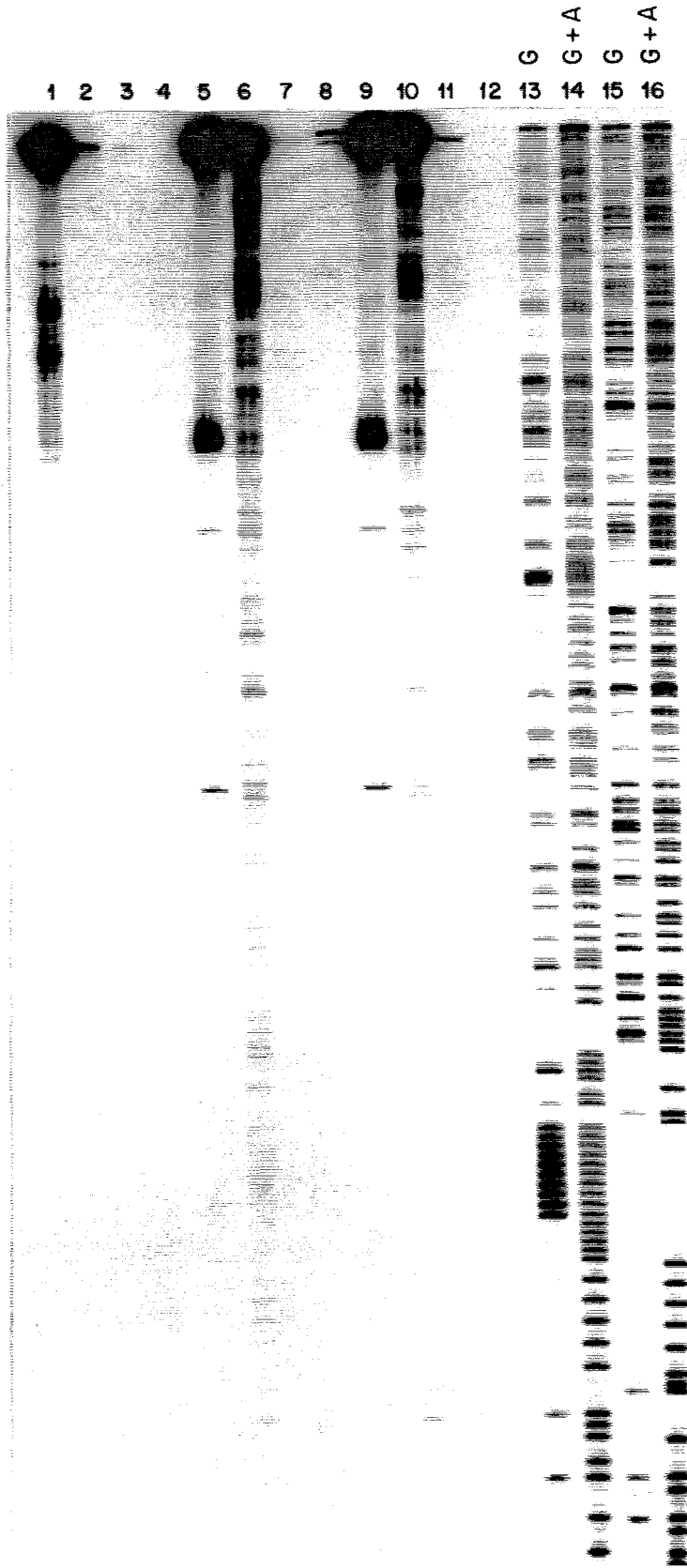


Figure 62. S1 nuclease probing of echinomycin binding to DNA: S1 nuclease unit study. Autoradiogram of high-resolution denaturing 8% polyacrylamide gel containing 5' (lanes 1-4 and 13-14) or 3' (lanes 5-12 and 15-16) ^{32}P end-labeled 628 bp *Eco* RI-*Bgl* I restriction fragment from plasmid pDMG10. S1 nuclease digestion of DNA was performed either in the absence of echinomycin, lanes 1-8, or in the presence of 50 μM echinomycin, lanes 9-12. DNA was digested with either no S1 nuclease (lanes 1, 5, 9), 6 units (lanes 2, 6, 10), 60 units (lanes 3, 7, 11) or 600 units (lanes 4, 8, 12) of S1 nuclease. Lanes 13 and 15 are the Maxam-Gilbert chemical sequencing G-specific reactions, lanes 14 and 16 the Maxam-Gilbert chemical sequencing purine-specific reactions on this DNA restriction fragment. Digestion conditions were 100 mM Tris / 100 mM NaOAc pH 4.7 with HCl, 0.5 mM ZnSO_4 , 10% (v/v) methanol, 200 μM calf thymus DNA bp and 0 or 50 μM echinomycin for 1 hour at 37°C.



from pDMG10 at various pH values. Lanes 1-6 show that the nuclease was active at and below pH 5.7 because the 5' radiolabel of the 628 bp *Eco* RI-*Bgl* I fragment from pDMG10 resides at the end of a 4 nucleotide (nt) single-stranded overhang generated by *Eco* RI digestion. 4 units of S1 nuclease removed greater than 95% of this label in the pH range 2.7-5.7 (Figure 61 lanes 1-4). At pH 7 and 8, the nuclease was inactive, shown by retention of the 5' label in lanes 5 and 6. On 3' end-labeled DNA, the label resides within a double-stranded region of DNA and was not removed by S1 nuclease unless the DNA was denatured. In the absence of echinomycin, S1 nuclease did not appreciably cleave the restriction fragment (lanes 7-12). Note that the 3' label was lost in lane 7, probably because of denaturing of the DNA duplex ends at pH 2.7. In the presence of 50 μ M echinomycin, S1 nuclease also failed to cleave the DNA to any significant extent throughout its active pH range (lanes 13-16). When larger amounts of S1 nuclease were employed for longer times at pH 4.7, similar results were obtained (Figure 62). Therefore, echinomycin did not impart any S1 nuclease hypersensitivity at or adjacent to its binding sites on the 628 bp restriction fragment from pDMG10.

In the presence of echinomycin, KMnO_4 modifies T residues within the A-T segment but not those at strong echinomycin binding sites.

KMnO_4 , like OsO_4 , is a chemical probe specific for thymidine residues. Both are believed to act by oxidizing thymidine residues across the 5,6 double bond.^{106,107} This lesion can then be developed into a DNA strand break by Maxam-Gilbert chemical sequencing workup. In general, B-DNA is unreactive to both these reagents and they react specifically with partially or wholly unwound T residues.^{84,107,108} In our hands, both reagents gave nearly identical results, but KMnO_4 gave a consistently better signal/noise ratio. KMnO_4 had the further advantage of being much less toxic than OsO_4 . KMnO_4 modification of the 628 bp fragment from pDMG10 is shown in Figure 63. In the absence of echinomycin (lanes 1 and 10) KMnO_4 did not significantly modify the DNA. In the

presence of 6.25 to 50 μM echinomycin, several T residues became reactive to KMnO_4 (lanes 2-5 and 11-14). Densitometric analysis of these results is shown in Figure 64. T residues at strong echinomycin binding sites such as 5'-TCGA-3' failed to react with KMnO_4 even at 50 μM echinomycin, but T residues within the A-T segment distal to the 5'-TCGA-3' sites were reactive to KMnO_4 at the lowest echinomycin concentrations tested (Figure 63). At 50 μM echinomycin, all except the last 5' T residues within the A-T segment reacted moderately with KMnO_4 (Figure 63, lanes 2 and 11 and Figure 64 B). Furthermore, the reaction pattern was 3' shifted and looked much like the DEP-adenosine reactivity pattern shown in Figure 57 H. No clear pattern appeared for the other T residues reactive to KMnO_4 in the presence of echinomycin except that T residues at strong echinomycin binding sites did not react with the probe: The palindromic sequence 5'-AGGATCCT-3' is a moderate echinomycin binding site and only the 3' extreme T residue was moderately KMnO_4 -reactive, but the T residues within the sequence 5'-TCGT-3', a strong echinomycin binding site, did not react with KMnO_4 even at 50 μM echinomycin (Figure 64).

Neocarzinostatin (NCS) and Bleomycin $\text{A}_2\cdot\text{Fe(II)}$ (BLM) footprinting of echinomycin.

NCS and BLM are naturally occurring antibiotics that damage DNA by oxidative degradation of the deoxyribose moiety.^{11,109,110} Unlike $\text{MPE}\cdot\text{Fe(II)}$ or $\text{EDTA}\cdot\text{Fe(II)}$, NCS and BLM each exhibit a moderately strong sequence binding/cleavage preference, NCS preferring to cleave at A or T residues and BLM at GT, GC and GG sequences. Both BLM and NCS appear to bind and damage DNA via the minor groove, although the modes of DNA binding and cleavage mechanisms differ for each reagent (see Discussion). NCS and BLM damage to the 628 bp fragment from pDMG10 is shown in Figure 65. In the absence of echinomycin, NCS damage to DNA was modest and showed the expected sequence preference (lanes 2 and 13). The A-T-rich segment at the bottom third of the gel

Figure 63. KMnO_4 reactivity in the presence of echinomycin. Autoradiogram of high resolution denaturing 8% polyacrylamide gel containing 5' (lanes 1-7) or 3' (lanes 8-14) ^{32}P end-labeled 628 bp *Eco* RI-*Bgl* I restriction fragment from plasmid pDMG10. Lanes: 1 and 10, KMnO_4 /piperidine cleavage of unbound DNA, 2-5 and 11-14, KMnO_4 /piperidine cleavage of DNA in the presence of 6.25, 12.5, 25 or 50 μM echinomycin, respectively. Lanes 6 and 8 are the Maxam-Gilbert chemical sequencing G-specific reactions, lanes 7 and 9 the Maxam-Gilbert chemical sequencing purine-specific reactions on the 628 bp DNA fragment. Reaction conditions were 100 mM Tris / 100 mM NaOAc pH 7.0 with HCl, 200 μM calf thymus DNA bp, 10% (v/v) methanol, 0-50 μM echinomycin and 50 μM KMnO_4 . KMnO_4 modification was for 15 minutes at 37°C.

KMnO ₄ /ECH					Δ	Δ	KMnO ₄ /ECH						
-	+	+	+	+	⊖	⊖	⊖	⊖	-	+	+	+	+
└──────────┘									└──────────┘				
1	2	3	4	5	6	7	8	9	10	11	12	13	14

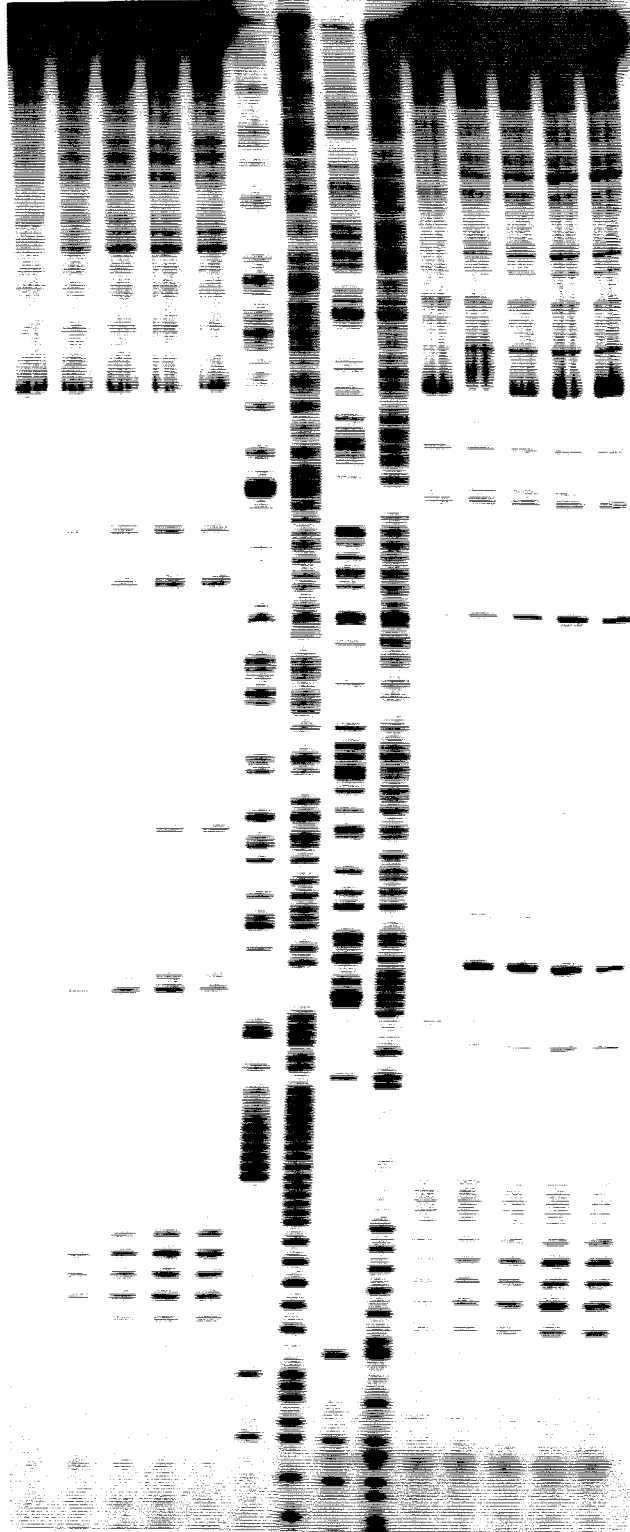
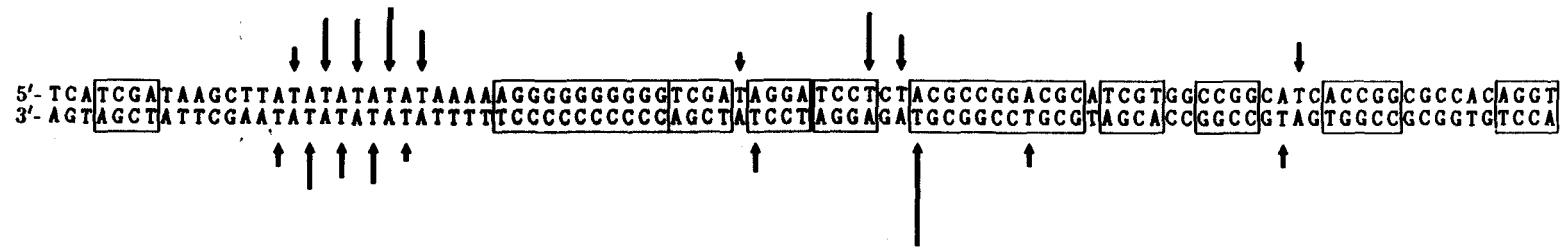
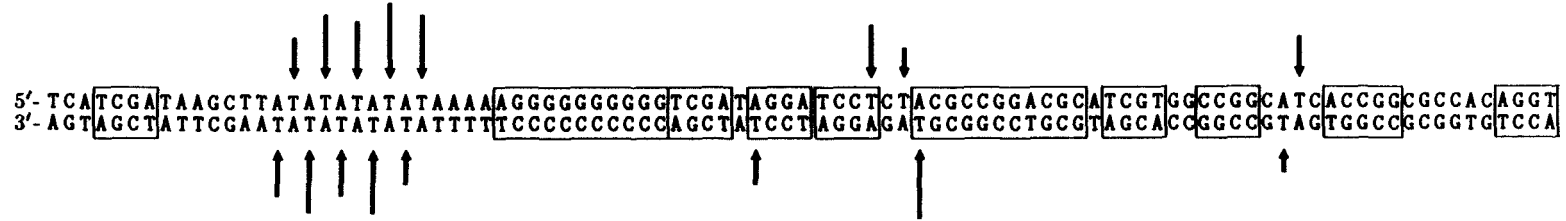


Figure 64. KMnO_4 /piperidine cleavage patterns in the presence of 12.5 μM echinomycin (A) or 50 μM echinomycin (B) on about 90 bp of the 628 bp restriction fragment from plasmid pDMG10, as determined by densitometry of the autoradiogram in Figure 63. KMnO_4 /piperidine cleavage patterns are shown as arrows with height proportional to cleavage enhancement at each nucleotide compared to KMnO_4 /piperidine cleavage of unbound DNA. Boxes represent the echinomycin binding sites on this fragment independently determined by $\text{MPE}\cdot\text{Fe(II)}$ footprinting.

A



B



was subject to uniform damage by NCS. The NCS cleavage ladder actually resembled an MPE·Fe(II) cleavage ladder missing the rungs at GC-rich sequences. In the presence of 12.5 or 50 μ M echinomycin (Figure 65, lanes 3-4 and 14-15) mild but significant changes appeared in the NCS-mediated cleavage patterns of DNA. The most visible of these changes occurred at the A-T-rich segment near the bottom of the gel. NCS-mediated cleavage of this segment in the presence of echinomycin had the form of a well when compared to cleavage in the absence of drug. There was slight inhibition of NCS action at the center of the A-T segment that was accompanied by a spreading and intensification of NCS-mediated cleavage at both ends of the A-T segment (compare Figure 65 lane 2 with 4 and lane 13 with 15). This pattern was even more evident in Figure 66, which shows NCS cleavage of the 628 bp fragment from plasmid pDMAG10. NCS efficiently cleaved the A-T segment in the absence of echinomycin (Figure 66 lanes 1 and 4). 12.5 or 50 μ M echinomycin inhibited NCS cleavage at the center of the A-T segment and enhanced NCS cleavage at the ends of the A-T segment (compare Figure 66 lane 1 with lanes 2-3 and lane 4 with lanes 5-6). Densitometric analysis of the NCS cleavage inhibition by echinomycin on pDMG10 is presented in Figure 67 A and B. NCS-mediated cleavage inhibition by echinomycin is shown as bars and NCS-mediated cleavage enhancement by echinomycin is shown as arrows (Figure 67A and B). Changes in NCS action at other sequences on this fragment showed that NCS damage to DNA was inhibited within and enhanced directly adjacent to strong echinomycin binding sites. On average, the patterns of NCS cleavage inhibition by echinomycin were shifted to the 3' side and agreed well with the echinomycin binding sites determined by MPE·Fe(II) footprinting. However, the inherent specificity of NCS for damaging A or T residues makes it a limited reagent for footprinting a G-C specific DNA binding ligand such as echinomycin.

Bleomycin cleavage of the 628 bp DNA restriction fragment in the absence of echinomycin gave a more intense and specific pattern than did neocarzinostatin (Figure 65 lanes 5 and 16). BLM cleavage of the A-T-rich segment showed an apparent strand

Figure 65. Neocarzinostatin (NCS) and Bleomycin $A_2 \cdot Fe(II)$ (BLM) footprinting of echinomycin. Autoradiogram of high-resolution denaturing 8% polyacrylamide gel containing 5' (lanes 1-9) and 3' (lanes 10-18) ^{32}P end-labeled 628 bp *Eco* RI-*Bgl* I restriction fragment from plasmid pDMG10. Lanes: 1 and 12, intact DNA standards subjected to 100 mM NaOH / 0.1 mM EDTA / heat workup; 2 and 13, NCS cleavage of unbound DNA; 3-4 and 14-15, NCS cleavage of DNA in the presence of 12.5-50 μ M echinomycin, respectively; 5 and 16, BLM cleavage of unbound DNA, 6-7 and 17-18, BLM cleavage of DNA bound by 12.5-50 μ M echinomycin, respectively; 8 and 10, Maxam-Gilbert chemical sequencing G-specific reactions; 9 and 11, Maxam-Gilbert chemical sequencing purine-specific reactions on the 628 bp fragment. Reaction conditions were 100 mM Tris / 100 mM NaOAc pH 7.0 with HCl, 200 μ M calf thymus DNA bp, 10% (v/v) methanol, 0, 12.5 or 50 μ M echinomycin and either 4 units of NCS (protein + chromophore in 15 mM NaOAc pH 5.0, Bristol Laboratories) or 4 μ M BLM (Blenoxane) / 4 μ M FAS. In addition, NCS reactions contained 10 mM 2-mercaptoethanol and BLM reactions contained 4 mM dithiothreitol (DTT). Cleavage of DNA was allowed to proceed for 20 minutes at 37°C and the DNA was precipitated and rinsed with ethanol. BLM cleavage products were ready for application to the gel at this point, but NCS cleavage products were developed by heating the DNA in 100 mM NaOH / 0.1 mM EDTA for 30 minutes at 90°C. The mixture was then cooled, reprecipitated from ethanol and vacuum-dried before application onto the polyacrylamide gel.

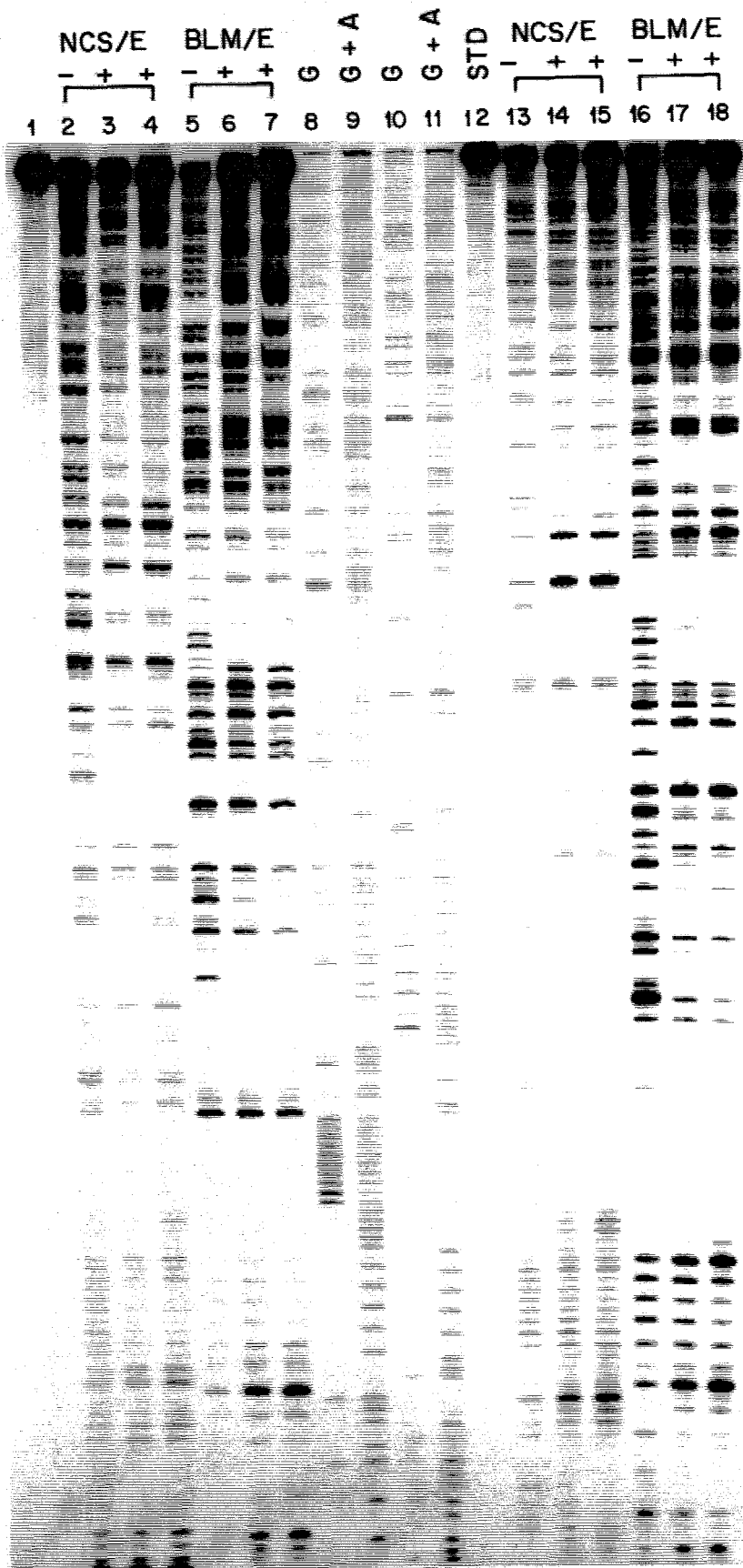


Figure 66. Neocarzinostatin (NCS) footprinting of echinomycin. Autoradiogram of high-resolution denaturing 8% polyacrylamide gel containing 5' (lanes 1-3 and 7-8) and 3' (lanes 4-6) ^{32}P end-labeled 628 bp *Eco* RI-*Bgl* I restriction fragment from plasmid pDMAG10. Lanes: 1 and 4, NCS cleavage of unbound DNA; 2-3 and 5-6, NCS cleavage of DNA bound by 12.5-50 μM echinomycin; 7, Maxam-Gilbert chemical sequencing G-specific reaction; 8, Maxam-Gilbert chemical sequencing purine-specific reaction on this restriction fragment. Reaction conditions were 100 mM Tris / 100 mM NaOAc pH 7.0 with HCl, 0.025 mM ZnSO_4 , 200 μM calf thymus DNA bp, 10% (v/v) methanol, 4 units of NCS (protein + chromophore in 15 mM NaOAc pH 5.0, Bristol Laboratories) and 10 mM 2-mercaptoethanol. NCS damage progressed for 15 minutes (dark) at 37°C and samples were then subjected to heat/base workup.

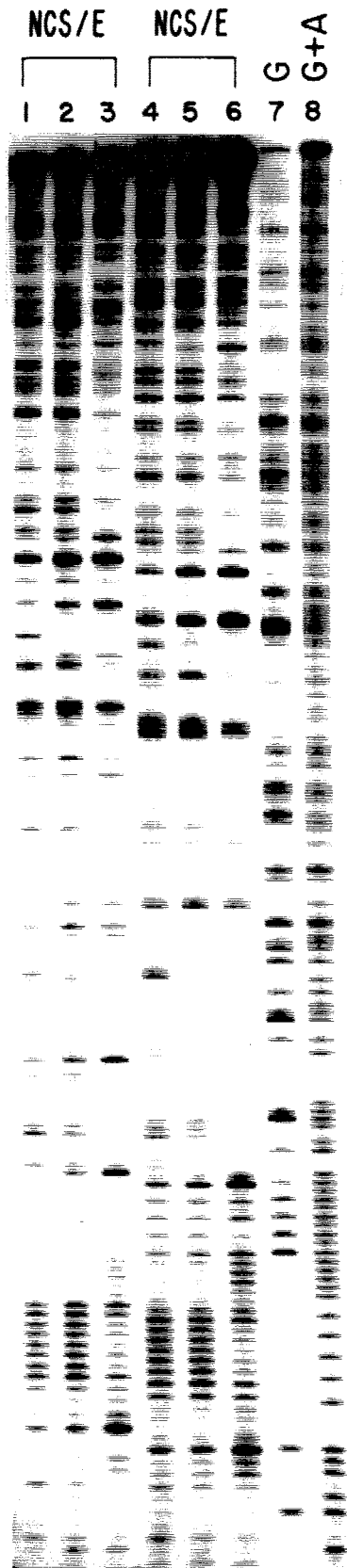
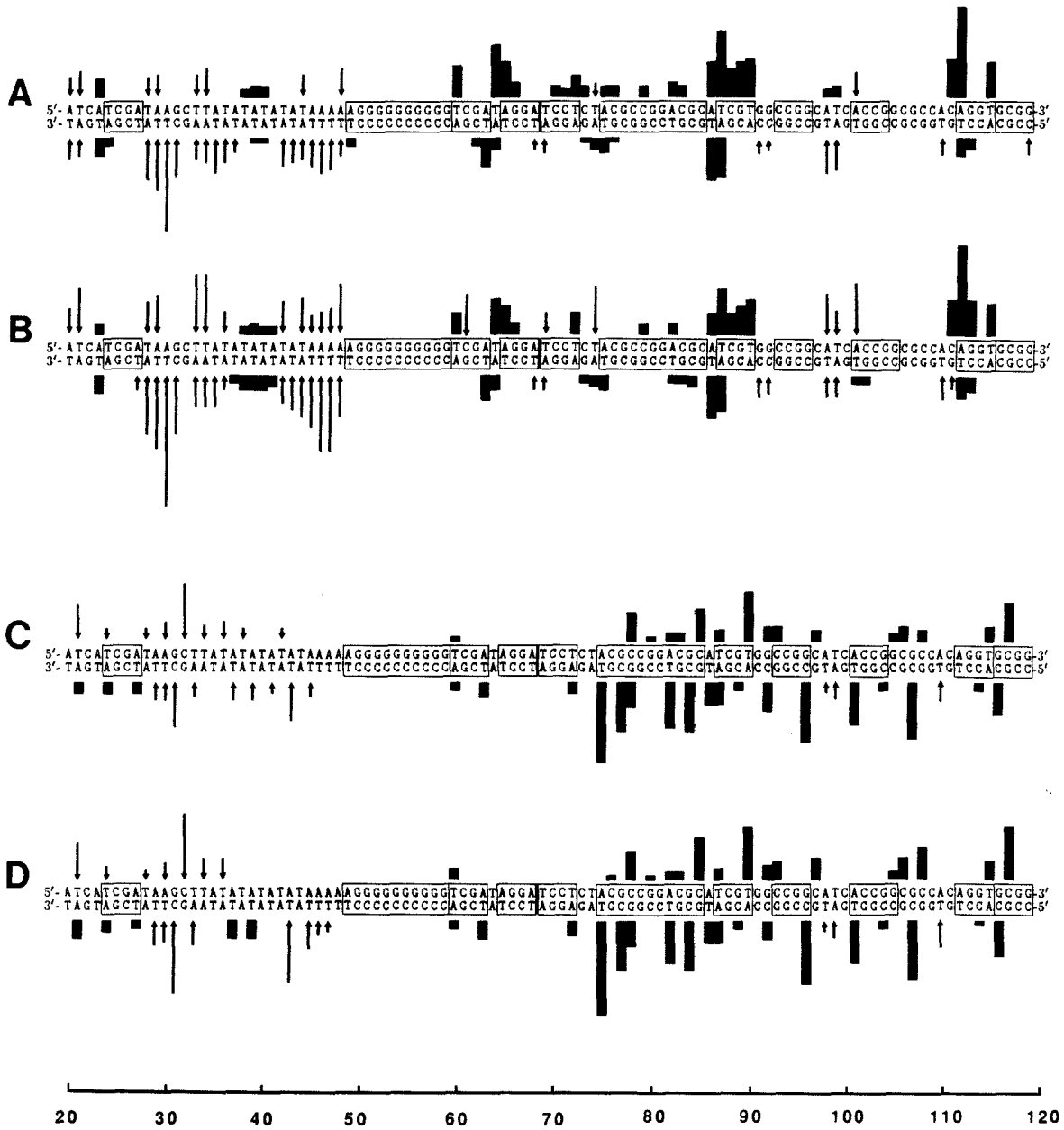


Figure 67. Densitometric analysis of NCS and BLM footprinting of echinomycin. Differential DNA cleavage patterns produced by neocarzinostatin (A-B) or bleomycin $A_2 \cdot Fe(II)$ (C-D) in the presence of $12.5 \mu M$ echinomycin (A and C) or $50 \mu M$ echinomycin (B and D) on about 100 bp of the 628 bp pDMG10 restriction fragment, as determined by densitometry of the autoradiogram in Figure 65. Differential neocarzinostatin (NCS) and bleomycin $A_2 \cdot Fe(II)$ (BLM) DNA cleavage patterns are shown as bars with height proportional to NCS or BLM cleavage inhibition and as arrows with height proportional to NCS or BLM cleavage enhancement at each nucleotide compared to NCS or BLM cleavage of unbound DNA. Boxes are the assigned echinomycin binding sites independently determined by MPE $\cdot Fe(II)$ footprinting on this restriction fragment. The scale at the bottom is as in Figures 57 and 59.



preference, cleaving this segment only weakly on the 5' strand while cleaving the 3' labeled strand quite efficiently (compare the bottom third of Figure 65 lanes 5 and 16). In the presence of 12.5 or 50 μ M echinomycin (lanes 6-7 and 17-18), BLM cleavage patterns on this fragment changed markedly. BLM cleavage inhibition predominated in the top half of each of these lanes, whereas BLM cleavage modulation was more complex on the lower half of each of these lanes. BLM cleavage of the A-T segment in the presence of echinomycin resembled a well: Echinomycin protected the core of the A-T segment from BLM cleavage and rendered the outer edges of the A-T segment more susceptible to BLM cleavage (compare lane 5 with lane 7 and lane 16 with 18 in Figure 65). This is shown in graphic form to the left of Figure 67 C and D, bars showing BLM cleavage inhibition and arrows showing BLM cleavage enhancement. This inhibition/enhancement pattern was similar to that obtained with NCS under similar conditions (compare Figure 67 A and C, B and D). Inhibition of BLM cleavage by echinomycin over the upper half of Figure 65 is plotted to the right in Figure 67 C and D. BLM cleavage inhibition by echinomycin is shifted to the 3' side and mapped to the echinomycin binding sites independently determined by MPE·Fe(II) footprinting. As with NCS, the inherent sequence specificity of BLM limited its use as a footprinting reagent.

Distamycin A abolishes reactivity of the A-T segment toward DEP in the presence of echinomycin.

The 17 bp run of A-T rich DNA in the 628 bp *Eco* RI-*Bgl* I fragment of pDMAG10 is sandwiched by two strong echinomycin binding sites, 5'-TCGA-3'. We tested the ability of distamycin A or echinomycin to affect DNA binding of each other when their individual binding sites were juxtaposed. Figure 68 presents the autoradiogram containing the results of this test. In the absence of either drug, MPE·Fe(II) produced its usual even ladder of DNA cleavage products (lanes 2 and 19). 4 μ M distamycin A (lanes 4 and 21) protected virtually all of the 17 bp A-T-rich sequence from cleavage by MPE·Fe(II). This is seen as a

Figure 68. MPE·Fe(II) and DEP/piperidine footprinting of echinomycin and distamycin A. A. Autoradiogram of high-resolution denaturing 8% polyacrylamide gel containing 5' (lanes 1-15) or 3' (lanes 16-30) ³²P end-labeled 628 bp Eco RI-Bgl I restriction fragment from plasmid pDMAG10. Lanes: 1 and 18, buffered, intact DNA (STD); 2 and 19, MPE·Fe(II) cleavage of unprotected DNA; 3 and 20, MPE·Fe(II) cleavage of DNA in the presence of 50 μM echinomycin (E); 4-5 and 21-22, MPE·Fe(II) cleavage of DNA in the presence of 4-10 μM distamycin A (D); 6-7 and 23-24, MPE·Fe(II) cleavage of DNA in the presence of 50 μM echinomycin plus 4-10 μM distamycin A, respectively (E+D, echinomycin added first); 8 and 25, DEP/piperidine cleavage of unbound DNA; 9-10 and 26-27, DEP/piperidine cleavage of DNA in the presence of 4-10 μM distamycin A; 11 and 28, DEP/piperidine cleavage of DNA in the presence of 50 μM echinomycin; 12-13 and 29-30, DEP/piperidine cleavage of DNA in the presence of 50 μM echinomycin plus 4-10 μM distamycin A (echinomycin added first); 14 and 16, Maxam-Gilbert chemical sequencing G-specific reactions; 15 and 17, Maxam-Gilbert chemical sequencing purine-specific reactions on this fragment. Reaction conditions were 100 mM Tris / 100 mM NaOAc pH 7.0 with HCl, 200 μM calf thymus DNA bp, and 10% (v/v) methanol. MPE·Fe(II) reactions also contained 4 μM MPE, 8 μM FAS and 1 mM sodium L-ascorbate. DEP reactions contained 68 mM DEP. After initial equilibration of drugs and MPE·Fe(II), MPE·Fe(II) cleavage was allowed to proceed for 35 minutes at 37°C. DEP modification of DNA was allowed to proceed for 10 minutes at 37°C.

Figure 69. Densitometric analysis of MPE·Fe(II) and DEP/piperidine footprinting of echinomycin and distamycin A. (A-E) are the MPE·Fe(II) cleavage inhibition patterns in the presence of 4 μ M distamycin A (A), 10 μ M distamycin A (B), 50 μ M echinomycin (C), 4 μ M distamycin A + 50 μ M echinomycin (D) or 10 μ M distamycin A + 50 μ M echinomycin (E) on about 100 bp of the 628 bp *Eco* RI-*Bgl* I restriction fragment from plasmid pDMAG10, as determined by densitometry of the autoradiogram in Figure 68. (F-H) are the DEP/piperidine cleavage patterns on the same 100 bp of DNA in the presence of 50 μ M echinomycin (F), 4 μ M distamycin A + 50 μ M echinomycin (G) or 10 μ M distamycin A + 50 μ M echinomycin (H), as determined by densitometry of Figure 68. MPE·Fe(II) cleavage inhibition patterns are shown as histograms or bars with height proportional to the reduction of MPE·Fe(II) cleavage at each nucleotide compared to MPE·Fe(II) cleavage of unbound DNA. DEP/piperidine cleavage patterns are shown as arrows with height proportional to the enhancement of DEP/piperidine cleavage at each nucleotide compared to DEP/piperidine cleavage of unbound DNA. Boxes are the assigned echinomycin or distamycin A binding sites based on the model in References 4, 16 and 88.

4 μ M Dist



10 μ M Dist



50 μ M Ech



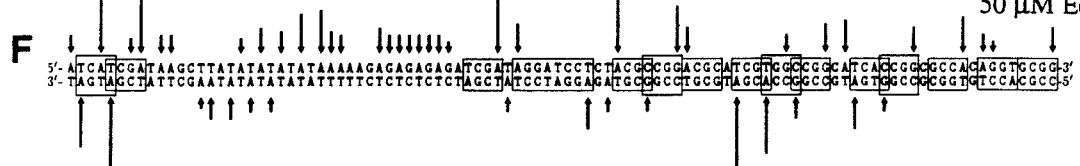
50 μ M Ech + 4 μ M Dist



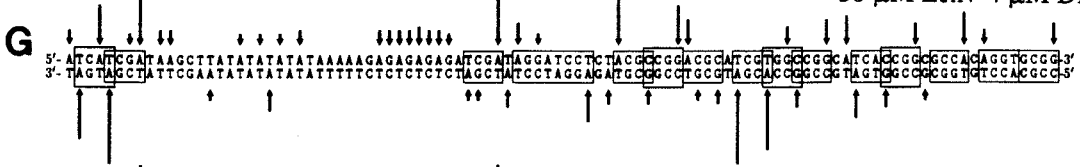
50 μ M Ech + 10 μ M Dist



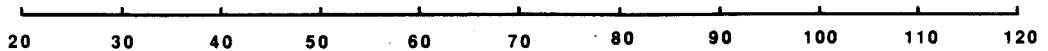
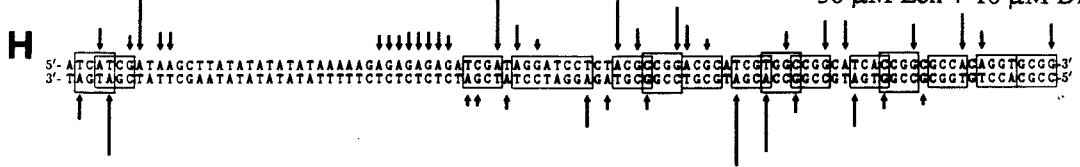
50 μ M Ech



50 μ M Ech + 4 μ M Dist



50 μ M Ech + 10 μ M Dist



large gap in the MPE·Fe(II) cleavage pattern when compared to control cleavage of unbound DNA. Higher concentrations of distamycin A (lanes 5 and 22) protected the same region as well as some less A-T-rich DNA from MPE·Fe(II) cleavage. This is presented in graphic form as Figure 69 A and B. 50 μ M echinomycin alone (lanes 3 and 20) protected several regions of DNA on this fragment from MPE·Fe(II) cleavage. The protected regions mapped to the sequences (5'-3') TCATCGA, TCGA, AGGATCCT, ACGCCGGACGC, TCGT, CCGG, TCACCGG, AGGT and GCGG (Figure 69 C). It was readily apparent that echinomycin and distamycin A each bind entirely different DNA sequences on this fragment (compare Figure 68 lane 3 with lanes 4-5, lane 20 with lanes 21-22 and Figure 69 C to A and B). When 50 μ M echinomycin was allowed to bind the restriction fragment and distamycin A was added subsequently, the resulting MPE·Fe(II) cleavage inhibition patterns closely resembled a simple summation of the MPE·Fe(II) cleavage patterns produced by each drug in the absence of the other (Figure 68 lanes 6-7, lanes 23-24 and Figure 69 D and E). It appeared that on this restriction fragment, echinomycin and distamycin do not compete with one another for DNA binding.

Echinomycin and distamycin A differed not only in their DNA sequence binding preferences, but also in their abilities to enhance DEP-purine hyperreactivity upon binding to DNA. In the absence of either drug, DEP/piperidine did not cleave the DNA to a significant extent (Figure 68 lanes 8 and 25). Both 4 and 10 μ M echinomycin failed to enhance any significant DEP-purine reactivity (lanes 9-10 and 26-27). As seen before on a similar restriction fragment, 50 μ M echinomycin dramatically enhanced DEP-purine reaction at and adjacent to its binding sites (lanes 11 and 28). However, addition of 4 and 10 μ M distamycin A to DEP-DNA reactions containing echinomycin selectively and almost totally inhibited DEP reaction of the adenosine residues within the A-T rich segment (compare lane 11 with lanes 12-13 and lane 28 with lanes 29-30). Figure 69 F-H presents the densitometric analysis of these results. Note that reactivity of all the other purines to DEP was not significantly affected by the addition of distamycin A to the system.

Distamycin A therefore selectively abolished the DEP reactivity of purines at its binding sites.

NaCl concentration dependence of echinomycin induced DEP-purine reactivity.

Figure 70 shows the DEP/piperidine cleavage patterns in the presence of 0 or 50 μM echinomycin over the entire aqueous solubility range of NaCl. In the absence of echinomycin (lanes 1-6 and 17-22), DEP did not modify the 628 bp fragment from pDMG10 to a significant extent. There was no NaCl concentration dependence upon the DEP reactivity of this DNA fragment in the absence of echinomycin. This result implied that high or low NaCl concentrations did not cause gross structural rearrangements to occur on this DNA fragment in the absence of echinomycin. DEP/piperidine cleavage in the presence of 50 μM echinomycin produced a number of intense cleavage bands on the autoradiogram (lanes 7-12 and 23-28). As before on this restriction fragment, these cleavage bands mapped to the first and/or fourth base pair positions of echinomycin binding sites with the exception of the A-T-rich segment at the bottom quarter of the gel. Densitometric analyses of results are presented in Figure 71. Two previously undetected 5'-GGGG-3' echinomycin binding sites were seen within the G10 run and showed the 1,4 pattern of DEP/purine reaction (see Figure 71 B and C).

Significant modulation of the DEP/piperidine cleavage patterns produced by echinomycin occurred over the range of "zero" NaCl to saturated NaCl. Overall DEP/piperidine cleavage outside echinomycin binding sites was inversely proportional to NaCl concentration (Figure 70 lanes 7-12 and 23-28). The DEP reactivity of adenosine residues within the A-T segment decreased markedly on progressing from 10 mM to 1.0 M to saturated NaCl (Figure 71 A-C). Further, the DEP reactivity of adenosine residues adjacent to assigned echinomycin binding sites decreased with increasing NaCl concentration. Several examples include the base pairs at positions 64, 99 and 120-121.

Figure 70. DEP/piperidine footprinting of echinomycin: NaCl concentration dependence. Autoradiogram of high-resolution denaturing 8% polyacrylamide gel containing either 5' (lanes 1-14) or 3' (lanes 15-28) ³²P end-labeled 628 bp *Eco* RI-*Bgl* I restriction fragment from plasmid pDMG10. DEP/piperidine cleavage was performed either without drug (lanes 1-6 and 17-22) or in the presence of 50 μM echinomycin (lanes 7-12 and 23-28) at "0" mM NaCl (no added salt, lanes 1,7,17,23), 10 mM NaCl (lanes 2,8,18,24), 1.0 M NaCl (lanes 3,9,19,25), 4.0 M NaCl (lanes 5,11,21,27) or saturated NaCl (lanes 6,12,22,28). Lanes 13 and 15 are the Maxam-Gilbert chemical sequencing G-specific reactions, lanes 14 and 16 the Maxam-Gilbert chemical sequencing purine-specific reactions on this DNA restriction fragment. Reaction conditions were 10 mM Tris.HCl pH 7.4, 0, 0.01, 0.1, 1.0, 4.0 or saturated NaCl, 200 μM calf thymus DNA bp, 10% (v/v) methanol and 68 mM DEP. Reaction was for 15 minutes at room temperature.

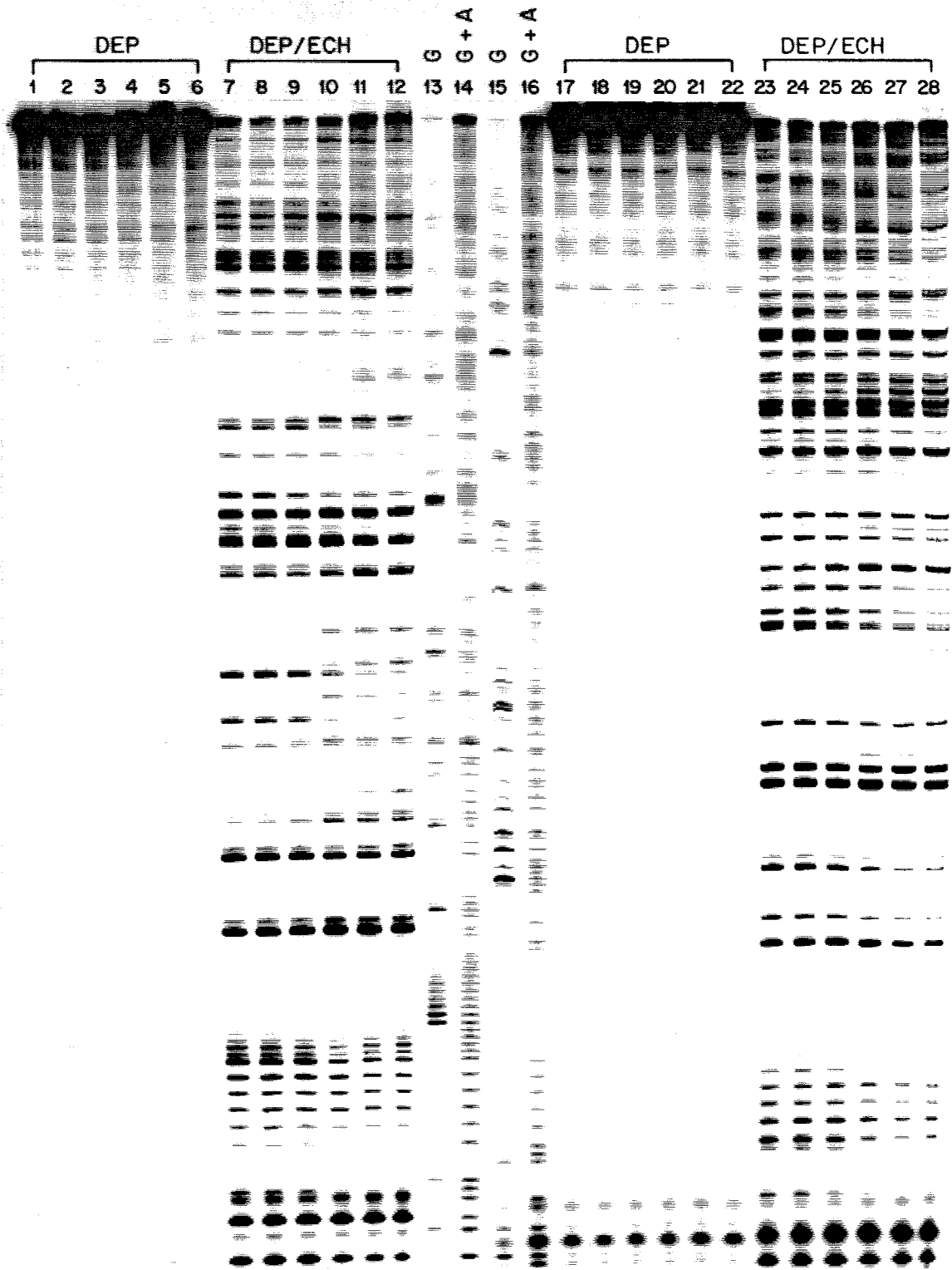
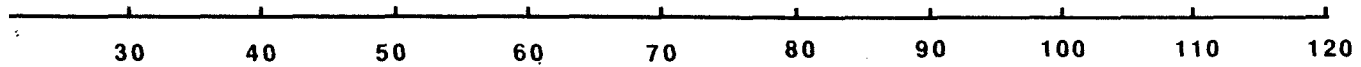
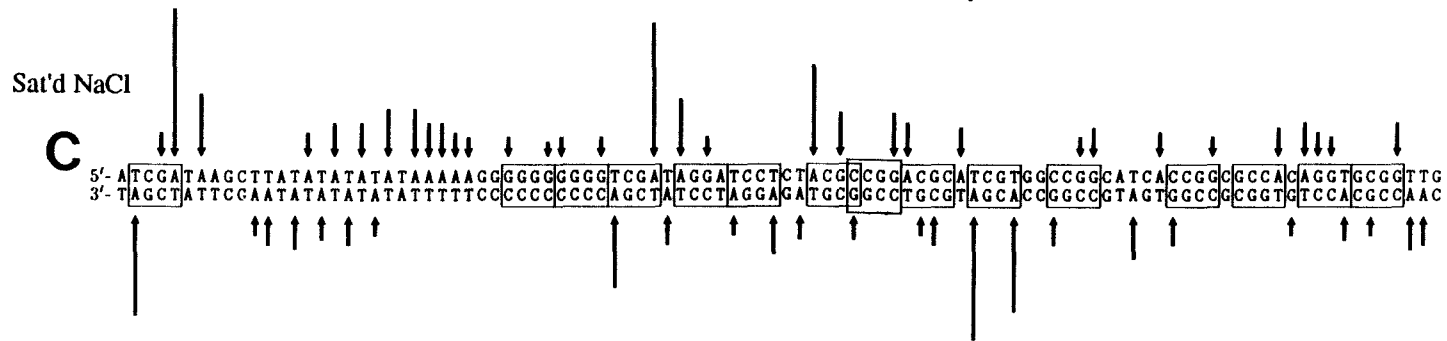
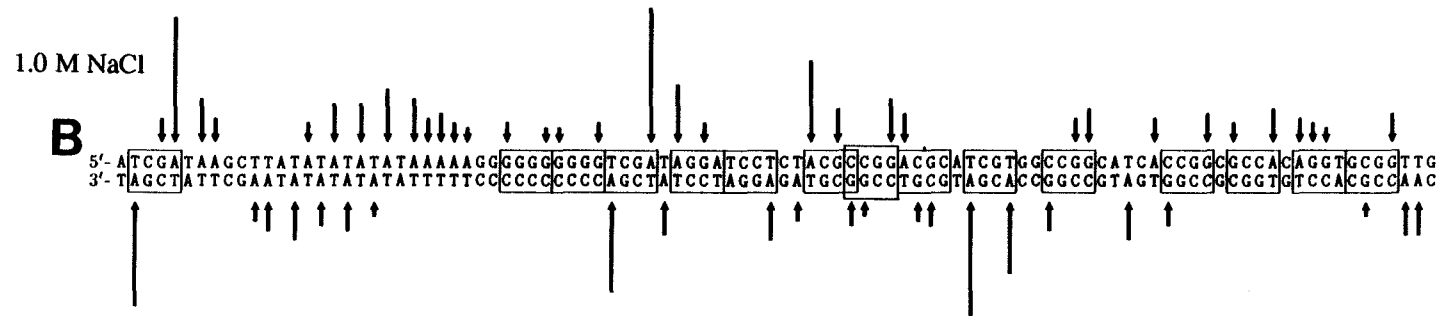


Figure 71. NaCl concentration dependence of DEP/piperidine cleavage patterns in the presence of 50 μ M echinomycin on about 100 bp of the 628 bp *Eco* RI-*Bgl* I restriction fragment from plasmid pDMG10, as determined by densitometry of the autoradiogram in Figure 70. DEP/piperidine cleavage patterns at 50 μ M echinomycin plus 10 mM NaCl (A), 1.0 M NaCl (B) or saturated NaCl (C) are shown as arrows with height proportional to the enhancement of DEP/piperidine cleavage at each nucleotide compared to DEP/piperidine cleavage of unbound DNA at the same NaCl concentration. Boxes are the assigned echinomycin binding sites based on DEP/piperidine cleavage at the first and/or fourth base pair positions of four base pair echinomycin binding sites containing a central 5'-3' CG, CC, GG or CA dinucleotide.⁸⁸ The scale at bottom corresponds to the first 5' thymidine of the *Eco* RI site of pDMG10 defined as position 1.



Within strong echinomycin binding sites, the dependence of NaCl concentration upon DEP reactivity was less clear. Adenosine residues on both strands within the 5'-TCGA-3' site starting at position 24 reacted more intensely with DEP as NaCl concentration increased. A similar increase in DEP-purine reactivity with increasing NaCl concentration was seen at the sites (5'-3') GGGG, AGGA, ACGC, TCGT and CCGG. However, a second 5'-TCGA-3' site at position 60 showed increased adenosine-DEP reactivity on the upper strand and decreased adenosine-DEP reactivity on the lower strand as NaCl concentration increased. In general, DEP-purine reactivity within strong echinomycin binding sites increased with increasing NaCl concentration and DEP-purine reactivity adjacent or distal to strong echinomycin binding sites decreased with increasing NaCl concentration. Similar results were obtained using 10 mM to 4 M MgCl₂ (data not shown). In addition, the clarity of this autoradiogram also allowed the assignment of two new 5'-GGGG-3' echinomycin binding sites within the G10 segment present in plasmid pDMG10.

pH dependence of DEP/piperidine cleavage.

Figure 72 shows DEP/piperidine cleavage patterns in the presence of 0 or 50 μ M echinomycin in tris-acetate (TA) buffer pH 2.7, 3.7, 4.7, 5.7, 7.0 or 8.0. In the absence of echinomycin, DEP/piperidine cleavage of the 628 bp fragment from pDMG10 was very weak (lanes 1-6 and 17-22). At the lowest pH values employed, slightly greater cleavage was observed at most adenosine residues, probably because of slow depurination (deadenylation) of the DNA at pH 2.7 and 3.7. Other than this, no significant DEP/piperidine cleavage occurred without echinomycin over the pH range 2.7 to 8.0. This implied that acidic conditions alone do not grossly affect the structure of this DNA restriction fragment. Addition of 50 μ M echinomycin to the system gave the usual pattern of intense DEP/piperidine cleavage bands (lanes 7-12 and 23-28). Progressing from reactions conducted at pH 2.7 to those performed at pH 8.0, some DEP/piperidine cleavage

Figure 72. DEP/piperidine footprinting of echinomycin: pH dependence of the reaction. Autoradiogram of high-resolution denaturing 8% polyacrylamide gel containing 5' (lanes 1-14) or 3' (lanes 15-28) ^{32}P end-labeled 628 bp *Eco* RI-*Bgl* I DNA restriction fragment from plasmid pDMG10. DEP/piperidine cleavage was performed either without drug (lanes 1-6 and 17-22) or in the presence of 50 μM echinomycin (lanes 7-12 and 23-28) at pH 2.7 (lanes 1,7,17,23), pH 3.7 (lanes 2,8,18,24), pH 4.7 (lanes 3,9,19,25), pH 5.7 (lanes 4,10,20,26), pH 7.0 (lanes 5,11,21,27) or pH 8.0 (lanes 6,12,22,28). Lanes 13 and 15 are the Maxam-Gilbert chemical sequencing G-specific reactions, lanes 14 and 16 the Maxam-Gilbert chemical sequencing purine-specific reactions on this DNA fragment. DEP reaction conditions were 100 mM Tris / 100 mM NaOAc pH 2.7, 3.7, 4.7, 5.7, 7.0 or 8.0 with HCl, 10% (v/v) methanol, 200 μM calf thymus DNA bp, 0 or 50 μM echinomycin and 68 mM DEP. DEP modification of DNA was for 10 minutes at 37°C.

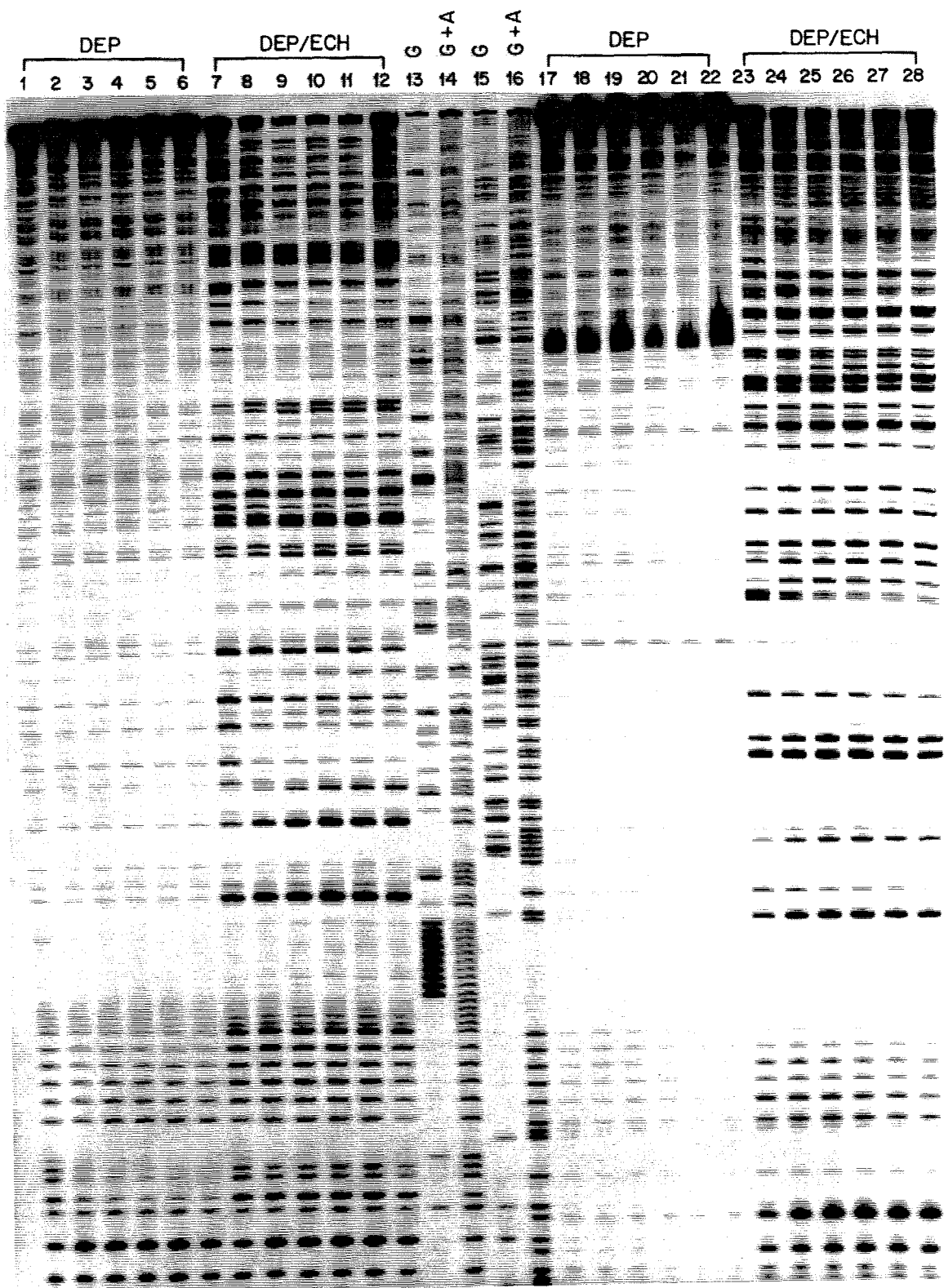
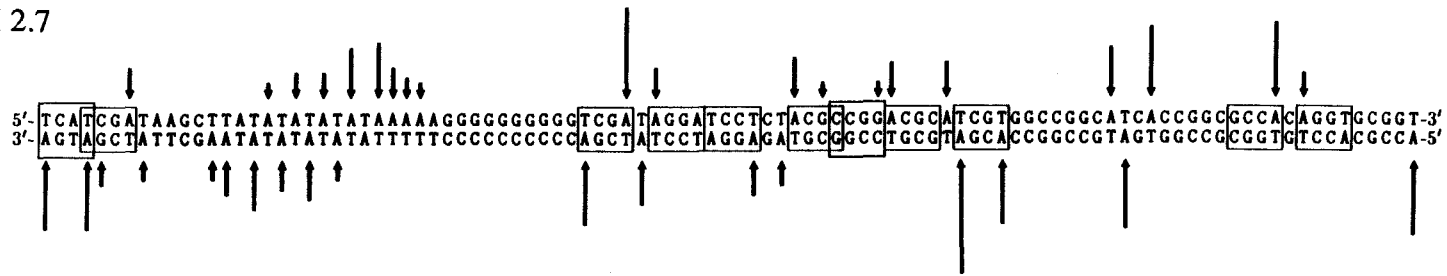


Figure 73. pH dependence of DEP/piperidine cleavage patterns in the presence of 50 μ M echinomycin on about 100 bp of the 628 bp fragment from pDMG10, as determined by densitometry of the autoradiogram in Figure 72. DEP/piperidine cleavage patterns at 50 μ M echinomycin in buffer pH 2.7 (A), pH 4.7 (B) or pH 7.0 (C) are shown as arrows with height proportional to the enhancement of DEP/piperidine cleavage at each nucleotide compared to DEP/piperidine cleavage of unbound DNA in the same pH buffer. Boxes are the assigned echinomycin binding sites based on DEP-purine reactivity at the first and/or fourth base pair positions of four base pair echinomycin binding sites centered around the dinucleotides 5'-3' CG, CC, GG or CA.⁸⁸ The scale at the bottom corresponds to that shown in Figure 71.

pH 2.7

A



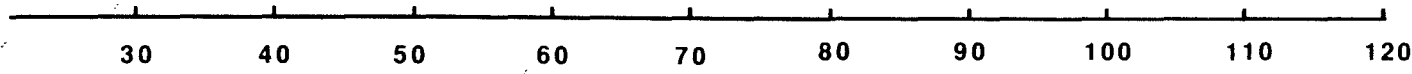
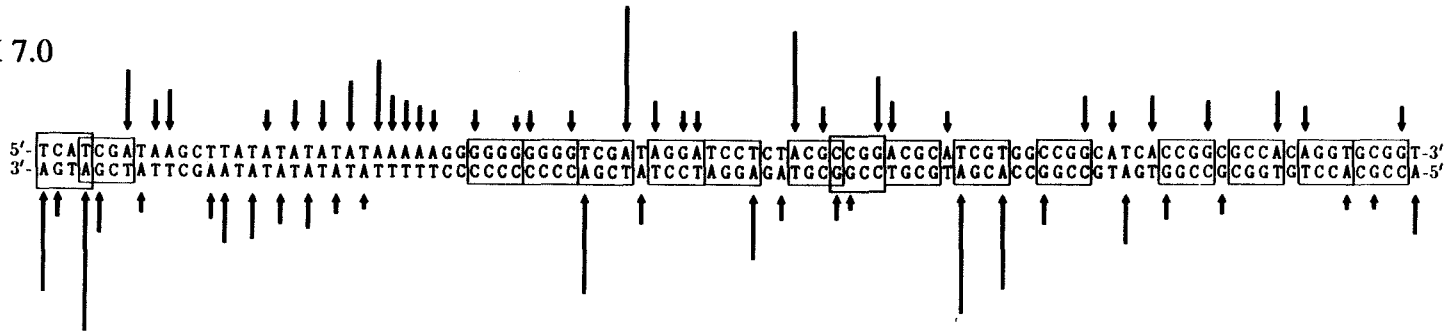
pH 4.7

B



pH 7.0

C



bands intensified while others diminished. These findings are presented graphically in Figure 73. For most purines, the change in DEP reactivity was moderate throughout the pH 2.7 to 8.0 range tested. DEP reactivity at the A-T segment in the presence of echinomycin remained essentially constant, tapering off slightly at higher pH values. Inspection of Figure 73 A-C shows a general trend in the observed DEP-purine reactivity at echinomycin binding sites: As pH increased, the degree of guanosine-DEP reactivity increased gradually, whether the G was within or adjacent to an echinomycin binding site. The dependence of DEP-adenosine reactivity upon pH was slightly different. Within echinomycin binding sites, DEP-adenosine reactivity increased with increasing pH, whereas the opposite was true of DEP-adenosine reactivity adjacent to echinomycin binding sites. For example, compare adenosine-DEP reaction at the 5'-TCGA-3' echinomycin binding site (positions 60-64) to that at the sequence 5'-ATCA-3' (positions 98-101) in Figure 73 A-C.

DISCUSSION

Structure of $d(A-T)_n$ segments.

Alternating A-T copolymeric DNA segments have the capacity to adopt an array of non-B-form DNA structures. Based on previous x-ray diffraction,¹¹¹ NMR¹¹² and nuclease digestion studies,¹¹³ Klug *et al.*¹¹⁴ suggested that $d(A-T)_n$ sequences adopt an "alternating B-DNA" structure in order to maximize 5'-A-T-3' base overlap. Recent nuclease digestion studies by Suggs and Wagner¹¹⁵ support the hypothesis that $d(A-T)_n$ structure consists of a dinucleotide repeat with an alternating sugar-phosphate backbone structure, even when the $d(A-T)_n$ segment is buried within a large DNA fragment. McClellan *et al.*¹⁰⁸ reached a similar conclusion using micrococcal nuclease and OsO_4 to probe the structure of a $d(A-T)_{16}$ segment imbedded within a plasmid DNA. Thus, in the

absence of any torsional stress or unusual buffer conditions; i.e., high salt or low pH, $d(A-T)_n$ segments appear to exist in a non-B-DNA structure.

Under conditions of negative supercoiling, $d(A-T)_n$ segments within DNA are readily extruded into cruciform structures to relieve torsional stress. Extensive studies detailing cruciform extrusion have been carried out by Lilley and co-workers^{34,35,87,108,116} and by others^{36,86} using chemical probes, nuclease hypersensitivity and 2-D gel electrophoresis to characterize cruciform formation. Cruciform extrusion is facile for alternating $d(A-T)_n$ sequences when n is greater than about 8-10. Other non-B-form structures are available to $d(AT)_n$. McLean *et al.*¹¹⁷ and Wang *et al.*¹¹⁸ showed that alternating A-T base pairs can also adopt the left-handed Z-form when flanked by short $d(C-G)_n$ sequences. As will be discussed below, the $d(T-A)_6$ tract hyperreactive to DEP in the presence of echinomycin appears to adopt yet another structure, that of partially unwound DNA.

The $d(T-A)_6$ segment hyperreactive to DEP in the presence of echinomycin is not a cruciform or single-stranded DNA.

The DEP-adenosine hyperreactivity patterns produced at the A-T segment of pDMG10 in the presence of 50 μ M echinomycin were shifted to the 3' side and covered most of this A-T segment (Figures 57, 69 and 76). This pattern is inconsistent with the formation of a cruciform loop at the A-T-rich segment in the presence of echinomycin because DEP modifies cruciform structure intensely and specifically at purine residues within the single-stranded loop region of the cruciform.^{86,87} Also, no torsional stress was available to extrude the A-T segment into a cruciform because all DEP modification reactions were performed on relaxed, linear DNA restriction fragments. It is possible that bound echinomycin molecules provide a microenvironment of torsional stress that is due to local helix unwinding, but this is unlikely to be large enough to induce cruciform extrusion. Furthermore, the $d(T-A)_6$ stretch of alternating copolymer within the entire A-T stretch is

probably too short to adopt a cruciform structure, except under forcing conditions.¹⁰⁸ Other observations argued against cruciform formation and/or single-strand character at the A-T segment were the lack of S1 nuclease hypersensitivity of this segment (Figures 61 and 62) and the failure of bromoacetaldehyde (BAA) to react with adenosine residues at the A-T segment in the presence of 50 μ M echinomycin (data not shown). Both these reagents are powerful probes of single-stranded nucleic acids¹¹⁹⁻¹²², and their failure to act suggested that echinomycin did not induce single-stranded character in the A-T segment. We would also have expected to see a diminution in MPE·Fe(II) mediated cleavage at the loop region of a cruciform because MPE·Fe(II) specifically binds double-stranded nucleic acids.¹²³ This diminution of MPE·Fe(II) cleavage was not observed. A similar argument is true for DNase I digestion because Drew¹²⁴ and Drew and Travers¹²⁵ showed that DNase I recognizes the twin sugar-phosphate backbones in the minor groove of right-handed DNA. DNase I actually cleaves some of the residues within the A-T segment more efficiently in the presence of echinomycin, inconsistent with cruciform formation or single-stranded character of this segment.

The d(T-A)₆ segment does not form Z-DNA in the presence of echinomycin.

d(T-A)_n sequences do not readily undergo the B \rightarrow Z transition. Although d(T-A)₂ can adopt the Z conformation when flanked by d(G-C)_n sequences,¹¹⁷ d(A-T)_n base pairs in Z-DNA are less stable than d(G-C)_n base pairs in this conformation.¹¹⁸ The d(T-A)₆ segment contained within plasmids pDMG10 and pDMAG10 was neither flanked by d(G-C)_n sequences nor under any torsional stress when subjected to DEP treatment. In the presence of echinomycin, the DEP-reactivity of adenosine residues within the A-T segment decreased with increasing NaCl concentration (Figures 70 and 71). High NaCl concentrations are known to assist the B \rightarrow Z transition.^{24,126} Because adenosines within Z-DNA are extremely reactive to DEP,⁸³ the results of Figures 70 and 71 are

contrary to Z-DNA formation within the A-T segment in the presence of echinomycin. The pattern of KMnO_4 reactivity also argues against Z-DNA formation at the A-T segment in the presence of echinomycin. As with OsO_4 ,^{84,107} we would have expected to observe KMnO_4 modification only at B-Z junctions, but Figures 63 and 64 show KMnO_4 to modify regions putatively *within* the Z-DNA regions. Clearly, the A-T rich segment of the plasmids studied cannot be forming Z-DNA in the presence of echinomycin.

Discussion up to this point has focussed on what structures are *not* adopted by the A-T-rich segment in the presence of echinomycin. We are confident that it is not B-DNA, not Z-DNA, not single-stranded DNA and not a cruciform loop. This description is informative, but not very specific. Below we present a model in which the A-T-rich segment is partially unwound by a distal echinomycin binding event.

Influence of echinomycin upon A-T segment structure.

The dependence of DEP-adenosine reactivity at the A-T segment upon echinomycin concentration suggests that a distal echinomycin binding event causes a structural rearrangement to occur within the A-T segment. Figure 57 E-H shows that DEP reactivity of adenosine residues within the A-T segment grew in intensity and spread over most of the A-T segment as echinomycin concentration was increased. This finding is consistent with a model where a structural rearrangement nucleates at the core of the A-T segment at low echinomycin concentrations and then propagates to cover most of the A-T segment at high echinomycin concentrations. We do not believe that binding of echinomycin to the A-T segment is responsible for the increased DEP-adenosine reactivity. Because three side-by-side copies of the sequence 5'-TATA-3' occur within the A-T segment, we would have expected to see a repeating pattern of DEP-adenosine reactivity if echinomycin were to bind those sites. Such a pattern was not observed. Further, MPE-Fe(II), DNase I and EDTA-Fe(II) footprinting methods failed to detect strong echinomycin binding to the A-T

segment. The pattern of KMnO_4 reaction within the A-T segment also supports the idea that echinomycin does not bind to the A-T rich segment (see below).

KMnO_4 specifically modifies thymidine residues in unwound and single-stranded DNAs by addition to the 5,6 double bond. KMnO_4 is not subject to direct in-line attack by nucleophilic base positions as are DEP, DMS and other alkylating/acylating reagents. Instead, the permanganate "sits down" upon the 5,6 double bond of thymidine and oxidizes this bond to disrupt base aromaticity. Base damage is then converted into a DNA strand break by conventional Maxam-Gilbert chemical sequencing workup.⁷⁹ B-DNA is unreactive toward KMnO_4 , probably because this form of the polymer does not provide enough room for KMnO_4 to approach the thymidine 5,6 double bond in a geometry productive for oxidation. Figures 64 and 65 show that KMnO_4 does not modify T residues at strong echinomycin binding sites such as (5'-3') TCGA and TCGT, even at high echinomycin binding densities. Echinomycin binding to these sites unwinds the DNA, yet in the presence of the drugs, KMnO_4 failed to react with T residues at these sequences. A simple explanation for this finding is that stacking of the antibiotic quinoxaline ring(s) blocks vertical approach of KMnO_4 upon the 5,6 double bond of unwound thymidine residues. KMnO_4 modification of T residues within the A-T segment increased with increasing echinomycin concentration (Figure 64 lanes 2-5 and 11-14, Figure 65 A and B). If echinomycin were to bind the A-T segment, we would have expected an opposite trend in the KMnO_4 reactivity of T residues because the intercalated quinoxaline rings should block KMnO_4 modification of thymidine residues within the A-T segment. As seen for DEP-adenosine reactivity, the KMnO_4 -thymidine reactivity pattern starts at the core of the A-T segment, then intensifies and spreads throughout the entire segment as echinomycin concentration increases. This pattern of KMnO_4 reactivity is consistent with progressive unwinding of the A-T segment as echinomycin concentration increases.

Neocarzinostatin and Bleomycin probing of the A-T segment in the presence of echinomycin.

Figures 65 and 67 show that NCS and BLM cleavage inhibition by echinomycin bound to the 628 bp pDMG10 fragment mapped primarily to the echinomycin binding sites independently determined by MPE·Fe(II) footprinting. There also appeared a modicum of NCS and BLM cleavage enhancement adjacent to the defined echinomycin binding sites, especially at higher echinomycin binding densities. NCS and BLM cleavage of the A-T segment in the presence of 12.5 or 50 μ M echinomycin was remarkably similar. In each case, 12.5 μ M echinomycin rendered the ends of the A-T segment more susceptible to NCS and BLM cleavage relative to NCS/BLM cleavage of unbound DNA. 50 μ M echinomycin accentuated the NCS/BLM cleavage enhancement at the ends of the A-T segment and protected a few bases at the core of the A-T segment from NCS or BLM cleavage (Figure 67 B and D).

The nonprotein chromophore of neocarzinostatin (NCS-C) is responsible for DNA damage by NCS and is known to intercalate into DNA.^{127,128} NCS-C cleaves the polymer by thiol-catalyzed abstraction of the sugar 5' proton primarily at A and T residues.¹⁰⁹ The preferred binding site for the NCS-C is 5'-GNT-3', with intercalation at the G-N step and cleavage at T.¹²⁹ The DNA-binding mode of bleomycin is less clearly defined. The issue as to whether BLM binds via intercalation, groove binding or a combination of both modes remains to be resolved, but it is clear that BLM also cleaves DNA by oxidative degradation of the sugar residue, primarily by H4' abstraction.^{11,110} BLM preferentially cleaves at the pyrimidine sugar in the sequences 5'-3' GT and GC.^{11,110} It is surprising that two such different reagents gave similar cleavage modulation patterns at the A-T segment in the presence of echinomycin. Particularly interesting is the inhibition of NCS-C and BLM cleavage at the core of the A-T segment at high echinomycin binding densities.

In the absence of other data, the simplest interpretation is that echinomycin occupies a 5'-ATAT-3' site at the A-T segment core and thus blocks cleavage there by NCS-C and

BLM. However, MPE·Fe(II) failed to detect any binding of echinomycin to this segment. Because MPE and NCS-C have similar DNA binding affinities^{104,129} and both bind via intercalation, we would expect NCS-C to readily displace weakly bound echinomycin at the A-T segment as would MPE·Fe(II), resulting in no cleavage inhibition. This pattern was not observed. An alternative explanation is that NCS-C recognizes a more complex and specific DNA structure and that long-range unwinding of the A-T segment by echinomycin disrupts the structure recognized by the NCS-C, thus lowering its affinity and cleavage intensity at the points of maximal DNA unwinding/unstructuring. It is particularly interesting that NCS-C cleavage inhibition occurred only at the core of the A-T segment. According to our model, unwinding of the A-T segment nucleates at the same positions where maximal NCS-C cleavage inhibition occurred, consonant with the latter interpretation of the NCS-C cleavage inhibition data. However, we cannot rule out the possibility that NCS-C is detecting weakly bound echinomycin at the core of the A-T segment. We feel that the same is true for the observed inhibition of BLM cleavage at the core of this segment. Another interesting feature of the NCS-C and BLM cleavage patterns at the A-T segment in the presence of echinomycin is the cleavage enhancement at both ends of the segment. This pattern is reminiscent of the enhanced OsO₄ reactivity at B-Z junctions in DNA.^{84,107} We thus interpret the NCS-C and BLM cleavage intensity maxima at or near the ends of the A-T segment to indicate a junction between canonical B-DNA outside the A-T segment and an unwound DNA structure within the A-T segment in the presence of echinomycin. It may be that the structure of this junction is preferentially recognized by both NCS-C and BLM. Partial unwinding at these "junction" sequences may facilitate intercalation and/or recognition of DNA by NCS-C and BLM, leading to more efficient cleavage, while extensive unwinding at the core of the A-T-rich segment may displace the recognition elements, leading to decreased BLM and NCS-C cleavage there.

Conditions affecting B-DNA stability.

Distamycin A.

Distamycin A is known to stabilize B-form DNA and can tip the B-Z and B-A equilibrium in favor of the B-form by binding to and thus stabilizing this form.^{2,42} We believe that distamycin A also disfavors the putative unwinding of the A-T segment induced by a distal echinomycin binding event. Figures 68 and 69 show that on the 628 bp fragment from pDMAG10, distamycin A and echinomycin did not directly compete with one another for binding sites. Also, echinomycin induced a DEP reactivity pattern at the A-T segment of the fragment virtually identical to that produced under similar conditions on plasmid pDMG10. While distamycin A failed to induce any DEP-purine reactivity even at 10 μ M concentrations, this drug selectively inhibited DEP-adenosine reaction at the A-T segment in the presence of 50 μ M echinomycin (Figure 69 F-H). This inhibition cannot be due to direct steric blockage of DEP action by distamycin A because DEP modifies DNA in the major groove (purine N7), whereas distamycin A binds in the minor groove of DNA. We believe that distamycin A binding to the A-T-rich segment stabilizes the DNA within that region such that long-range helix unwinding by a distal bound echinomycin can no longer take place.

NaCl concentration and pH dependence of DEP reactivity.

Addition of sodium chloride to the buffer appeared to have a similar effect as did distamycin A upon DEP-adenosine reactivity at the A-T segment in the presence of echinomycin. Figures 70 and 71 show that as NaCl concentration increased, DEP-adenosine reactivity within the A-T segment decreased. This observation suggests that higher sodium chloride concentrations stabilize the A-T segment, making it more difficult to deform. Alternatively, high NaCl concentrations may stabilize the A-T segment to such a degree that weak echinomycin binding to the region is depressed, but we favor the interpretation that high NaCl concentrations stabilize the A-T segment and prevent its

unwinding by echinomycin bound at least 6 bp away. Variation of buffer pH in the range 2.7 to 8.0 had little effect on the DEP-adenosine reactivity at the A-T segment in the presence of echinomycin (Figure 72 lanes 7-12 and 23-28). A small decrease in DEP reactivity at the A-T segment occurred at higher pH values, but this is likely an artifact that is due to enhanced adenosine depurination at lower pH, independent of the presence of echinomycin. Therefore, whatever structural rearrangement underlies the DEP-adenosine reactivity at the A-T segment is not detectably dependent upon buffer pH.

Summary.

An array of enzymatic and chemical probes was used to characterize the structure of an A-T-rich DNA sequence in the presence of echinomycin. We find that echinomycin binding at least 6 bp away from the A-T-rich segment appears to induce a structural rearrangement within this segment that is neither B-form DNA, single-stranded DNA, Z-form DNA, nor a cruciform loop. Instead, a distal echinomycin binding event on contiguous DNA appears to transmit helix unwinding into the A-T segment, rendering the segment reactive to DEP and KMnO_4 . We believe this to be another form of "telestability" or long-range stabilization of DNA structure by DNA-binding ligands.¹³⁰

Other sequences affected by echinomycin binding.

To investigate whether the structure of sequences other than $d(\text{A-T})_n$ can be affected by adjacent echinomycin binding, we constructed a series of plasmids containing a repeating, non-echinomycin-binding sequence immediately adjacent to a strong echinomycin binding site:

5' ATATATATATAAAAANNNNNNNNNTCGA 3'

ACACACACAC pDMAC10

AGAGAGAGAG pDMAG10

GCGCGCGCGCG pDMGC11.

The d(A-T)₆dA₅ sequence serves as a "buffer sequence" and next, a 10-11 bp tract of repeating DNA sequence (underlined) was juxtaposed 5' to a strong echinomycin binding site, (5'-3') TCGA. We then tested to see whether echinomycin binding to 5'-TCGA-3' can transmit helix deformation into different sequences at the N₁₀₋₁₁ segment. The results presented below suggest that under appropriate conditions, echinomycin can alter the structure of a variety of repeating DNA sequences adjacent to its binding sites. Apparently, the ability to modify DNA structure is a general property of echinomycin binding to DNA and may be a prime example of a small molecule acting as an allosteric effector on biopolymer structure.

pDMAC10

Figure 74 displays the pH dependence of DEP-purine reactivity within the 628 bp fragment from pDMAC10. pDMAC10 is identical to pDMG10 described above except that the 10 bp poly G tract was replaced by a 10 bp alternating A-C segment. As seen with pDMG10, DEP did not react with the DNA in the absence of echinomycin over the pH range 2.7-8.0 (Figure 74 lanes 1-6 and 17-22). 50 μ M echinomycin produced a typical DEP-purine reactivity pattern (lanes 7-12 and 23-28), but a new set of DEP-reactive purines appeared that was not seen with pDMG10. These are seen in lanes 7-12 as a set of alternating dark-light-dark-light-dark bands approximately one-third of the way from the gel bottom. Alternate adenosine residues within the AC10 segment reacted with DEP to give this pattern, presented in histogram form in Figure 76 A-C. This pattern was suggestive of an ordered, non-B-DNA structure. Interestingly, the guanosine residues on the complementary GT10 strand did not react with DEP even in the presence of echinomycin. This is likely because the 5-methyl group of a T residue immediately 3' to a G residue sterically blocks the guanosine N7 from reacting with DEP.⁸³ DEP-adenosine reactivity within the AC10 segment was most intense at low pH (compare Figure 76 A and C). More interesting was the reactivity pattern of this segment at neutral pH: Although the

alternation of dark-light bands persisted, adenosine-DEP reaction within the AC10 segment gradually decreased *away* from the strong 5'-TCGA-3' echinomycin binding site at the 3' end of the AC10 tract. This immediately suggested that echinomycin binding to the 5'-TCGA-3' site transmitted helix unwinding into the adjacent AC10 segment and that the degree of helix unwinding and thus DEP-adenosine reactivity progressively decreased away from the strong echinomycin binding site.

We do not believe that echinomycin bound to the AC10 segment because BLM cleavage of the GT10 strand was unimpaired in the presence of 50 μ M echinomycin (data not shown). However, MPE·Fe(II) and DNase I cleavage of the AC10 segment was inhibited by 12.5 and 50 μ M echinomycin (Figure 75 lanes 2-4, 19-21 and lanes 5-7, 22-24). Within this segment, the magnitude of DNase I and MPE·Fe(II) cleavage inhibition was directly proportional to the enhancement of DEP-adenosine reactivity by echinomycin (compare Figure 75 lanes 8-13 and 25-30 with the MPE·Fe(II) and DNase I cleavage lanes). This correlation suggested two different explanations for the observed DEP-adenosine reactivity at the AC10 sequence: Either echinomycin bound to half of the AC10 segment closest the 5'-TCGA-3' site or echinomycin bound at the 5'-TCGA-3' site induced a structural transition to occur within the AC10 segment such that DNase I and MPE·Fe(II) no longer recognized this DNA. As yet, we cannot distinguish between these possibilities, but either would be a novel characteristic of echinomycin binding to DNA. Direct binding by echinomycin would be unusual because the 5'-ACAC-3' sites at the segment do not fit the preferred echinomycin binding sequences 5'-NCGN-3' very well. Further, it is questionable why echinomycin would inhibit MPE·Fe(II) and DNase I cleavage on only one-half of the AC10 segment closest the 5'-TCGA-3' site. We favor the interpretation that echinomycin disrupts the AC10 structure enough to prevent recognition and cleavage by DNase I and MPE·Fe(II), but more study is required to substantiate this view.

Figure 74. DEP/piperidine footprinting of echinomycin: pH dependence of the reaction. Autoradiogram of high-resolution denaturing 8% polyacrylamide gel containing 5' (lanes 1-14) or 3' (lanes 15-28) ^{32}P end-labeled 628 bp *Eco* RI-*Bgl* I DNA restriction fragment from plasmid pDMAC10. DEP/piperidine cleavage was performed either without drug (lanes 1-6 and 17-22) or in the presence of 50 μM echinomycin (lanes 7-12 and 23-28) at pH 2.7 (lanes 1,7,17,23), pH 3.7 (lanes 2,8,18,24), pH 4.7 (lanes 3,9,19,25), pH 5.7 (lanes 4,10,20,26), pH 7.0 (lanes 5,11,21,27) or pH 8.0 (lanes 6,12,22,28). Lanes 13 and 15 are the Maxam-Gilbert chemical sequencing G-specific reactions, lanes 14 and 16 the Maxam-Gilbert chemical sequencing purine-specific reactions on this DNA fragment. DEP reaction conditions were 100 mM Tris / 100 mM NaOAc pH 2.7, 3.7, 4.7, 5.7, 7.0 or 8.0 with HCl, 10% (v/v) methanol, 200 μM calf thymus DNA bp, 0 or 50 μM echinomycin and 68 mM DEP. DEP modification of DNA was for 10 minutes at 37°C.

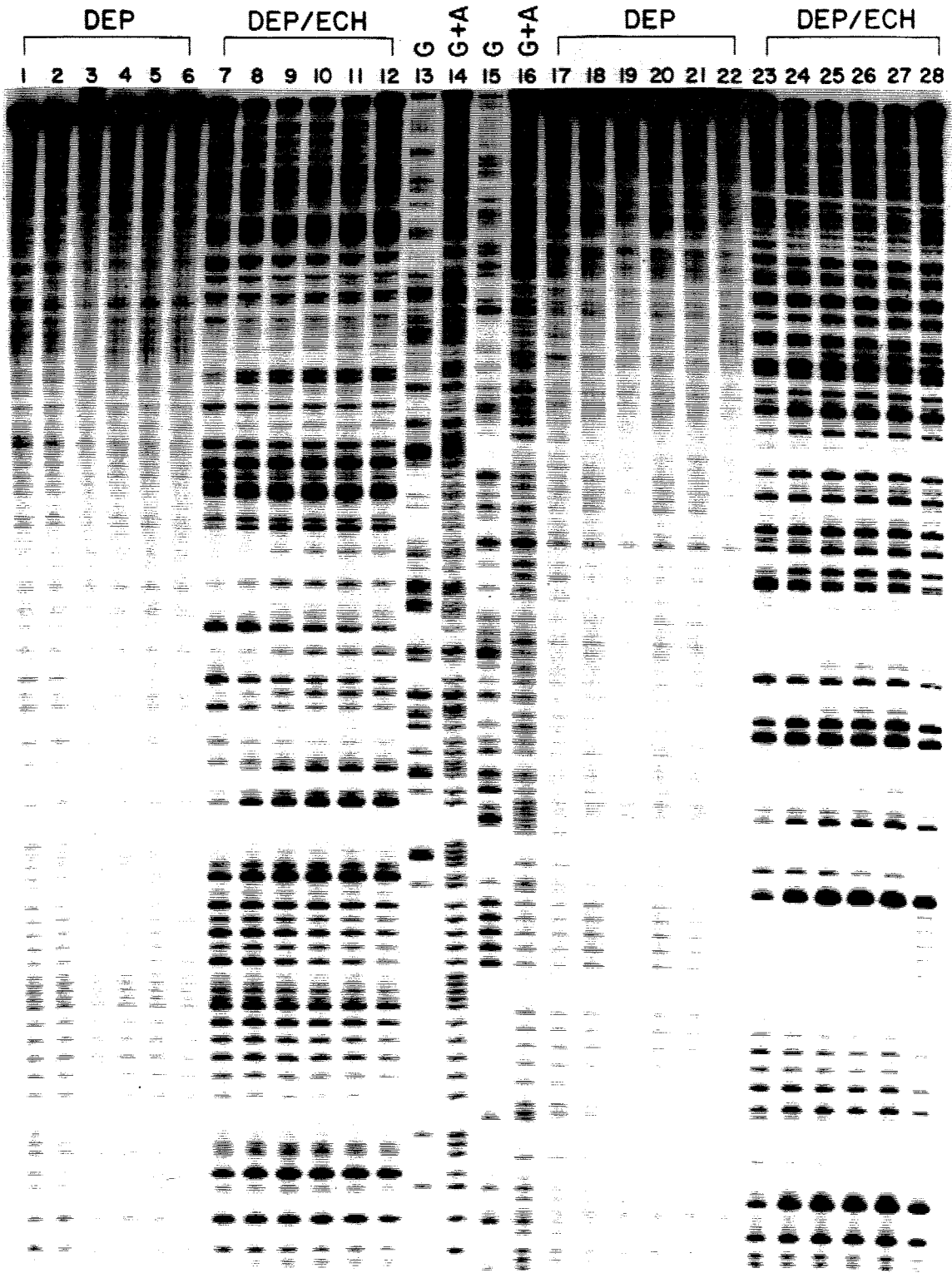


Figure 75. DNase I, MPE·Fe(II) and DEP/piperidine footprinting of echinomycin on a large DNA restriction fragment. Autoradiogram of 5' (lanes 1-15) and 3' (lanes 16-30) ³²P end-labeled 628 bp *Eco* RI-*Bgl* I restriction fragment from plasmid pDMAC10. Lanes: 1 and 18, buffered, intact DNA (STD); 2-4 and 19-21, MPE·Fe(II) cleavage of DNA in the presence of 0, 12.5 or 50 μM echinomycin, respectively; 5-7 and 22-24, DNase I cleavage of DNA in the presence of echinomycin at 0, 12.5 or 50 μM, respectively; 8-10 and 25-27 DEP/piperidine cleavage of DNA (TA buffer) in the presence of 0, 12.5 or 50 μM echinomycin, respectively; 11-13 and 28-30, DEP/piperidine cleavage of DNA (TKMC buffer) in the presence of 0, 12.5 or 50 μM echinomycin, respectively; 14 and 16, Maxam-Gilbert chemical sequencing G-specific reactions; 15 and 17, Maxam-Gilbert chemical sequencing purine-specific reactions on this restriction fragment. MPE·Fe(II) digestion of DNA was performed for 35 minutes at 37°C in 100 mM Tris / 100 mM NaOAc pH 7.0 with HCl (TA buffer), 200 μM calf thymus DNA bp, 10% (v/v) methanol, 4 μM MPE, 8 μM FAS, 0, 12.5 or 50 μM echinomycin and 1 mM sodium L-ascorbate. DNase I digestions were performed for 3 minutes at room temperature with 1.32 ng of DNase I in 10 mM Tris·HCl pH 7.9 / 10 mM KCl / 10 mM MgCl₂ / 5 mM CaCl₂ (TKMC buffer), 200 μM calf thymus DNA bp, 10% (v/v) methanol and 0, 12.5 or 50 μM echinomycin. DEP reactions were performed for 10 minutes at 37°C in either TA or TKMC buffer, 200 μM calf thymus DNA bp, 10% (v/v) methanol and 0, 12.5 or 50 μM echinomycin.

	MPE/E		DNase I/E		DEP/E					G	G + A	G	G + A	STD	MPE/E		DNase I/E		DEP/E											
STD	-	+	+	-	+	+	-	+	+	-	+	+	G	G + A	G	G + A	STD	-	+	+	-	+	+	-	+	+	-	+	+	
	┌───┐			┌───┐			┌───┐										┌───┐			┌───┐			┌───┐							
	1	2	3	4	5	6	7	8	9	10	11	12	13	14	15	16	17	18	19	20	21	22	23	24	25	26	27	28	29	30

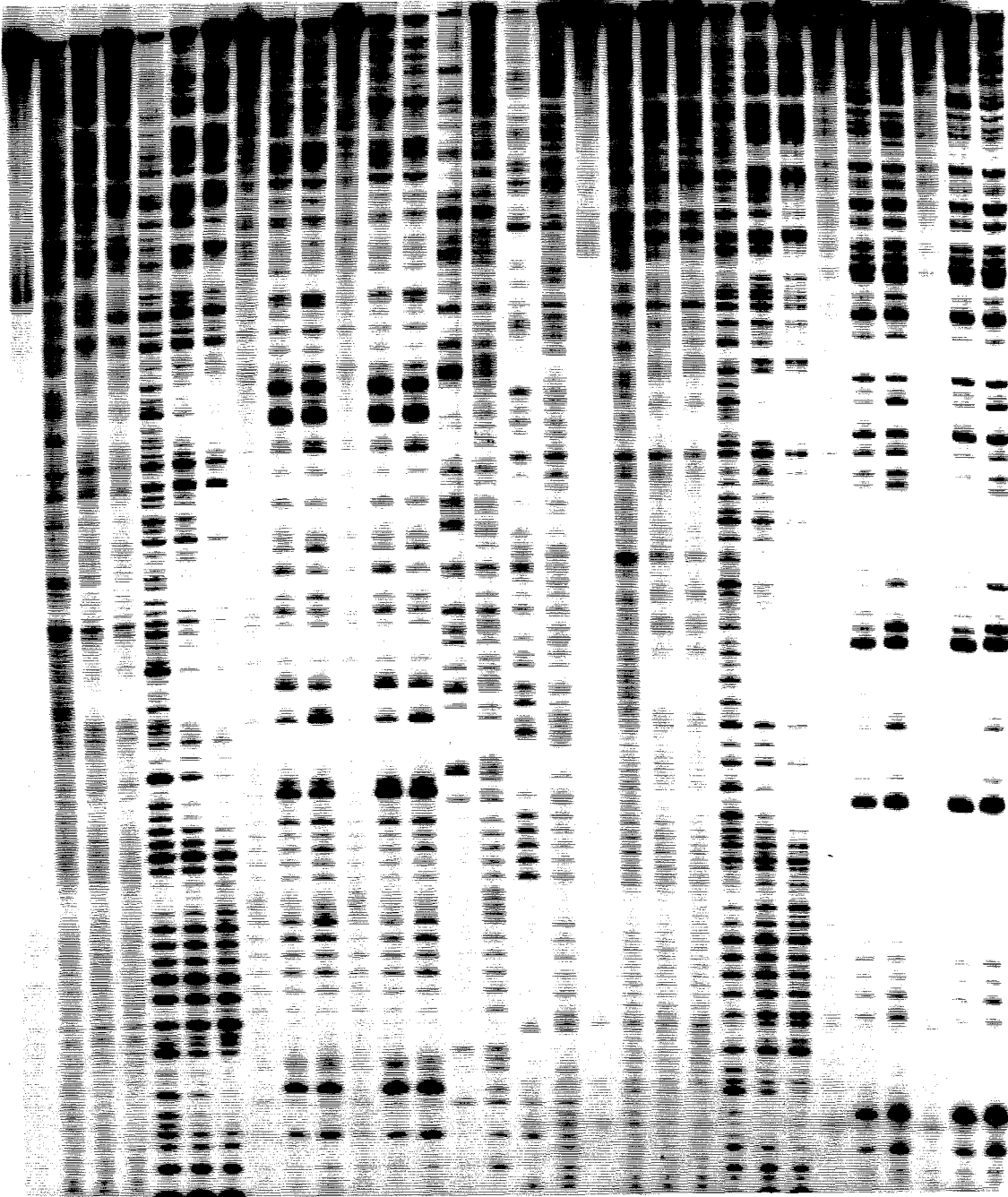


Figure 76. pH dependence of DEP/piperidine cleavage patterns in the presence of 50 μ M echinomycin on about 100 bp of the 628 bp fragment from pDMAC10 (A-C) or pDMAG10 (D-F), as determined by densitometry of the autoradiograms in Figures 74 and 77, respectively. DEP/piperidine cleavage patterns at 50 μ M echinomycin in buffer pH 2.7 (A and D), pH 4.7 (B and E) or pH 7.0 (C and F) are shown as arrows with height proportional to the enhancement of DEP/piperidine cleavage at each nucleotide compared to DEP/piperidine cleavage of unbound DNA in the same pH buffer. Boxes are the assigned echinomycin binding sites based on DEP-purine reactivity at the first and/or fourth base pair positions of four base pair echinomycin binding sites centered around the dinucleotides 5'-3' CG, CC, GG or CA.⁸⁸ The scale at the bottom corresponds to that shown in Figure 71.

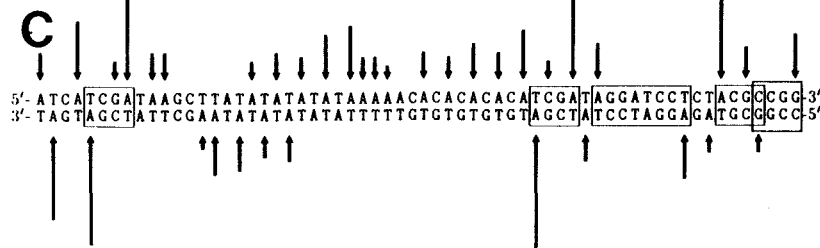
pH 2.7



pH 4.7



pH 7.0



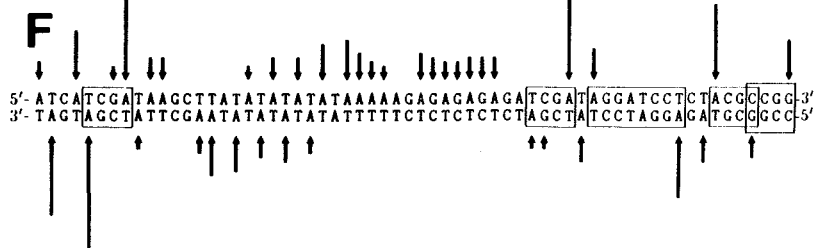
pH 2.7



pH 4.7



pH 7.0



pDMAG10

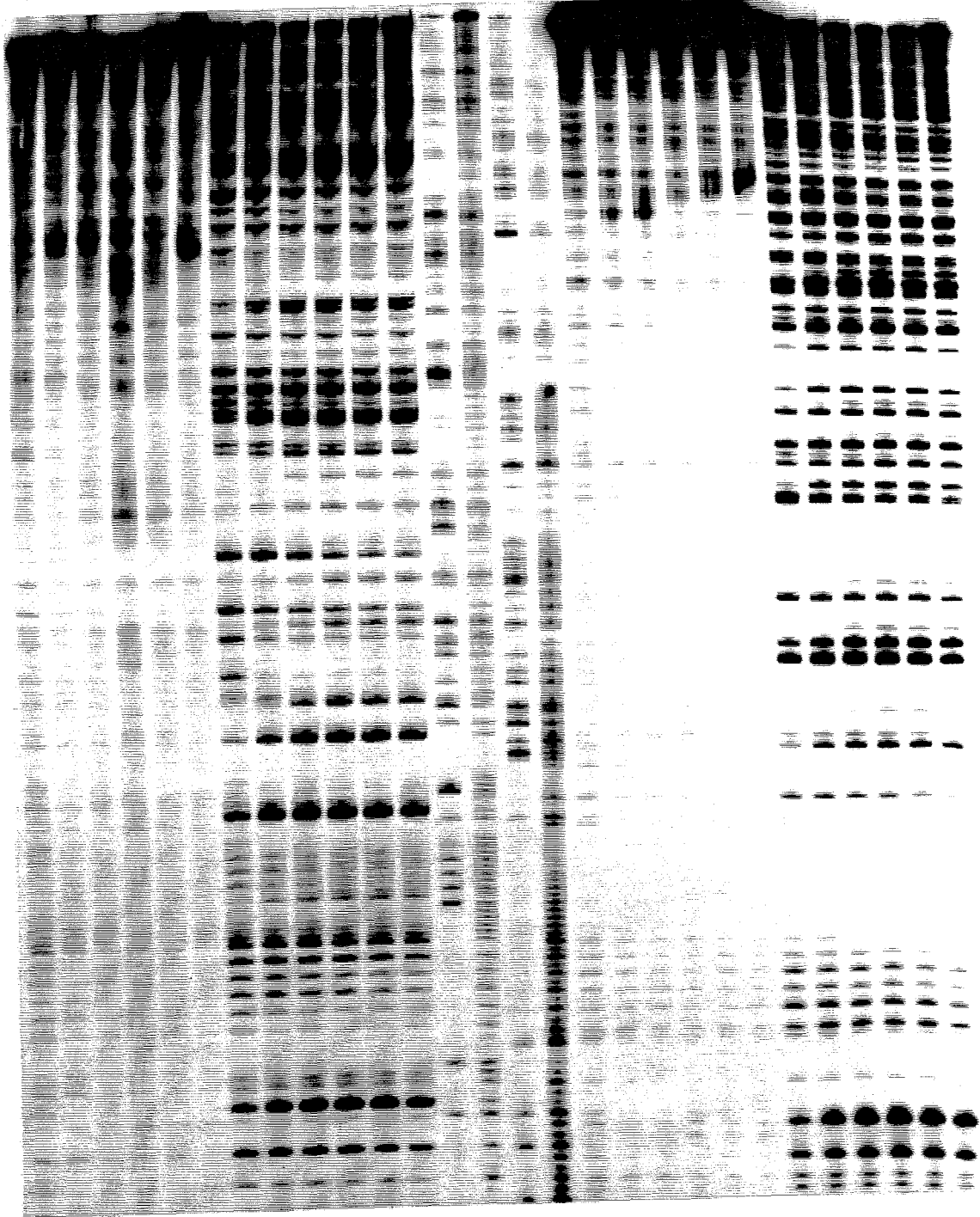
When the G10 or AC10 segment adjacent the 5'-TCGA-3' site was replaced by a 10 bp (A-G)₅ repeat (AG10 segment), a different pattern of DEP-purine reactivity was produced in the presence of echinomycin. Figure 77 shows the pH dependence of DEP/piperidine cleavage on the 628 bp pDMAG10 fragment. All conditions were as in the analogous studies on pDMG10 and pDMAC10. Lanes 7-12 show weak DEP-purine reactivity within the AG10 segment in the presence of 50 μ M echinomycin. Adenosine residues at this block of purines reacted preferentially with DEP at pH 3.7 and below, whereas above this pH value, both A and G residues in the AG10 segment were modified weakly by DEP (Figure 76 D-F presents the densitometric analysis of these results). We also favor a model wherein echinomycin binding to the 5'-TCGA-3' site at the 3' end of the AG tract deforms the AG segment, rendering it reactive toward DEP. We do not believe that echinomycin binds directly to the AG repeat because NCS cleavage of the AG repeat (the complementary CT strand) was actually *enhanced* by the presence of 50 μ M echinomycin (Figure 66 lanes 4-6). The amount of DEP reaction at the AG10 segment suggests that this segment was not subject to a large amount of unstructuring by echinomycin. Nonetheless, some type of unstructuring was apparently detectable and was dependent upon echinomycin.

pDMGC11

This plasmid places an 11 bp alternating G-C copolymer adjacent to the 5'-TCGA-3' site at position 60, but is identical in all other respects to the plasmids described thus far (see Experimental section for plasmid construction). Under identical conditions used to analyze pDMG10, pDMAC10 and pDMAG10, the GC11 segment showed no increased reactivity to DEP in the presence of echinomycin at different pH (Figure 78). However, if NaCl concentration was varied instead of pH, the GC11 segment became reactive to DEP only in the presence of echinomycin (Figure 79).

Figure 77. DEP/piperidine footprinting of echinomycin: pH dependence of the reaction. Autoradiogram of high-resolution denaturing 8% polyacrylamide gel containing 5' (lanes 1-14) or 3' (lanes 15-28) ^{32}P end-labeled 628 bp *Eco* RI-*Bgl* I DNA restriction fragment from plasmid pDMAG10. DEP/piperidine cleavage was performed either without drug (lanes 1-6 and 17-22) or in the presence of 50 μM echinomycin (lanes 7-12 and 23-28) at pH 2.7 (lanes 1,7,17,23), pH 3.7 (lanes 2,8,18,24), pH 4.7 (lanes 3,9,19,25), pH 5.7 (lanes 4,10,20,26), pH 7.0 (lanes 5,11,21,27) or pH 8.0 (lanes 6,12,22,28). Lanes 13 and 15 are the Maxam-Gilbert chemical sequencing G-specific reactions, lanes 14 and 16 the Maxam-Gilbert chemical sequencing purine-specific reactions on this DNA fragment. DEP reaction conditions were 100 mM Tris / 100 mM NaOAc pH 2.7, 3.7, 4.7, 5.7, 7.0 or 8.0 with HCl, 10% (v/v) methanol, 200 μM calf thymus DNA bp, 0 or 50 μM echinomycin and 68 mM DEP. DEP modification of DNA was for 10 minutes at 37°C.

DEP DEP/ECH G G+A G G+A DEP DEP/ECH
1 2 3 4 5 6 7 8 9 10 11 12 13 14 15 16 17 18 19 20 21 22 23 24 25 26 27 28



The 629 bp fragment from pDMGC11 reacted weakly with DEP in the absence of echinomycin throughout the aqueous solubility range of NaCl (Figure 79 lanes 1-6 and 17-22). 50 μ M echinomycin at "normal" salt concentrations gave the usual purine-DEP reactivity pattern at its strong binding sites and at the A-T segment distal to these binding sites (Figure 79 lanes 7-9 and 23-25). None of the guanosine residues within the GC11 tract reacted with DEP in these lanes. As NaCl concentration was increased to 4.0 M and finally to saturation, a few of the G residues at the center of the GC11 sequence reacted moderately with DEP (lanes 11-12 and 27-28). Adenosine-DEP reactivity at the neighboring A-T segment showed the opposite trend, A residues reacting more feebly with DEP as NaCl concentration increased. Under appropriate conditions, echinomycin thus appeared capable of transforming even an adjacent $d(G-C)_n$ segment into a structure reactive to DEP. The nature of the DEP reactivity at G residues within the GC11 segment at high salt is not yet clear. This may reflect nonspecific binding of echinomycin to the GC11 segment as echinomycin is known to approach *monointercalative* binding at higher ionic strength.⁵⁹ We also speculate that the observed reactivity may be caused by the GC11 segment adopting the Z-form. High salt is known to favor the Z-form of $d(G-C)_n$ polymers^{24,126}, and echinomycin binding adjacent the GC11 segment may facilitate the B \rightarrow Z transition by destabilizing the B-form of this sequence. This hypothesis has not been tested, but an interesting experiment presents itself: Poly $d(G-Me^5C)_n$ is known to undergo the B \rightarrow Z transition at lower salt than poly $d(G-C)_n$.²⁴ It would be interesting to see if the GC11 segment becomes reactive to DEP at lower salt concentrations in the presence of echinomycin when the the C residues of this tract are 5-methylated by the action of *Hha* I methylase. If DEP-guanosine reaction at the GMe^5C11 tract were to occur at lower salt than observed for the GC11 tract in the presence of echinomycin, then it would appear that echinomycin binding adjacent a $d(G-C)_n$ sequence may shift the B-Z equilibrium toward the Z-form.

CONCLUSION

We found that purines within a number of repeating DNA sequences adjacent or distal to strong echinomycin binding sites became reactive to DEP in the presence of echinomycin. Because B-DNA and the repeating DNA sequences were unreactive to DEP in the absence of echinomycin, it appeared that adjacent or distal echinomycin binding events disrupted the structure of these sequences. The structure of a d(T-A)₆ segment at least 6 bp away from a strong echinomycin binding site was characterized with an array of chemical and enzymatic probes. Based on the cleavage/base modification patterns of these probes in the presence and absence of echinomycin, we believe that echinomycin binding at least 6 bp away causes unwinding to occur at the center of a contiguous d(T-A)₆ sequence of DNA. Under various conditions, purines within the sequences d(A-G)₅·d(C-T)₅, d(A-C)₅·d(G-T)₅ and d(G-C)₅G·dC(G-C)₅ become reactive to DEP only in the presence of echinomycin when these sequences were adjoined to a strong echinomycin binding site. The structures of the DEP reactive forms of these sequences are as yet uncharacterized, but the ability of echinomycin to render them reactive to DEP suggests that echinomycin can alter the structure of many DNA sequences adjacent to or near its binding sites.

Figure 78. DEP/piperidine footprinting of echinomycin: pH dependence of the reaction. Autoradiogram of high-resolution denaturing 8% polyacrylamide gel containing 5' (lanes 1-14) or 3' (lanes 15-28) ³²P end-labeled 629 bp *Eco* RI-*Bgl* I DNA restriction fragment from plasmid pDMGC11. DEP/piperidine cleavage was performed either without drug (lanes 1-6 and 17-22) or in the presence of 50 μM echinomycin (lanes 7-12 and 23-28) at pH 2.7 (lanes 1,7,17,23), pH 3.7 (lanes 2,8,18,24), pH 4.7 (lanes 3,9,19,25), pH 5.7 (lanes 4,10,20,26), pH 7.0 (lanes 5,11,21,27) or pH 8.0 (lanes 6,12,22,28). Lanes 13 and 15 are the Maxam-Gilbert chemical sequencing G-specific reactions, lanes 14 and 16 the Maxam-Gilbert chemical sequencing purine-specific reactions on this DNA fragment. DEP reaction conditions were 100 mM Tris / 100 mM NaOAc pH 2.7, 3.7, 4.7, 5.7, 7.0 or 8.0 with HCl, 10% (v/v) methanol, 200 μM calf thymus DNA bp, 0 or 50 μM echinomycin and 68 mM DEP. DEP modification of DNA was for 10 minutes at 37°C.

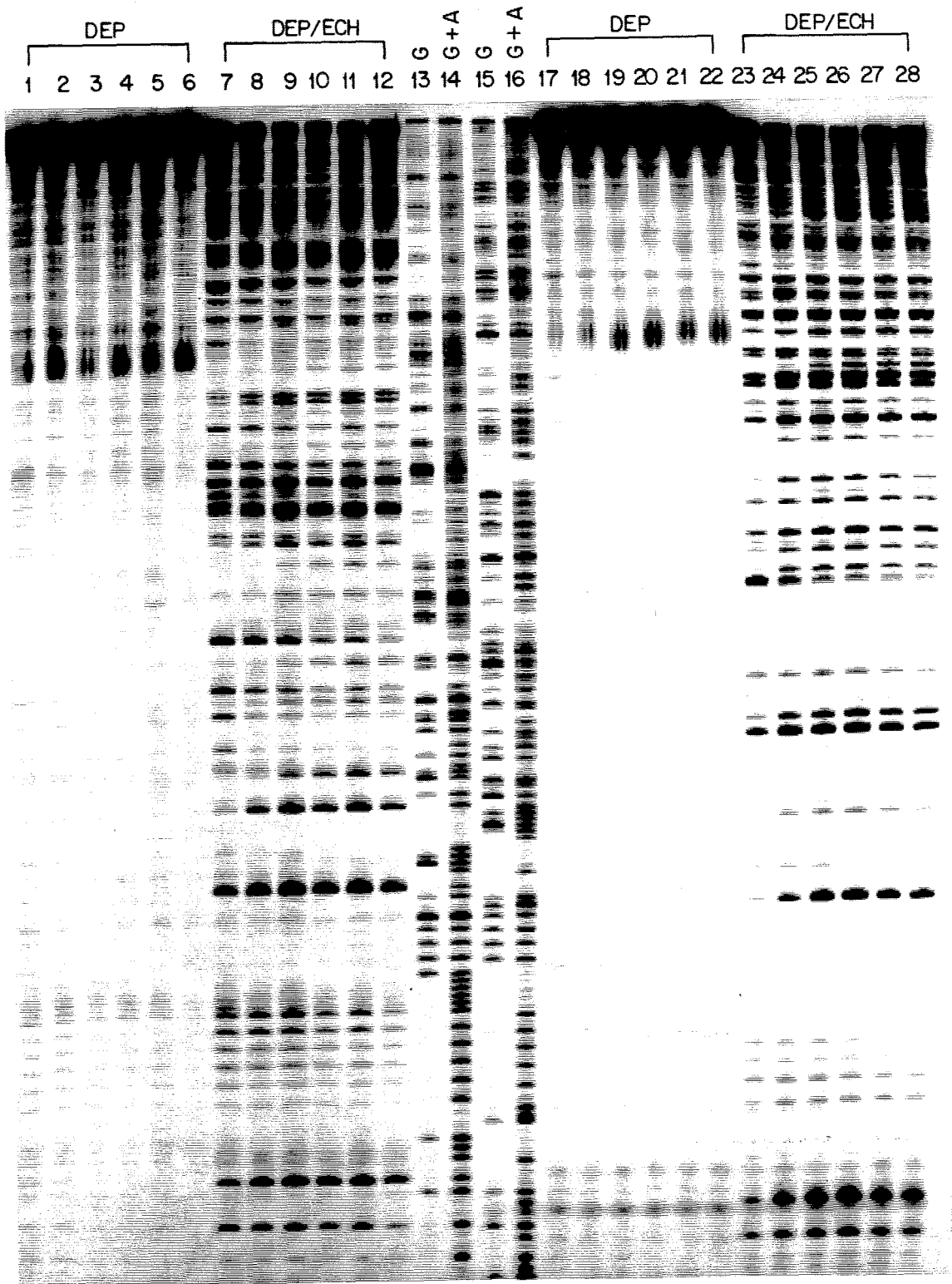
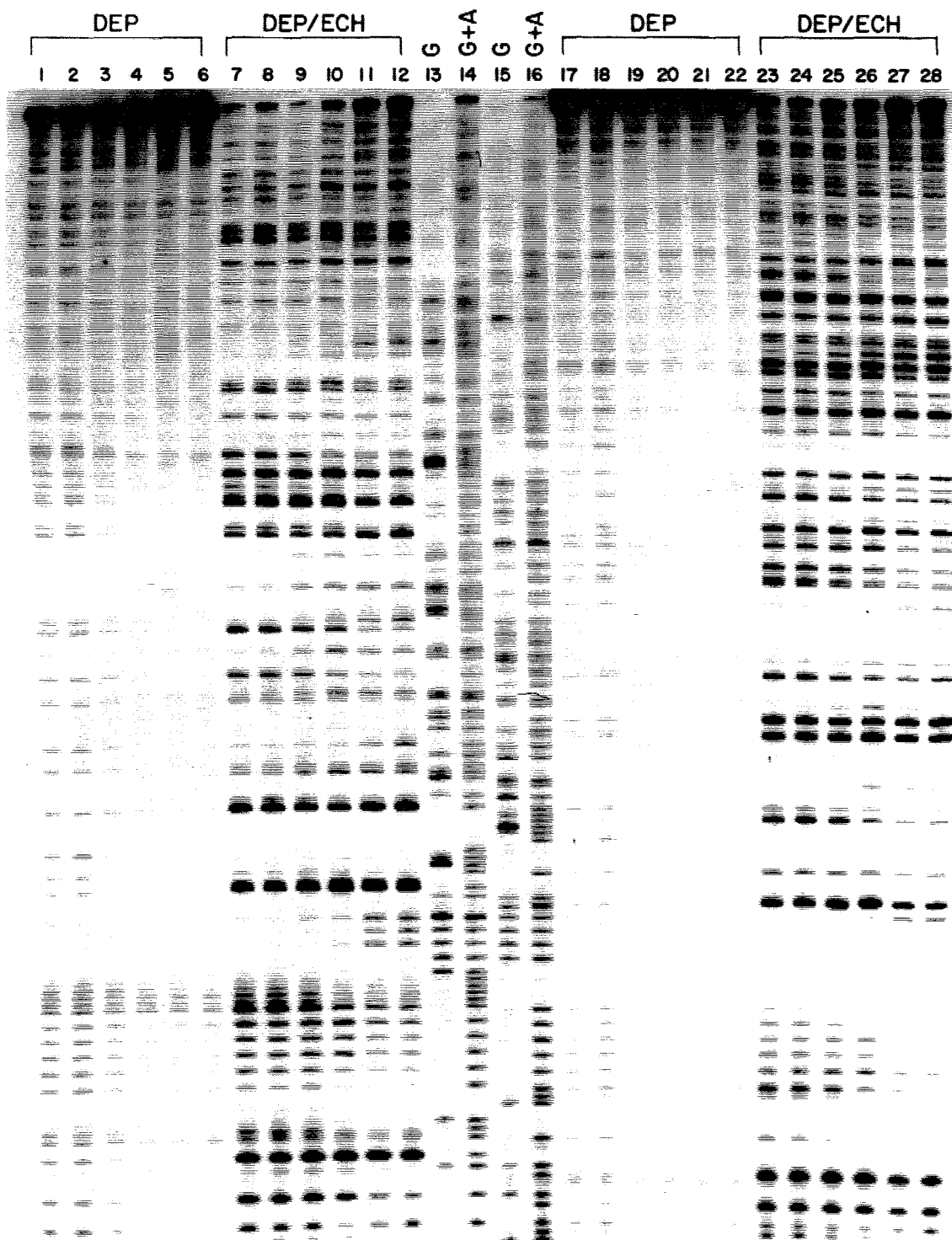


Figure 79. DEP/piperidine footprinting of echinomycin: NaCl concentration dependence. Autoradiogram of high-resolution denaturing 8% polyacrylamide gel containing either 5' (lanes 1-14) or 3' (lanes 15-28) ^{32}P end-labeled 628 bp *Eco* RI-*Bgl* I restriction fragment from plasmid pDMGC11. DEP/piperidine cleavage was performed either without drug (lanes 1-6 and 17-22) or in the presence of 50 μM echinomycin (lanes 7-12 and 23-28) at "0" mM NaCl (no added salt, lanes 1,7,17,23), 10 mM NaCl (lanes 2,8,18,24), 1.0 M NaCl (lanes 3,9,19,25), 4.0 M NaCl (lanes 5,11,21,27) or saturated NaCl (lanes 6,12,22,28). Lanes 13 and 15 are the Maxam-Gilbert chemical sequencing G-specific reactions, lanes 14 and 16 the Maxam-Gilbert chemical sequencing purine-specific reactions on this DNA restriction fragment. Reaction conditions were 10 mM Tris·HCl pH 7.4, 0, 0.01, 0.1, 1.0, 4.0 or saturated NaCl, 200 μM calf thymus DNA bp, 10% (v/v) methanol and 68 mM DEP. Reaction was for 10 minutes at 37°C.



CHAPTER 3

Experimental

EXPERIMENTAL

Reagents and Materials.

In general, the highest purity reagents available were used without further purification except for formamide that was recrystallized three times prior to use. Water was purified through a Milli-Q® system (Millipore Corp, Bedford, MA) comprised of a coarse organic removal cartridge, two ion-exchange cartridges, a fine "polishing" organic removal cartridge and two filters. This water was used exclusively for HPLC buffers.

Echinomycin was the generous gift of Dr. Matthew Suffness of the National Cancer Institute Natural Products Center. This sample was used as received. Solutions of echinomycin were made in spectrophotometric grade methanol, and concentrations were determined spectrophotometrically using $\epsilon_{325\text{nm}}=11,550 \text{ l mol}^{-1}$.¹⁴ The antibiotic was protected from light at all times and stock solutions were stored at +4° or -20°C. Suppliers for all other materials can be found in the accompanying source list.

<u>Restriction Endonucleases</u>	<u>Source</u>
<i>Bam</i> HI	Boehringer-Mannheim (BMB)
<i>Bgl</i> I	BMB
<i>Eco</i> RI	BMB
<i>Hind</i> III	BMB
<i>Taq</i> I	New England Biolabs (NEBL)
 <u>DNA Modification Enzymes</u>	
Deoxyribonuclease, bovine pancreatic (DNase I)	Worthington
DNA Polymerase I, large fragment (Klenow)	BMB, NEBL
Ribonuclease A	Sigma

S1 Nuclease	BMB
<i>Taq</i> I methylase	NEBL
T4 DNA ligase	NEBL
T4 Polynucleotide kinase	BMB
<u>Chemicals</u>	
Acetic Acid (99.7+%, ACS reagent grade)	Aldrich
Acetonitrile (glass distilled, UV grade)	Burdick & Jackson
Acrylamide	BMB, Bio-Rad
Agarose (Sea Kem [®] , Sea Plaque [®])	FMC Corp.
Boric Acid	J. T. Baker
Diethyl pyrocarbonate	Aldrich
Dimethyl sulfate	Aldrich
EDTA	Baker
Ethyl chloroformate	Kodak
Formamide	BMB
Formic Acid	Aldrich
2-Mercaptoethanol	Aldrich
4,5,6-triaminopyrimidine sulfate	Aldrich
2,4-diamino-6-hydroxypyrimidine	Aldrich
NaNO ₂	Aldrich
Na ¹⁵ NO ₂ (>99% enriched)	Cambridge Isotope Labs
Phenol (redistilled)	Bethesda Research Labs (BRL)
Triethylamine (HPLC grade)	Fisher
Tris·HCl, Tris Base	Sigma, BMB
Urea	BRL

Radionucleotides

γ - ³² P ATP (>5000 Ci/mmol) (purified, aqueous)	Amersham Corp.
α - ³² P dATP (~3000 Ci/mmol) (purified, aqueous)	Amersham Corp.

Antibiotics

Actinomycin D	Calbiochem
Ampicillin	Sigma
Bleomycin (Blenoxane)	Bristol
Chloramphenicol	Parke-Davis
Distamycin A	BMB
Echinomycin	NCI, Natural Products Center
Neocarzinostatin	Bristol
Tetracycline	Sigma

Instrumentation.

All ¹³C NMR spectra were recorded on a JEOL FX-90Q spectrometer using a 1-second pulse delay for proton decoupling. Acquisition was normally for 2-3 hours, but the [5-¹⁵N]-carbethoxyamino-2,4-diamino-6-hydroxypyrimidine spectrum was acquired overnight to enhance the signal of carbons split by the ¹⁵N. ¹H NMR spectra were recorded on a JEOL GX400 spectrometer. All NMR spectra were obtained in DMSO-d₆ and this solvent was also used as internal standard for the assignment of chemical shifts. Electron impact and fast atom bombardment mass spectrometry was performed by the Midwest Center for Mass Spectrometry at the University of Nebraska, Lincoln, Nebraska. Infrared spectrometry was performed exclusively on a Shimadzu IR-435 instrument using

KBr pellets. Electronic spectra were obtained using either a Perkin-Elmer Lambda 4C or a Beckman Model 25 UV-Visible spectrophotometer.

Buffers.

All buffers prepared with double-distilled or Milli-Q® quality H₂O were sterilized either by autoclaving or by filtering (0.45 or 0.20 μM) where necessary. Buffers used for restriction endonuclease digestions and DNA modifying enzymes were as suggested by the manufacturer. One exception was *Taq* I Methylase, where it was necessary to use 2 mM S-adenosylmethionine (SAM) instead of the 80 μM SAM recommended by New England Biolabs. Compositions of the other buffers used for chemical and enzymatic footprinting are listed below:

TN Buffer

10 mM Tris·HCl pH 7.4
50 mM NaCl

TKMC Buffer

10 mM Tris·HCl pH 7.9
10 mM KCl
10 mM MgCl₂
5 mM CaCl₂

TE Buffer

10 mM Tris·HCl pH 8.0
1 mM EDTA

TBE Buffer (High-resolution gels)

100 mM Tris pH 8.3
100 mM H₃BO₃
2 mM EDTA

TA Buffer

100 mM Tris
100 mM NaOAc
pH 2.7, 3.7, 4.7,
5.7, 7.0 or 8.0
with HCl

STE Buffer

100 mM NaCl
10 mM Tris·HCl pH 8.0
1 mM EDTA

TAE Buffer (Agarose gels)

40 mM Tris
5 mM NaOAc
1 mM EDTA
to pH 7.9 w/ Acetic Acid

Formamide loading Buffer

80% (v/v) Formamide
1X TBE buffer
Bromophenol Blue
Xylene Cyanol

Oligonucleotide synthesis and purification.

All oligodeoxyribonucleotides were synthesized by machines employing solid-phase phosphite-triester chemistry.¹³¹⁻¹³³

10 μ mol scale oligonucleotides.

10 μ mol scale syntheses were performed on an Applied Biosystems (Foster City, CA) model 380 A DNA synthesizer. Oligonucleotides were constructed with β -cyanoethyl phosphoramidites, and the terminal 5' dimethoxytrityl (DMT) protecting group was left attached to the oligomer to assist in purification. After deprotection in NH_4OH (55°C, 12-24 h), the NH_4OH /oligonucleotide solution was allowed to cool to room temperature. This was then injected directly onto a Pharmacia FPLC[®] (Fast Protein Liquid Chromatography, Pharmacia-LKB Biotech, Piscataway, NJ) system for purification. Six to eight separate 1.25 - 1.5 μ mol injections of each oligonucleotide were chromatographed on an HR 10/10 MONO Q[®] cation exchange column using denaturing conditions. The solvent gradient program used for purification is shown schematically in Figure 80. The flow rate was 1.5 ml/min and buffers were: A, 10 mM ultrapure NaOH (Morton-Thiokol) / 0.5 M NaCl; B, 10 mM ultrapure NaOH / 1.5 M NaCl.

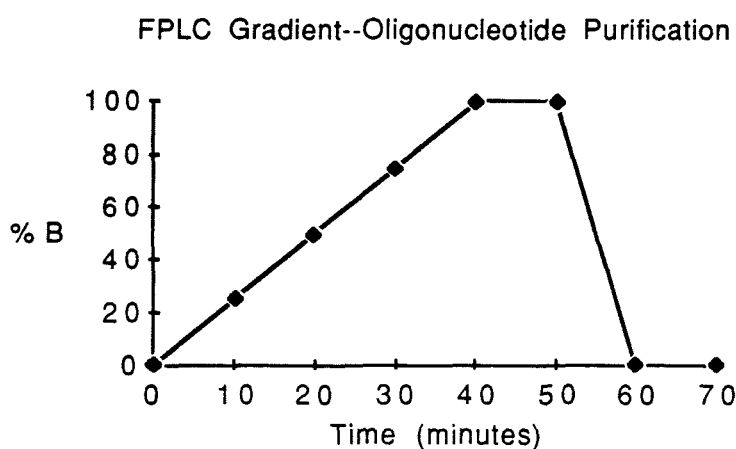


Figure 80. FPLC[®] solvent gradient program used for large-scale oligonucleotide purification.

A typical chromatogram produced under this method is shown in Figure 81. All material not retaining a 5' DMT group elutes early in the gradient whereas oligonucleotides with the 5' DMT group attached elute at nearly 100% B or ~1.5 M NaCl. Note the excellent resolution between 5' DMT-on and 5' DMT-off material.

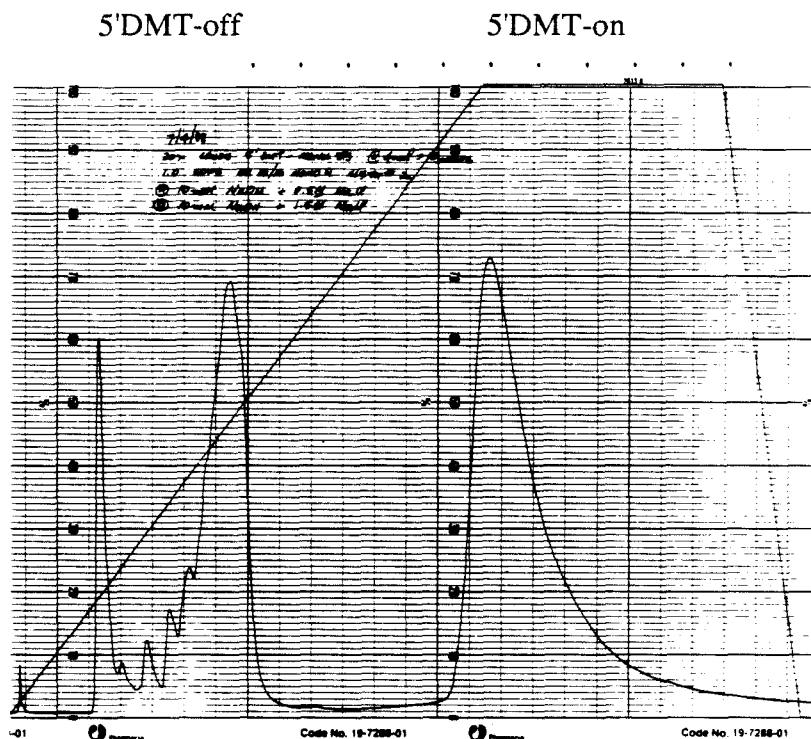


Figure 81. Typical FPLC[®] chromatogram illustrating the resolution between DMT-on and DMT-off oligonucleotides.

Fractions corresponding to the late-eluting material were collected and neutralized by adding 1/10 volume of 100 mM HCl. The six to eight injections of each 10 μ mol scale oligonucleotide yielded about 50 to 60 mL of 5' DMT-on fractions. The volume of these pooled fractions was reduced to ca. 15 mL (saturated NaCl) via lyophilization on a Savant Speedvac (Savant Instruments, Farmingdale, NY) and the NaCl was removed by extensive dialysis (6 X 1L) against H₂O. Dialyzed product was then reduced in volume to 4 mL via lyophilization and the 5' DMT group removed by adding either 1 mL of glacial acetic acid

(ACS reagent, 99.7%+) or 4 mL of 1% (v/v) trifluoroacetic acid to the 4 mL of dialyzed product. DMT removal at room temperature was allowed to continue for 20 minutes (acetic acid) or 5 minutes (trifluoroacetic acid). After incubation with acid, excess concentrated NH_4OH was added to the detritylated oligonucleotide to prevent depurination and the mixture was lyophilized to dryness. This mixture was resuspended in 2.2 mL of 2% (w/v) NaOAc pH 5.2 and then precipitated by adding 6 mL of absolute ethanol to the tube. Large masses of white flocculent material usually appeared immediately upon adding ethanol to the DNA. The mixture was then frozen at -80°C overnight and centrifuged for 30 minutes at 10 K rpm, 4°C in a Beckman J2-21 centrifuge using a JA-20 rotor plus rubber adapter. The supernatants were discarded, the pellet rinsed with 2 mL of 70% ethanol and dried under vacuum. FPLC[®] analysis of the purified material showed a single, sharp peak with no evidence of contaminating shoulder or forepeaks. Concentration and oligonucleotide purity was determined spectrophotometrically in 1X STE buffer pH 8.0, assuming $\epsilon_{260\text{nm}} \sim 10,000 \text{ l mol}^{-1} \text{ bp}^{-1} \text{ cm}^{-1}$ per residue for a mixed sequence oligonucleotide. 260nm/280nm ratios were typically 1.8-1.9, indicating that the oligonucleotide was free of protein. Typical yield for a purified 10 μmol scale 34 residue oligonucleotide was 35 milligrams or about 30% assuming 100% coupling efficiency. Although FPLC[®] and polyacrylamide gel electrophoresis showed these oligonucleotides to be extremely pure, upon radiolabeling with T4 polynucleotide kinase and $\gamma\text{-}^{32}\text{P}$ ATP, we consistently observed about four to five closely spaced bands in the autoradiogram of high-resolution denaturing gels. This pattern was consistent whether acetic or trifluoroacetic acid was used to remove the DMT group. Other than this problem, the manually detritylated oligonucleotides behaved as expected and showed ideal hybridization to their respective complementary strands. To obtain clean radioactively labeled material for gel electrophoretic analysis, we found it necessary to re-synthesize each oligonucleotide on the 1 μmol scale and to remove the terminal 5' DMT group on the machine. However, the manually deprotected oligonucleotides were used in

the large-scale DEP-DNA reactions and as carrier DNA in the reactions containing radiolabeled oligonucleotides.

1 μ mol scale oligonucleotides.

1 μ mol scale oligonucleotide syntheses were performed on either an Applied Biosystems model 380 A or a Beckman System 1 Plus DNA synthesizer. The terminal 5' DMT group was removed by the machine and after deprotection in NH_4OH (55°C, 24 h) and removal of NH_4OH , oligonucleotides were purified by electrophoresis on a high-resolution denaturing 15 or 20% polyacrylamide gel. Oligonucleotides were visualized by UV shadowing over an activated TLC plate, were excised from the gel with a scalpel and were then electroeluted from the gel slice using an Elutrap[®] (Schleicher & Schuell, Keene, NH). Electrophoresis buffer salts were removed from the oligonucleotide by passage over a prepacked Sephadex[®] G-25 column (Pharmacia-LKB Biotech, Piscataway, NJ).

5' End-labeling of oligonucleotides.

About 100-200 pmol of single-stranded oligonucleotide in buffer was incubated with 50 μCi γ -³²P ATP and 30 units of T4 polynucleotide kinase for 30 minutes at 37°C. Kinase was then denatured by incubation at 65°C for 15 minutes. Unincorporated radionucleotide was then removed with a G-15 Sephadex[®] spun-column¹³⁴ and then 1/10 volume of 10X STE buffer and a twofold molar excess of unlabeled complementary strand was added to the labeled oligonucleotide. The sample was mixed, heated at 90°C for 5 minutes in a temperature block heater and then the oligonucleotides were allowed to anneal overnight by removing the heat block from its base and placing it in a covered styrofoam box. After cooling overnight, about 1.25 nmol of the same unlabeled oligonucleotide duplex was added to the labeled material as carrier DNA. The labeled DNA was then precipitated with ethanol, rinsed with 70% ethanol and dried under vacuum prior to use.

Large-scale oligonucleotide hybridization.

1 μmol each of two complementary single-stranded oligonucleotides in H_2O were combined in a screw-capped glass vial and lyophilized to dryness. They were then dissolved in 4 mL of 1X STE buffer supplemented with 4 mM MgCl_2 , mixed thoroughly and then heated at 90°C for 10 minutes in a heat block. The block containing the oligonucleotide mixture was then removed from its electrical base and placed in a closed styrofoam box to allow the oligonucleotides to cool slowly overnight. After cooling, the mixtures were vortexed briefly and were then stored at -20°C until ready for use.

DEP/piperidine footprinting of echinomycin and ethidium bromide on oligonucleotide duplexes 47+48 to 60+61.

In a 1.5 mL microcentrifuge tube, a 193 μL solution of buffered singly $5'$ ^{32}P end-labeled oligonucleotide duplex, echinomycin or ethidium bromide, methanol and unlabeled FPLC[®]-purified oligonucleotide duplex was incubated for 1 hour at room temperature in the dark. Next, 7 μL of neat diethyl pyrocarbonate (DEP) was added to and mixed with the solution. DEP modification was allowed to proceed for 30 minutes at room temperature in the dark. Final reaction conditions were 100 mM Tris / 100 mM NaOAc pH 7.0 with HCl (TA buffer), 0.3 mM MgCl_2 , 600-700 μM oligonucleotide duplex bp, 10% (v/v) methanol, 0 or 120-140 μM echinomycin (echinomycin:DNA bp = 1:5), 0 or 3.0-3.6 mM ethidium bromide (ethidium bromide:DNA bp = 5:1) and 200-230 mM DEP (DEP:bp ~300 equivalents). DEP reaction was terminated and DNA binding drugs removed by extracting the reaction mixture three times each with 200 μL of H_2O saturated *n*-butanol. DEP control cleavage reactions were treated exactly as those containing echinomycin or ethidium bromide, except for the omission of the DNA-binding ligand. The DNA was then precipitated with ethanol, rinsed with 70% ethanol and then vacuum-dried on a Speedvac concentrator. The resulting pellet was resuspended in 300 μL of freshly diluted 100 mM piperidine, divided into three portions and heated for 15, 30 or 60 minutes at 90°C . After

heating, the reactions were centrifuged briefly and then lyophilized twice to remove piperidine. The Cerenkov radiation of each sample was measured with a Beckman LS 3801 liquid scintillation counter and the samples were then dissolved in formamide loading buffer to a specific activity of 4,000 cpm μL^{-1} . 4 μL of each sample was then loaded onto a high-resolution denaturing 15% polyacrylamide gel for electrophoretic separation of the cleavage products.

Product analysis: Large-scale reaction of DEP with oligonucleotide duplexes 47+48 to 60+61.

100 nmol of duplex oligonucleotide (32-36 base pairs in length) in ~400 μL of 100 mM NaCl / 10 mM Tris·HCl pH 8 / 1 mM EDTA / 4 mM MgCl_2 was placed in a 3 dram glass, screw-cap vial containing 1000 μL of 5X TA buffer pH 7.0. To this was added H_2O , methanol and either no drug, or 1600-1800 μL of 10 mM ethidium bromide in H_2O or 320-360 μL of 2000 μM echinomycin in methanol. The solutions were mixed and allowed to equilibrate for 2 hours in the dark at room temperature. After this equilibration period, 160-180 μL of neat DEP was added to the mixture; the vials were then sealed with Teflon tape, covered with Al foil and shaken for 30 minutes at room temperature on a mechanical "wrist-action" shaker. After addition of the DEP, reaction volume was exactly 5000 μL and contained 10% (v/v) methanol, 1X TA buffer, 0.3 mM MgCl_2 , 640-720 μM oligonucleotide DNA bp, 3.2-3.6 mM ethidium bromide, 128-144 μM echinomycin and 220-240 mM DEP. The molar ratios of drug to DNA bp remained constant at ~5:1 for ethidium bromide and ~1:5 for echinomycin. About 330 equivalents of DEP to DNA bp were used for each reaction. After shaking, drugs and DEP were extracted twice with 5 mL dry *n*-butanol and twice with 5 mL H_2O saturated *n*-butanol. This also reduced the reaction volume to about 2.5 mL. The extracted reaction mixture was then desalted by loading onto a rinsed, prepacked G-25 Sephadex[®] column (Pharmacia NAP-25). The sample was eluted with 3.5 mL H_2O into a screw-cap vial and then lyophilized to dryness using a Speedvac

concentrator. The lyophilizate was redissolved in 1800 μL of H_2O , after which 200 μL of ACS reagent grade (96%+) formic acid was added. A light precipitate formed after addition of the acid and persisted after mixing. The vial was capped tightly, sealed with teflon tape and then incubated at 60°C for 24 hours in a circulating water bath to depurinate the DNA. After heating, the mixture had cleared and it was then allowed to cool to room temperature. It was then lyophilized to dryness, resuspended in 1 mL of H_2O and then lyophilized again to remove trace formic acid. After the second lyophilization, the residue was resuspended in 1 mL H_2O by brief sonication and extensive agitation. To remove nucleic acid fragments produced during the depurination, the suspension was applied to an H_2O -rinsed 500 mg disposable SAX column (strong anion exchange, PGC scientifics, Gaithersburg, MD) and allowed to drip slowly through the column. The column was then eluted with 4mL of H_2O by gravity feed. The eluents were lyophilized to dryness in a 1.5 mL microcentrifuge tube and then resuspended in 35 μL of H_2O for HPLC analysis. The samples were centrifuged for 8-10 minutes at 14,000 rpm in a microcentrifuge to remove particulates and 35 μL of cleared solution was then transferred to a 100 μL (conical center) HPLC autosampler vial containing 3 μL of saturated *p*-anisaldehyde (in H_2O) as internal standard.

HPLC chromatography.

All separations were performed on a Hewlett-Packard HP1090M instrument equipped with a diode array detector and an autosampler. 10 μL of sample was injected for each chromatographic run and components were resolved on a C_2/C_{18} mixed-bed reversed-phase column 4.6 mm in diameter by 20 cm in length (Mino RPC™ S 5/20 Pharmacia-LKB Biotech, Piscataway, NJ). A guard column packed with the same C_2/C_{18} resin was always used. Buffers A (20 mM triethylammonium acetate TEAA pH 7.0) and B (20 mM TEAA pH 7.0 + 50% CH_3CN) prepared by diluting a 1.0 M TEAA pH 7.0 stock solution were filtered and sonicated for ~10 minutes prior to analysis. Reagents used in the buffers were the highest purity available, including HPLC grade triethylamine (Fisher), ACS

reagent grade glacial acetic acid (Aldrich), Milli-Q[®] purified H₂O and glass-distilled acetonitrile (Burdick & Jackson). Two different solvent gradients were employed to separate DEP-purine adducts, RAMP3 and RAMP9, and these are depicted in Figures 82 and 83.

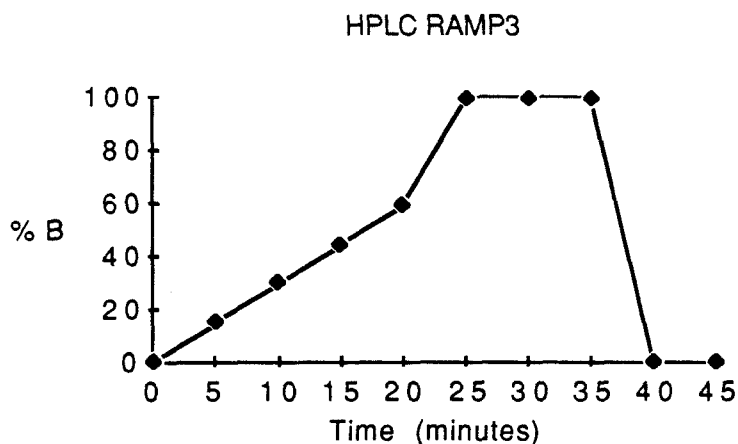


Figure 82. Schematic diagram of HPLC solvent gradient RAMP3.

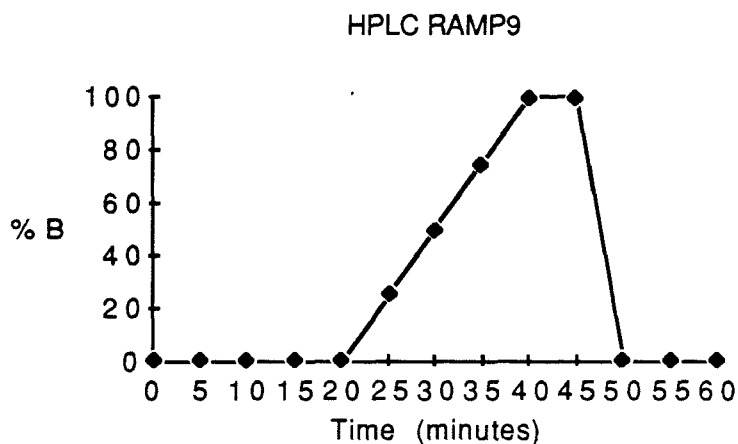


Figure 83. Schematic diagram of HPLC solvent gradient RAMP9.

In each case, the solvent flow rate was 0.5 mL min⁻¹ and detection was at 254 nm (10 nm bandwidth) versus a reference wavelength of 510 nm (10 nm bandwidth). Peak spectra were collected from 210 to 400 nm and a 90-second wash of the injection syringe was performed between each run to prevent sample carry-over.

Synthesis of 5-carbethoxyamino-4,6-diaminopyrimidine hydrochloride (X).

5 g (22.4 mmol) of 4,5,6-triaminopyrimidine sulfate was suspended in 75 mL of H₂O and the suspension added to 50 grams of Amberlite® IRA-400(OH) anion exchange resin in a 150 mL screw-cap centrifuge bottle. The mixture was mechanically shaken for three hours at room temperature, after which all of the sulfate salt dissolved. The slurry was filtered and the resin rinsed with about 25 mL of H₂O to give a pale-yellow filtrate with pH ca. 11. The filtrate was frozen overnight at -80°C and then lyophilized to dryness to give 1.81 grams (65%) of 4,5,6-triaminopyrimidine as pale-yellow needles. 22.5 MHz proton decoupled ¹³C NMR (DMSO-d₆) δ 106.6, 147.6, 151.5 ppm, all singlets relative to internal standard DMSO at 39.5 ppm. The free base was stored under argon in the dark at 4°C. Synthesis of 5-carbethoxyamino-4,6-diaminopyrimidine hydrochloride was carried out essentially as described by Leonard *et al.*⁹⁴ 1.25 g (10 mmol) of 4,5,6-triaminopyrimidine was stirred with 50 mL of dry pyridine at 0°C to give a suspension. To the stirring suspension was added 2.16 g (20 mmol) of ethyl chloroformate dropwise over a period of 30 minutes. During the course of ethyl chloroformate addition, the suspension cleared to give an orange solution. Stirring at 0°C was continued for another 1.5 hours in a stoppered flask, and the pyridine was then stripped from the reaction mixture on a rotovap to give a yellow-orange gum. The gum was resuspended in 90 mL of absolute ethanol and divided between two 50 mL polypropylene centrifuge tubes. Centrifugation for 5 minutes at 1500 rpm in a clinical centrifuge separated the mixture into a large white mass under a clear, deep-orange supernatant. The supernatant was removed and each tube extracted with another 45 mL of absolute ethanol. The extraction/centrifugation was performed a total of

four times and the supernatant was clear by the fourth extraction. The massive white pellet was filtered, rinsed with cold absolute ethanol and then dried to give 1.6 g (68%) of 5-carbethoxyamino-4,6-diaminopyrimidine hydrochloride (X) as a pale yellow powder. 400 MHz ^1H NMR (DMSO- d_6) δ 1.23 (t, 3H), 4.05 (q, 2H), 7.66 (broad s, 3H, exchanged with D_2O), 8.17 (2s, 2H); 22.5 MHz proton decoupled ^{13}C NMR (DMSO- d_6) δ 14.4, 60.7, 93.1, 147.2, 154.4, 156.4 ppm (all singlets) relative to internal DMSO- d_6 standard at 39.5 ppm; Exact mass (positive ion FAB) for $\text{C}_7\text{H}_{15}\text{N}_5\text{O}_2^+$, calculated: 198.0991, found: 198.0995; IR (KBr) 3150, 2700, 1640, 1250 cm^{-1} ; UV (20 mM TEAA pH 7.0 / 15.3% CH_3CN) λ_{max} 217, 260 nm.

Synthesis of 2,4,5-triamino-6-hydroxypyrimidine sulfate (C).

The synthesis below is an adaptation of two previous procedures.^{98,135} 252 mg (2 mmol) of 2,4-diamino-6-hydroxypyrimidine was dissolved in 7.2 mL of 1.0 M HCl and was then stirred in a brine / ice- H_2O bath at between -5° and 0°C to give a suspension. To this stirred suspension was added dropwise over 20 minutes 212 mg (3.1 mmol) of NaNO_2 dissolved in 750 μL of H_2O . A heavy, bright-pink precipitate formed immediately upon adding the first few drops of the NaNO_2 solution. The temperature of the reaction was kept between -5° and 0°C during NaNO_2 addition by stirring rapidly within a relatively large volume brine / ice- H_2O bath. When the NaNO_2 addition was complete, the cooling bath was removed and the mixture stirred for 1 hour while warming to room temperature. Solid NaHCO_3 was added portionwise until the pH of the mixture was approximately 8. The bright-pink solid was rinsed with cold H_2O and resuspended in ca. 15 mL H_2O for further reaction. The pink solid was judged to be 5-nitroso-2,4-diamino-6-hydroxypyrimidine based on identical appearance and solubility properties with reference material. The nitroso compound is virtually insoluble, failing to dissolve in H_2O , 1 M HCl, 1 M NaOH, CH_2Cl_2 , DMSO or DMF. The resuspended nitroso compound was heated to reflux (110°C) in a 25 mL flask fitted with a Kugelrohr condenser. About 5 drops of 1.0 M

NaOH were then added, followed by the portionwise addition of 760 mg (4.4 mmol) solid $\text{Na}_2\text{S}_2\text{O}_4$ (sodium dithionite, sodium hydrosulfite). At this point, the mixture began to clear. Another 380 mg (2.2 mmol) of $\text{Na}_2\text{S}_2\text{O}_4$ was added portionwise and the mixture turned a clear pale orange color. Reflux was continued for another 2-3 minutes and then the mixture was acidified by adding about 10-20 drops of 50% (v/v) H_2SO_4 . Heating was continued for another 30 seconds to 1 minute, after which the heat was removed and the solution allowed to cool to room temperature. After a few hours, a pale-yellow precipitate formed. The precipitate was filtered, rinsed with 95% ethanol, absolute ethanol, ether and was then dried under vacuum overnight to give 463 mg (96% for two steps) of 2,4,5-triamino-6-hydroxypyrimidine sulfate as pale-yellow needles. 2,4,[5- ^{15}N]-triamino-6-hydroxypyrimidine sulfate was synthesized in the same fashion except that >99% enriched $\text{Na}^{15}\text{NO}_2$ (Cambridge Isotope Laboratories) was used as the nitrogen source. This gave 453 mg (94%) of 2,4,[5- ^{15}N]-triamino-6-hydroxypyrimidine sulfate as pale-yellow needles.

Synthesis of 5-carbethoxyamino-2,4-diamino-6-hydroxypyrimidine (Y) and [5- ^{15}N]-carbethoxyamino-2,4-diamino-6-hydroxypyrimidine.

239 mg (1mmol) of 2,4,5-triamino-6-hydroxypyrimidine sulfate was stirred with 10 mL of H_2O plus 3.5 mL of saturated NaHCO_3 to give a light purple solution. Next, 200 μL (227 mg, 2.1 mmol) of ethyl chloroformate was added all in one portion and the stirring continued at room temperature. Within 5 minutes, a white precipitate began to form with the evolution of some gas. Stirring was continued for another 4 h, after which the precipitate was filtered and then rinsed with H_2O . The retentate was then recrystallized from ca. 15 mL of hot H_2O to give yellow needles. The first crop of crystals was filtered, rinsed with absolute ethanol, ether, dichloromethane and was then dried under vacuum overnight. The first crop of crystals gave 60 mg (28%) of 5-carbethoxyamino-2,4-diamino-6-hydroxypyrimidine. 400 MHz ^1H NMR: (DMSO-d_6) δ 1.17 (t, 3H), 3.96 (q, 2 H), 5.73

(s, 2H, exchanged with D₂O), 6.09 (s, 2H, exchanged with D₂O), 7.27 (s, 1H, exchanged with D₂O), 9.87 (s, 1H, exchanged with D₂O); 22.5 MHz proton decoupled ¹³C NMR: (DMSO-d₆) δ 14.7, 59.7, 89.5, 153.4, 155.9, 160.1, 161.6 (all singlets) relative to internal DMSO-d₆ at 39.5 ppm; IR (KBr) 3250, 1720, 1690, 1630, 1480, 1340, 1240 cm⁻¹; UV (20 mM TEAA pH 7.0) λ_{max} 216 nm, 270 nm; m/e 213 (M⁺, C₇H₁₁N₅O₃), with major decomposition products at m/e 167 (C₅H₅N₅O₂, loss of ethoxy group) and 140 (C₄H₆N₅O, loss of carbethoxy group)

[5-¹⁵N]-carbethoxyamino-2,4-diamino-6-hydroxypyrimidine was synthesized exactly as was the all ¹⁴N-compound, except that 2,4,[5-¹⁵N]-triaminopyrimidine sulfate was used as precursor. This gave a first crop of 63 mg (29%) of [5-¹⁵N]-carbethoxyamino-2,4-diamino-6-hydroxypyrimidine as yellow needles. 22.5 MHz proton decoupled ¹³C NMR: (DMSO-d₆) δ 14.7 (s), 59.7 (s), 89.5 (d, J=19Hz), 153.4 (s), 155.9 (d, J=26Hz), 160.1 (s), 161.7 (s) relative to internal DMSO-d₆ at 39.5 ppm; m/e 214 (M⁺, C₇H₁₁N₄O₃¹⁵N), with major decomposition products at m/e 168 (C₅H₅N₄O₂¹⁵N, loss of ethoxy group) and 141 (C₄H₆N₄O¹⁵N, loss of carbethoxy group).

Plasmid Construction.

A series of plasmids was constructed to investigate the sequence and length dependence of allosteric effects that were due to echinomycin binding to DNA. Figure 84 depicts the construction of plasmid pDMG10. The other plasmids were constructed in a similar fashion. Each plasmid was constructed by hybridizing a pair of 5' phosphorylated synthetic oligonucleotides to give a short duplex possessing cohesive *Bam* HI and *Hind* III termini. Table 6 lists the oligonucleotides used to construct the plasmids. Each duplex was ligated (16°C overnight) into the 4.0 kilobase (kb) *Bam* HI-*Hind* III fragment of plasmid pBR322. The resulting ligation mixture was used to transform *E. coli* strain HB101 according to the standard CaCl₂ procedure, pp. 250-251 of Reference 134. Recombinant

clones were selected for ampicillin resistance and tetracycline sensitivity because deletion of the small *Bam* HI-*Hind* III fragment from pBR322 disrupts the gene responsible for tetracycline resistance.¹³⁶ Milligram quantities of each recombinant plasmid were isolated according to the procedure that follows. Restriction mapping and chemical sequencing confirmed each construct. The inserted sequence is contained in the ~628 bp *Eco* RI-*Bgl* I fragment for each plasmid. The exact size of this fragment differs for each plasmid: 623 bp for both pDMG5 and pDMAT5; 628 bp for pDMG10, pDMAT10, pDMAG10 and pDMAC10; 629 bp for pDMGC11.

Table 6. Oligonucleotides Used for Plasmid Construction.

Plasmid (size)	Oligonucleotide duplex
pDMG5 (4049 bp)	5'AGCTTATATATATATAAAAAGGGGGTTCGATAG 3' 3'ATATATATATATTTTTCCCCCAGCTATCCTAG 5'
pDMAT5 (4049 bp)	5'AGCTTATATATATATAAAAATATATTCGATAG 3' 3'ATATATATATATTTTTATATAAGCTATCCTAG 5'
pDMG10 (4054 bp)	5'AGCTTATATATATATAAAAAGGGGGGGGGTTCGATAG 3' 3'ATATATATATATTTTTCCCCCCCCCAGCTATCCTAG 5'
pDMAT10 (4054 bp)	5'AGCTTATATATATATAAAAATATATATATATTCGATAG 3' 3'ATATATATATATTTTTATATATATATAGCTATCCTAG 5'
pDMAG10 (4054 bp)	5'AGCTTATATATATATAAAAAGAGAGAGATCGATAG 3' 3'ATATATATATATTTTTCTCTCTCTAGCTATCCTAG 5'
pDMAC10 (4054 bp)	5'AGCTTATATATATATAAAAACACACACATCGATAG 3' 3'ATATATATATATTTTTGTGTGTGTAGCTATCCTAG 5'
pDMGC11 (4054 bp)	5'AGCTTATATATATATAAAAAGCGCGCGCGTCGATAG 3' 3'ATATATATATATTTTTCGCGCGCGCAGCTATCCTAG 5'

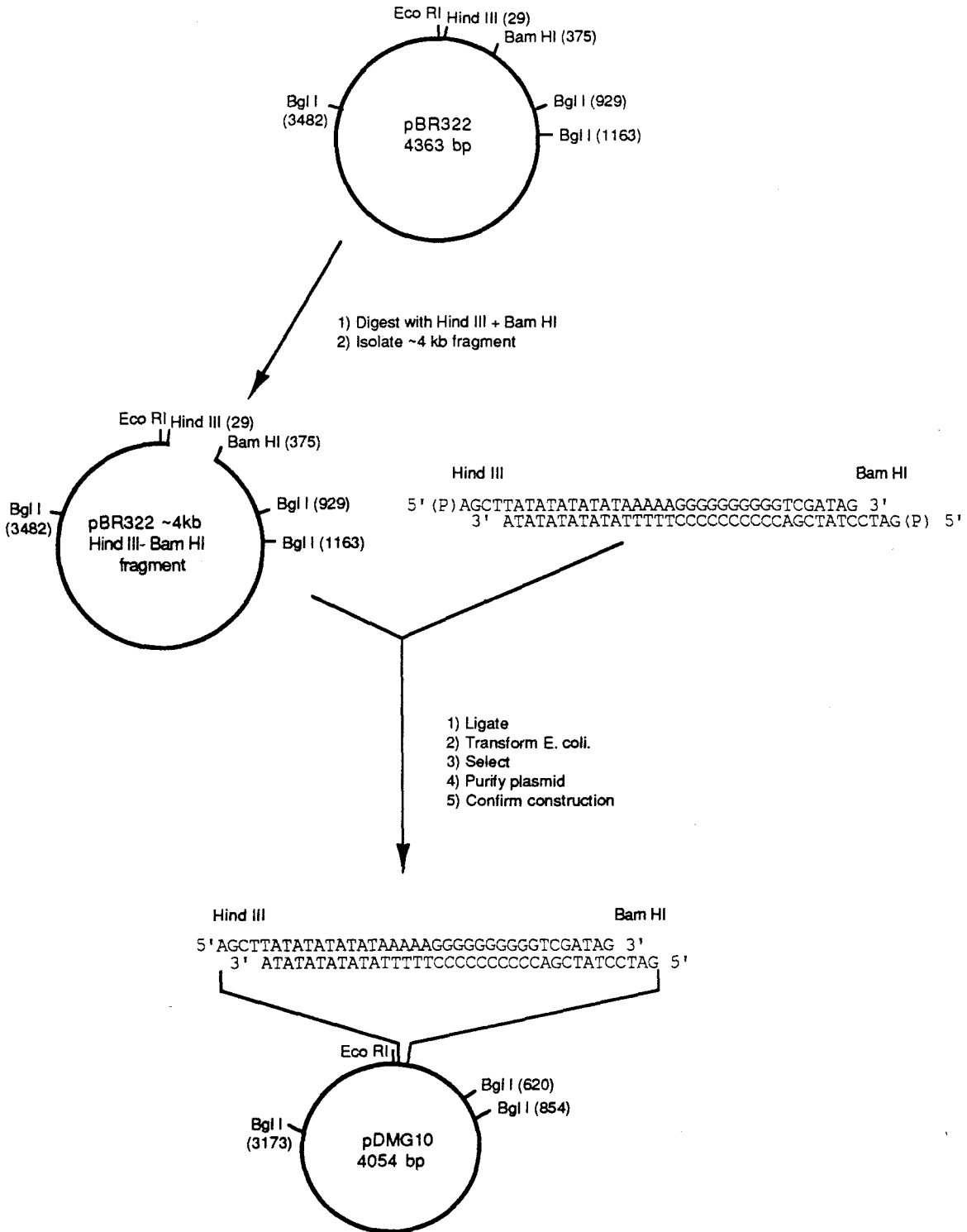


Figure 84. Construction scheme for plasmid pDMG10.

Plasmid Preparation.

The following practical protocol was supplied by Dr. Lianna Johnson of Caltech and is an adaptation of the method described in Reference 137.

Media Preparation and Growth of Bacteria.

Prepare 2 liters of Vogel-Bonner media (1 liter in each of two 2 liter-erlenmeyer flasks). Recipe for 1 liter of Vogel-Bonner media is as follows:

2 g casamino acids
20 mL 50X Vogel-Bonner salts
50 mL autoclaved 1 mg/mL thymine
water to give 980 mL total volume.

Autoclave the above media and allow to cool to room temperature, add:

20 mL sterile (autoclaved) 20% w/v D-glucose
2 mL ampicillin (25 mg/mL, filtered sterile 0.2 μ m)
1 mL thiamine·HCl (1 mg/mL, filtered sterile 0.2 μ m).

Inoculate 1 liter of Vogel-Bonner minimal media with 4 mL of an overnight culture of bacteria in L-broth containing 50 ug/mL ampicillin (to keep selective pressure on to increase yield of plasmid). Grow the cells in 37°C incubator shaker until O.D.₅₉₀ = 0.6 to 0.9. Amplify by adding 2 mL 100 mg/mL chloromycetin sodium succinate (chloramphenicol) per 1 liter of culture (100 mg/mL solution is made by adding 10 mL sterile water via syringe to a 1 g vial of chloramphenicol and shaking until it has completely dissolved). Continue shaking of cultures at 37°C for 12-17 hours.

Cell Harvest and Lysis.

1. Chill cells in the 2-liter growth flasks on ice bath with frequent agitation. Load chilled cells into 500 mL bottles, balance with a double pan balance. Spin at 5000 rpm at 4°C for 20 min. Discard supernatants and wipe bottles dry.

2. Resuspend the cell pellets in 4-6 mL of 25% sucrose/50 mM Tris pH 8. Transfer the resuspended cells to a 70Ti (polycarbonate) tube and add:
 - 1.6 mL 5 mg/mL lysozyme (prepared just before use) and let sit on ice for 5 min with occasional stirring, then add:
 - 5 mL 0.5 M EDTA pH 8 and let sit on ice for 5 min with occasional stirring.
3. One tube at a time, add 12 mL 10% Triton X-100/50 mM Tris pH 8/60 mM EDTA pH 8 and shake vigorously until the lysates clear (looks like shampoo that's been shaken). Usually the process takes about 20 to 30 sec. Try to avoid clumping of lysates.
4. Balance tubes to within 0.01 g difference, load into Ti 70 rotor. Spin in ultracentrifuge at 30,000 rpm at 4°C for 30 min.
5. Pour supernatants into 50 mL polypropylene centrifuge tubes and avoid gluey junk near cell debris.
6. Add 350 μ L of 2 mg/mL RNaseA (DNase free) and incubate for 20 min at 37°C.
7. Add 1/3 volume (6 to 7 mL) of 30% PEG 8000/1.5 M NaCl to each tube, shake to mix and incubate 30 min to 8 hours on ice (longer the time of incubation equals better yield).
8. Centrifuge the PEG/NaCl mixture at 6000 rpm for 20 min at 4°C and discard supernatant.
9. Resuspend pellet in 2-5 mL of cold 10X TE buffer (100 mM Tris-HCl/10 mM EDTA pH 8) using a glass rod.
10. Set up the first CsCl isopycnic banding run. For every 500 mL of original culture, use one 40 mL quick seal tube. For 2 liters of original culture, combine the following:
 - 119.04 g CsCl (ultrapure)
 - pellets in 10X TE from step 9
 - 6.4 mL of 10 mg/mL EtBr
 - 1X TE buffer to give a final weight of 228 g (this equals 160 mL of 48% w/w CsCl and has density of 1.55 g/mL).

Stir to dissolve the CsCl and load into 4 VTi50 tubes. Balance to within 0.01 g difference and seal the tubes using the Beckman tube sealer. Allow the tube sealer to warm up for 10

to 20 min before using. Load the tubes into the VTi50 rotor, put spacers and caps in place and start the first gradient at 42,000 rpm for 20 hrs at 17°C.

11. Pull lower (plasmid) band (using UV illumination) by puncturing the quick-seal® tube about 1 cm below band with an 18 gauge needle and a 10 mL syringe. Keep needle bevel up and protect DNA from excessive exposure to UV light.

12. Transfer bands from step 11 into VTi65 tubes (5 mL tube volume) and fill tubes with CsCl filling solution if necessary (48% CsCl and 400 µg/mL EtBr). Balance the tubes again to 0.01 g difference, seal and load into VTi65.2 rotor.

13. Spin at 55,000 rpm at 17°C for 12 hrs.

14. Extract plasmid band as before in step 11, but use a 3 mL syringe.

15. Extract EtBr with 1X TE saturated isoamyl alcohol. About 12-15 extractions of 1 volume each are needed (DNA is in the aqueous layer at the bottom). Check for EtBr presence with transilluminator.

16. Dialyze plasmid vs. 1X TE pH 8 buffer at 4°C. The dialysis requires 4-5 changes over a period of 24 hrs.

17. Check O.D.₂₆₀ and O.D.₂₈₀ of the dialyzed plasmid for concentration and purity.

Radiolabeling of the *Eco* RI-*Bgl* I restriction fragments.

A uniquely labeled *Eco* RI-*Bgl* I restriction fragment containing the desired insert was obtained by linearizing plasmid pDMG10 (or any of the other plasmids described) with *Eco* RI and then labeling the 5' termini with T4 polynucleotide kinase and γ -³²P ATP or by labeling the 3' termini with the large fragment (Klenow enzyme) of *E. coli*. DNA polymerase I and α -³²P dATP. The fragment containing inserted sequence was liberated by digestion of the labeled DNA with *Bgl* I. An *Eco* RI + *Bgl* I double digest of each recombinant DNA plasmid above gives rise to four DNA restriction fragments, ~300 bp, ~628 bp, ~900 bp and ~2200 bp. The ~628 bp fragment contains the inserted sequence at

~30 bp from the labeled *Eco* RI end. After *Bgl* I digestion of the labeled DNA, the restriction fragments were separated by electrophoresis through a 1.5% low-melting agarose gel. The desired fragment was then excised from the gel and then extracted from the agarose with phenol. A practical protocol for the preparation of purified, uniquely end-labeled 628 bp **Eco* RI-*Bgl* I fragment from plasmid pDMG10 is presented below:

5' Labeling

15 µg *Eco* RI digested, dephosphorylated
pDMG10
29 µL H₂O
5 µL 10X T4 kinase buffer
5 µL 10mg/mL DTT, fresh
10 µL γ -³²P ATP ~100 µCi
1 µL T4 polynucleotide kinase (10 units/µL)
50 µL

Incubate:
20 minutes, 37°C

Add:
1 µL T4 polynucleotide kinase (10 units/µL)

Incubate:
20 minutes 37°C

Precipitate twice with ethanol, vacuum dry pellet for ca. 3-5 minutes on Speedvac.

Bgl I digest

15 µg 5' or 3' end-labeled pDMG10, dried pellet
40 µL H₂O
5 µL 10X *Hinf* I buffer
resuspend for 10-15 minutes at 37°C
1 µL 2-mercaptoethanol (100 mM, freshly prepared)
4 µL *Bgl* I (8 units/µL, Boehringer)
50 µL

3' Labeling

15 µg *Eco* RI digested pDMG10
18 µL H₂O
5 µL 10X Hae III buffer
5 µL 10 mg/mL DTT (freshly
prepared)
12 µL α -³²P dATP ~120 µCi
5 µL dTTP, 10 mM pH 7
5 µL Klenow fragment (5 units/µL)
50 µL

25 minutes, 25°C

5 µL dTTP, 10 mM pH 7
5 µL dATP, 10 mM pH 7

10 minutes, 25°C

Incubate for 1-2 hours at 37°C; check digest on minigel.

If digest is complete via minigel, reduce volume to ~35 μ L via Speedvac, add ~5 μ L ficoll loading buffer + dyes and apply to a 1.5% low-melting agarose gel in the cold room.

Electrophorese @ 20-30V overnight, stain with ethidium bromide. Excise the second smallest (~628 bp) band and trim away excess agarose not containing DNA, transfer slice to 1.5 mL microcentrifuge tube.

Extraction of DNA from agarose:

To the gel slice containing radiolabeled DNA add:

5 volumes (relative to gel slice volume) of 1X TE buffer pH 8, incubate at 65°C for 10-15 minutes to melt gel slice.

Add: 1 volume (relative to total gel slice + TE volume) of H₂O saturated phenol, vortex vigorously and centrifuge at room temperature for 3-4 minutes at 14000 rpm.

Transfer: top (aqueous) layer to a clean 1.5 mL tube; avoid carrying fluffy white material.

Repeat extraction: 1X with 1 volume phenol:chloroform:iso-amyl alcohol 25:24:1, (save top layer), 1X with 1 volume chloroform:iso-amyl alcohol 24:1 (save top layer) and 3-5X with 1 volume dry *n*-butanol to reduce volume and to extract ethidium bromide (save bottom layer).

Precipitate DNA with ethanol, rinse with 70% ethanol and vacuum-dry. Redissolve to a specific activity of ca. 15000-20000 cpm/ μ L and store at 4°C in an acrylic shielding box.

MPE•Fe(II) footprinting.

Three different but similar protocols were used for MPE•Fe(II) footprinting.

Unless stated otherwise, all incubations were performed in the dark.

1) MPE•Fe(II) footprinting in TN buffer. A buffered 16 μ L solution containing purified end-labeled restriction fragment, echinomycin, methanol, and sonicated, deproteinized calf thymus DNA was incubated for 15 minutes at 37°C. Next, 2 μ L of an 80 μ M MPE / 160 μ M Fe(NH₄)₂(SO₄)₂ (FAS) solution was added, the mixture was vortexed to mix and allowed to equilibrate another 15 minutes at 37°C. DNA strand scission was initiated by adding 2 μ L of a freshly prepared 40 mM dithiothreitol (DTT) solution. Cleavage at 37°C was terminated after 20 minutes by freezing on dry ice, followed by two

precipitations from ethanol. The final concentrations in the 20 μL reaction mixture were 400 μM DNA bp, 1X TN buffer pH 7.4, 8 μM MPE, 16 μM FAS, 10% (v/v) methanol, 4 mM DTT and 0, 12.5, 25, 50 or 100 μM echinomycin.

2) MPE·Fe(II) footprinting of echinomycin in the absence of methanol. A 40 μL solution of buffered, purified end-labeled DNA restriction fragment, sonicated, deproteinized calf thymus DNA, echinomycin and 10% (v/v) methanol was incubated for 15 minutes at 37°C. This mixture was then lyophilized to dryness, redissolved in 34 μL of H_2O and allowed to stand for 20 minutes at 37°C. Next, 2 μL of an 80 μM MPE / 160 μM FAS solution was added; the mixture was vortexed and allowed to stand another 15 minutes at 37°C. MPE·Fe(II)-mediated strand scission was initiated by addition of 4 μL of a freshly prepared 10 mM sodium L-ascorbate solution and continued for 2 minutes at 37°C before termination by freezing and ethanol precipitation. Prior to addition of ethanol, the 40 μL reaction mixture contained 1X TN buffer pH 7.4, 200 μM DNA bp, 4 μM MPE / 8 μM FAS and 0, 12.5 or 50 μM echinomycin.

3) MPE·Fe(II) footprinting in Tris-acetate (TA) buffer. Incubation was as in (1) above except that strand scission was continued for 25 to 35 minutes at 37°C. Final concentrations prior to reaction termination were 1X TA buffer pH 7.0, 200 μM DNA bp, 0 or 50 μM echinomycin, 10% (v/v) methanol, 4 μM MPE, 8 μM FAS and 1 mM sodium L-ascorbate. For simultaneous footprinting of two drugs, a second incubation step was added to allow the second drug to bind the DNA.

EDTA·Fe(II) Footprinting.

A 40 μL solution of buffered, end-labeled DNA restriction fragment, sonicated, deproteinized calf thymus DNA, 10% (v/v) methanol and 0, 12.5 or 50 μM echinomycin was incubated for 15 minutes at 37°C in the dark. This solution was lyophilized to dryness on a Speedvac concentrator and then re-equilibrated in 32 μL of H_2O for 20 minutes at 37°C. Next, 4 μL of a 2 mM EDTA ($\text{Na}_2\cdot\text{H}_2\text{O}$) / 2 mM FAS solution was added; the

mixture was then vortexed and allowed to stand for another 15 minutes at 37°C. DNA strand scission was initiated by the addition of 4 μL of a freshly prepared 10 mM sodium L-ascorbate solution. After mixing, cleavage was allowed to proceed for 10 minutes at 37°C and was terminated by the addition of 150 μL of cold absolute ethanol to the reaction mixture. The DNA was then precipitated from ethanol and dried under vacuum in preparation for loading onto high-resolution denaturing polyacrylamide gels. Final concentrations prior to reaction termination were 1X TN buffer, 200 μM calf thymus DNA bp, 0, 12.5 or 50 μM echinomycin, 200 μM EDTA / 200 μM FAS and 1 mM sodium L-ascorbate.

DNase I footprinting.

A 36 μL solution of buffered, end-labeled DNA restriction fragment, sonicated, deproteinized calf thymus DNA and methanol or echinomycin (dissolved in methanol) was incubated (dark) for 15 minutes at 37°C. Next, 4 μL of a freshly prepared 330 ng/mL solution of DNase I (bovine pancreatic deoxyribonuclease I, Worthington) was added to the wall of the microcentrifuge tube and then vortexed to mix with the buffered DNA and to initiate DNA strand scission. Cleavage was terminated after 2 to 3 minutes at room temperature by the addition and mixing of 5 μL of 3 M ammonium acetate / 250 mM EDTA solution. The DNA was then precipitated with ethanol, rinsed with 70% ethanol and vacuum-dried. Final concentrations in the reaction mixture prior to termination were 1X TKMC buffer, 200 μM calf thymus DNA bp, 10% (v/v) methanol, 0, 6.25, 12.5, 25 or 50 μM echinomycin and 1.32 ng of DNase I.

DEP footprinting.

A buffered 38 μL solution containing purified end-labeled DNA restriction fragment, methanol or echinomycin (dissolved in methanol) and sonicated, deproteinized calf thymus DNA was incubated (dark) for 15 minutes at 37°C. Next, 2 μL of a freshly

made 5-fold dilution of DEP in methanol was added; the mixture was vortexed and then incubated for 10 minutes at 37°C. The final concentrations in the 40 µL modification reactions were 1X TA buffer, pH 2.7, 3.7, 4.7, 5.7, 7.0 or 8.0, 200 µM calf thymus DNA bp, 10% (v/v) methanol, 0 to 50 µM echinomycin and 68 mM DEP. DEP modification reactions were terminated by ethanol precipitation, rinsing with 70% ethanol and then vacuum-drying. The dried, modified DNA pellet was resuspended in 100 µL of freshly diluted 100 mM piperidine and then heated at 90°C for 15 minutes (5' label) or 5 minutes (3' label) to effect strand scission at the bases modified by DEP. Piperidine was removed by two lyophilizations, and the DNA was then dissolved in formamide loading buffer in preparation for high-resolution denaturing gel electrophoresis. Control DEP modification reactions lacked only echinomycin and were treated exactly as were samples containing echinomycin. This procedure can also be used with TN and TKMC buffers and with different DNA bp concentrations.

DMS footprinting.

A 48 µL solution of buffered, 5' end-labeled oligonucleotide duplex, purified carrier duplex oligonucleotide, methanol and echinomycin or ethidium bromide was incubated (dark) at room temperature for 30 minutes. Then 2 µL of a dimethyl sulfate (DMS) solution (saturated in H₂O) was added; the mixture was then vortexed and allowed to stand for 15 minutes (dark) at room temperature. DMS modification was terminated by adding 4 µL of neat 2-mercaptoethanol to the solution and then mixing. The DMS-modified DNA was then precipitated with ethanol, rinsed with 70% ethanol and then vacuum-dried. The resulting pellet was redissolved in freshly diluted 100 mM piperidine and heated in a tightly capped 600 µL microcentrifuge tube at 90°C for 30 minutes. The condensate was returned to the bottom of the tube by brief centrifugation and the mixture was lyophilized twice to remove piperidine before loading onto high-resolution denaturing polyacrylamide gels. Final concentrations prior to termination were 1X TA buffer pH 3.7 or 8.0, 680 µM

oligonucleotide bp, 136 μ M echinomycin or 3.9 mM ethidium bromide, 10% (v/v) methanol and a 25-fold dilution of saturated DMS in H₂O.

KMnO₄ footprinting.

A 36 μ L solution of buffered, end-labeled DNA restriction fragment, sonicated, deproteinized calf thymus DNA and methanol or echinomycin (in methanol) was incubated for 15 minutes at 37°C. Next, 4 μ L of a freshly prepared 500 μ M KMnO₄ solution was added; the mixture was vortexed and then incubated for another 15 minutes at 37°C. KMnO₄ modification was terminated by ethanol precipitation and rinsing, followed by vacuum-drying. The dried pellet was then resuspended in 100 μ L of freshly diluted 100 mM piperidine, heated for 15 minutes at 90°C and then lyophilized twice prior to loading on sequencing gels. Final concentrations in the modification reactions before precipitation were 1X TA buffer pH 7.0, 200 μ M calf thymus DNA bp, 10% (v/v) methanol, 0, 6.25, 12.5, 25 or 50 μ M echinomycin and 50 μ M KMnO₄.

Bleomycin A₂·Fe(II) (BLM) and Neocarzinostatin (NCS) footprinting.

A 32 μ L solution of buffered end-labeled DNA restriction fragment, sonicated, deproteinized calf thymus DNA, and methanol or echinomycin (in methanol) was incubated in the dark for 15 minutes at 37°C. Next, 4 μ L of either NCS (Bristol, 1 unit/ μ L in 15 mM NaOAc pH 5.0) or 4 μ L of a freshly prepared 40 μ M BLM (Blenoxane, Bristol) / 40 μ M FAS solution was added, mixed and the resulting solution incubated another 5 minutes in the dark at 37°C. Different thiol sources were then added to each mixture in order to initiate DNA cleavage: For NCS reactions, 4 μ L of a freshly prepared 100 mM 2-mercaptoethanol solution was added and for BLM reactions, 4 μ L of a freshly prepared 40 mM dithiothreitol (DTT) solution was added. After addition of thiol, the reactions were mixed and then incubated for 20 minutes in the dark at 37°C, after which DNA strand scission was interrupted by ethanol precipitation and rinsing followed by vacuum-drying. The final

concentrations in the 40 μL reaction mixtures before ethanol precipitation were 1X TA buffer pH 7.0, 200 μM calf thymus DNA bp, 0, 12.5 or 50 μM echinomycin, 10 mM 2-mercaptoethanol or 4 mM DTT and 4 μM bleomycin / 4 μM FAS or 0.1 unit / μL of NCS.

High-Resolution Denaturing Polyacrylamide Gel Electrophoresis.

DNA cleavage products produced in footprinting reactions were separated on high-resolution denaturing 8% or 15% polyacrylamide gels. The acrylamide was crosslinked 1:20 with bis-acrylamide, and the gels also contained 50% (w/v) urea and 1X TBE buffer. All gels were wedge-shaped, having a thicker bottom to enhance resolution and to more evenly resolve the products of DNA cleavage. Dimensions for all 8% gels were 34 cm (w) x 40 cm (l) x 0.2 mm (comb) x 0.6 mm (base). 15% gels had the same length and width but were 0.4 mm thick at the comb and 1.2 mm thick at the base. We used the Bethesda Research Laboratories Model S2 sequencing apparatus exclusively for high-resolution gel electrophoresis. Prior to loading samples, gels were pre-electrophoresed for 1 hour at 1500 V with 1X TBE as the running buffer. Samples in formamide loading buffer were denatured by heating at 90°C for 2 minutes after which they were placed in a polyethylene glycol mold kept at -20°C. This process was more effective than wet ice in preventing renaturation of the DNA samples. Approximately 4 μL of sample was loaded onto each lane of the pre-electrophoresed gel with an Eppendorf® ultramicro pipettor. Prior to denaturation and loading, the Cerenkov radiation of each sample was measured and the samples were then made to a common specific activity (ca. 4000 cpm μL^{-1}) so that uniform amounts of radiolabeled material could be applied to each lane without having to change the pipettor setting. This is important because loading 28 to 30 lanes on a gel requires a significant amount of time, and the DNA can renature during loading if pipettor settings have to be changed for each lane. After application of samples to the gel, 1500 V was again applied and the gel electrophoresed for 2-4 hours until the bromophenol blue marker dye had migrated 40 cm (8% gels) or 25 cm (15% gels) from the origin. After this, the gel was

transferred to a sheet of Whatman 3 MM chromatography paper and was then dried under vacuum at 80°C using a Bio-Rad slab gel dryer. 15% gels contained ca. 2-3% glycerol to prevent cracking during the drying process. 8% gels were dried for 90 minutes, 15% gels for 3-4 hours, and then were allowed to cool to room temperature on the gel dryer while still under vacuum. They were then placed in an aluminum cassette and allowed to expose Kodak X-OMat XAR-5 film. An intensification screen was used for the exposure of 15% gels at -80°C, whereas all 8% gel exposures were made at room temperature without intensification screens. Typically, the ~15,000 cpm loaded per lane gave a good image after 12 hours of intensified exposure or after about 3.5 to 4 days exposure without intensifier. After developing, the autoradiograms were cut and then scanned with an LKB model 2222 XL laser densitometer.

Chemical Sequencing Reactions.

The Maxam-Gilbert chemical sequencing G and G+A specific reactions were performed as described in the original reference ⁷⁹, except that 100 mM piperidine was used instead of the 1.0 M piperidine for strand scission at the points of modified bases. We found this concentration of piperidine to give a cleaner background with the purine specific reactions. However, we do not know if 100 mM piperidine is sufficient to cleave at the points of pyrimidine modification. Optimum DMS methylation times were about 90 seconds for the 628 bp restriction fragments and about 8 minutes for the ~34 bp oligonucleotides. Optimum formic acid treatment was for 4 minutes on the 628 bp restriction fragments and 15 minutes on the ~34 bp oligonucleotides. All incubations were performed at room temperature (20-22°C).

REFERENCES

1. Waring, M. J. (1981) *Annu. Rev. Biochem.* **50**, 159-192.
2. Zimmer, C. (1975) *Prog. Nucl. Acid Res. Mol. Biol.* **15**, 285-318.
3. Kopka, M. L., Yoon, C., Goodsell, D., Pjura, P. & Dickerson, R. E. (1985) *Proc. Natl. Acad. Sci. USA* **82**, 1376-1380.
4. Dervan, P. B. (1986) *Science* **232**, 464-471.
5. Coll, M., Frederick, C. A., Wang, A.H.-J. & Rich, A. (1987) *Proc. Natl. Acad. Sci. USA* **84**, 8385-8389.
6. Hurley, L. H. & Needham Van Devanter (1986) *Acc. Chem. Res.* **19**, 230-237.
7. Quigley, G. J., Wang, A.H.-J., Ughetto, G., van der Marel, G. van Boom, J. H. & Rich, A. (1980) *Proc. Natl. Acad. Sci. USA* **77**, 7204-7208.
8. Tomasz, M., Chowdary, D., Lipman, R., Shimotakahara, S., Viero, D., Walker, V. & Verdine, G. L. (1986) *Proc. Natl. Acad. Sci. USA* **83**, 6702-6706.
9. Tomasz, M., Lipman, R., Chowdary, D., Pawlak, J., Verdine, G. L. & Nakanishi, K. (1987) *Science* **235**, 1204-1208.
10. Lee, S. H. & Goldberg, I. H. (1989) *Biochemistry* **28**, 1019-1026.
11. Hecht, S. M., Ed. (1978) *Bleomycin: Chemical, Biochemical, and Biological Aspects*, Springer-Verlag, New York, Heidelberg and Berlin.
12. Muller, W. & Crothers, D. M. (1968) *J. Mol. Biol.* **35**, 251-290.
13. Hollstein, U. (1974) *Chem. Rev.* **74**, 625-652.
14. Low, C. M. L., Drew, H. R. & Waring, M. J. (1984) *Nucleic Acids Res.* **12**, 4865-4879.
15. Wang, A. H.-J., Ughetto, G., Quigley, G. J., Hakoshima, T., van der Marel, G. A., van Boom, J. H. & Rich, A. (1984) *Science* **225**, 1115-1121.
16. Van Dyke, M. M. [sic] & Dervan, P. B. (1984) *Science* **225**, 1122-1127.
17. Harshman, K. D. & Dervan, P. B. (1985) *Nucleic Acids Res.* **13**, 4825-4835.
18. Teng, M. Usman, N., Frederick, C. A. & Wang, A. H.-J. (1988) *Nucleic Acids Res.* **16**, 2671-2690.
19. Van Dyke, M. W. & Dervan, P. B. (1983) *Biochemistry* **22**, 2373-2377.
20. Gao, X. & Patel, D. J. (1989) *Biochemistry* **28**, 751-762.
21. Watson, J. D. & Crick, F. H. C. (1953) *Nature* **171**, 737-738.

22. Fuller, W., Wilkins, M. H. F., Wilson, H. R. & Hamilton, L.D. (1965) *J. Mol. Biol.* **12**, 60-80.
23. Shakked, Z., Rabinovich, D., Cruse, W. B. T., Egert, E., Kennard, O., Salisbury, S. A. & Viswamitra, M. A. (1981) *Proc. Roy. Soc. London Ser. B* **231**, 479-487.
24. Rich, A., Nordheim, A. & Wang, A. H.-J. (1984) *Annu. Rev. Biochem.* **53**, 791-846.
25. Saenger, W. (1984) in *Principles of Nucleic Acid Structure*, pp. 276-282, Springer-Verlag, New York, Heidelberg and Berlin.
26. Mirkin, S. M., Lyamichev, V. I., Drushlyak, K. N., Dobrynin, V. N., Filippov, S. A., & Frank-Kamenetskii, M. D. (1987) *Nature* **330**, 495-497.
27. Htun, H. & Dahlberg, J. E. (1988) *Science* **241**, 1791-1796.
28. Koo, H. S., Wu, H. S. & Crothers, D. M. (1986) *Nature* **320**, 501-506.
29. Burkhoff, A. M. & Tullius, T. D. (1987) *Cell* **48**, 935-943.
30. Zahn, K. & Blattner, F. R. (1987) *Science* **236**, 416-422.
31. Felsenfeld, G., Davies, D. R. & Rich, A. (1957) *J. Am. Chem. Soc.* **79**, 2023-2024.
32. Felsenfeld, G. & Miles, H. T. (1967) *Annu. Rev. Biochem.* **36**, 407-448.
33. Moser, H. E. & Dervan, P. B. (1987) *Science* **238**, 645-650.
34. Lilley, D. M. J. (1986) in *The Role of Cyclic Nucleic Acid Adducts in Carcinogenesis and Mutagenesis* (Singer, B. & Bartsch, H., Eds.), pp. 83-99 International Agency for Research on Cancer, Lyon.
35. Sullivan, K. M. & Lilley, D. M. J. (1987) *J. Mol. Biol.* **193**, 397-404.
36. Haniford, D. B. & Pulleyblank, D. E. (1985) *Nucleic Acids Res.* **12**, 4343-4363.
37. Kahn, A. S. & Roe, B. A. (1988) *Science* **241**, 74-79.
38. Taylor, J. S., Schultz, P. G. & Dervan, P. B. (1984) *Tetrahedron* **40**, 457-465.
39. Schultz, P. G. & Dervan, P. B. (1984) *J. Biomol. Struct. Dynam.* **1**, 1133-1147.
40. Schultz, P. G. & Dervan, P. B. (1983) *Proc. Natl. Acad. Sci. USA* **80**, 6834-6837.
41. Youngquist, R. S. & Dervan, P. B. (1985) *Proc. Natl. Acad. Sci. USA* **82**, 2565-2567.
42. Youngquist, R. S. (1988) Ph. D. Thesis, California Institute of Technology, Pasadena, California.

43. Youngquist, R. S. & Dervan, P. B. (1987) *J. Am. Chem. Soc.* **109**, 7564-7565.
44. Dervan, P. B. & Sluka, J. P. (1986) *Stud. Org. Chem. (Amsterdam) 25 New Synth. Methodol. Funct. Interesting Compd.*, 307-322.
45. Wade, W. S. & Dervan, P. B. (1987) *J. Am. Chem. Soc.* **109**, 1574-1575.
46. Griffin, J. H. & Dervan, P. B. (1987) *J. Am. Chem. Soc.* **109**, 6840-6842.
47. Kuroya, M., Ishida, N., Katagiri, K., Shoji, J., Yoshida, T., Mayama, M., Sato, K., Matsuura, S., Niinome, Y. & Shiratori, O. (1961) *J. Antibiotics Ser. A* **14**, 324-329.
48. Katagiri, K., Yoshida, T. & Sato, K. (1975) in *Antibiotics III: Mechanism of Action of Antimicrobial and Antitumor Agents* (Corcoran, J. W. & Hahn, F. E., Eds.), pp. 235-251, Springer-Verlag, Berlin, Heidelberg and New York.
49. Ward, D. C., Reich, E. & Goldberg, I. H. (1965) *Science* **149**, 1259-1263.
50. Foster, B. J., Claggett-Carr, K., Shoemaker, D. D., Suffness, M., Plowman, J., Trissel, L. A., Grieshaber, C. K. & Leyland-Jones, B. (1986) *Investig. New Drugs* **3**, 403, 410.
51. Barton, J. K. (1988) *Chem. Eng. News* **66**, 30-42.
52. Keller-Schierlein, W., Mihailovic, M. Lj. & Prelog, V. (1959) *Helv. Chim. Acta* **42**, 305-322.
53. Dell, A., Williams, D. H., Morris, H. R., Smith, G. A., Feeney, J. & Roberts, G. C. K. (1974) *J. Am. Chem. Soc.* **97**, 2497-2502.
54. Martin, D. G., Mizesak, S. A., Biles, C., Stewart, J. C., Baczynskyj, L. & Meulman, P. A. (1975) *J. Antibiotics* **28**, 332-336.
55. Sato, K., Shiratori, O. & Katagiri, K. (1967) *J. Antibiotics Ser. A* **20**, 270-276.
56. Waring, M. J. & Wakelin, L. P. G. (1974) *Nature* **252**, 653-657.
57. Waring, M. J., Wakelin, L. P. G. & Lee, J. S. (1975) *Biochim. Biophys. Acta* **407**, 200-212.
58. McGhee, J. D. & von Hippel, P. H. (1974) *J. Mol. Biol.* **86**, 469-489.
59. Wakelin, L. P. G. & Waring, M. J. (1976) *Biochem. J.* **157**, 721-740.
60. Lee, J. S. & Waring, M. J. (1978) *Biochem. J.* **173**, 115-128.
61. Sen, D. & Gilbert, W. (1988) *Nature* **334**, 364-366.
62. Lee, J. S. & Waring, M. J. (1978) *Biochem. J.* **173**, 129-144.
63. Low, C. M. L., Fox, K. R., Olsen, R. K. & Waring, M. J. (1986) *Nucleic Acids Res.* **14**, 2015-2033.

64. Wang, J. C. (1974) *J. Mol. Biol.* **89**, 783-801.
65. Cheung, H. T., Feeney, J., Roberts, G. C. K., Williams, D. H., Ughetto, G. & Waring, M. J. (1978) *J. Am. Chem. Soc.* **100**, 46-54.
66. Ughetto, G. & Waring, M. J. (1977) *Mol. Pharmacol.* **13**, 579-584.
67. Galas, D. J. & Schmitz, A. (1978) *Nucleic Acids Res.* **5**, 3157-3170.
68. Low, C. M. L., Olsen, R. K. & Waring, M. J. (1984) *FEBS Lett.* **176**, 414-420.
69. Hoogsteen, K. (1959) *Acta Crystallogr.* **12**, 822-823.
70. Singh, U. C., Pattabiraman, N., Langridge, R. & Kollman, P. A. (1986) *Proc. Natl. Acad. Sci. USA* **83**, 6402-6406.
71. Ughetto, G., Wang, A. H.-J., Quigley, G. J., van der Marel, G. A., van Boom, J. H. & Rich, A. (1985) *Nucleic Acids Res.* **13**, 2305-2323.
72. Quigley, G. J., Ughetto, G., van der Marel, G. A., van Boom, J. H., Wang, A. H.-J. & Rich, A. (1986) *Science* **232**, 1255-1258.
73. Wang, A. H.-J., Ughetto, G., Quigley, G. J. & Rich, A. (1986) *J. Biomol. Struct. Dynam.* **4**, 319-342.
74. Gao, X. & Patel, D. J. (1988) *Biochemistry* **27**, 1744-1751.
75. Patel, D. J. (1974) *Biochemistry* **13**, 2396-2402.
76. Feigon, J., Denny, B. A., Leupin, W. & Kearns, D. R. (1984) *J. Med. Chem.* **27**, 450-465.
77. Gao, X. & Patel, D. J. (1989) *Quart. Rev. Biophys.* in press.
78. Lawley, P. D. & Brookes, P. (1963) *Biochem. J.* **89**, 127-138.
79. Maxam, A. M. & Gilbert, W. (1980) *Methods Enzymol.* **65**, 499-560.
80. Peattie, D. A. & Gilbert, W. (1980) *Proc. Natl. Acad. Sci. USA* **77**, 4679-4682.
81. Ehresmann, C., Baudin, F., Mougel, M., Romby, P., Ebel, J.-P. & Ehresmann, B. (1987) *Nucleic Acids Res.* **15**, 9109-9128.
82. Mougel, M., Philippe, C., Ebel, J.-P., Ehresmann, B. & Ehresmann, C. (1988) *Nucleic Acids Res.* **16**, 2825-2839.
83. Herr, W. (1985) *Proc. Natl. Acad. Sci. USA* **82**, 8009-8013.
84. Johnston, B. A. & Rich, A. (1985) *Cell* **42**, 713-724.
85. Runkel, L. & Nordheim, A. (1986) *J. Mol. Biol.* **189**, 487-501.
86. Scholten, P. M. & Nordheim, A. (1986) *Nucleic Acids Res.* **14**, 3981-3993.

87. Furlong, J. C. & Lilley, D. M. J. (1986) *Nucleic Acids Res.* **14**, 3993-4007.
88. Mendel, D. & Dervan, P. B. (1987) *Proc. Natl. Acad. Sci. USA* **84**, 910-914.
89. Portugal, J., Fox, K. R., McLean, M. J., Richenberg, J. L. & Waring, M. J. (1988) *Nucleic Acids Res.* **16**, 3655-3670.
90. Fox, K. R. & Grigg, G. W. (1988) *Nucleic Acids Res.* **16**, 2063-2075.
91. Jeppesen, C. & Nielsen, P. E. (1988) *FEBS Lett.* **231**, 172-176.
92. McClelland, M. (1981) *Nucleic Acids Res.* **9**, 6795-6804.
93. Leonard, N. J., McDonald, J. J. & Reichmann, M. E. (1970) *Proc. Natl. Acad. Sci. USA* **67**, 93-98.
94. Leonard, N. J., McDonald, J. J., Henderson, R. E. L. & Reichmann, M. E. (1971) *Biochemistry* **10**, 3335-3342.
95. Vincze, A., Henderson, R. E. L., McDonald, J. J. & Leonard, N. J. (1973) *J. Am. Chem. Soc.* **95**, 2677-2682.
96. Henderson, R. E. L., Kirkegaard, L. H. & Leonard, N. J. (1973) *Biochim. Biophys. Acta* **294**, 356-364.
97. Silverstein, R. M., Bassler, G. C. & Morrill, T. C. (1981) in *Spectrometric Identification of Organic Compounds*, pp. 249-303, John-Wiley & Sons, New York.
98. Traube, W. (1900) *Ber.* **33**, 1371-1383.
99. McLean, M. J. & Waring, M. J. (1988) *J. Mol. Recognition* **1**, 138-151.
100. Gilbert, D. E., van der Marel, G. A. van Boom, J. H. & Feigon, J. (1989) *Proc. Natl. Acad. Sci. USA* in press.
101. Van Dyke, M. W. & Dervan, P. B. (1983) *Nucleic Acids Res.* **11**, 5555-5567.
102. Tullius, T. D. & Dombroski, B. A. (1986) *Proc. Natl. Acad. Sci. USA* **83**, 5469-5473.
103. Schultz, P. G. & Dervan, P. B. (1983) *J. Am. Chem. Soc.* **105**, 7748-7750.
104. Herzberg, R. P. & Dervan, P. B. (1984) *Biochemistry* **23**, 3934-3945.
105. Vogt, V. M. (1973) *Eur. J. Biochem.* **33**, 192-200.
106. Kochetkov, N. K. & Budovskii, E. J., Eds. (1972) In *Organic Chemistry of Nucleic Acids, Part B* pp. 287-288, Plenum Press, London and New York.
107. Galazka, G., Palecek, E., Wells, R. D. & Klysik, J. (1986) *J. Biol. Chem.* **261**, 7093-7098.

108. McClellan, J. A., Palecek, E. & Lilley, D. M. J. (1986) *Nucleic Acids Res.* **14**, 9291-9309.
109. Kappen, L. S. & Goldberg, I. H. (1983) *Biochemistry* **22**, 4872-4878.
110. Hecht, S. M. (1986) *Acc. Chem. Res.* **19**, 383-391.
111. Viswamitra, M. A., Kennard, O., Shakked, Z., Jones, P. G., Sheldrick, G. M., Salisbury, S. & Falvello, L. (1978) *Nature* **273**, 687-690.
112. Patel, D. J. & Tonelli, A. E. (1974) *Biopolymers* **13**, 1943-1964.
113. Scheffler, I. E., Elson, E. L. & Baldwin, R. L. (1968) *J. Mol. Biol.* **36**, 291-304.
114. Klug, A., Jack, A., Viswamitra, M. A., Kennard, O., Shakked, Z. & Steitz, T. (1979) *J. Mol. Biol.* **131**, 669-680.
115. Suggs, J. W. & Wagner, R. W. (1986) *Nucleic Acids Res.* **14**, 3703-3716.
116. Lilley, D. M. J. (1988) *Trends in Genetics* **4**, 111-114.
117. McLean, M. J., Blaho, J. A., Kilpatrick, M. W. & Wells, R. D. (1986) *Proc. Natl. Acad. Sci. USA* **83**, 5884-5888.
118. Wang, A., H.-J., Hakoshima, T., van der Marel, G., van Boom, J. H. & Rich, A. (1984) *Cell* **37**, 321-331.
119. Kohwi-Shigematsu, T., Gelin, R. & Weintraub, H. (1983) *Proc. Natl. Acad. Sci. USA* **80**, 4389-4393.
120. Kohwi-Shigematsu, T., Manes, T. & Kohwi, Y. (1987) *Proc. Natl. Acad. Sci. USA* **84**, 2223-2227.
121. McLean, M. J., Larson, J. E., Wohlrab, F. & Wells, R. D. (1987) *Nucleic Acids Res.* **15**, 6917-6935.
122. Kohwi, Y. & Kohwi-Shigematsu, T. (1988) *Proc. Natl. Acad. Sci. USA* **85**, 3781-3785.
123. Kean, J. M., White, S. A. & Draper, D. E. (1985) *Biochemistry* **24**, 5062-5070.
124. Drew, H. R. (1984) *J. Mol. Biol.* **176**, 535-557.
125. Drew, H. R. & Travers, A. A. (1985) *Nucleic Acids Res.* **13**, 4445-4467.
126. Pohl, F. M. & Jovin, T. M. (1972) *J. Mol. Biol.* **67**, 375-396.
127. Povirk, L. F. & Goldberg, I. H. (1980) *Biochemistry* **19**, 4773-4780.
128. Kappen, L. S., Goldberg, I. H. & Liesch, J. M. (1982) *Proc. Natl. Acad. Sci. USA* **79**, 744-748.
129. Lee, S. H. & Goldberg, I. H. (1989) *Biochemistry* **28**, 1019-1026.

130. Burd, J. F., Wartell, R. M., Dodgson J. B. & Wells, R. D. (1975) *J. Biol. Chem.* **250**, 5109-5113.
131. Matteucci, M. D. & Caruthers, M. H. (1981) *J. Am. Chem. Soc.* **103**, 3185-3191.
132. Beaucage, S. L. & Caruthers, M. H. (1981) *Tetrahedron Lett.* **22**, 1859-1862.
133. Atkinson, T. & Smith, M. (1984) In *Oligonucleotide Synthesis: A Practical Approach* (Gait, M. J., Ed.), pp. 35-81, IRL Press, Oxford and Washington D. C.
134. Maniatis, T., Fritsch, E. F. & Sambrook, J. (1982) In *Molecular Cloning: A Laboratory Manual*, pp. 466-467, Cold Spring Harbor Laboratory, Cold Spring Harbor, NY.
135. Evans, R. M., Jones, P. G., Palmer, P. J. & Stephens, F. F. (1956) *J. Chem. Soc.* 4106-4113.
136. Sutcliffe, J. G. (1979) *Cold Spring Harbor Symp. Quant. Biol.* **43**, 77-90.
137. Tanaka, T. & Weisblum, B. (1975) *J. Bacteriol.* **121**, 354-362.